Thermodynamic Modeling of the Mg-Al-Li-Na-H System for Solid State Hydrogen Storage Applications

Saida Abdessameud

A Thesis

In the Department

of

Mechanical and Industrial Engineering

Presented in Partial Fulfillment of the Requirements

For the Degree of Doctor in Philosophy (Mechanical Engineering) at

Concordia University

Montreal, Quebec, Canada

August, 2016

CONCORDIA UNIVERSITY
School of Graduate Studies

This is to certify that the thesis prepared

By: Saida Abdessameud

Entitled: Thermodynamic Modeling of the Mg-Al-Li-Na-H system for Solid State Hydrogen Storage Applications

and submitted in partial fulfillment of the requirements for the degree of

DOCTOR OF PHILOSOPHY (Mechanical Engineering)

complies with the regulations of the University and meets the accepted standards with respect to originality and quality.

Signed by the final examining committee:

_____Chair
Dr. Rabin Raut

_____External Examiner
Dr. Jacques Huot

_____External to program
Dr. Fuzhan Nasiri

_____Examiner
Dr. Paula Wood Adams

_____Examiner
Dr. Hoi Dick Ng

_____Thesis Supervisor
Dr. Mamoun Medraj

Approved by _____
Chair of Department or Graduate Program Director

2016 _____
Dr. , Dean
Faculty of Engineering & Computer Science

ABSTRACT

Thermodynamic Modeling of the Mg-Al-Li-Na-H System for Solid State Hydrogen Storage Applications
Saida Abdessameud, PhD
Concordia University, 2016

In this work a thermodynamic database describing the Mg-Al-Li-Na-H system was constructed using thermodynamic modeling through the CALPHAD method. The constructed database was used to assess the hydrogen storage properties of the system at different pressures and temperatures and to understand the phase relationships and reactions mechanisms.

The liquid phase in the binary systems was reassessed using the modified quasichemical model (MQM) or taken from the literature. Since hydrogen atoms occupy the interstitial positions in the solid phases, terminal solid solution phases were described using the compound energy formalism (CEF). Two sublattices were used where Mg, Al, Li, and Na atoms mix randomly in the first sublattice to allow for their mutual solubility and H atom and vacancy mix in the second sublattice. All the gases included in this study were considered ideal. The calculated phase diagrams and thermodynamic properties were compared to experimental data from the literature and showed good agreement. The ternary systems were extrapolated from the corresponding binaries using the asymmetric Kohler-Toop technique where H is singled out as the asymmetric component. In this study, all the calculations were performed using the FactSage software where all the cited models are already coded and implemented.

The constructed database allowed the calculation of pressure-composition isotherms of MgH_2-10 wt. % NaH, Mg-10 at. % Al and Mg-4 at. % Al. Phase diagrams, pressure temperature diagrams, and reaction pathways of the composites MgH_2-AlH_3, MgH_2-$NaAlH_4$, MgH_2-Na_3AlH_6, and MgH_2-$AlLiH_4$/$AlLi_3H_6$ were calculated and showed good agreement with the experimental data from the literature. The results provided more details about the de/hydrogenation processes, the amount and composition of phases, and the effect of the pressure and temperature. It is found that Al and Li when added to Mg improve the hydrogen potential of the system and the most promising compositions were predicted.

The strategy used in this study will allow the experimental investigations to focus on the kinetics aspect of the de/hydrogenation reactions for these alloys.

Dedication

To my parents

To my sisters and brothers

Acknowledgements

I express my sincere gratitude to Professor Mamoun Medraj for his guidance, cooperation, and support during the accomplishment of this work. Also, I am grateful for his valuable comments, the trust, and the freedom he gave me to do this work.

I wish to thank all (former and current) TMG members for their continuous support and the atmosphere of a research family they built up.

I like to express my profound thanks to Dr. Mezbahul-Islam for his support, his help in using FactSage software, and his cooperation in this work.

I sincerely thank Professor Jack Huot and his group members from IRH for allowing me to use their laboratory to realize some experimental work. Even though, these experiments were not used for this thesis, it was a wonderful experience to work with them.

Thanks are not the words enough to express my feelings to my parents for their selfless love and support during all my life. They always keep encouraging me to move forward in my studies.

I like to thank my brothers and sisters; especially Fatma-Zohra and her husband Kamel and their kids, Rym, Nassim and Lina, for providing the family atmosphere that I need.

Last but not least, I thank Maamar Bouchouka for supporting my PhD work; his encouragements have made all these possible.

Special thank to the natural sciences and engineering research council NSERC for financial support of the project through NSERC Hydrogen Canada Network (H_2Can).

Contributions of the Authors

This thesis was prepared in manuscript-based format. The entire contents represent results that have been published in the form of an unaltered original J. article and materials that are submitted for publication, or the clearly duplicated text of one or more published papers of which the student is the author or co-author. The complete citation for the published papers is provided below:

- **Chapter 2**: S. Abdessameud, M. Mezbahul-Islam and M. Medraj, "Thermodynamic modeling of hydrogen storage capacity in Mg-Na alloys", *The Scientific World J. 2014 (Article ID 190320, 16 pages),* (2014)

- **Chapter 3**: S. Abdessameud and M. Medraj, "Understanding the hydrogen storage behavior of promising Al-Mg-Na compositions using thermodynamic modeling", *Materials for Renewable and Sustainable Energy 5(2),* pp. 1-29, (2016)

- **Chapter 4**: S. Abdessameud and M. Medraj, "Thermodynamic analysis of the hydriding process of Mg-Al-Li-Na alloys", *CALPHAD: Computer Coupling of Phase Diagrams and Thermochemistry (54),* pp. 54–66, (2016)

M. Mezbahul-Islam contributed in the first published paper on the assessment of the Mg-Na and Na-H systems.

Table of Contents

List of Figures

List of Tables

Chapter 1: Introduction

1.1 Hydrogen storage

Increasing energy demand, climate change, and limited fossil fuel reserves are the world's most urgent concerns and sources of insecurity for life on earth. Keller et al. [1] examined these issues, and presented valuable arguments for the potential of hydrogen as an alternative "energy carrier". Hydrogen is abundant and can be produced using renewable energy resources. It enables high-energy conversion efficiency devices such as fuel cells and internal combustion engines (ICEs) with no CO_2 emissions. Klebanoff *et al.* [2] provided a description of the existing hydrogen power technologies and their main applications.

However, the potential of hydrogen as the fuel of the future depends on the development of appropriate storage solutions. Hydrogen can be stored in various physical states (solid, liquid, gas, chemical compounds); for a review of all the hydrogen storage methods, one can refer to the book entitled "Hydrogen Storage Technology, Materials and Applications" edited by Klebanoff [3]. It is concluded that for most hydrogen energy applications, an adapted storage method is required prior hydrogen usage. In this work, a special attention is given to the storage of hydrogen in the form of chemical compounds or alloys, where hydrogen atoms are bounded with other elements, and particularly to metal hydrides and complex hydrides. A review of all the materials investigated/used for hydrogen storage applications is presented in the book entitled "Handbook of Hydrogen Storage: New Materials for Future Energy Storage" edited by Hirsher [4].

The US department of energy DOE highlights the importance of hydrogen energy for light-duty vehicles by its "centers of excellence for solid-state hydrogen storage". Recently, Klebanoff and Keller [5] presented a summary of 5 years of solid-state hydrogen storage research in the DOE metal hydride center of excellence (MHCoE). The main focus of the MHCoE is to develop and validate new on-board reversible hydrides for vehicular applications. The term "On-board reversible" means that the hydrogen desorption and re-absorption is realized on-board the vehicle or "in place" which implies specific conditions of temperature and pressure. The MHCoE established quantitative system storage technical targets for their research programs [5]. The main issues (goals) addressed are: hydrogen capacity (9wt%), reversibility and cycle life (1000

cycles), thermodynamics (PME full cell operating temperature of 85°C at 5 bar), kinetics (5-kg hydrogen charge in 4.2 min), material's stability and hydrogen purity (less than 200 ppm contamination). It should be noted that no material has been identified that satisfies all the selected goals [5]. However, materials that merit further study have been identified using interim targets as guidelines (the material should: have a hydrogen capacity of 5wt%, be 50% reversible, release hydrogen below 350°C, loose less than 1000 ppm for a single cycle, release and reabsorb hydrogen in less than 24 hours). Klebanoff and Keller [5] reported that from the 94 materials systems investigated, 84 were not selected for further study. The main limitations of these materials are poor kinetics and reversibility, which prevent the study of their thermodynamic properties and reaction mechanisms. It is worth noting that these limitations are related to the present lack of knowledge on reactions mechanisms and kinetics. Significant amount of research is still needed to improve the understanding of these aspects of hydrogen storage materials. The elements that are selected for the current study encompass some of the materials that were recommended for further studies by MHCoE.

1.2 Metal hydrides

Huot [6] reviewed the fundamental characteristics of metal hydrides for hydrogen storage applications and provided valuable references for in depth details about their historical development and applications. In this section, the main characteristics and aspects of metal hydrides related to this work are presented.

Hydrides can be divided in three categories according to the nature of bonding of hydrogen with the host metal, such as ionic (or saline), covalent, and metallic hydrides, which confers different physical properties to the hydrides. Reversibility of a metal hydride depends on the nature of hydrogen-atom bonding (the stronger the bonding the less reversible the hydride). In order of decreasing level of reversibility, metal hydrides can be ordered as: metallic, ionic, and then covalent [6]. For most metals and alloys, hydrogen is bound in the interstitial (octahedral and tetrahedral) sites of the host material. Intermediate cases (mixed ionic-covalent bonding) are referred to as complex hydrides [3].

Most of the binary metal hydrides (elemental hydrides) are too stable (have large negative heat of formation) for practical applications. The heat of formation is significantly reduced for

hydrides formed from intermetallic compounds AB, AB_2, A_2B, and AB_5 (A is an element which forms a stable hydride and B another element which does not form a stable hydrides) [6]. Chandra [7] and Chao and Klebanoff [8] reviewed the properties of intermetallics and interstitial metal hydrides for hydrogen storage applications. It should be noted that, except MgH_2 and Mg_2NiH_4, metal hydrides contain less than 3 wt% H_2 [3].

1.2.1 Thermodynamics of hydride formation

Many metals and alloys react with hydrogen gas to form metal hydrides according to equation (1.1). Where M is a metal, a solid solution alloy or an intermetallic compound, MH_x is the hydride and x is the hydrogen to metal molar ratio H/M.

$$M + \frac{x}{2} H_2 \rightarrow MH_x \qquad (1.1)$$

Figure 1.1 shows a schematic representation of the process and the pressure-composition isotherms (PCIs), characteristic of the thermodynamics of hydride formation [9]. The left side of Figure 1.1 shows the PCIs for hydrogen absorption in a typical metal. The dissociation of molecular hydrogen into hydrogen atoms starts in the vicinity of metal surface (and certain intermetallic compounds). Hydrogen atoms dissolve exothermically in the metal and form an interstitial solid solution α-phase (shown in the left hand side of the PCIs in Figure 1.1) which is followed by a lattice expansion proportionally to hydrogen concentration by approximately 2 to 3 $Å^3$ per hydrogen atom [10]. As the concentration of hydrogen atoms in the metal is increased, the hydride phase (β-phase) nucleates and grows due to the formation of H-H bond with anisotropic volume expansion (corresponding to 10 to 20% of the metal lattice) in (α + β) region shown in the plateau region (ideally flat) of the PCIs characteristic of the coexistence of the two phases. The length of the plateau determines the amount of hydrogen that can be stored reversibly with small pressure variations. As a consequence of lattice expansion, lattice defects and internal strain fields are formed which end in decrepitating of brittle host metals [6]. The end of the plateau is followed by the steep rise of the hydrogen pressure with hydrogen concentration, which is characteristic of the β phase. The right hand side of Figure 1.1 shows the Van't Hoff Plot, the representation of the Van't Hoff equation given by equation (1.2), which relates the equilibrium pressure P_{eq} to the enthalpy and entropy of formation of the metal hydride

ΔH and ΔS, respectively. Peq^0 is a reference pressure. The stability of the metal hydride is characterized by the enthalpy term.

$$\mathrm{Ln}\left(\frac{P_{eq}}{P_{eq}^{0}}\right) = \left(\frac{\Delta H}{R}\right)\frac{1}{T} - \left(\frac{\Delta S}{R}\right) \qquad (1.2)$$

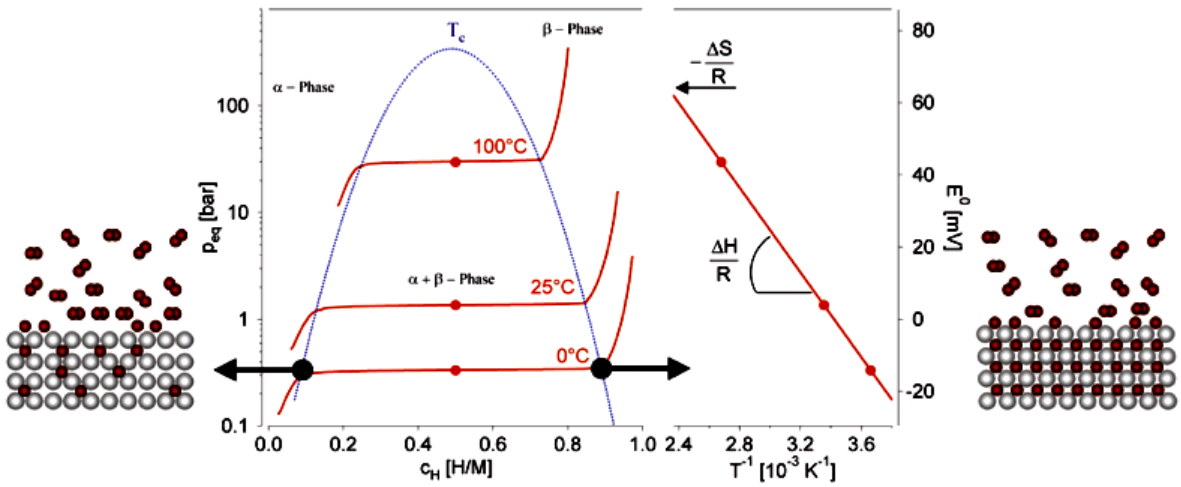

Figure 1.1: Schematic representation of the Pressure-Concentration-Isotherms (PCIs) (on the left hand side) and Van 't Hoff Plot for a hydrogen absorbent (on the right hand side) [9]

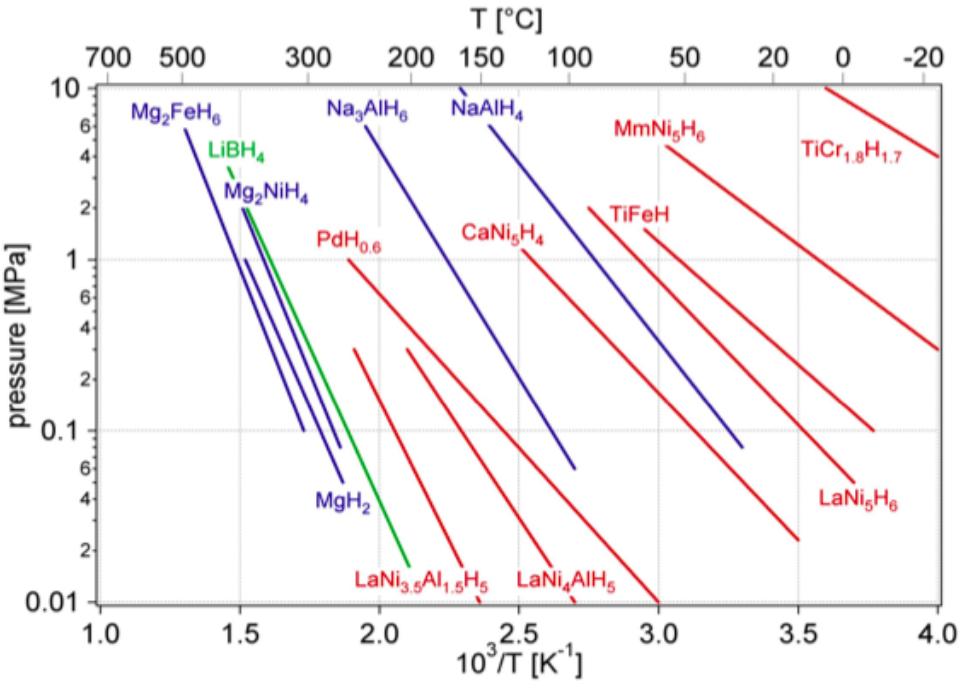

Figure 1.2: Van 't Hoff Plots of selected hydrides [9]

In practice, the plateaus shown in Figure 1.1 are sometimes slopped and desorption equilibrium pressure are lower than absorption ones (hysteresis) due to defects and inhomogeneities in the materials. Hydrides are classified according to their ΔH and temperature of decomposition. Figure 1.2 shows the Van't Hoff plot for several selected metal hydrides [9]. It has been shown that partial substitution of a constituent element in the host lattice of a binary compound could significantly alter the hydrogen storage properties [9]. An example is shown in Figure 1.2 where Züttel [9] has shown the influence of stabilisation of $LaNi_5$ hydride by the partial substitution of Ni by Al. The stability of a hydride is given by the value of the heat of formation ΔH (the higher ΔH the more stable the hydride), which is given by the slop of the Van't Hoff plot multiplied by the gas constant R as shown in Figure 1.1.

1.2.2 Complex metal hydrides

Complex metal hydrides are very promising for hydrogen storage applications due to their hydrogen capacity and lightweight. These materials contain mixed ionic-covalent bonding and are composed of metal cations (such as Li^+, Na^+, K^+, Mg^{2+}, Ca^{2+}, etc.) strongly bounded (ionic bond) to complex anions. Complex metal hydrides are classified according to the complex hydrogen-containing anions (covalent bond within anions) such as alanates (AlH_4^- or AlH_6^{3-}), borohydrides (BH_4^-), amides (NH_2^-), and imides (NH^-). Jain *et al*. [11] provided a review of the crystal structures and (de)/hydrogenation properties data of these complex hydrides. Stavila *et al*. [12] provided an updated review. However, these hydrides suffer from slow kinetics, high desorption temperatures, and/or reversibility for on-board applications.

1.3 Magnesium and its alloys for hydrogen storage

Magnesium and its alloys stand as promising candidates for hydrogen storage because of their hydrogen storage capacity, light weight, the abundance of magnesium in the earth's crust, and low cost compared to alternative systems. In fact, magnesium forms MgH_2 hydride, which contains 7.6wt. % hydrogen [13]. But, its formation from bulk magnesium and gaseous hydrogen is extremely slow and in thermodynamic equilibrium a plateau pressure of 1 bar requires a temperature of about 300°C which corresponds to an enthalpy of formation of -78 kJ/mole H_2 [13].

Sakintuna *et al.* [13] and Jain *et al.* [14] conducted literature reviews on magnesium and its alloys as hydrogen storage systems. The investigations on magnesium hydrides found in the literature focus mainly on improving the sorption kinetics by ball milling and using catalysts, and decreasing desorption temperature (or reaction enthalpy) [14].

In order to lower reaction enthalpy, many experiments have been conducted where Mg has been alloyed with other elements and thus, formed stable Mg-based compounds. As an example, Mg_2Ni forms a ternary hydride, Mg_2NiH_4, with 3.6 wt. % H_2 and a decomposition temperature of 280°C at 1 bar and shows improved kinetics [15]. However, it contains lower hydrogen capacity than MgH_2 and its working conditions are still not suitable for practical applications [15].

1.3.1 Thermodynamic destabilization

Vajo *et al*. [16] tried to destabilize MgH_2 by adding Si. They [16] found that the dehydrogenation reaction proceeds according to reaction (1.3)

$$2\,MgH_2 + Si \rightarrow Mg_2Si + 2\,H_2 \qquad (1.3)$$

The energy diagram of MgH_2/Si presented by Vajo et al. [16] is shown in Figure 1.3. It is shown that the formation of Mg_2Si reduces the enthalpy of dehydrogenation of the system from 75.3 kJ/mol for MgH_2 to 36.4 kJ/mol for MgH_2+1/2 Si [16]. Dehydrogenation temperature of the MgH_2+1/2 Si [16] was estimated to be 20°C at 1 bar pressure [16]. Nevertheless, Si reduced the hydrogen capacity of the system and the (de)/hydrogenation kinetics was very poor.

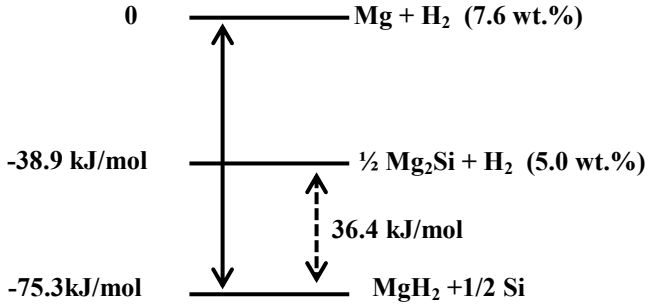

Figure 1.3: Energy diagram showing MgH_2 destabilization through the formation of Mg_2Si alloy upon dehydrogenation [16]

In general, thermodynamic destabilization results in decreasing the enthalpy (temperature) of dehydrogenation of a system. It occurs through alloy formation upon dehydrogenation of a system where the hydride is mixed with additives (compounds or hydrides). For a two

components system, hydride destabilization involves the reaction (1.4) [16] (AH_x and BH_y are binary or more complex hydrides):

$$n\,AH_x + m\,BH_y \rightarrow A_nB_m + \frac{1}{2}(nx + my)\,H_2 \qquad (1.4)$$

1.4 CALPHAD method

The CALPHAD method [17] is a powerful tool in phase equilibrium studies and materials development. It is based on the fact that multicomponent phase diagram calculations are possible if the thermodynamic properties are known.

Thermodynamic modeling through the CALPHAD method is to define appropriate thermodynamic models for all the phases in a system and to express the related Gibbs energy functions in terms of temperature, pressure and composition. Different models are used for different phases based on the characteristics of each phase and adjustable thermodynamic parameters are used. The mathematical expressions of Gibbs energy functions used in this work are given in Chapter 2. The total Gibbs energy is the sum of Gibbs energy of all the phases multiplied by their mole fractions. The derived Gibbs energy functions should reproduce the thermodynamic properties and the experimentally determined phase diagrams. For that purpose, thermodynamic, crystallographic, and phase diagram experimental data are collected from the literature and are critically evaluated to remove inconsistency and contradiction.

Once the thermodynamic parameters of binary systems are successfully optimized considering all the reliable data, the CALPHAD method allows the calculation of higher order systems by extrapolation techniques, which are based on the summation of the binary and the ternary excess parameters using various geometrical weightings of the mole fractions [18]. There are three main techniques for the extrapolation; symmetric such as Kohler [19] and Muggianu [20] models and asymmetric such as Kohler-Toop [21] and Muggianu-Toop [18] models.

The symmetric methods consider all the components as chemically similar and do not differentiate between them, whereas asymmetric methods considers that one of the binaries behaves differently than the two other binaries for which the common component is singled out as the asymmetric component. Geometric constructions for the cited models are presented in Figure 1.4 [22]. In the present study, hydrogen is singled out as the asymmetric component since M-H systems (M is a metal) behave very differently than any metals systems.

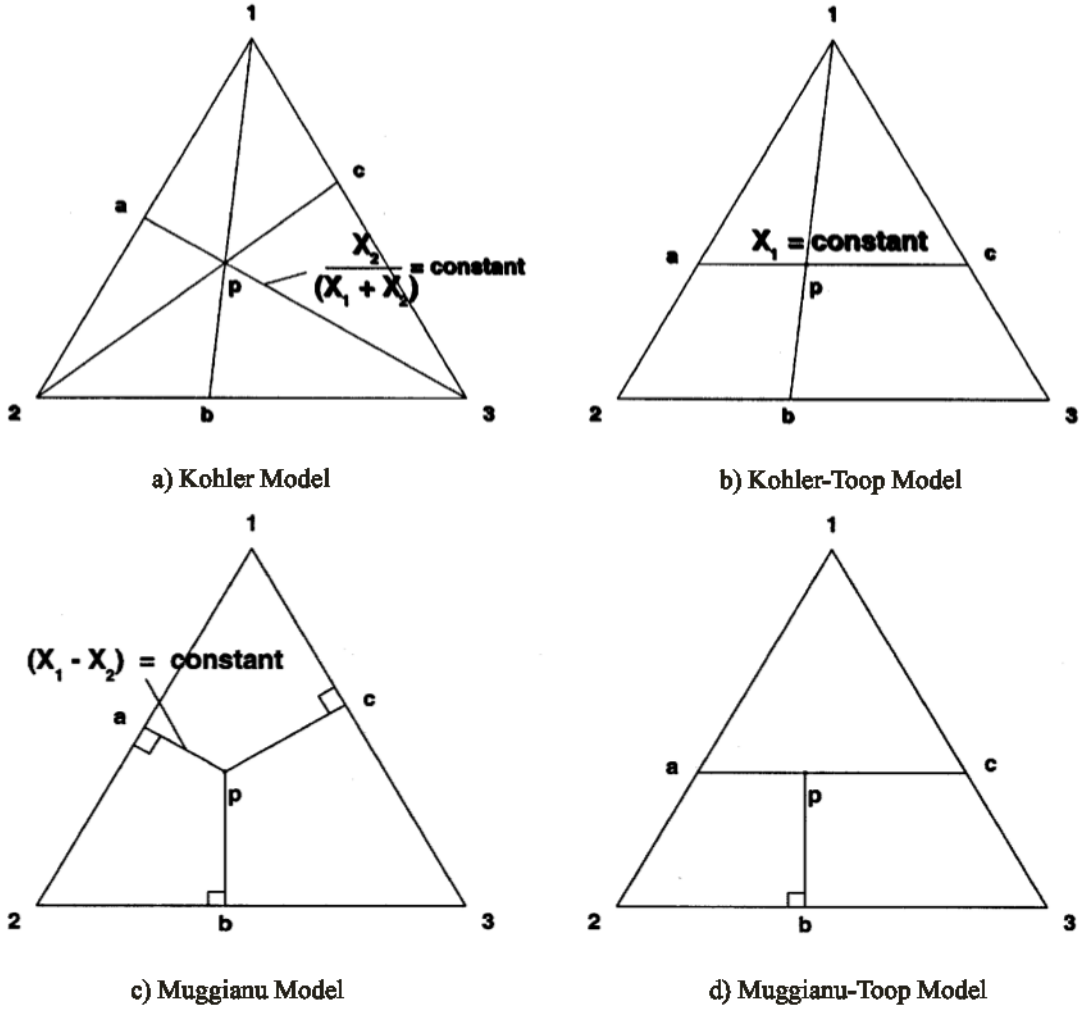

Figure 1.4: Different "geometric" models for ternary extrapolation from optimized binary data [22]

In this work, the thermodynamic model used for the solid solutions is the compound energy formalism or sublattice model [23] while the modified quasichemical model in the pair approximation [24] is used for the liquid solution. These thermodynamic models are already coded and implemented in the FactSage software [25], which can access the databases containing the model parameters. Details of the thermodynamic models are given in section 3 of chapters 2-4.

1.5 Research objectives and approach

A suitable material for on-board hydrogen storage applications is still missing despite the huge amount of work devoted to this issue during the last decade. The suitability of a system for hydrogen storage can be first assessed by the thermodynamic properties (the equilibrium temperatures and pressures of hydrogenation/dehydrogenation reactions) of the metal-hydrogen system. This system should reversibly absorb and release a certain amount of hydrogen at moderate temperature and pressure.

The CALPHAD method is being used to develop a thermodynamic database for the light metal hydrides, especially for magnesium alloys. The constructed database provides a tool to identify promising systems for hydrogen storage, to evaluate the reaction path (as function of temperature and pressure), and to understand the related processes.

The present work permits to evaluate the effect of adding alloying elements or mixing different hydrides on hydrogen release temperature. The maximum decrease in this temperature represents potential significant improvement in the hydrogen storage capacity of the system.

This strategy will enhance the chance of obtaining the most suitable alloys for hydrogen storage applications instead of the traditional empirical trial and error experimentation involving the production of numerous different alloy compositions. Not much research work tackling this issue could be found in the literature. Establishing a thermodynamic database for all the promising additives to Mg will definitely reduce the experimental work required to find the alloys with the best hydrogen storage capacity and thermodynamic properties.

This work will not provide any information about the kinetics of the reactions and catalysis processes. However, it will allow focusing the experimental work on the most promising compositions that have suitable equilibrium thermodynamic properties.

The work will focus on the Mg-Al-Li-Na-H system and will address the following specific objectives:

- Evaluation of all the available experimental and theoretical data on the system. Critical assessment of these data is essential for the thermodynamic modeling.
- Thermodynamic modeling of the binary systems in the Mg-Al-Li-Na-H system.

All the binary systems: Mg-Al, Mg-Li, Mg-Na, Mg-H, Al-Li, Al-Na, Al-H, Li-Na, Li-H, and Na-H are assessed or reassessed in this work to provide uniformity of the thermodynamic models used in this work.

- The constituent ternary systems: Mg-Al-Li, Mg-Al-Na, Mg-Al-H, Mg-Li-Na, Mg-Li-H, Mg-Na-H, Al-Li-Na, Al-Li-H, Al-Na-H, and Li-Na-H are extrapolated from the constituent binary systems. Experimental data are used when available.
- Combination of the thermodynamic description of the Mg-Al-Li-Na-H system in a self-consistent database.
- Using the constructed multicomponent database to predict the phase relations and various thermodynamic properties of any composition in the system. Hence, the database will be used to identify the most promising compositions in this system suitable for hydrogen storage application.
- Using computational thermodynamics to evaluate reaction path, to compare with the available experimental data, and to understand the related processes.

Chapter 2. Thermodynamic modeling of hydrogen storage capacity in Mg-Na alloys

Abstract

Thermodynamic modeling of the H-Mg-Na system is performed for the first time in this work in order to understand the phase relationships in this system. A new thermodynamic description of the stable $NaMgH_3$ hydride is performed and the thermodynamic models for the H-Mg, Mg-Na and H-Na systems are reassessed using the modified quasichemical model for the liquid phase. The thermodynamic properties of the ternary system are estimated from the models of the binary systems and the ternary compound using CALPHAD technique. The constructed database is successfully used to reproduce the pressure-composition isotherms for MgH_2 +10 wt.% NaH mixtures. Also, the pressure-temperature equilibrium diagram and reaction paths for the same composition are predicted at different temperatures and pressures. Even though it is proven that H-Mg-Na does not meet the DOE hydrogen storage requirements for on-board applications, the best working temperatures and pressures to benefit from its full catalytic role are given. Also, the present database can be used for thermodynamic assessments of higher order systems.

Key words: Magnesium hydrides, hydrogen storage, thermodynamic modeling, perovskite.

2.1 Introduction

Hydrogen stands as an ideal fuel for the future reducing the dependence on oil and the environmental problems arising from the use of fossil fuels. Hydrogen can be used for power generation through fuel cells. Hydrogen fuel cells have a wide range of potential applications ranging from micro-fuel cells that power portable electronics to mobile applications [26]. The transition to hydrogen energy is hindered by technical barriers related to storage problems. Solid state hydrogen storage materials, such as light-weight metal hydrides, complex and chemical hydrides have been widely investigated due to their small volume, low equilibrium pressure, safety advantages and high storage capacity [11, 13, 15, 27, 28].

Magnesium and its alloys stand as promising candidates for hydrogen storage. In fact, magnesium hydride MgH_2 contains 7.6 wt.% hydrogen [13], but it suffers from extremely slow hydriding kinetics. A temperature of about 300°C is required for a plateau pressure of 1 bar at thermodynamic equilibrium, which corresponds to an enthalpy of formation of -78 kJ/mol H_2 [13]. The investigations of magnesium hydrides found in the literature focus on decreasing desorption temperature, enhancing the kinetics and cycle life and lowering their reactivity with air and oxygen [29-31]. Mixing with other compounds and/or incorporating new elements have been shown to be effective strategies to tune the thermodynamic properties of MgH_2 [29, 32]. The literature shows that the search of new alloys, suitable for hydrogen storage, is somewhat a trial and error method, involving numerous experiments. Also, hydrogen is a flammable gas, which makes this search more difficult. The effort and time of experiments can be reduced significantly with the application of thermodynamic calculation. Hence, a self-consistent thermodynamic database of the H-Mg-Me system (Me is one metal or more) will be very useful for identifying the most promising hydrogen storage alloys and for studying the effect of adding minor elements or mixing hydrides on the storage capability.

In recent years, the Mg-based perovskite-type hydrides, especially $NaMgH_3$, have received considerable attention for hydrogen storage applications [33-39]. In addition, to its high gravimetric and volumetric hydrogen densities (6 wt.% and 88 kg/m^3), $NaMgH_3$ demonstrates reversible hydrogen storage properties [40]. The crystal structure of $NaMgH_3$ has been identified as orthorhombic *perovskite* with the space group of *Pnma* (*$GdFeO_3$*-type structure) [37]. Recently, it has been found that NaH hydride addition greatly improves the hydrogen storage properties of MgH_2 because of the formation of $NaMgH_3$ [41]. Fast hydrogen mobility in $NaMgH_3$ has been revealed by H atom nuclear magnetic resonance (HNMR) study and related to its *perovskite* structure [42]. Therefore, it is believed that, in a mixture of MgH_2 and $NaMgH_3$, hydrogen gas adsorption and dissociation are activated by $NaMgH_3$ grains, which offer fast diffusion pathway for hydrogen atoms into MgH_2 [38, 41]. Also, it has been found that $NaMgH_3$ forms during the destabilization reactions of many complex hydrides [43-49].

Consequently, accurate thermodynamic description of H-Mg-Na system is required as a building block of a larger database of H-Mg-Me. In the present work, thermodynamic modeling is used to provide a self-consistent database, which can be used to predict hydrogen storage properties of

the H-Mg-Na system for the whole composition range. The H-Mg-Na system is modeled using FactSage software [25].

2.2 Literature review

2.2.1 H-Mg system

No complete experimental phase diagram of the Mg-H system could be found in the literature. An extensive literature review of the H-Mg system has been presented by San-Martin and Manchester [50] and later by Zeng *et al*. [51]. But some of the experimental data [52, 53] were not cited by San-Martin and Manchester [50] and are added in this work. Experimental investigations on phase equilibria were performed by different researchers [50, 54-56]. Only one temperature-composition isobar profile at 1.013 bar was predicted by Shapovalov *et al*. [57]. The H-Mg system consists of hcp-Mg (the interstitial solid solution of H in Mg) and β-MgH_2 in addition to the liquid and gas phases. Two invariant equilibria have been confirmed by San-Martin and Manchester [50] in this system; L → hcp-(Mg) + gas and hcp-(Mg) + gas → MgH_2. According to Stampfer *et al*. [56], from the measured pressure-composition isotherms (PCI), the composition of β-MgH_2 after a complete hydriding reaction was $MgH_{1.99\pm0.01}$. In this work, this phase is treated as a stoichiometric compound. The equilibrium absorption/desorption pressure of the β-MgH_2 was investigated by different authors [58-63]. According to Krozer *et al*. [62], the equilibrium formation pressure of MgH_2 is very close to its decomposition pressure. Stampfer *et al*. [56] collected 129 data points in the measurement of the dissociation pressures of β-MgH_2 in the temperature range 587-849 K with uncertainties of 0.35 bar and 1 K. These results are used in this work because they are self-consistent and in excellent agreement with the results published by Ellinger *et al*. [64], Reilly *et al*. [65] and other groups [57, 66-68]. The enthalpy and entropy of formation of β-MgH_2 have been calculated from PCI measurements using Van't Hoff plot by many researchers [56, 64-69].

Wolf *et al*. [52] determined the standard entropy (S_0= 30.64±0.05 $JK^{-1}mol^{-1}$) and the specific heat capacity function: $c_p(T)=(2.8711+0.11061T+68611T^{-2})$ $JK^{-1}mol^{-1}$ within the range 298-373 K for MgH_2 using adiabatic low temperature calorimetry and differential scanning calorimetry (DSC). Bogdanovic *et al.* [53] determined the average desorption enthalpy at an average temperature of 683 K using calorimetric measurements. They used the results published by Wolf

et al. [52] to calculate the enthalpy and entropy of formation of MgH_2. These results [52, 53] are used as first approximation in the present work together with the previously reported PCIs results.

Hydrogen solubility in magnesium has been investigated several times [55, 57, 63, 70-74]. Stampfer *et al.* [56] calculated the equilibrium hydrogen solubility in solid magnesium, hcp-(Mg), at five different temperatures from the PCI measurement assuming that the decomposition of MgH_2 was complete at the end of the isotherm. A modified Sieverts apparatus was used by Koeneman *et al.* [63] to determine the solubility of hydrogen in magnesium between 328 and 1048 K. The results of Koeneman *et al.* [63] are in good agreement with those published later by Huang *et al.* [71] and Shapovalov *et al.* [55, 57]. Popovic *et al.* [74] measured the solubility of hydrogen in solid magnesium. But their [74] values are lower than those reported earlier [33, 35, 41, 49] and are not considered in the present work. The data obtained by Shapovalov *et al*. [57] using the conventional methods for high temperatures are also lower because of the possible losses of hydrogen.

Thermodynamic modeling of the H-Mg system was conducted by Zeng *et al*. [51]. But the hydrogen solubility in the molten magnesium was neglected in their [51] work and the liquid phase was treated as an ideal solution. Recently, Harvey and Chartrand [75] modeled the hydrogen solubility in liquid magnesium using the modified quasichemical model taking into account the solubility of hydrogen in the liquid magnesium. Their optimized thermodynamic parameters for the liquid phase are used in the present work and thus, the other phases are remodelled to be consistent with the new liquid and to take into account the new experimental data of Wolf et al. [52] and Bogdanovic *et al.* [53].

2.2.2 H-Na system

The H-Na system was reviewed by San-Martin and Manchester [76]. Based on some of the earlier studies [77-79], they [76] predicted that at atmospheric pressure the maximum solubility of H in solid Na should be less than 8×10^{-5} at.%. Since no experimental measurement of the solubility could be found in the literature, their [76] prediction will be used during optimization in the present work. The solubility of H in liquid Na was measured by several researchers [80-85] in the mid 1900's in the temperature range 373 to 723 K at the atmospheric pressure. All these measurements showed a consistent trend of increased H solubility in liquid Na with

increasing temperature. These results will be compared with the present thermodynamic modeling.

The H-Na system has one stable compound, NaH. The melting point of NaH was determined by thermal analysis by Sukuratov *et al.* [86] as 911±2 K at 107.3 bar and 911±2 K at 207.3 bar. Another measurement by Kiostermeier and Franck [87] showed the melting point of NaH to be 905±2 K at 106 bar which is in accord with Sukuratov *et al.* [86]. The kinetic studies on the rate of reaction and thermal decomposition of NaH were carried out by [88, 89]. Prochazka and Nedved [88] studied the effect of CO on H during the reaction and suggested the CO acts as a precursor. Gwyther and Whittingham [89] measured the rate of H removal from Na+NaH mixtures by continuous evacuation and purging by argon in the temperature range of 533-693 K. They also reported the rate of H desorption from unsaturated solutions of NaH in liquid Na at ≤673 K.

Crystallographic study of the Na-H system was performed by several researchers [90-93] using X-ray diffraction. NaH has an fcc crystal structure ($Fm\bar{3}m$) with a prototype of NaCl. The XRD measurement by Kuznetsov and Shkrabkina [93] at different temperatures did not show any phase transformation of NaH up to the decomposition temperature. They [93] also observed that the lattice parameter of NaH increases linearly from a = 0.4872 nm at room temperature to 0.5000 nm at 673 K. Later San-Martin and Manchester [76] reported the following equation to fit the data of Kuznetsov and Shkrabkina [93]:

$$a = 0.487017 + 0.32X10^{-4}T \ (293 < T < 683\ K)$$

Qiu *et al*. [94] also calculated the lattice parameter of NaH as 0.4857 nm using first principle which is close to the reported values by [93].

The enthalpy of formation of NaH was determined by several groups using two different techniques: calorimetric methods [95-98] and dissociation pressure data [78, 86, 99]. In the calorimetric methods the enthalpy values are measured from the difference between the heat of reaction of NaH and that of Na, with water [76] as it is the most common medium due to the well-known c_p. For the second method, the dissociation pressures of hydrides are measured usually over a temperature range. Using these data, the enthalpy of formation at the atmospheric pressure is determined from the slope of the van't Hoff plot (*log P vs 1/T*) [76]. The enthalpy of

formation of NaH that was reported by various groups [78, 96, 97, 99] is fairly in agreement with each other and will be compared with the present calculation. The heat capacity of NaH was measured by Sayre and Beaver [100] in the temperature range 60 to 90 K using an adiabatic calorimeter. Their [100] reported c_p values will be compared with the present calculation.

A partial phase diagram of the Na-H system was presented by Predel [101]. Later Qiu *et al.* [94] assessed the H-Na system combining experimental data from the literature and first principle calculation based on density functional theory to supplement the thermodynamic properties of this system. Qiu *et al*. [94] modeled the Na-H liquid with the random solution model and bcc phase with the sub-lattice model. Heat capacity in the temperature range from 0 to 2000 K was calculated by first principle calculations. They [94] also presented the heat of formation of NaH, decomposition pressure and hydrogen solubility in liquid Na.

2.2.3 Mg-Na system

The experimental work and thermodynamic modeling of the Mg-Na system was carried out by several groups [102-106]. The main feature of Mg-Na system is the large immiscibility in the liquid phase. No experimental data regarding the critical temperature as well as the shape of the immiscibility gap could be found in the literature. The solubility of Na in solid Mg as well as Mg in solid Na is negligible. Pelton [105] estimated ~0.5 at.% Na solubility in Mg by assuming Henrian behavior of the solution and employing Van't Hoff equation to back calculate the solubility. This is rather small solubility and since there is no experimental evidence, no solubility of Na in Mg is considered in the present work.

Mathewson [102] employed thermal analysis and determined the composition and temperature of the monotectic (liquid1 → liquid2 + hcp-(Mg)) reaction to be 2 at.% Na and 911 K. He [102] reported the composition of liquid2 to be ~98.6 at.% Na at 911 K. Klemm and Kunze [104] reported Mg-Na phase diagram with the monotectic temperature of 910 K. Although they [104] mentioned this as a peritectic reaction instead of monotectic, the temperature of the thermal event agreed well with the results of Mathewson [102]. Pelton [105] extracted the composition of the monotectic liquid2 from Klemm and Kunze's [104] reported phase diagram as ~92.7 at.% Na and used this value in his assessment. The composition (~98.6 at.% Na) reported by Mathewson [102] could be associated with higher error due to the use of a glass container which usually reacts with Mg-Na liquid [105]. Hence during optimization the composition of liquuid 2 reported

by Klemm and Kunze [104] will be used since they used iron crucibles. Lantratov [103] reported the temperature dependent solubility of Na in liquid Mg. The solubility of Na increases from 2.1 at.% at 911 K to 2.7 ± 0.1 at.% Na at 973 K.

Lantratov [103] measured the activities of Na and Mg in the liquid along the complete composition range by EMF method at 973 K which exhibited strong positive deviation from ideality due to the limited solubility. In a recent study, Zhang *et al.* [106] presented a thermodynamic model of the Mg-Na system as the constituent binary of the Al-Mg-Na ternary system. They [85] employed the random solution model for the liquid phase and calculated the Mg-Na phase diagram and the activities of Mg and Na in the liquid.

2.2.4 H-Mg-Na system

Only one ternary compound, $NaMgH_3$, has been reported in the H-Mg-Na system. The standard enthalpy of formation of $NaMgH_3$ was determined by Bouamrane *et al.* [35] as - 231 ± 4 kJ/mol, by calorimetry using its reaction with diluted hydrochloric acid (0.5 M HCl). The hydrogen desorption and absorption properties of $NaMgH_3$ have been investigated for the first time by Ikeda *et al.* [40] using XRD, thermogravimetry, differential thermal analysis and hydrogen pressure composition PCI measurements. They [40, 107] reported that 5.8 ± 0.2 wt.% hydrogen has been released from the sample during two endothermic reactions. Hydrogen was desorbed after only 8 min at 673 K and $NaMgH_3$ formed under 10 bar of hydrogen at 673 K [40]. Only one PC isotherm at 673 K was reported [40] showing two plateau pressures of 1.5 and 0.4 bar confirming that $NaMgH_3$ decomposes in two-steps according to the following reactions [40]:

$$NaMgH_3 \rightarrow NaH + Mg + H_2 \qquad 4\ wt.\%\ H_2 \qquad (2.1)$$

$$NaH \rightarrow Na\ (l) + 1/2\ H_2 \qquad 2\ wt.\%\ H_2 \qquad (2.2)$$

The enthalpy change of reaction (2.1) was calculated by Ikeda *et al.* [40], using Van't Hoff plot; $\Delta H(298\ K) = 88\ kJ/molH_2$. Using this value and the reported standard heat of formation of NaH, - 114.1 $kJ/molH_2$ [108], as enthalpy change for reaction (2.2), the standard enthalpy of formation of $NaMgH_3$ was estimated to be - 96.7 kJ/mol H_2 [40] or -145 kJ/mol. PCIs of $NaMgH_3$ during decomposition were reported by Komya *et al.* [39] at 673, 698 and 723 K. For the isotherm measured at 673K, the plateau pressures were around 1 and 0.4 bar for reactions (2.1) and (2.2),

respectively. The enthalpy and the entropy changes of these reactions have been calculated using the Van't Hoff plot. By calculating the sum of the enthalpy changes of reaction (2.1) and (2.2), the standard enthalpy of formation of $NaMgH_3$ was wrongly estimated by these authors to be -210±17 kJ/mol H_2 [39]; they did not pay attention to the units used (kJ/molH_2). Hence, heat of formation of this compound will be recalculated in the present work using their [39] enthalpy values for reactions (2.1) and (2.2). PCIs of $NaMgH_3$ during decomposition were reported by Ikeda *et al.* [37] at 653, 673 and 693 K. Pottmaier *et al.* [49] investigated the thermodynamic properties of $NaMgH_3$ using high pressure DSC, PCI measurements and density functional theory calculations (DFT). Enthalpy and entropy of reaction (2.1) were calculated from PCI measurements at 650, 670, 680, 700 and 723 K [49]. Pottmaier *et al.* [49] used their results together with the experimental and calculated values from the literature to estimate the thermodynamic properties of $NaMgH_3$ using the CALPHAD approach. It should be pointed out that, for the PCIs published by Ikeda *et al.* [37], Komya *et al*. [39] and Pottmaier *et al.* [49], the plateaus were slopped and very limited data points were collected within them. In addition to that, the quality of the data given by Pottmaier *et al.* [49] is poor especially at 650 and 670 K; the plateaus are not flat with large pressure variations. A slow kinetics, an insufficient time for each equilibrium measurement or an insufficient pressure resolution might be the causes of these problems and might have led to erroneous enthalpy and entropy determination from Van't Hoff plot. Later on, Sheppard *et al.* [109] investigated the kinetic and thermodynamic data of $NaMgH_3$ decomposition. PCIs showing the first reaction decomposition at 671.4, 683.8, 691.9, 702.8 and 712.9 K were reported. All the above-mentioned problems have been avoided by Sheppard *et al*. [109] by waiting longer (more than 2 h) to reach true thermodynamic equilibrium for each sorption step. The plateau curves were wide and flat with negligible hysteresis. For all these reasons the experimental data reported by Sheppard *et al*. [109] are used in the present optimization of the H-Mg-Na system. The thermodynamic properties of $NaMgH_3$ obtained from PCIs and DSC by different authors are summarized in Table 2.5. Since there is no information regarding the homogeneity range of $NaMgH_3$ in the literature, this compound is treated as stoichiometric in this work. Thermodynamic modeling of the H-Mg-Na system for the whole composition range is conducted for the first time in the present study.

2.3 Thermodynamic modeling

2.3.1 Pure elements

The Gibbs energy functions of the pure elements (Mg, Na) are taken from the SGTE (Scientific Group Thermo data Europe) compilation of Dinsdale [110]. These data are taken in reference to the Stable Element Reference (SER) at 298.15 K and 1 bar. Liquid monoatomic hydrogen is not stable under normal conditions; its Gibbs energy has been estimated by Harvey *et al.* [56] and is reported in Table 2.1. The c_p values of the gases included in this study, i.e. H_2, H, Mg, Mg_2, MgH, Na, Na_2 and NaH, are taken from NIST-JANAF thermochemical tables [111] compiled by FactPS database [25].

2.3.2 Stoichiometric compounds

The Gibbs energy of a binary stoichiometric phase is given by:

$$G^{\phi} = x_i {}^0G_i^{\phi_1} + x_j {}^0G_j^{\phi_2} + \Delta G_f \qquad (2.4)$$

Where x_i and x_j are mole fractions of the components *i* and *j* of the compound denoted by *f*. ${}^0G_i^{\phi_1}$ and ${}^0G_j^{\phi_2}$ are the Gibbs energy of components *i* and *j* in their standard state. $\Delta G_f = a + b\,T$ is the Gibbs energy of formation per mole of atoms of the stoichiometric compound. The parameters *a* and *b* are obtained by optimization. The stoichiometric compounds in the H-Mg-Na system are: MgH_2, NaH and $NaMgH_3$.

2.3.3 Liquid phase

Modified quasichemical model is used to describe the liquid phase for all the binaries. This model uses the energy of pair formation to define the excess Gibbs energy. According to [112], the excess energy is expressed as:

$$\Delta g_{AB} = \Delta g^{o}_{AB} + \sum_{i\geq 1} g^{i0}_{AB} X^{i}_{AA} + \sum_{j\geq 1} g^{0j}_{AB} X^{j}_{BB} \qquad (2.5)$$

Where Δg^{o}_{AB}, Δg^{i0}_{AB} and Δg^{0j}_{AB} are the parameters of the model and are expressed as functions of temperature ($\Delta g^{o}_{AB} = a + bT$). The short range ordering in the liquid is expressed by the atom to atom coordination number 'Z' and is given by:

$$\frac{1}{Z_A} = \frac{1}{Z^A_{AA}}\left(\frac{2n_{AA}}{2n_{AA}+n_{AB}}\right) + \frac{1}{Z^A_{AB}}\left(\frac{n_{AB}}{2n_{AA}+n_{AB}}\right) \qquad (2.6)$$

$$\frac{1}{Z_B} = \frac{1}{Z_{BB}^B}\left(\frac{2n_{BB}}{2n_{BB}+n_{AB}}\right) + \frac{1}{Z_{BA}^B}\left(\frac{n_{AB}}{2n_{BB}+n_{AB}}\right) \qquad (2.7)$$

Z_{AA}^A and Z_{AB}^A are the values of Z_A when all nearest neighbours of an A atom are A's, and when all nearest neighbours of A atom are B's, respectively. The same applies to Z_{BB}^B and Z_{BA}^B. All binary liquid thermodynamic parameters have been interpolated using the asymmetric Kohler-Toop technique [112]. According to Qiao *et al.* [113], H is singled out as the asymmetric component since Mg-Na system shows significantly different thermodynamic characteristics than both Mg-H and Na-H. In the current work, no ternary parameters are added to the liquid model.

2.3.4 Gas phase

In the pressure range of interest, the non-ideal contribution of pressure to the Gibbs energy for the gases is very small. Therefore, the gases included in this work are taken as ideal gases. The gas phase is described by the ideal solution model as:

$$G = x_i\ G_i^{\phi} + x_j\ G_j^{\phi} + RT[x_i \ln x_i + x_j \ln x_j] \qquad (2.8)$$

where *i* and *j* are the gas constituents; $G_i^{\phi} = {}^0G_i^{\phi} + RTLnP$ and *P* is the pressure.

2.3.5 Solid solution phases

Hydrogen atoms occupy interstitial positions in the solid magnesium; hcp-Mg; and sodium; bcc-Na. These phases are described by a two sublattice model where the first sublattice is occupied by the metal atoms and the second one by hydrogen atoms and vacancies; $(M)_a(H, Va)_c$. The Gibbs energy is described by the equations:

$$G = G^{ref} + G^{ideal} + G^{excess} \qquad (2.9)$$

$$G^{ref} = \sum y_i^l y_j^m \ldots y_k^q\ {}^0G_{(i:j:\ldots:k)} \qquad (2.10)$$

$$G^{ideal} = RT\sum_l f_l \sum_i y_i^l \ln y_i^l \qquad (2.11)$$

$$G^{excess} = \sum y_i^l y_j^l y_k^m \sum_{\gamma=0}{}^{\gamma}L_{(i,j):k} \times (y_i^l - y_j^l)^{\gamma} \qquad (2.12)$$

where *i, j, ... k* are components or vacancy, *l, m* and *q* represent sublattices. y_i^l is the site fraction of component *i* on sublattice *l*. f_l is the fraction of sublattice *l* relative to the total lattice sites. ${}^0G_{(i:j:..k)}$ represents a real or a hypothetical compound energy. ${}^{\gamma}L_{(i,j)}$ represent the interaction

parameters which describe the interaction within the sublattice. According to Frisk [114] the number of sites on each sublattice $(M)_a(H, Va)_c$ is *a=2* and *c=1* for the hcp-(Mg) phase and *a=1* and *c=3* for bcc-(Na) phase. To allow for the solubility of Na in hcp-(Mg) and Mg in bcc-(Na), Mg and Na are allowed to mix randomly in the first sublattice. Therefore, the hcp-(Mg) phase and bcc-(Na) in the ternary system are described by the two sublattices $(Mg,Na)_2(H,Va)_1$ and $(Na,Mg)_1(H,Va)_3$, respectively.

2.4 Results and discussion

The thermodynamic parameters optimized in the present work for the H-Mg-Na system are given in Table 2.1.

Table 2.1*: Optimized model parameters for the different phases in the H-Mg-Na system (J/mole)*

Phase	Model	Parameters	
Liquid	MQM	$g^0_{H(l)} = 74{,}266.7 - 26.2456T + 20.7856T\ln T$	[75]
		$Z^{Mg}_{MgH} = Z^{H}_{MgH} = 6, \Delta g^{o}_{MgH} = -18{,}049.78$	[75]
		$Z^{Na}_{NaH} = Z^{H}_{NaH} = 6, \Delta g^{0}_{NaH} = -39{,}245.92 + 8.45T$	
		$\Delta g^{10}_{NaH} = 12{,}133.6 - 0.711T$	This work
		$\Delta g^{01}_{NaH} = -66{,}944 + 8.368T$	
		$Z^{Mg}_{MgNa} = 4.5, Z^{Na}_{MgNa} = 6, \Delta g^{o}_{MgNa} = 7{,}660.0 + 2.9T$	This work
hcp-(Mg)	Sublattice $(Mg,Na)_2(H,Va)_1$	${}^0G^{Mg_2H}_{Mg:H} = 173{,}217.6 - 242.672T + 2G(Mg_{cph}) + 1/2G(H_2, gas)$	
		${}^0G^{Na_2H}_{Na:H} = 2G(Na_{cph}) + 1/2G(H_2, gas)$	
		${}^0G^{Mg_2}_{Mg:Va} = 2G(Mg_{cph})$	This work
		${}^0G^{Na_2}_{Na:Va} = 2G(Na_{cph})$	
		${}^0L^{cph}_{Mg,Na:Va} = 79{,}496 + 16.736T$	
bcc-(Na)	Sublattice $(Na,Mg)_1(H,Va)_3$	${}^0G^{NaH_3}_{Na:H} = G(Na_{bcc}) + 3/2G(H_2, gas)$	
		${}^0G^{MgH_3}_{Na:H} = G(Mg_{bcc}) + 3/2G(H_2, gas)$	
		${}^0G^{Na}_{Na:Va} = G(Na_{bcc}); {}^0G^{Mg}_{Mg:Va} = G(Mg_{bcc})$	This work
		${}^0L^{bcc}_{Na::H,Va} = -5{,}569.8; {}^1L^{bcc}_{Na::H,Va} = -2{,}092.9$	
		${}^0L^{bcc}_{Na,Mg:Va} = 30{,}000$	
MgH_2	Stoichiometric	${}^{Solid}G^0_{MgH_2} = -82{,}842.15 + 25.42T - 2.87T\ln T - 55.30\times10^{-3}T^2 - 34{,}305.5T^{-1}$	This work
NaH	Stoichiometric	${}^{Solid}G^0_{NaH} = -75{,}767.99 + 293.72T - 48.69T\ln T - 0.26\times10^{-3}T^2 + 1.80\times10^{-8}T^3 + 632{,}658.0T^{-1}$	This work
$NaMgH_3$	Stoichiometric	${}^{Solid}G_{NaMgH_3} = -157{,}905.82 + 185.83T - 33.6T\ln T - 61.27\times10^{-3}T^2$	This work

2.4.1 H-Mg system

The optimized thermodynamic parameters obtained by Harvey and Chartrand [75] using the MQM for the liquid phase are used in the present work. The hcp-(Mg) is modeled using $(Mg)_2(H, Va)_1$ two sub-lattice model [114] as discussed in section 3.5. No excess terms have been employed to represent hcp-(Mg). MgH_2 is considered as a stoichiometric compound. The gas species H, H_2, Mg, Mg_2 and MgH are treated as ideal gases. All the parameters for this system are listed in Table 2.1.

The calculated enthalpy and entropy of formation of magnesium hydride MgH_2 are given in Table 2.2 together with experimental data from the literature. Very good consistency can be seen between the calculated values and the experimental data [52, 55, 58, 63-66, 68, 116] except for some deviation from the results published by Selvam *et al.* [59], Ellinger *et al.* [64] and Pederson *et al.* [69]. Considering the consistency among the other six works, this deviation can be related to the quality of the PCIs and the slow kinetics, which can lead to erroneous values of the equilibrium pressures.

***Table 2.2**: Enthalpy and entropy of formation of MgH_2*

ΔH ($kJ/molH_2$)	ΔS ($J/molH_2.K$)	Temperature range (K)	Reference
-77.3	-136.9	298	This work
-77.4 ± 4	-138 ± 3	549-623	[65]
-74.4	-135	587-849	[56]
-70	-126	573-673	[69]
-78.2	_	573-616	[68]
-78.31	-140.07	513-633	[67]
-79	_	575-629	[66]
-66.9	_	450	[64]
-70.7	-119	590	[59]
-76.2	_	574	[115]
-74.05±1.3	_	683	[53]

The calculated Mg-rich part of the Mg-H phase diagram at 1bar is presented in Figure 2.1(a) compared with experimental hydrogen solubility data in solid magnesium. The entire phase diagram at 1bar is shown in Figure 2.1(b).

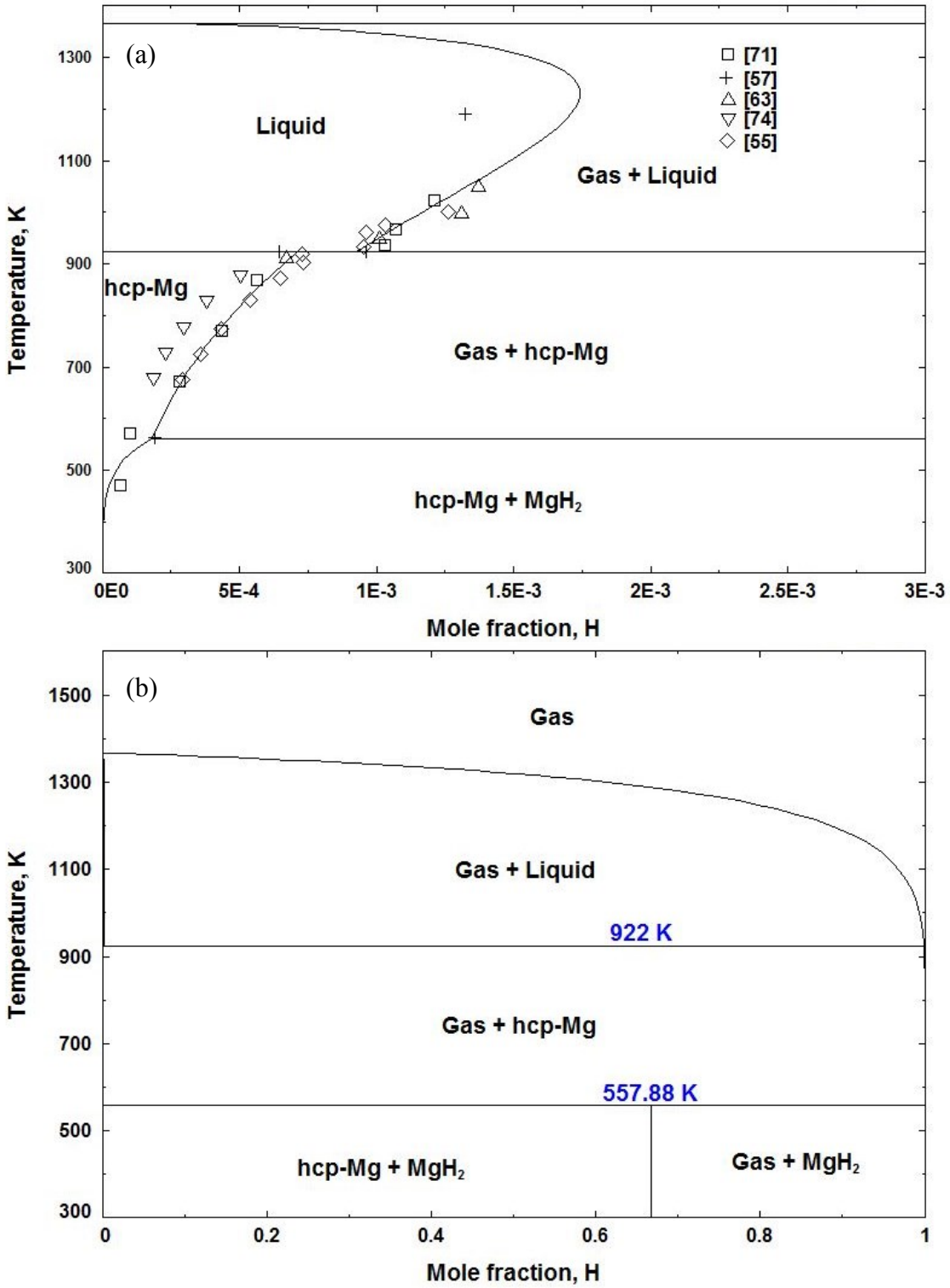

Figure 2.1 Calculated Mg-rich part of Mg-H phase diagram at 1 bar compared with experimental hydrogen solubilities in solid magnesium data from literature (a) and the calculated Mg-H phase diagram over the entire temperature range (b) at 1 bar.

It can be seen in Figure 2.1(a) that there is a good agreement between the calculated phase diagram at 1 bar and the selected experimental data except for the results of Popovic *et al*. [74] who differed from otherwise consistent results of [54, 56, 62, 70]. According to the present calculations, the eutectic type reaction L → hcp-(Mg) + gas occurs at 0.0923 at.% hydrogen and 922 K which agrees well with that calculated by Zeng *et al*. (0.093 at.% H and 922.8 K) [51]. There is no measured decomposition temperature for MgH_2 at the atmospheric pressure. However, the present work predicts that MgH_2 decomposes to hcp-(Mg) and H_2 at 557.88 K, this value is about 3 K lower than that predicted by Zeng *et al*. [51].

The calculated dissociation pressure of MgH_2 as function of temperature is presented in Figure 2.2(a), which shows good agreement with the experimental data from the literature. The present results show that the thermodynamic functions used in this work describe the H-Mg system in a broader pressure range more accurately than those reported by Zeng *et al.* [51]. In fact, Zeng *et al*. [51] unlike the current work did not achieve agreement with the experimental results above 150 bar. They blamed this inconsistency on the experimental data. The pressure-temperature diagram of MgH_2 is presented in Figure 2.2(b) to show the stability of the different phases. It is predicted that MgH_2 decomposes directly to liquid and gas above 919.5 K and 618.8 bar.

In order to compare with the experimental data of [56, 64], the H-Mg phase diagrams at 30.48 bar and 236 bar are also calculated in the present work as shown in Figure 2.3(a) and 2.3(b), respectively.

The dissociation temperature of MgH_2 is predicted to be 700 K at 30.48 bar and 832 K at 236 bar which agrees very well with the values reported by Stampfer *et al*. [56] (700 K at 30.48 bar) and by Ellinger *et al*. [64] (834 K at 236 bar). It can be seen in Figure 2.3 that the temperature of the reaction L → hcp-Mg + gas does not change a lot with pressure.

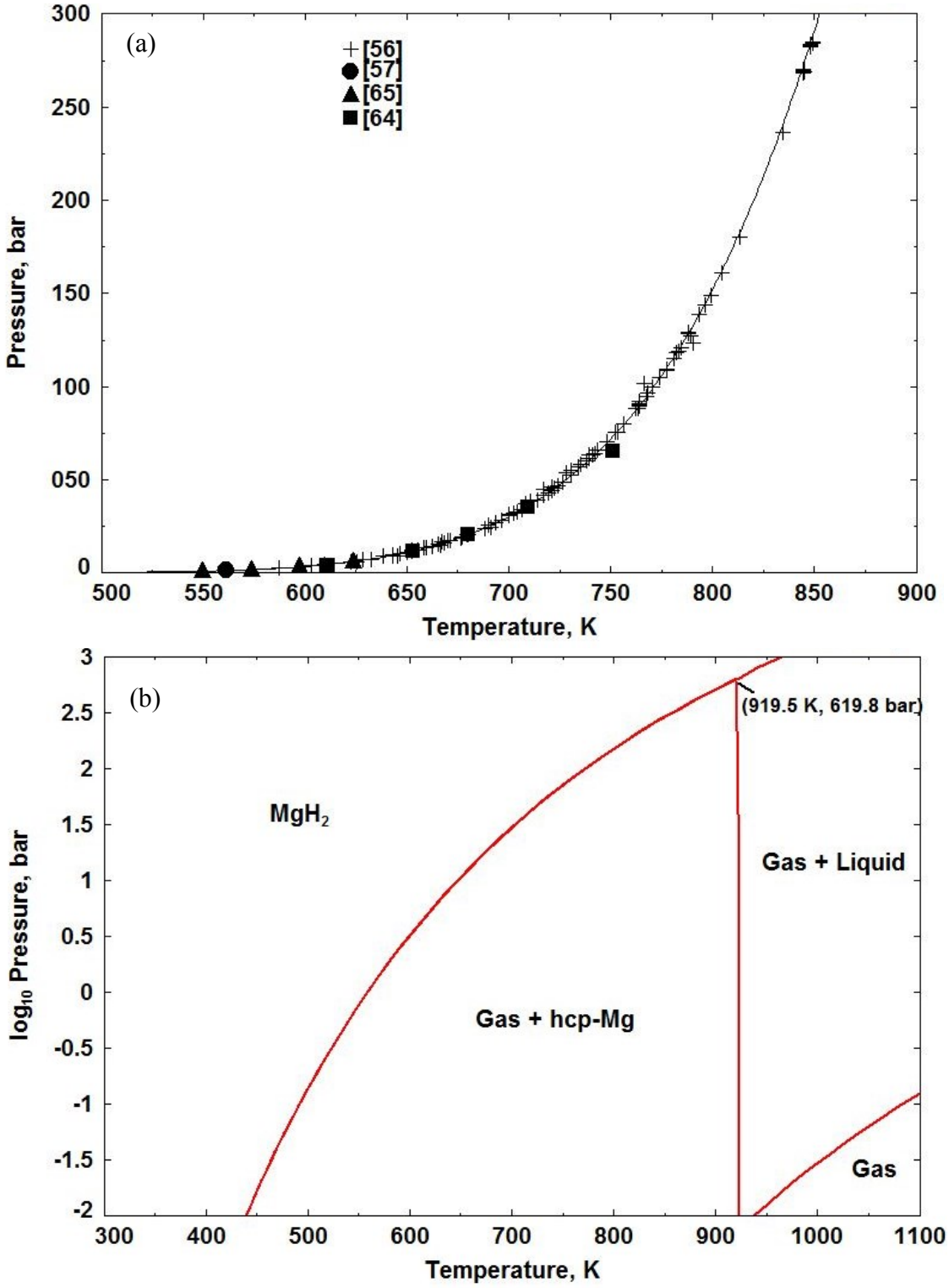

Figure 2.2 a) The dissociation pressure of MgH_2 calculated in this work compared to experimental data, b) Predicted pressure-temperature diagram of MgH_2

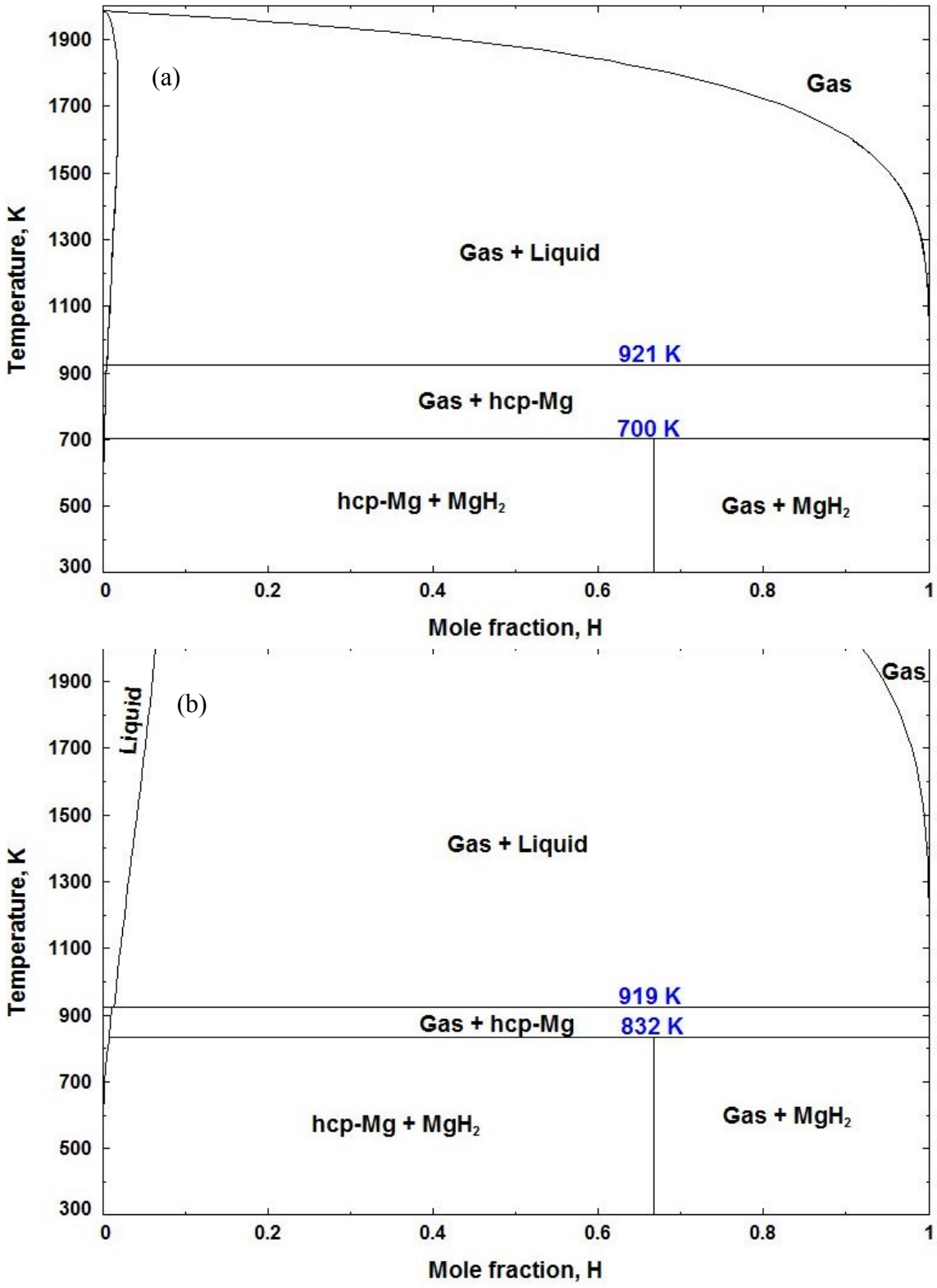

Figure 2.3 Calculated Mg-H phase diagram at: a) 30.48 bar, b) 236 bar

2.4.2 H-Na system

The liquid phase of the H-Na system is modeled using the modified quasi-chemical model. The solution has been considered random with no preferential short range ordering. The parameters of the model are determined considering the experimental data of H solubility in liquid Na. The bcc-(Na) is modeled using the compound energy formalism employing $(Na)_1(H, Va)_3$ two sub-lattice model [114] as mentioned in section 3.5. This model has been adopted from Qiu *et al*. [94]. Two excess terms are used to describe this phase. NaH is considered as a stoichiometric compound. The 'c_p' ranges ($0 < T < 298.15$ K and $298.15 < T < 2000$ K) of solid NaH have been optimized in this work to comply with the experimental data of the phase diagram as well as the thermodynamic properties. The gas species H, H_2, Na, Na_2 and NaH are treated as ideal gases. All the parameters for this system are listed in Table 2.1.

The calculated phase diagram of H-Na system at 1 bar is presented in Figure 2.4. There is only one intermediate compound NaH in the system, which decomposes at 700 K to liquid and gas. The H solubility in liquid Na has been found ~0.23 at.% at 700 K which is in good agreement with the proposed solubility limit of ~0.2 at.% by San-Martin and Manchester [76].

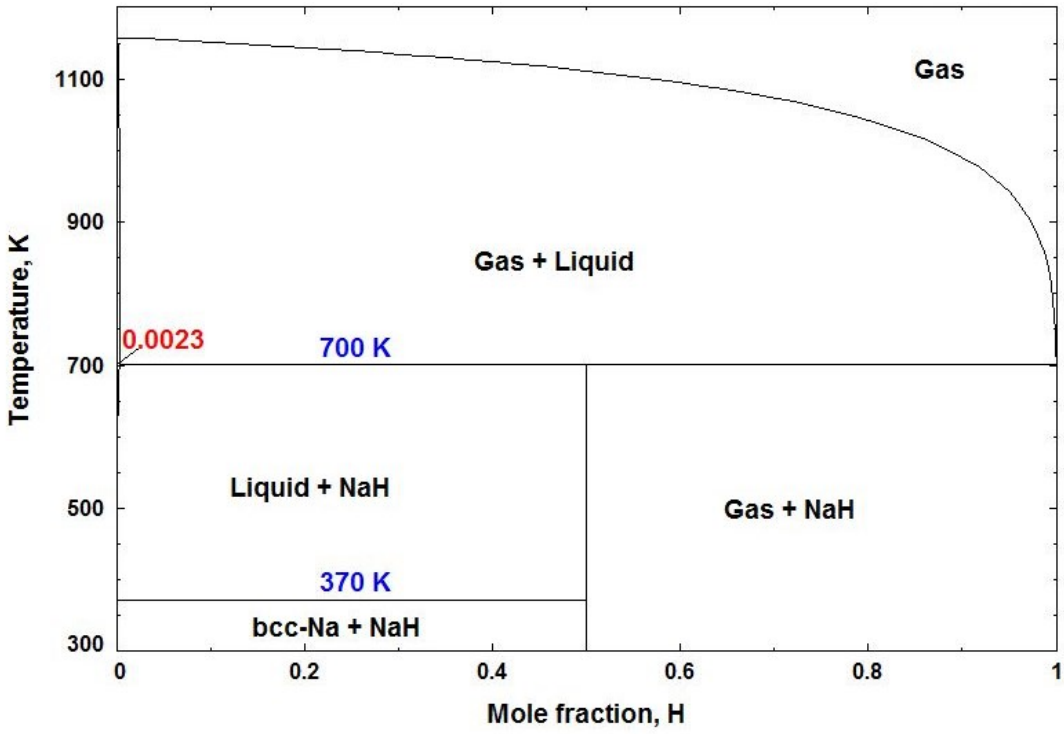

Figure 2.4 Calculated H-Na phase diagram at 1 bar

In order to visualize the impact of pressure on the H solubility in liquid Na, the Na-H phase diagram has been calculated at 150 bar and 200 bar as shown in Figures 2.5 (a) and (b). It can be seen that the solubility increases from ~0.23 at.% (700 K) to ~4.0 at.% (983 K) from the ambient pressure to the 200 bar. The melting temperature of NaH is 911 K and 905 K at 200 and 115 bar respectively in the present work. This is in agreement with the measured value of 911±2 K at 207.3 bar by Sukuratov *et al.* [86] and 905±2 K at 106 bar by Klostermeier and Franck [87]. The critical temperature (T_c) for the immiscibility in the liquid is 1569 K in the present calculation as shown by the dotted line in Figures 2.5(b) which agrees with the 1500±70 K estimated by Klostermeier and Franck [87].

Several measurements [80-85] on the H solubility in liquid Na were found in the literature. The solubility values are very small. Hence to compare the experimental data with the present calculation a phase diagram of *Temperature vs log H/Na* is plotted in Figure 2.6. This diagram shows the Na-rich side of the phase diagram from 371 to 900 K. The solubility values are in general agreement with those from the literature. The cutoff point of the calculation in FactSage program is 1×10^{-5}. Therefore dotted lines have been used in the Figure to extend parting lines of the phases. Some of the experimental solubility data [80, 81, 83] do not agree well with the present calculation. However, San-Martin and Manchester [76] noted that these measurements suffered from contamination due to the reaction of Na with glass walls. Therefore, during optimization only the other experimental data reported by Meacham *et al.* [84] and Vissers *et al.* [85] were given higher weight in the present work.

The chemical potential diagram for the H-Na system calculated in the present study is shown in Figure 2.7. The diagram shows reasonable agreement with the experimental data from the literature [78, 79, 86, 87]. It can be seen from this diagram that with increasing pressure, the dissociation temperature of NaH increases until ~114 bar (at 911 K) where melting of this compound occurs. After this point the slope of the curve decreases as no more NaH can dissolve in the liquid. This indicates the immiscibility of the two liquids. Similar observations were also reported by Qiu *et al.* [94] .

The enthalpy of formation of the solid NaH has been determined as: -56.98 kJ/mol, which is consistent with the available experimental data as can be seen in Table 2.3.

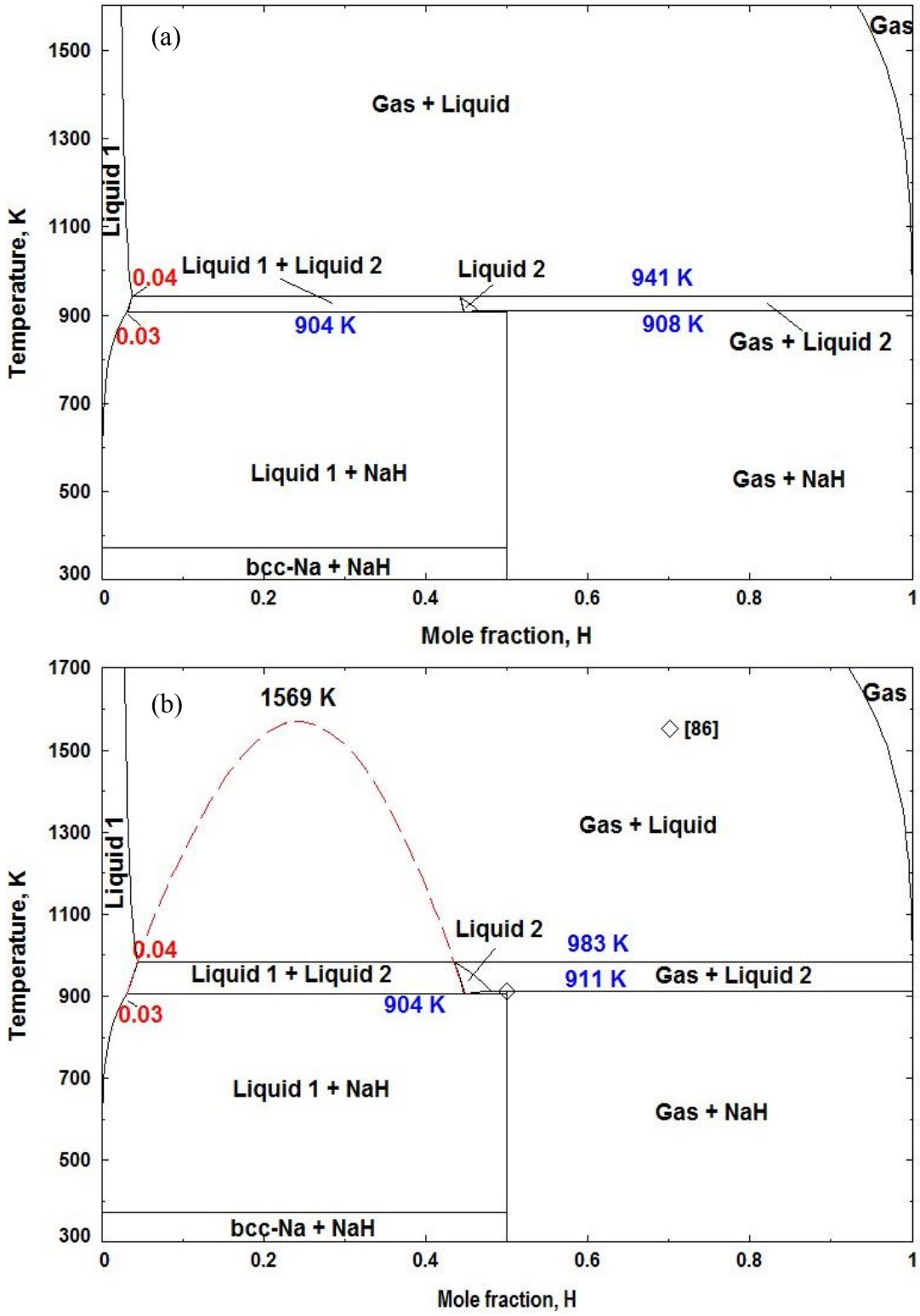

Figure 2.5 The Na-H phase diagram calculated at: (a) 150 bar and (b) 200 bar showing the metastable immiscibility gap

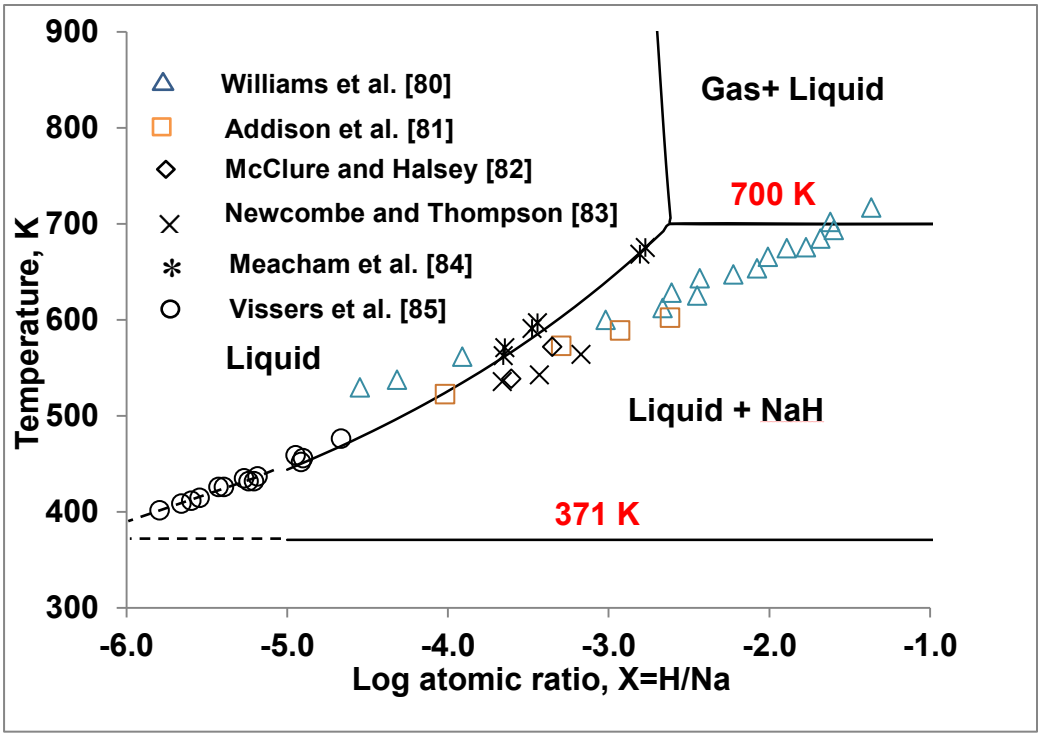

Figure 2.6 Calculated hydrogen solubility in the liquid Na system at 1 bar pressure in comparison to the experimental data in the literature

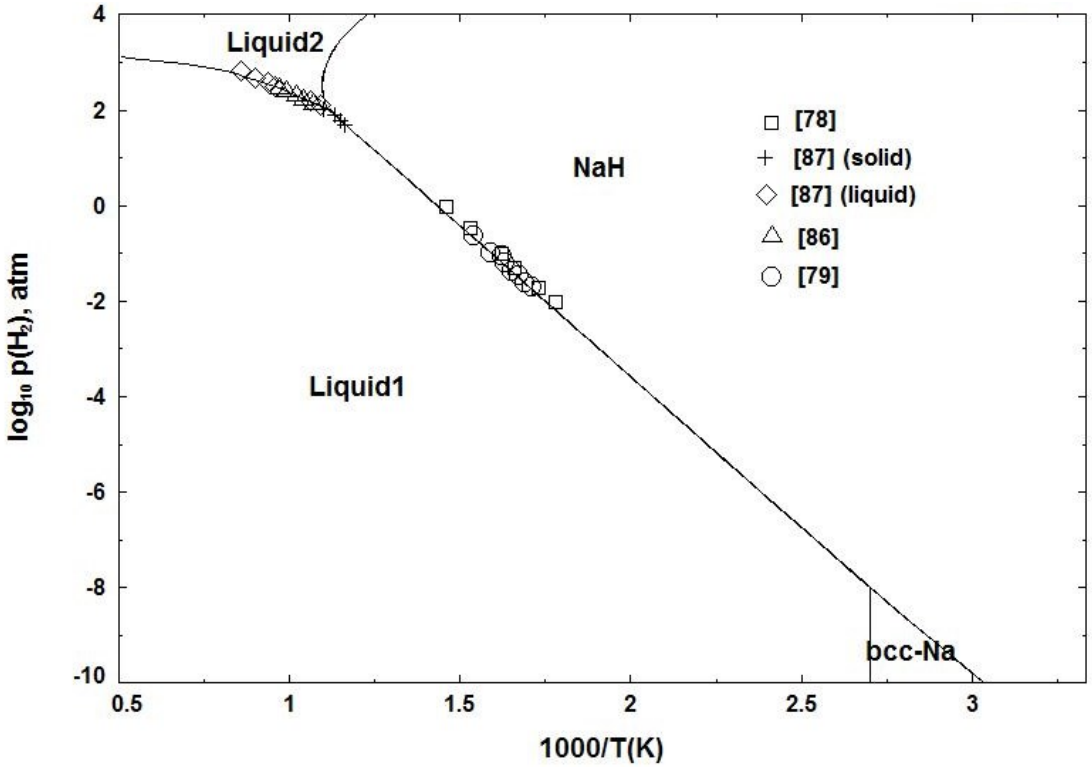

Figure 2.7 Calculated dissociation pressure of NaH in comparison with the experimental data from the literature

The calculated heat capacity of solid NaH with the available experimental data from Sayre and Beaver [100] is shown in Figure 2.8. In order to obtain reliable agreement with experimental data, the Gibbs energy of the solid NaH in the temperature range $0 < T < 298.15$ K has been determined in this work. The Gibbs energy of this compound at higher temperatures ($298.15 < T < 2000$ K) is taken from Qiu *et al.* [94].

***Table 2.3**: Enthalpy of formation of the NaH phase*

Enthalpy of formation kJ/mole	Temperature K	Reference
- 56.98	298	This work
- 58.4±1.2	623	[78, 99]
- 56.9±1.1	298	[97]
- 56.44±0.17	298	[96]

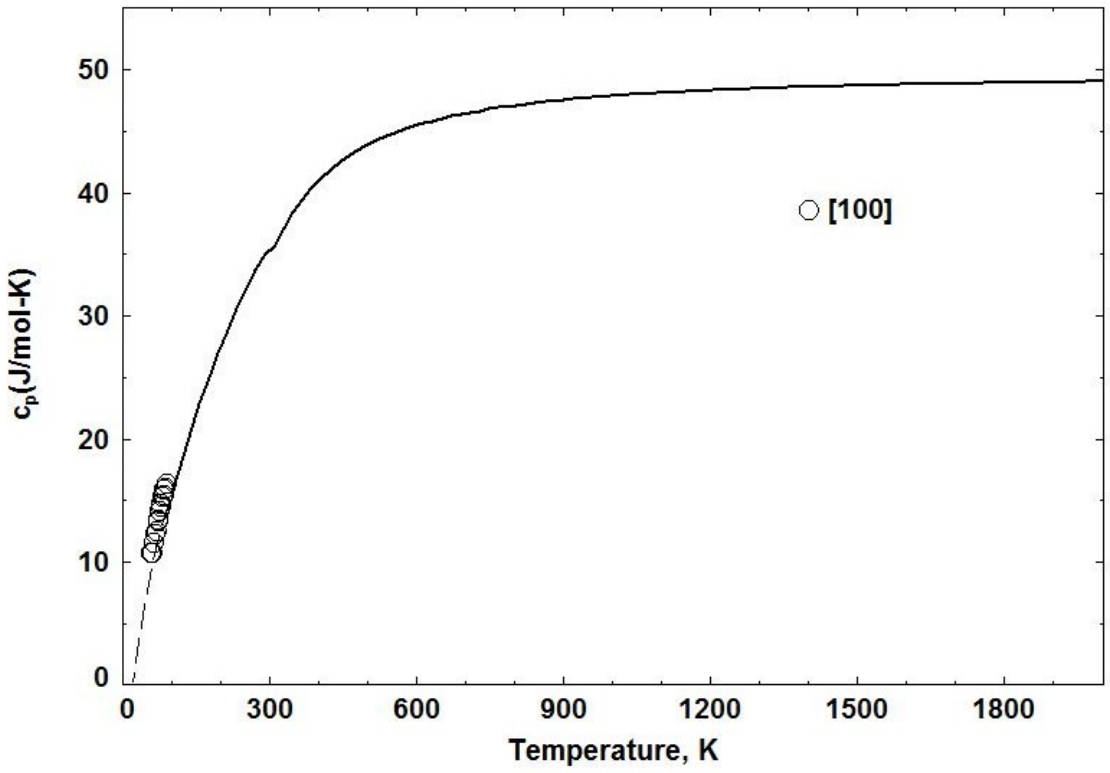

Figure 2.8 Calculated heat capacity c_p of NaH in comparison with experimental data

2.4.3 Mg-Na system

The calculated phase diagram of the Mg-Na system is presented in Figure 2.9. The thermodynamic model parameters obtained for the system are given in Table 2.1. The calculated phase diagram is in good agreement with the experimental data form the literature [102-106]. However, it differs a little from the calculation of Zhang *et al.* [106] at high temperature when the gas phase interacts with the liquid immiscibility gap. Zhang *et al.* [106] reported the Gas→liquid2 transformation at 97.01 at.% Na which was found at 92.5 at.% Na in the present work. Since there is no experimental data for this reaction the present prediction is acceptable. The composition and temperature of the invariant reactions in the Mg-Na system calculated in the present work are compared with the experimental data from the literature Table 2.4. Activities of Mg and Na in the liquid at 973 K are calculated and presented in Figure 2.10. The calculated Mg activity is in good agreement with the experimental measurements by Lantratov [103]. The Na activity shows deviation from that of Lantratov [103] in the liquid immiscibility gap. However, the experimental data showed unrealistic activity of almost equal to unity and was not possible to obtain without deviating from the experimental phase diagram.

Table 2.4: *Invariant reactions in the Mg–Na system*

Reaction	Temp/K	Composition, Na (at.%)			Reference
Gas→liquid2	1153	92.5			This study
	1157	97.016			Modeling [107]
Liquid1→hcp-Mg + liquid2	910	2.25	0.11	93.21	This study
	910	2.10	0.033	92.70	Modeling [107]
	911	2.0±0.1			Experiment [102]
	911	2.1		98.6	Experiment [104]
	910	1.6		92.7	Experiment [103]
Liquid2→hcp-Mg + bcc-Na	371	99.97	1.0×10^{-3}	100	This study
	371	99.98	4.15×10^{-4}	100.00	Modeling [107]
	371				Experiment [102]
	371				Experiment [103]

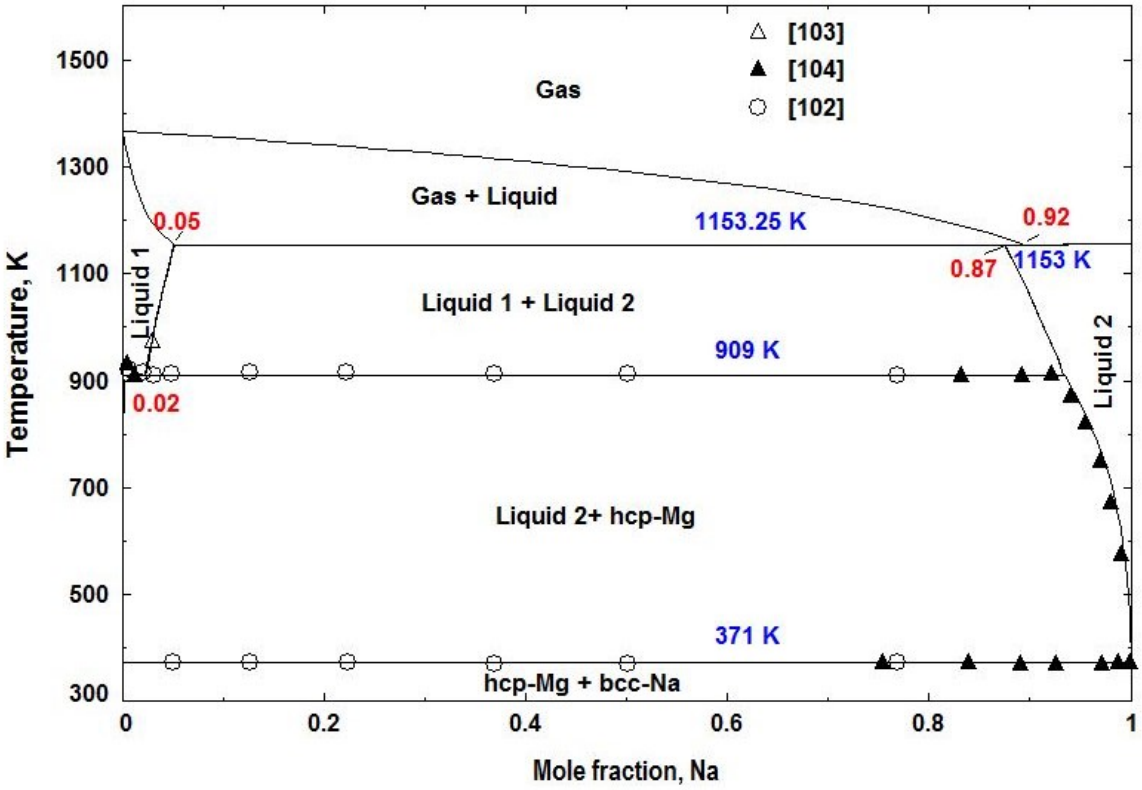

Figure 2.9 Calculated phase diagram for Mg–Na system in comparison with the experimental

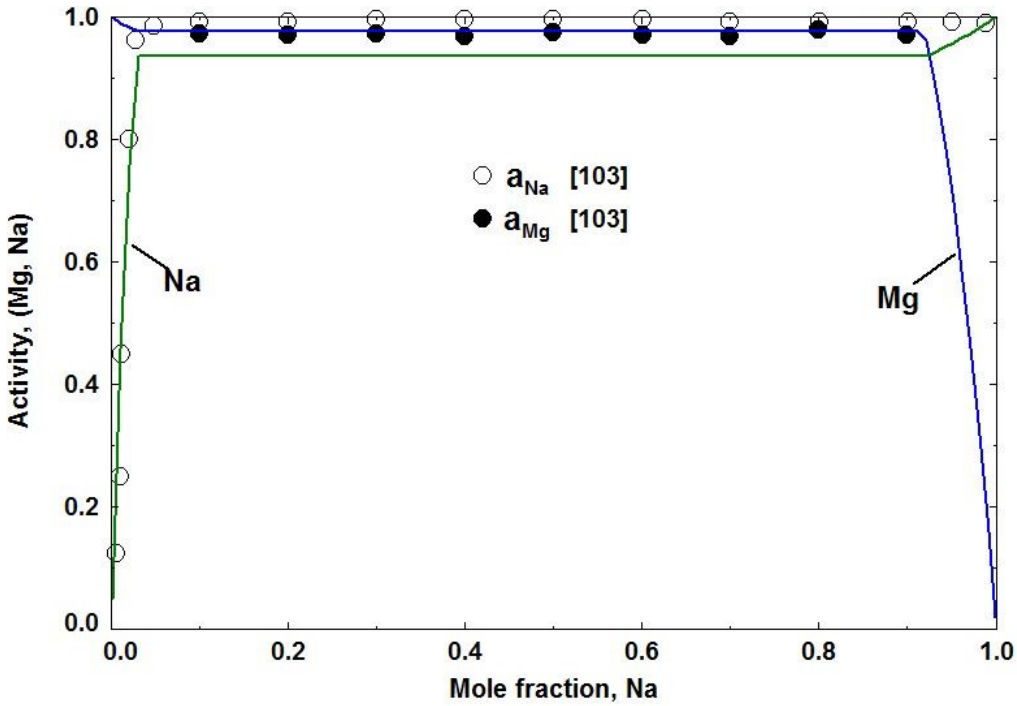

Figure 2.10 Calculated activities of liquid Na and liquid Mg at 973 K in comparison with the experimental data

2.4.4 H-Mg-Na system

Calculated changes in enthalpy and entropy for reactions (2.1) and (2.2) and enthalpy and entropy of formation of $NaMgH_3$ are given in Table 5 in comparison with experimental data from the literature. There is a good consistency between the calculated heat of formation of $NaMgH_3$ in this work and the experimental values reported in the literature [15, 17, 18, 89] except for the DSC results published by Bouamrane *et al.* [35], which are higher. This can be attributed to the use of DSC for the measurement of thermodynamic properties of the hydrides instead of PCI method, which is more accurate due to its reliance on the change in volume. The calculated enthalpy and entropy of reactions (2.1) and (2.2) are in very good agreement with the values reported by Sheppard *et al*. [109]. Agreement is also shown between the calculated enthalpy of reaction (2.1) with Ikeda *et al.* [40] as well as between the calculated entropy of reaction (2.2) and Komya *et al.* [39]. As discussed in section 2.4, all the other differences are related to the PCIs quality and poor kinetics in [37, 39, 49].

***Table 2.5**: Thermodynamic properties of $NaMgH_3$ decomposition from PCI and DSC experiments*

Reaction 2.1		Reaction 2.2		Δ_fH^0 ($NaMgH_3$) (kJ/mol)	Reference
ΔH (kJ/mol H_2)	ΔS (J/mol H_2 K)	ΔH (kJ/mol H_2)	ΔS (J/mol H_2 K)		
85.45	127.2	114	154.2	-142.44	This work
_	_	_	_	-231**	[35]
88 ± 0.9	_	_	_	-145*	[40]
93.9 ± 6	116.2 ± 9	102.2 ± 4	125.9 ± 6	-145*	[37]
94 ± 15	140 ± 22	116 ± 2	165 ± 3	-152*	[39]
92	123	_	_	_	[49]
86.6 ± 1	132.2± 1.3	117	168.2	-145.1*	[109]

**: the values are (re)calculated in this work using ΔH values reported in the literature; **: data obtained by DSC measurements.*

The calculated PCI profiles at various temperatures are presented in Figure 2.11 in comparison with the experimental data reported by Sheppard *et al*. [109]. It has been reported by these authors [109] that the samples used for the PCI measurements were composed of 84.3 wt.%

$NaMgH_3$, 4.7 wt.% NaH, and 11.0 wt.% MgO. In the present work, the hydrogen wt.% desorbed from the samples has been recalculated to consider only the $NaMgH_3$ content assuming no reaction between H_2, MgO and NaH. The hydrogen content of the samples was calculated by subtracting the hydrogen desorbed from the total hydrogen content before desorption (6 wt.%). These results (Figure 2.11) show that the model used to describe the $NaMgH_3$ reproduces the equilibrium pressures at different temperatures. The calculated PCI at 671.4 K in comparison with the experimental one, show that there is agreement between the theoretical and the measured hydrogen content of the first sample. It can be seen that the amount of hydrogen desorbed from the samples is decreasing after each experiment probably because of incomplete hydriding or dehydriding reactions and very sluggish kinetics.

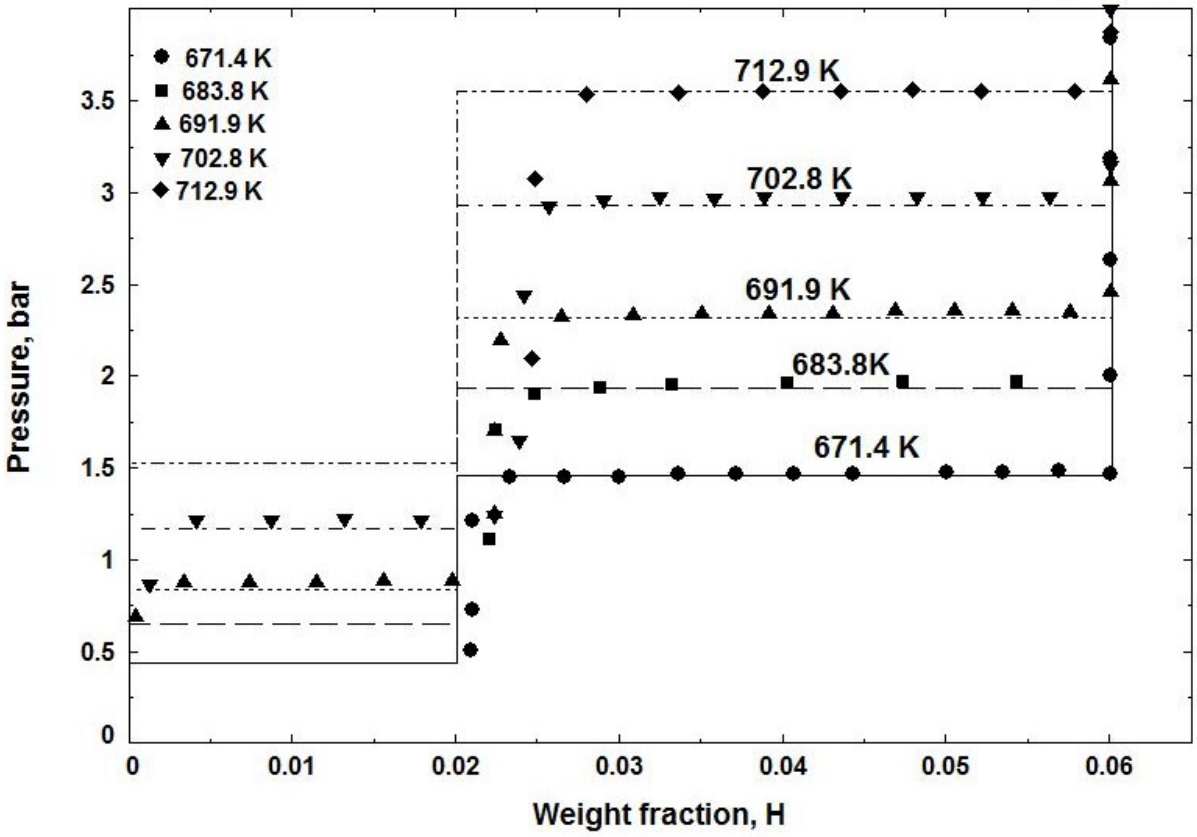

Figure 2.11 Calculated PCIs for $NaMgH_3$ at various temperatures compared to experimental data reported by Sheppard et al. [109]

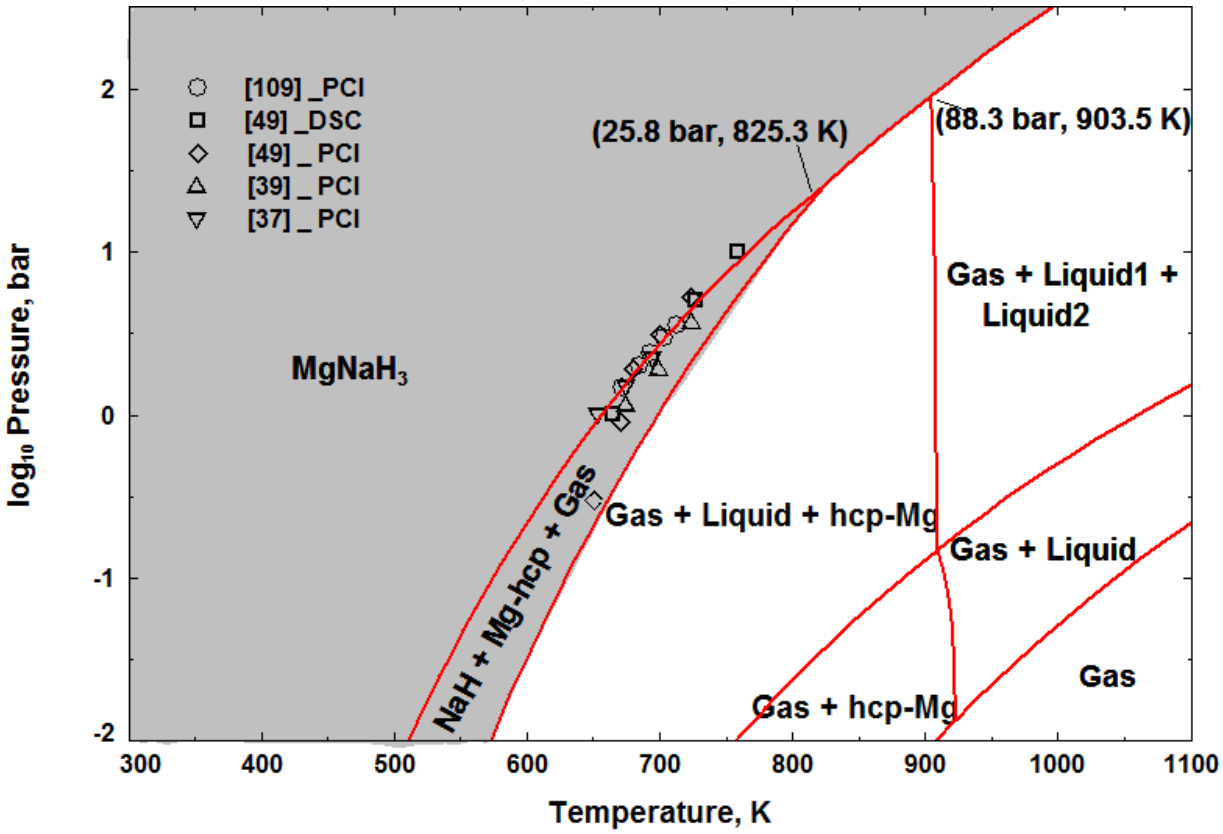

Figure 2.12 Calculated Pressure-Temperature equilibrium diagram for $NaMgH_3$ in comparison with experimental data from the literature

The calculated pressure-temperature diagram of $NaMgH_3$ is presented in Figure 2.12 in relation to experimental data from the literature. There is good agreement between the calculated and the experimental data except for the PCI results obtained by Pottmaier *et al.* [49] at 650 K. This deviation was expected because of the poor quality of the PCIs reported by Pottmaier *et al.* [49] due to very low kinetics especially for low temperature experiments as discussed before. Figure 2.12 indicates that $NaMgH_3$ is stable up to higher temperatures when the pressure is increased (up to ~ 900 K at ~ 100 bar). However, the stability region for NaH is relatively small. It can be seen in Figure 2.12 that the two-step decomposition of $NaMgH_3$ through reactions (2.1) and (2.2), transforms into a single step decomposition: ($NaMgH_3 \rightarrow$ Liquid + hcp-(Mg) + Gas) from 825.3 K and 25.8 bar.

Pottmaier *et al.* [49] observed an important decrease in hydrogen capacity of $NaMgH_3$ after 15 cycles of hydrogenation/dehydrogenation and observed at the end of the measurements that

metallic Na segregated into isolated blocks which, according to these authors [49], caused this loss in capacity. Sheppard *et al.* [109] reported a dramatic reduction in the rehydrogenation reaction kinetics of the products (Na (l) and hcp-(Mg)) to form $NaMgH_3$ and supported Pottmaier *et al.* [49] conclusion. This suggests that avoiding liquid Na during the decomposition of $NaMgH_3$, significantly improves the kinetics and prevents capacity degradation. According to the present calculation the best working temperatures and pressures for $NaMgH_3$ are shown as the shaded region in Figure 2.12 as this region avoids the liquid formation.

It has been shown by Wang *et al.* [41] that the addition of 10 wt.% of NaH greatly improved the hydrogen storage properties and the hydrolysis properties of MgH_2 due to the formation of $NaMgH_3$. As mentioned earlier, the perovskite structure allows fast hydrogen mobility and gives $NaMgH_3$ the catalytic role necessary for hydrogen storage capacity improvement of MgH_2. In Figure 2.13, the calculated vertical section of Mg-Na-H system along the composition line MgH_2-NaH at 1 bar and 100 bar is presented. Figure 2.13 shows that when 10 wt.% of NaH is added to MgH_2, $NaMgH_3$ forms. Also, all phase transformations with temperature at 1 bar and at 100 bar can be inferred from this figure. Since this figure does not provide the relative amounts of each phase, phase assemblage diagrams are calculated as will be discussed below.

Calculated PCI curves for the MgH_2 + 10 wt.% NaH mixtures at 623 and 673 K are shown in Figure 2.14(a) in comparison with the results published by Wang *et al.* [41]. The hydrogen content of the samples in [41] has been recalculated assuming that the initial samples hydrogen capacity is 7.3 wt.% based on the chemical formulae assuming stoichiometric amounts. At 673 K, three plateau pressures are shown in the calculated PCI curve (see arrows A, B and C in Figure 2.14b). The higher plateau (A) corresponds to the decomposition of MgH_2, the second (B) and the third (C) plateaus correspond to the decomposition of $NaMgH_3$ through reactions (2.1) and (2), respectively. At 623 K, only the first two plateaus are observed and the formation of liquid Na through reaction (2.2) is avoided. The last plateau (C in the PCI curve at 673 K) and the two last plateaus (in the PCI curve at 623 K) could not be observed by Wang *et al.* [41] and their reported plateau pressures are slightly lower than the current calculations. No information have been given by Wang *et al.* [41] about their PCI measurements conditions, but very few data points are shown in the published curves.

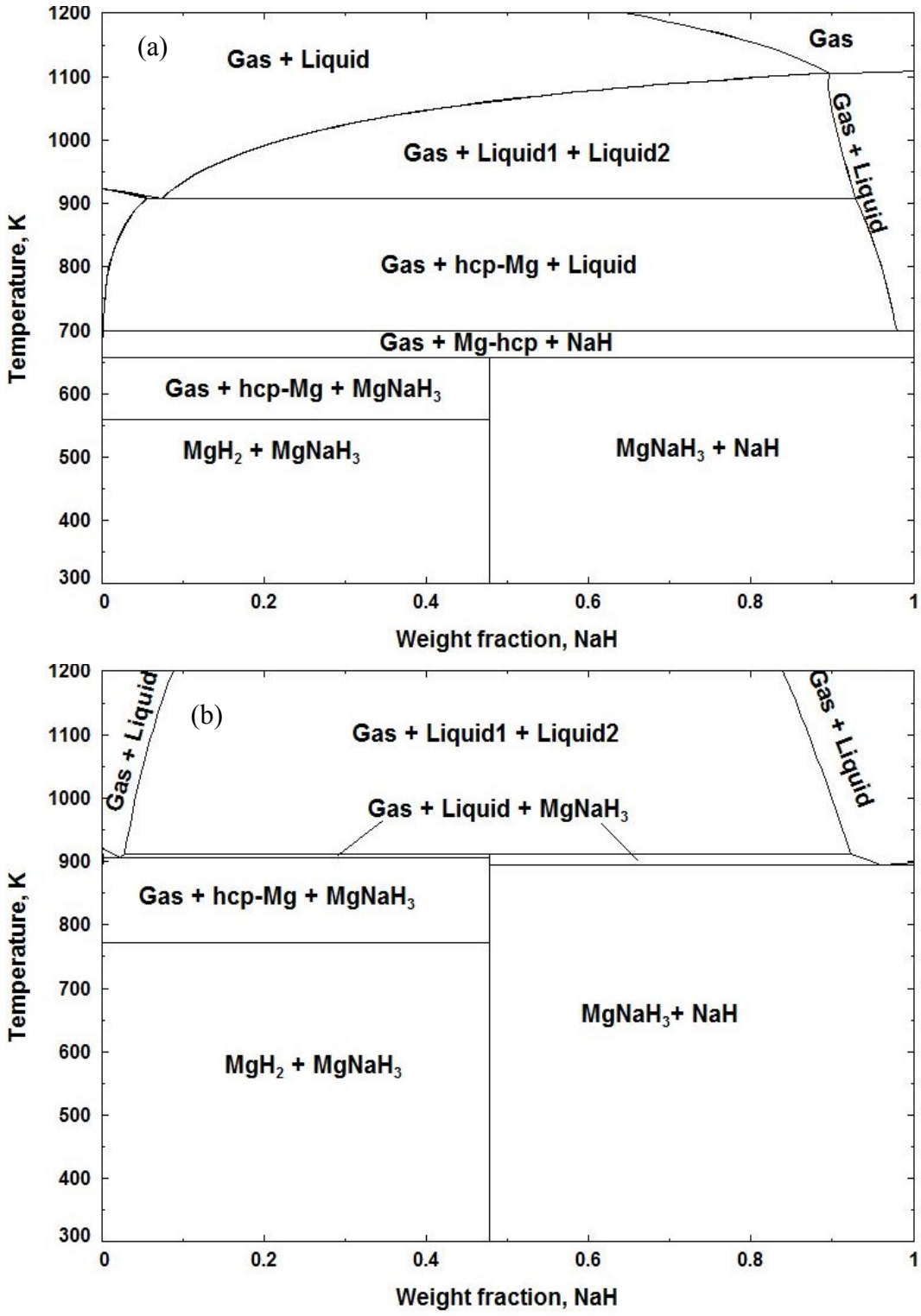

Figure 2.13 Calculated vertical section of Mg-Na-H system along the composition line MgH_2-NaH at (a): 1 bar and (b): 100 bar

It has been pointed out by Wang *et al.* [41] that their testing temperatures for kinetic measurements have been chosen below 623 K to avoid the decomposition of $NaMgH_3$, but according to the present calculations, $NaMgH_3$ decomposes at this temperature through reaction (2.1) and only reaction (2.2) is avoided during desorption in the pressure range of measurement.

The calculated pressure-temperature diagram for the MgH_2 + 10 wt.% NaH composition is shown in Figure 2.14(b). The plateau pressures at 673 K shown in Figure 2.14(a) (A, B and C) are also indicated by arrows in Figure 2.14(b). It can be seen that Figure 2.14(b) is a superimposition of Figure 2.2(b) (pressure-temperature diagram for MgH_2) and Figure 2.12 (pressure-temperature diagram for $NaMgH_3$) for temperatures below ~900 K. This result suggests that the thermodynamic properties of MgH_2 and $NaMgH_3$ are not affected when mixing MgH_2 with NaH. Only the amount of hydrogen desorbed from the mixture (the plateaus width) at each step changes with the amount of NaH added. In other words, from a thermodynamic point of view, addition of NaH to MgH_2 does not improve the hydrogen storage properties of MgH_2. In the contrary, the absorption/desorption kinetics is significantly improved as reported in the literature. For this purpose as well, the full potential of the catalytic role of $NaMgH_3$ can only be obtained if the processing conditions are set as shown by the shaded region in Figure 2.12.

The decomposition temperature and the amount of released hydrogen for any compositions of the H-Mg-Na system can be obtained at any pressure using the current database. The calculations for three different pressures (1, 0.1 and 1×10^{-4} bar) are discussed below.

The Calculated reaction path of the MgH_2 + 10 wt.% NaH at 1 and 0.1 bar is given in Figures 2.15(a) and 2.15(b), respectively. The reaction path at 1 bar is as follows: MgH_2 decomposes first at 557.8 K to hcp-(Mg) and 6 wt.% H_2 gas. $NaMgH_3$ decomposes second at 656 K to NaH, hcp-(Mg) and an additional 0.9 wt.% H_2 gas. At 697 K, NaH decomposes to liquid and an additional 0.4 wt.% H_2 gas. Slow decrease in the amount of liquid phase from 700 K is accompanied with the evaporation of Na. The total amount of gas phase is presented in dashed line. A second liquid phase appears at the melting point of magnesium and disappears at 933 K where Mg starts to evaporate with decreasing the amount of the liquid phase. At 0.1 bar, as expected, the decomposition temperatures of the hydrides, the evaporation points of Na and Mg and the sublimation point of Mg are lower.

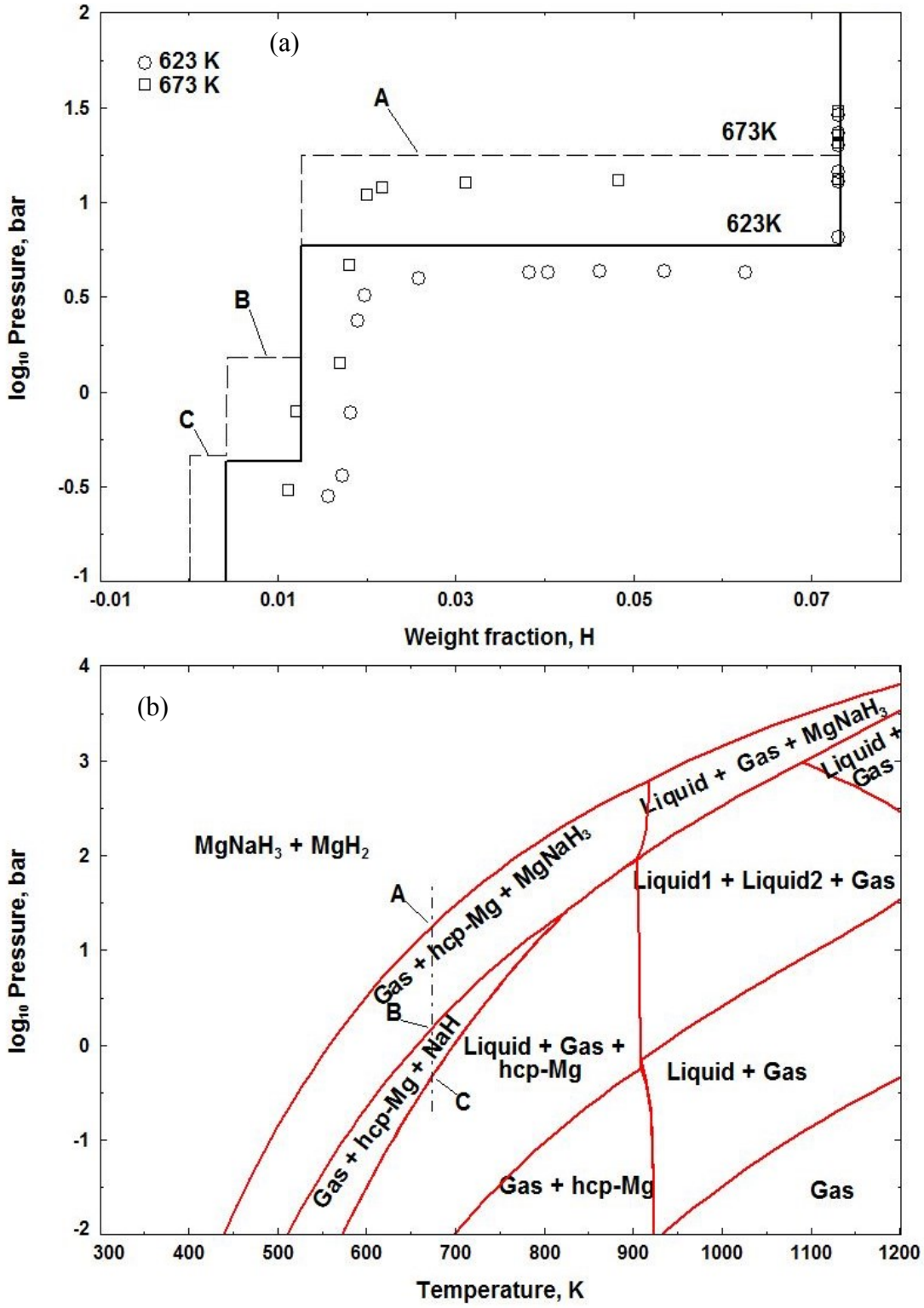

Figure 2.14 (a) Calculated P-C isotherm for MgH_2+10 wt. % NaH at 623 and 673 K compared to experimental data [41], (b) Calculated pressure temperature diagram for MgH_2+10 wt. % NaH

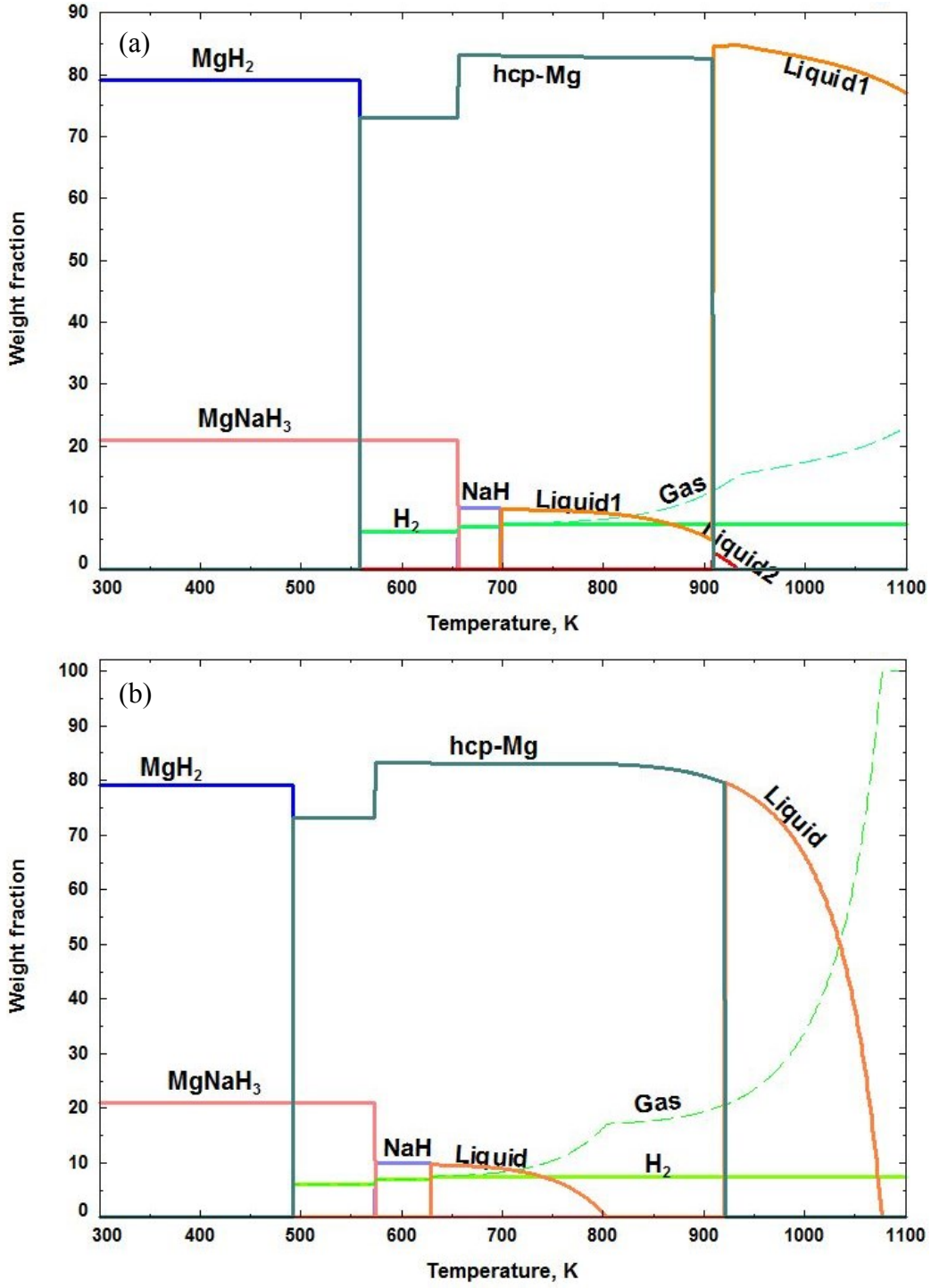

Figure 2.15 Calculated reaction path for MgH_2 + 10 wt. % NaH a: (a) 1 bar, (b) 0.1 bar

MgH_2 decomposes at 491 K to hcp-(Mg) and 6 wt.% H_2 gas and $NaMgH_3$ at 573 K liberating an additional 0.9 wt. % H_2 gas. NaH decomposes at 628 K to liquid and an additional 0.4 wt. % H_2 gas. According to the present calculation, at a pressure of 1×10^{-4} bar, MgH_2 decomposes at 366 K, $NaMgH_3$ at 418 K and NaH at 486 K. It is concluded in this work that MgH_2 will decompose at temperatures lower than 373 K with good kinetics at low pressures if mixed with a small amount of $NaMgH_3$.

2.5 Conclusion

A self-consistent thermodynamic database has been constructed to describe the H-Mg-Na system. Thermodynamic modeling of the constituent binary systems: H-Mg, H-Na and Mg-Na have been carried out. The modified quasi-chemical model is used to describe the liquid phase. Thermodynamic calculations of various phase diagrams and thermodynamic properties are compared with the experimental data and found to be in good agreement. The binary thermodynamic parameters of the liquid phases were interpolated using the asymmetric Kohler-Toop technique. The solid solution phases; hcp-Mg and bcc-(Na) are described by two-sublattice models as $(Mg,Na)_2(H,Va)_1$ and $(Na,Mg)_1(H,Va)_3$. The constructed database is used to predict the PCIs and the pressure-temperature diagram of the MgH_2 +10 wt.% NaH mixture. The calculations provide more insight about the reactions when compared to experimental data from the literature. The reaction path of the MgH_2 +10 wt.% NaH mixture is predicted at different pressures. In this study, it is demonstrated that H-Mg-Na system does not satisfy all the DOE requirements for on board hydrogen storage applications (desorption temperature < 373 K, at atmospheric pressure) but still very good candidate for high temperature applications. According to this work, at 1 bar, $NaMgH_3$ decomposes at 656 K to NaH and hcp-(Mg) liberating 6 wt.% of hydrogen gas. The present database is used to find the best working temperatures and pressures of $NaMgH_3$ to avoid its full decomposition and benefit from its full catalytic role when mixed with MgH_2. At pressures of 1, 0.1 and 10^{-4} bar, the limiting working temperature should be 697, 628 and 486 K, respectively. It is also found that MgH_2 decomposes at 366 K at a pressure of 10^{-4} bar. The present database can be used for further thermodynamic assessments of higher order systems.

Chapter 3. Understanding the hydrogen storage behaviour of Promising Al-Mg-Na compositions using thermodynamic modeling

Abstract

Thermodynamic modeling of the Al-Mg-Na-H system is performed in this work in order to understand the phase relationships and reaction mechanisms in this system. The Al-Na system is reassessed using the modified quasichemical model for the liquid phase. All the terminal solid solutions have been remodelled using the compound energy formalism. Thermodynamic properties of the ternary systems are estimated from the models of the binary systems and the ternary compound using CALPHAD method. Reaction pathways for the systems: MgH_2/AlH_3, $MgH_2/NaAlH_4$, and MgH_2/Na_3AlH_6 are calculated and compared to the experimental data from the literature. Details about the reaction mechanisms and temperatures, the amount of the products, and their composition are revealed and discussed in this work. The calculations show that in the composites $MgH_2/NaAlH_4$ and MgH_2/Na_3AlH_6, the components spontaneously destabilize mutually in specific relative amounts by forming $NaMgH_3$, which may play only a catalytic role on the decomposition of (MgH_2+Al) mixture, $NaAlH_4$, or Na_3AlH_6. Also, Al destabilizes MgH_2 and $NaMgH_3$ by forming β phase and reducing the decomposition temperatures of these hydrides by more than 50°C. The constructed database is successfully used to reproduce the pressure-composition isotherms (PCIs) for Mg-10at.%Al and Mg-4at.%Al alloys at 350°C. The results provide a better understanding of the reaction mechanisms in the PCIs found in the literature concerning the number of plateau pressures and their sloping. It is shown that the first plateau pressure observed during the PCIs of Al-Mg alloys depends on Al content and is higher than that of pure Mg. This difference is due to Al solubility in hcp-Mg.

Key words: Hydrogen storage, magnesium hydrides, sodium alanates, thermodynamic modeling.

3.1 Introduction

Hydrogen storage in light metal hydrides is considered as one of the most promising solutions

toward a hydrogen economy. Lots of efforts have been devoted last few decades to the search of a metal hydride that satisfies all the requirements for the development of hydrogen fuel cells which potential applications are ranging from micro-fuel-cells that power portable electronics to mobile applications. Magnesium hydride MgH_2 shows a great potential as a hydrogen storage material because of its high hydrogen storage capacities (7.6 wt.%), reversibility, and low cost [13]. However, it suffers from extremely slow hydriding kinetics and high decomposition temperature [13]. MgH_2 is predicted to decompose to hcp-Mg and H_2 at a temperature of 284.73°C and ambiant pressure [117]. Many studies have shown the possibility of lowering the decomposition temperature of MgH_2 and/or improving its hydriding kinetics by mixing with other elements or compounds. Another group of complex metal hydrides, alanates (or aluminohydrides, a family of complex hydrides containing aluminum and hydrogen), have attracted a great interest since the work of Bogdanovic [118] who demonstrated the reversibility of the hydrogenation of the Ti-enhanced alanates. Sodium alanate, $NaAlH_4$, decomposes in two steps with total hydrogen release of 5.6 wt.%. According to Qiu *et al.* [119], it is predicted that, at 1 bar, the first step proceeds at 21.45°C and the second one at 106.58°C. However, research is still needed to improve alanates' absorption/desorption kinetics. Recently, great efforts have been made to investigate hydrogen storage properties and reaction mechanisms in composites containing MgH_2 and some complex hydrides such as magnesium and sodium alanates where different explanations have been given about the observed processes [120-126]. However, no theoretical work has been conducted to better understand these experimental results.

In the present work, thermodynamic modeling is used to construct a self-consistent thermodynamic database that describes the Mg-Al-Na-H system and allows the prediction of its hydrogen storage performance and provides a basic understanding of the reaction mechanisms between the different phases in the system under equilibrium conditions. Recently, Abdessameud *et al.* [117] performed thermodynamic modeling of Mg-Na-H system and predicted its hydrogen storage properties over a wide range of temperatures and pressures. They [117] proved that the $MgNaH_3$ hydride does not affect the thermodynamics of MgH_2 and provided the best working conditions to benefit from its full catalytic role.

3.2 Literature review

This section is composed of two main parts. In the first part, a literature review about the thermodynamic properties and descriptions of the constituent binaries and ternaries in the Al-Mg-Na-H system is presented. In the second part, the most recent findings about the hydrogen storage properties in the Mg-Al-H and Mg-Al-Na-H systems are reviewed.

3.2.1 Termodynamic description of Mg-Al-Na-H system

The Mg-Al-Na-H system is modeled in the current work using FactSage software [25]. The constituent binary systems are modeled using the modified quasichemical model MQM for the liquid phase and the compound energy formalism for the solid solution phases. These binary systems are either taken from the literature [75, 127, 128] or from our previous work [117] or re-assessed in the current work (Al-Na). In many occasions the models found in the literature were adjusted to suit dealing with hydrogen. This will be ellaborated in the following sections. The thermodynamic properties of the ternary systems are estimated from the models of the binary systems and the ternary compounds using CALPHAD method.

Mg-Na-H system was reviewed and modeled for the first time in our previous work [117]. The constituent binaries (Mg-Na, Mg-H, and Na-H) were remodeled using the MQM for the liquid phase and three hydrides: MgH_2, NaH, and $MgNaH_3$, were described in this system [117]. The model parameters taken from [117] are used in this work.

3.2.1.1 Al-Mg system

The model parameters used to describe the liquid phase of the Al-Mg system are from Harvey [128] who used the MQM to model this phase. In [128], the terminal solid solutions were considered substitutional. Since this system is used for hydrogen storage purposes, the terminal solid solutions are considered interstitial and are adjusted in this work. For the compounds, all the parameters used in [128] are adopted in this work. The phase diagram consists of a liquid phase, terminal fcc-Al and hcp-Mg solid solutions, and three compounds β(Al_3Mg_2), γ ($Al_{12}Mg_{17}$) and ε ($Al_{30}Mg_{23}$).

3.2.1.2 Al-H system

San-Martin and Manchester [129] conducted a critical literature review and assessment of the Al-H system. Three stable phases have been reported in the system: liquid, fcc-Al solid solution

and gas. They [129] reported a eutectic-type reaction near the melting point of Al, (660.452°C) and hydrogen solubilities of 1.1×10^{-3} and 1.16×10^{-4} at% in liquid Al and in fcc-Al, respectively. Only one hydride AlH_3 was reported in the literature [130]. AlH_3 has a gravimetric density that exceeds 10 wt% and shows rapid dehydrogenation at low temperatures (<100°C) with a low heat of reaction (around -7 kJ/molH_2) which makes it a promising hydrogen storage material [130]. According to its thermodynamic properties, AlH_3 is metastable at ambiant conditions but its decomposition reaction suffers from poor kinetics [130]. Thus, after the first dehydrogenation, the resulting Al could be hydrogenated only at high pressure (10^6 MPa) and AlH_3 will not take part in the following hydrogenation/dehydrogenation cycles. Graetz *et al.* [130] published an extensive review about aluminum hydride as "a hydrogen and energy storage material". Qiu *et al.* [127] reviewed the existing thermodynamic properties of Al-H system and modeled it. The calculations made by Qiu *et al.* [127] showed good agreement with experimental data for hydrogen solubility in fcc-Al and thermodynamic properties of AlH_3. Later, thermodynamic modeling of hydrogen solubility in liquid Al was conducted by Harvey and Chartrand [75] using the MQM, showing better agreement with the available experimental data. Since MQM is used to describe the liquid phase in this work, the model parameters of Harvey and Chartrand [75] are used to describe the liquid phase in the present work. The model parameters given by Qiu *et al.* [127] for the AlH_3 hydride and fcc-Al phase are also adopted in this work.

3.2.1.3 Al-Na system

The Al-Na system has been extensively reviewed by Murray [131] and by Zhang *et al.* [106]. The Al-Na system has been assessed by Murray [131], Zhang *et al.* [106], and Qiu *et al.* [127]. The assessed phase diagram by Murray [131] shows a miscibility gap in the liquid phase, low solubility of Na in fcc-Al and of Al in bcc-Na and a monotectic reaction: Liquid1 → Liquid2 + fcc-Al at Na composition of 0.18 ± 0.02 at.%.

Because different models are used in this study for the liquid phase (MQM) and for the terminal solid solutions than previous assessments [106, 127, 131], the system is reassessed in the present work. Scheuber *et al.* [132] conducted solubility measurements of Na in liquid Al by heating under hydrogen gas and quenching. It should be noted that their results are uncertain due to hydrogen contamination as pointed out by Murray [131]. Fink *et al.* [133] carried out direct and differential thermal analysis measurement to investigate Al liquidus and monotectic reaction in

addition to electrical resistivity and metallographic measurements to investigate the Na solubility in solid Al. They [133] reported a monotectic composition and temperature of 0.18 at% Na and 932 K in addition to a maximum solubility of Na in fcc-Al of less than 0.003 at%. Two years later, Ransley and Neufeld [134] reported a lower value for the monotectic composition (0.14 at% Na occuring at 932 K) and more precise value of Na solubility in solid Al (0.0023 at% Na). Later, Na solubility in liquid Al measurements conducted by Hensen *et al.* [135] showed higher values compared to [132-134] and also increasing Na solubility with decresing temperature. Two years later, Fellner *et al.* [136] reported saturated solubility data (of Na in liquid Al) close to the results of [132-134]. Activity of Na in molten Al has been determined by Dewing [137] at 1293 and 1353 K and by Brisley and Fray [138] for super purity Al at 998 K. These data [137, 138] are used in the present work.

3.2.1.4 Al-Mg-H system

Rokhlin and Ivanchenko [139] conducted a literature review on the Al-Mg-H system. Harvey *et al.* [75, 128] reviewed the hydrogen solubility experimental data of Al-Mg liquid alloys and used them in assessing this system using the MQM. These authors [70, 123] obtained good agreement with the experimental data from the literature [70, 71, 140-142]. Therefore, their model parameters of the Al-Mg-H liquid are adopted in this work. In the present work, solubility of hydrogen in Al-Mg compounds ($\beta(Al_3Mg_2)$, $\gamma(Al_{12}Mg_{17})$ and $\varepsilon(Al_{30}Mg_{23})$) is neglected because no significant experimental evidence exists for hydrogen solubility in these compounds in the literature [143, 144].

Only one metastable ternary compound, $Mg(AlH_4)_2$ (with P-3m1 structure and a gravimetric density of 9.3 wt.%), has been reported in the literature [134]. Palumbo *et al.* [144] investigated the Al-Mg-H system using thermodynamic modeling and ab-initio calculations. However, they [144] focused their literature review on magnesium alanate $Mg(AlH_4)_2$. Thermodynamic description of the $Mg(AlH_4)_2$ compound has been provided later by Grove *et al.* [145] and their parameters are used as initial values in the present work.

Decomposition of $Mg(AlH_4)_2$ has been invesigated by different authors such as Mamatha *et al.* [146] and Varin *et al.* [147] using DSC and Kim *et al.* [148] using TG/MS and DSC and Iosub *et al.* [149] using XRD, TPD (temperature programmed desorption) and DSC. It has been concluded that magnesium alanate, $Mg(AlH_4)_2$, decomposes in two steps [148, 150] according to

the reactions:

$Mg(AlH_4)_2 \rightarrow MgH_2 + 2\ Al + 3\ H_2$ (7 wt.% H_2) (3.1)

$MgH_2 + 2\ Al \rightarrow ½\ \beta + ½\ Al + H_2$ (2.3 wt.% H_2) (3.2)

An enthalpy value of 1.7 kJ/mole for reaction (3.1) has been found by Mamatha *et al.* [146] while Varin *et al.* [147] reported a value close to zero. Iosub *et al.* [149] estimated that the enthalpy of reaction (3.1) is approaching 2 kJ/mole.

3.2.1.5 Al-Mg-Na system

No experimental thermodynamic data and no ternary compound have been reported in the literature for the Al-Mg-Na system.Thermodynamic modeling of the system has been performed by Zhang *et al.* [106] by combining the constituent binaries. Since MQM is used in this work, thermodynamic description of the system is predicted from extrapolation of the binaries cited in sections 3.2.1.1 and 3.2.1.3 (Al-Mg and Al-Na) and those assessed in our our previous paper (Mg-Na) [117].

3.2.1.6 Al-Na-H system

The Al-Na-H system has been reviewed and modeled by Qiu *et al.* [119] . Two ternary compounds have been reported in the literature[119], $NaAlH_4$ (with a tetragonal $I4_1/a$ structure) and Na_3AlH_6 which exists in two forms; α-Na_3AlH_6 at temperatures lower than 252°C (with a monoclinic P21/c structure) and β-Na_3AlH_6 at temperatures higher than 252°C (with cubic Fm-3m structure). $NaAlH_4$ decomposes in two steps as follows:

$NaAlH_4 \longrightarrow 1/3\ \alpha\text{-}Na_3AlH_6 + 2/3Al + H_2$ (3.7 wt.% H_2) (3.3)

$\alpha\text{-}Na_3AlH_6 \longrightarrow 3NaH + Al + 3/2H_2$ (1.9 wt.% H_2) (3.4)

Using the substitutional solution model, Qiu *et al.* [119] provided a thermodynamic description of the Al-Na-H liquid. They assessed the two compounds in the system using CALPHAD approach and first principle calculations. Their parameters [119] are used in this work for the compounds. However, since the MQM is used in the present work, the ternary liquid has been extrapolated from the constituent binaries described in sections 3.2.1.

3.2.2 Hydrogen storage behavior in Al-Mg-Na-H system

3.2.2.1 Al-Mg-H system

Recently, Liu *et al.* [151] investigated the decomposition reaction of $Mg(AlH_4)_2$ using TPD, DSC and XRD. They [151] reported that, after the first exothermic peak, two dehydrogenation overlapping endothermic peaks have been observed. XRD measurements at 200, 280, and 320°C showed that diffraction peaks of Al shifted towards lower angles indicating the increase of solubility of Mg in Al phase. According to these authors [151], the overall dehydrogenation reaction proceeds as follows (with the first reaction as exothermic):

$$Mg(AlH_4)_2 \xrightarrow{125\text{-}200^\circ C} MgH_2 + 2\ Al + 3\ H_2 \xrightarrow{250\text{-}320^\circ C} 7/9\ MgH_2 + 20/9\ Al_{0.9}Mg_{0.1} + 29/9\ H_2$$
$$\xrightarrow{320\text{-}440^\circ C} 6/9\ Al_{0.9}Mg_{0.1} + 7/15\ Al_3Mg_2 + 4\ H_2 \qquad (3.5)$$

In these equations, Liu *et al.* [151] referred to fcc-Al as $Al_{0.9}Mg_{0.1}$ by taking into account the value of the maximum solubility of Mg in fcc-Al at 320°C as 10 at.%. After recharging at 120-210°C and 100 bar of hydrogen pressure, only MgH_2 and Al formed [151].

Hydrogenation properties of Al-Mg alloy s have been widely investigated [120, 121, 125, 126, 152-155]. It has been found [152, 153] that β (Al_3Mg_2) and γ ($Al_{12}Mg_{17}$) phases can be hydrogenated reversibly to form (MgH_2 + Al) and (MgH_2 + β), respectively.

Shang *et al.* [155] showed that the de-hydrogenation of MgH_2 is improved when mixed with Al using mechanical alloying. Zaluska *et al.* [154] suggested that Al is involved in hydriding/de-hydriding reactions through the reaction:

$$n\ MgH_2 + m\ Al \rightarrow Mg_nAl_m + n\ H_2 \qquad (3.6)$$

Andreasen [156] reviewed the hydrogen storage properties of Al-Mg alloys and reported that Mg_nAl_m (in reaction 3.6) has been found to be mainly the β-phase.

Liu *et al.* [125] investigated the effect of Al on MgH_2 destabilization by ball milling mixtures of MgH_2 + AlH_3 and MgH_2 + Al (Molar ratio 1:1) and using DSC-MS (H_2) and XRD analysis. They found that when mixed with AlH_3, the dehydrogenation temperature of MgH_2 is reduced 55°C compared to MgH_2 alone because of the interaction between MgH_2 and the oxide-free Al which was formed from desorption of AlH_3. Also, Although AlH_3 is metastable and will not form after the first desorption reaction, MgH_2 + AlH_3 mixture showed improved hydrogen desorption/absorption kinetics compared to MgH_2 + Al.

Later, Liu *et al.* [126] investigated the hydrogen desorption properties of MgH_2/AlH_3 composites with molar ratios 1:1, 1:0.5, and 1:0.25. These authors found that the onset hydrogen desorption temperature of MgH_2 decreases when the amount of AlH_3 increases. The DSC and MS-H_2 results indicate that the mixtures MgH_2/AlH_3 exhibit a two-stage desorption process. The first one has been related to AlH_3 decomposition and the second one to the decomposition of MgH_2. Liu *et al.* [126] reported that the second stage is composed of two overlapping (peaks) desorption steps and showed that MgH_2 decomposes in two steps. In their work, XRD analysis of MgH_2 + 0.25 AlH_3 was performed on samples heated in the same conditions as the DSC-MS measurements at different temperatures. Liu *et al.* [126] concluded on the basis of DSC analysis and XRD results that desorption of Mg-Al-H alloys proceeds in two steps.

Andreasen [156] summarized the results of pressure-composition isotherms (PCIs) found in the literature and concluded that the de/hydrogenation of Al-Mg alloys is at least a two step process when β phase is present. Andreasen [156] also noted that, in most of the PCI studies on the Al-Mg alloys, the distinction of the plateau pressures was difficult and uncertain because of the sloping of the measured curves and concluded that the thermodynamic parameters of the Al-Mg-H alloys calculated from these curves should be verified by more experiments. Tanniru *et al.* [120] characterized the hydrogenation behaviour (in the temperature range of 180-280°C) and PCIs (in the temperature range of 275-400°C) of Mg-8 at.% Al alloys compared to pure Mg in order to investigate the effect of Al addition on hydrogen storage properties of magnesium hydride. The PCI results showed that only one plateau was observed for Mg and Mg-8 at.% Al alloys. However, the equilibrium pressure for hydride formation in Mg-8 at.% Al alloys were slightly higher compared to pure Mg and the calculated enthalpy was lower by less than 10%. The higher plateau pressures has been explained by the change of the thermodynamics of hydride formation due to the solubility of Al in hcp-Mg which, according to these authors [120], reduces the solubility of hydrogen in hcp-Mg. Also, slopped curves showing the rise of pressure with composition after the plateau region of the Al-Mg alloys has been observed by Tanniru *et al.* [120] and attributed to the hydrogenation of γ phase (to form MgH_2 and β). Later, Tanniru *et al.* [121] conducted PCI tests at 350°C for Mg-10 at.% Al and Mg-4 at.% Al alloys. In the PCI experiments of Tanniru *et al.* [121], the pressure was increased in small steps and sufficient time has been allowed to reach equilibrium in each step. For this reason, the results obtained by [121]

will be compared to the calculations conducted in this work. Samples at different hydrogenation/dehydrogenation steps have been analyzed using X-ray diffraction (XRD) and scanning electron microscopy (SEM) in order to study the microstructure evolution during PCIs. They [121] reported three steps for hydriding of Mg-10 at.% Al alloys corresponding to three plateaus in PCIs at 350°C. As for pure Mg, PCI curve at 350°C of Mg-4 at.% Al alloys showed the existence of only the first plateau with a continuous increase of the pressure with the absorbed hydrogen. They [121] attributed the absence of the second and the third plateau for Mg-4at.%Al alloys to the small amount of γ phase formed at the end of the first plateau. In addition, Tanniru *et al.* [121] showed that the first plateau pressure increases with Al content of the samples and attributed this increase to kinetics factors. These results will be discussed and compared with the calculations done in this work in section 3.4.2.1.

3.2.2.2 Al-Mg-Na-H system

Investigations on hydrogen properties of mixtures of complex hydrides have been subject to many studies [45, 122-124, 150, 157]. Hudson *et al.* [150] was the first to report that, in the alanate mixture 0.5 $Mg(AlH_4)_2$ + $NaAlH_4$, the dehydriding temperature of $NaAlH_4$ was lowered by 50°C and the desorption kinetics was 4 times faster. Sartori *et al.* [45] investigated the hydrogen storage properties of the composites $2MgH_2$ + NaH + 3Al hydrided at 80°C and 160 bar. They [45] described the decomposition reaction mechanism of the hydrided composite using TPD and XRD experiments. Ismail *et al.* [122-124] investigated the hydrogen storage properties and the reaction pathways of MgH_2-$NaAlH_4$ (4:1)/Na_3AlH_6 (4:1) composites using XRD, thermo-gravimetric analysis, DSC, TPD and isothermal sorption measurements. Ismail *et al.* [122] showed that dehydriding kinetics of MgH_2 and $NaAlH_4$ were significantly improved when mixed together and reported that these hydrides destabilize mutually. Ismail *et al.* [124] reported that during the first step of the dehydrogenation reactions of the MgH_2-Na_3AlH_6 (4:1) composite where $NaMgH_3$, Al, and H_2 are formed, the decomposition of Na_3AlH_6 starts at a temperature 55°C lower than the decomposition temperature of the as milled Na_3AlH_6. In the second step, MgH_2 reacts with Al to decompose and to form β (Al_3Mg_2) phase. The decomposition temperature of MgH_2 in the composite is also 55°C lower than the decomposition temperature of the as milled MgH_2 [124]. They [124] suggested that the observed

thermodynamic and kinetic destabilization is a consequence of the insitu formation of β and $NaMgH_3$ phases during the dehydrogenation reactions of the MgH_2-Na_3AlH_6 (or $NaAlH_4$) (4:1) composites. In this work, the mechanisms of these reactions are discussed based on thermodynamic calculations.

3.3 Thermodynamic modeling

3.3.1 Pure elements. The Gibbs energy functions of the pure elements (Al, Mg, Na) and of pure liquids Al, Mg, and Na are taken from the compilation of Dinsdale [110]. The Gibbs energy of liquid monatomic hydrogen has been estimated by Ransley and Talbot [158] and is listed in Table 3.1.

3.3.2 Stoichiometric compounds. In the Al-Mg-Na-H system, the compounds $Al_{30}Mg_{23}$, AlH_3, MgH_2, $Mg(AlH_4)_2$, NaH, $NaMgH_3$, $NaAlH_4$, and Na_3AlH_6 are considered as stoichiometric compounds. Gibbs energy of a stoichiometric compound depends only on the Gibbs energy of the components and the Gibbs energy of formation, which is optimized using the experimental data (ΔH and ΔS of formation) from the literature.

3.3.3 Gas phase. The Gibbs energies of the gases included in this study, that is, Al, Al_2, AlH, H, H_2, Mg, Mg_2, MgH, Na, Na_2, and NaH, are taken from FactPS database [25]. In the pressure range of interest, the non-ideal contribution of pressure to the Gibbs energy for the gases is very small. In fact, to account for the non-ideal contribution of hydrogen gas, Hemmes *et al.* [159] calculated the equation of state of hydrogen and other thermodynamic quantities in the range $p \leq 100$ GPa and $100 \leq T \leq 1000$ K. Numerical values of Gibbs energy and other quantities given in [159] have been used in this work to extrapolate the Gibbs free energy versus temperature of hydrogen gas at 100 bar and used in the calculations for comparison with the ideal gas model. A difference in temperatures of less than 3 K (at 100 bar) has been found. For this reason, all the gases are considered ideal gases.

3.3.4 Solid solution phase. Terminal solid solutions are modeled in this work using the compound energy formalism as hydrogen atoms occupy the interstitial positions in the solid phases fcc-Al, hcp-Mg, and bcc-Na. These phases are described by two sublattices were Al, Mg, and Na are mixed randomly in the first sublattice to allow for their mutual solubility. Hydrogen

atom and vacancy mix in the second sublattice. Therefore, as discussed in [117], $(Al,Mg,Na)_1(H,Va)_1$, $(Mg,Al,Na)_2(H,Va)_1$, and $(Na,Al,Mg)_1(H,Va)_3$ sublattices are used to model fcc-Al, hcp-Mg, and bcc-Na, respectively.

In the Al-Mg system, the compounds β (Al_3Mg_2) and γ ($Al_{12}Mg_{17}$) are taken from Harvey [128] where they are discribed by the sublattices $(Mg)_{10}(Al,Mg)_{24}(Al,Mg)_{24}$ and $(Al)_{19}(Al,Mg)_2(Mg)_{12}$ for γ and β, respectively.

3.3.5 Liquid phases. The modified quasichemical model (MQM) is used to model the liquid phase for all the binaries. Binary liquid parameters have been interpolated using the asymmetric Kohler-Toop technique where H is singled out as the asymmetric component as discussed in our previous paper [117]. No ternary parameters have been added to the liquid model.

Thermodynamic equations used to model different phases are explained in our previous paper [117].

3.4 Results and discussion

In section 3.4.1, the calculated thermodynamic properties and phase diagrams using the current database are presented for the binary and ternary phases discussed in section 3.2.1. The thermodynamic parameters used in the present work for the Al-Mg-Na-H system are given in Table 3.1.

Table 3.1*: Optimized model parameters for the different phases in the Al-Mg-Na-H system (J/mole)*

Liquid Phase (MQM)	
$g^0_{H(l)} = 74,266.7 - 26.2456T + 20.7856T\ln T$ $Z^{Mg}_{MgH} = Z^{H}_{MgH} = 6, \Delta g^{o}_{MgH} = -18,049.78$	[75]
$Z^{Na}_{NaH} = Z^{H}_{NaH} = 6, \Delta g^{0}_{NaH} = -39,245.92 + 8.45T;$ $\Delta g^{10}_{NaH} = 12,133.6 - 0.711T; \Delta g^{01}_{NaH} = -66,944 + 8.368T$ $Z^{Mg}_{MgNa} = 4.5, Z^{Na}_{MgNa} = 6, \Delta g^{0}_{MgNa} = 7,660.0 + 2.9T$	[117]
$Z^{Al}_{AlH} = Z^{H}_{AlH} = 6, \Delta g^{0}_{AlH} = -6,516.58 - 0.544T$ $Z^{Mg}_{MgAl} = Z^{Al}_{MgAl} = 6, \Delta g^{0}_{MgAl} = -2761.44 + 1.52716T; \Delta g^{10}_{MgAl} = -481.4 + 0.6276T$	[75]
$Z^{Al}_{AlNa} = Z^{Na}_{AlNa} = 6, \Delta g^{0}_{AlNa} = 203509.76 + 5.89944T; \Delta g^{10}_{AlNa} = -193133.44$	This work

Terminal Solid solutions (Compound Energy Formalism)

- hcp-(Mg) $(Mg,Na,Al)_2(H,Va)_1$

$^0G^{Mg_2}_{Mg:Va} = 2G(Mg_{hcp})$; $^0G^{Na_2}_{Na:Va} = 2G(Na_{hcp})$; $^0G^{Al_2}_{Al:Va} = 2G(Al_{hcp})$

$^0G^{Mg_2H}_{Mg:H} = 173,217.6 - 242.672T + 2G(Mg_{hcp}) + 1/2G(H_2, gas)$

$^0G^{Na_2H}_{Na:H} = 2G(Na_{hcp}) + 1/2G(H_2, gas)$; $^0G^{Al_2H}_{Al:H} = 100000 + 2G(Al_{hcp}) + 1/2G(H_2, gas)$ [117]

$^0L^{hcp}_{Mg,Na:Va} = 79,496 + 16.736T$

$^0L^{hcp}_{Mg,Al:Va} = 8288.059 - 8.75T$; $^1L^{hcp}_{Mg,Al:Va} = 414.886 - 6.109T$; $^0L^{hcp}_{Al,Na:Va} = 75132$ This work

- bcc-(Na) $(Na,Mg,Al)_1(H,Va)_3$

$^0G^{NaH_3}_{Na:H} = G(Na_{bcc}) + 3/2G(H_2, gas)$; $^0G^{MgH_3}_{Mg:H} = G(Mg_{bcc}) + 3/2G(H_2, gas)$;

$^0G^{AlH_3}_{Al:H} = G(Al_{bcc}) + 3/2G(H_2, gas)$

$^0G^{Na}_{Na:Va} = G(Na_{bcc})$; $^0G^{Mg}_{Mg:Va} = G(Mg_{bcc})$; $^0G^{Al}_{Al:Va} = G(Al_{bcc})$ [117]

$^0L^{bcc}_{Na:H,Va} = -5,569.8$; $^1L^{bcc}_{Na:H,Va} = -2,092.9$; $^0L^{bcc}_{Na,Mg:Va} = 30,000$

$^0L^{bcc}_{Al,Na:Va} = 27715$ [127]

$^0L^{bcc}_{Al,Mg:Va} = 5020.8$ [128]

- fcc-Al $(Al,Mg,Na)_1(H,Va)_1$

$^0G^{Al}_{Al:Va} = G(Al_{fcc})$; $^0G^{Mg}_{Mg:Va} = G(Mg_{fcc})$; $^0G^{Na}_{Na:Va} = G(Na_{fcc})$;

$^0G^{AlH}_{Al:H} = G(Al_{fcc}) + 1/2G(H_2, gas) + 100000$; $^0G^{NaH}_{Na:H} = G(Na_{fcc}) + 1/2G(H_2, gas) + 130T$

$^0L^{fcc}_{Al:H,Va} = -45,805 + 56.43T$ [127]

$^0G^{MgH}_{Mg:H} = G(Mg_{fcc}) + 1/2G(H_2, gas) + 100000$

$^0L^{fcc}_{Al:Mg,Va} = 3349.069 - 1.6763T$; $^1L^{fcc}_{Mg:Al,Va} = 169.787 - 3.05459T$; $^0L^{fcc}_{Al,Na:Va} = 77741.6$; $^0L^{fcc}_{Mg,Na:Va} = 20000$ This work

Nonstoichiometric compounds [128]

γ ($Al_{12}Mg_{17}$): $(Mg)_{10}(Al,Mg)_{24}(Al,Mg)_{24}$:

$G^{\gamma}_{Mg:Al:Al} = 10G(Mg_{hcp}) + 48G(Al_{fcc}) + 178762.96 - 203T$; $G^{\gamma}_{Mg:Mg:Al} = 34G(Mg_{hcp}) + 24G(Al_{fcc}) - 208742 + 78.474T$

$G^{\gamma}_{Mg:Al:Mg} = 34G(Mg_{hcp}) + 24G(Al_{hcp[}) + 359507.2 - 197.664T$; $G^{\gamma}_{Mg:Mg:Mg} = 58G(Mg_{hcp}) + 359153.4 - 174.58T$

β(A_3Mg_2): $(Al)_{19}(Al,Mg)_2(Mg)_{12}$:

$G^{\beta}_{Al:Al:Mg} = 12G(Mg_{hcp}) + 21\mathrm{G}(Al_{fcc})$-82110.6 $- 13.8072T$; $G^{\beta}_{Al:Mg:Mg} = 14G(Mg_{hcp}) + 19\mathrm{G}(Al_{fcc})$-72445.56-27.6144T

Stoichiometric compounds

MgH_2: $G^0_{MgH_2} = -82,842.15 + 25.42T - 2.87T\ln T - 55.30\square 10^{-3}T^2 - 34,305.5T^{-1}$ [117]

NaH: $G^0_{NaH} = -75,767.99 + 293.72T - 48.69T\ln T - 0.26\square 10^{-3}T^2 + 1.80\square 10^{-8}T^3 + 632,658.0T^{-1}$ [117]

$NaMgH_3$: $G_{NaMgH_3} = -157,905.82 + 185.83T - 33.6T\ln T - 61.27\square 10^{-3}T^2$ [117]

AlH_3: $G_{AlH_3} = -28,415 + 213.712933T - 41.75632T\ln T - 14.548469\square 10^{-3}T^2 + 446400T^{-1}$ [127]

ε ($Al_{30}Mg_{23}$): $G_{\varepsilon} = 23G(Mg_{hcp}) + 30\mathrm{G}(Al_{fcc})$-116327.71+1673.42T [128]

Al_2Li_3: $G_{Al_2Li_3} = 2G(Al_{fcc}) + 3G(Li_{bcc}) - 89{,}690 + 33.96T$ This work

Al_4Li_9: $G_{Al_4Li_9} = 4G(Al_{fcc}) + 9G(Li_{bcc}) - 438{,}967.89 + 69.28T$ This work

---

In section 3.4.2, thermodynamic calculations conducted to analyze and understand the hydrogen storage behaviour of the Al-Mg-H and Al-Mg-Na-H systems are presented in comparison with the experimental data cited in section 3.2.2.

3.4.1 Thermodynamic description of the Al-Mg-Na-H system

3.4.1.1 Al-Mg and Al-H systems

The calculated Al-Mg and Al-H phase diagrams at 1 bar are presented in Figures 3.1 and 3.2. Pressure temperature diagram for AlH_3 hydride is presented in Figure 3.2b. It can be seen that AlH_3 is not stable under ambient temperature and pressure conditions.

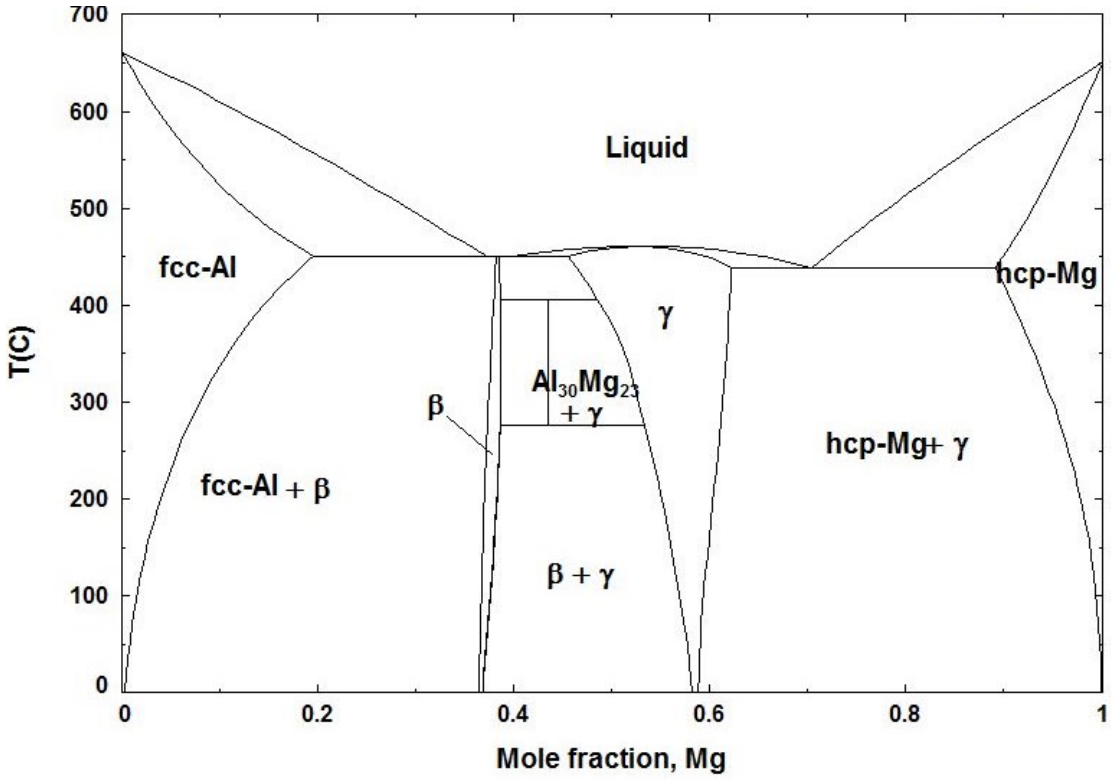

Figure 3.1 Calculated Al-Mg phase diagram at 1 bar

3.4.1.2 Al-Na system

The model parameters used in Al-Na system are listed in Table 3.1. For the liquid phase, the parameters have been determined using the Na solubility in liquid Al [132-136] and Na activity in liquid Al [137, 138] experimental data. The calculated Al-Na phase diagram is presented in Figure 3.3a. Figure 3.3b and 3.3c give an enlarged view of the Al-rich part of the calculated phase diagram in comparison with experimental data.

The experimental Na solubility in liquid Al results reported by Hensen *et al.* [135] are reported in Figure 3.3b for comparison and have not been considered reliable in this work because of their disagreement with all the data reported in the literature. The calculated Na solubility in liquid Al shown in Figure 3.3b are in reasonable agreement with the experimental data especially those reported by Fink *et al.* [133] . In fact, as pointed out by Murray [131], the results of Scheuber *et al.* [132] are not certain due to hydrogen contamination. As can be seen in Figure 3.3b, these results [132] are very close to those of Fellner *et al.* [136]. The experimental data reported by Ransley and Neufeld [134] have been given higher weight by Murray [131] and by Zhang *et al.* [106] in their assessment of the Al-Na system because of high purity Al and the experimental procedure used. The calculated phase diagram by Murray fits the phase diagram data of Ransley and Neufeld [134]. However, Murray [131] did not consider recent Na solubility data and Na activity in liquid Al. The results presented in this work are in reasonable agreement with those of Zhang *et al.* [106]. The invariant reactions in Al-Na system in comparison with experimental data and previous calculations are listed in Table 3.2.

Table 3.2*: Calculated invariant reactions in Al-Na system in comparison with data from the literature*

Reaction	Temperature (K)	Na concentration (at.%)			Reference
Gas + Liquid → Liquid1+Liquid2	1155[c]	100	0.27	100	This work
	1157[c]	100	0.238	100	[106]
Liquid1+Liquid2 → fcc-Al+Liquid2	932[c]	0.15	0.0023	100	This work
	932[c]	0.14	0.002	100	[106]
	932[c]	0.18	0.0023	100	[131]
	932[ex]	0.18	<0.003	100	[133]
	932[ex]	0.14	0.002	100	[134]
fcc-Al + Liquid2 → fcc-Al+bcc-Na	370.7[c]	100	0	100	This work
	371[c]	99.99	7.03×10^{-10}	100	[106]

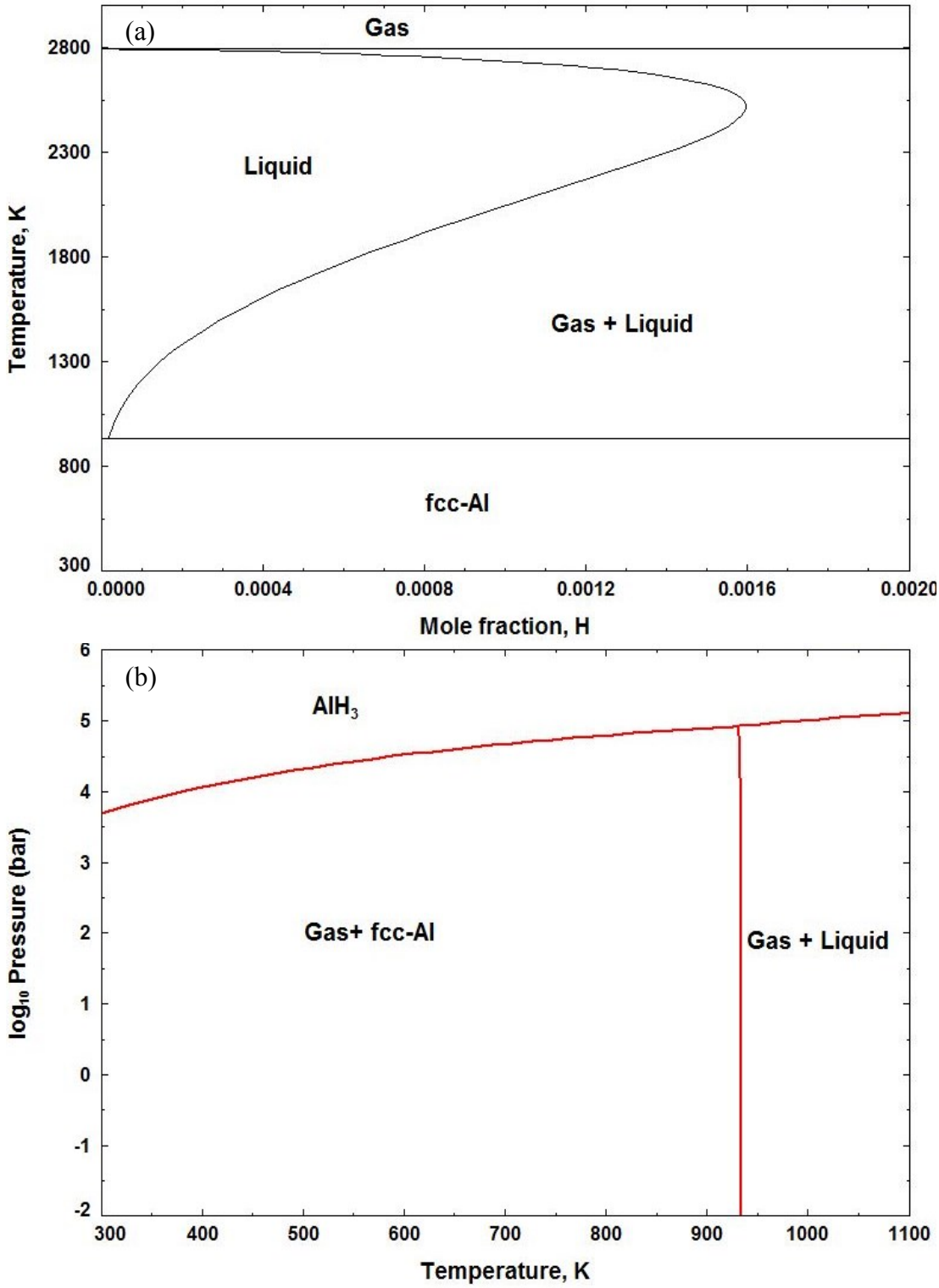

Figure 3.2 (a) Calculated Al-H phase diagram and (b) AlH_3 pressure temperature diagram

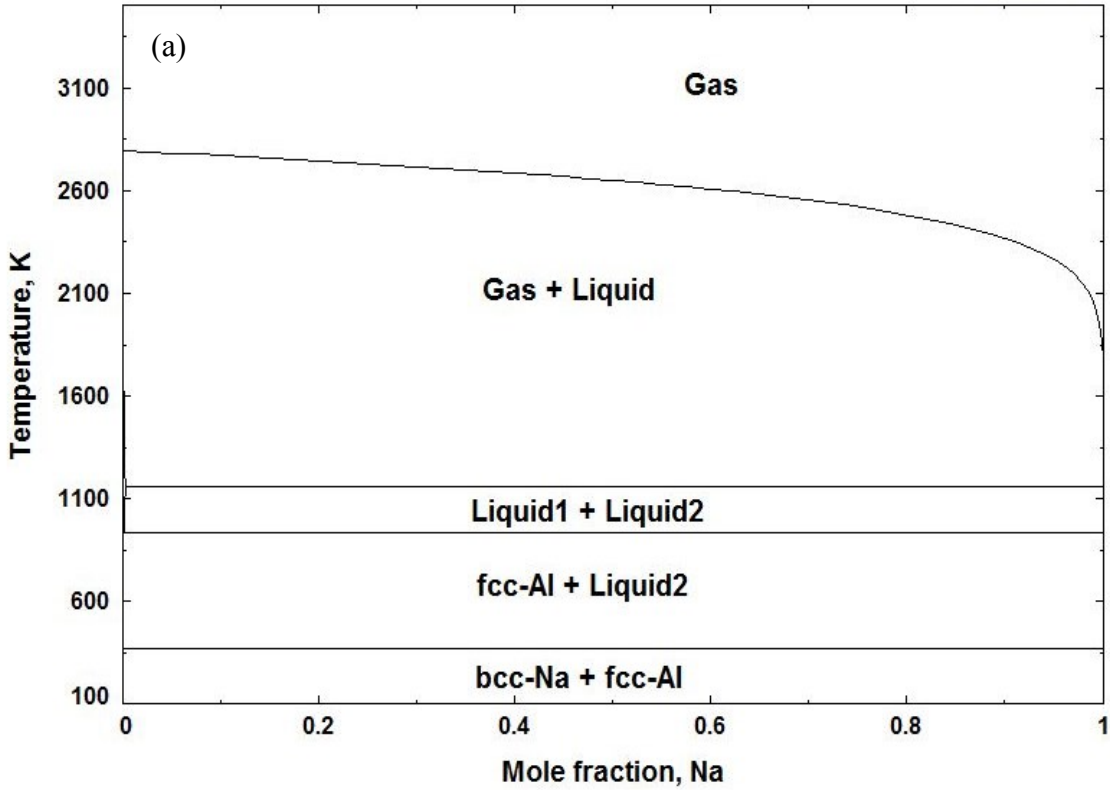
(a)
Gas
Gas + Liquid
Liquid1 + Liquid2
fcc-Al + Liquid2
bcc-Na + fcc-Al
Temperature, K
Mole fraction, Na
3100
2600
2100
1600
1100
600
100
0
0.2
0.4
0.6
0.8
1

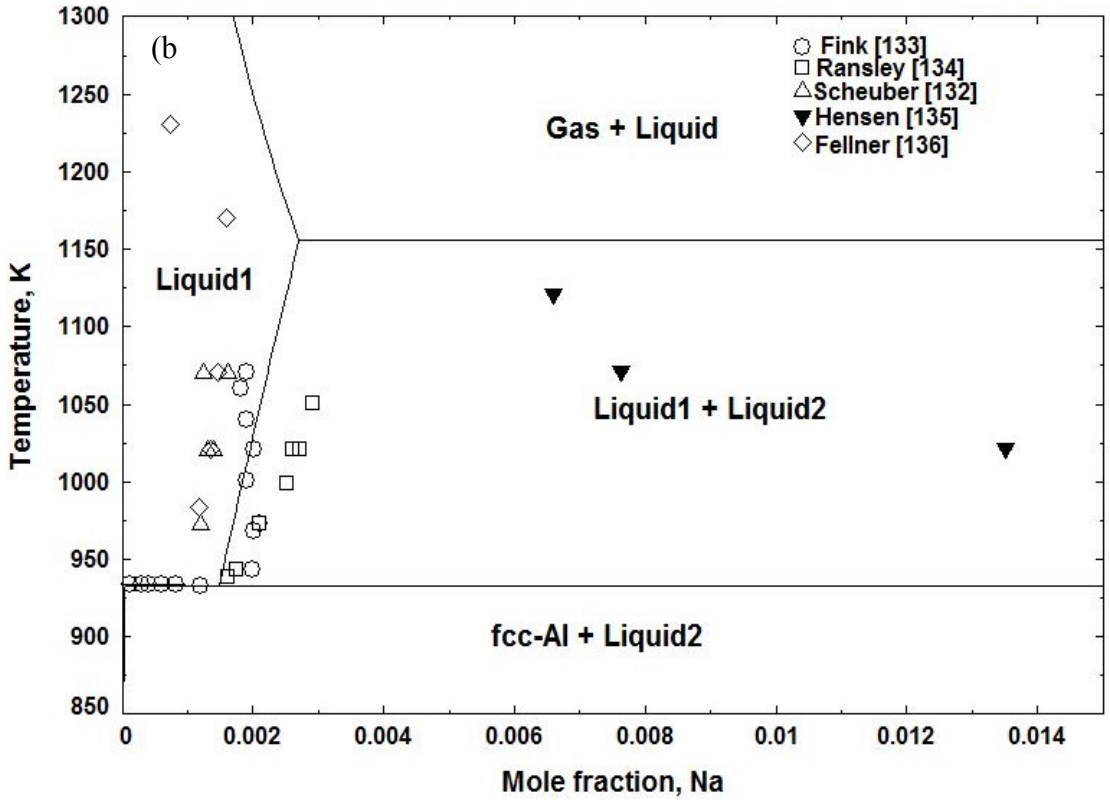
(b
Fink [133]
Ransley [134]
Scheuber [132]
Hensen [135]
Fellner [136]
Gas + Liquid
Liquid1
Liquid1 + Liquid2
fcc-Al + Liquid2
Temperature, K
Mole fraction, Na
1300
1250
1200
1150
1100
1050
1000
950
900
850
0
0.002
0.004
0.006
0.008
0.01
0.012
0.014

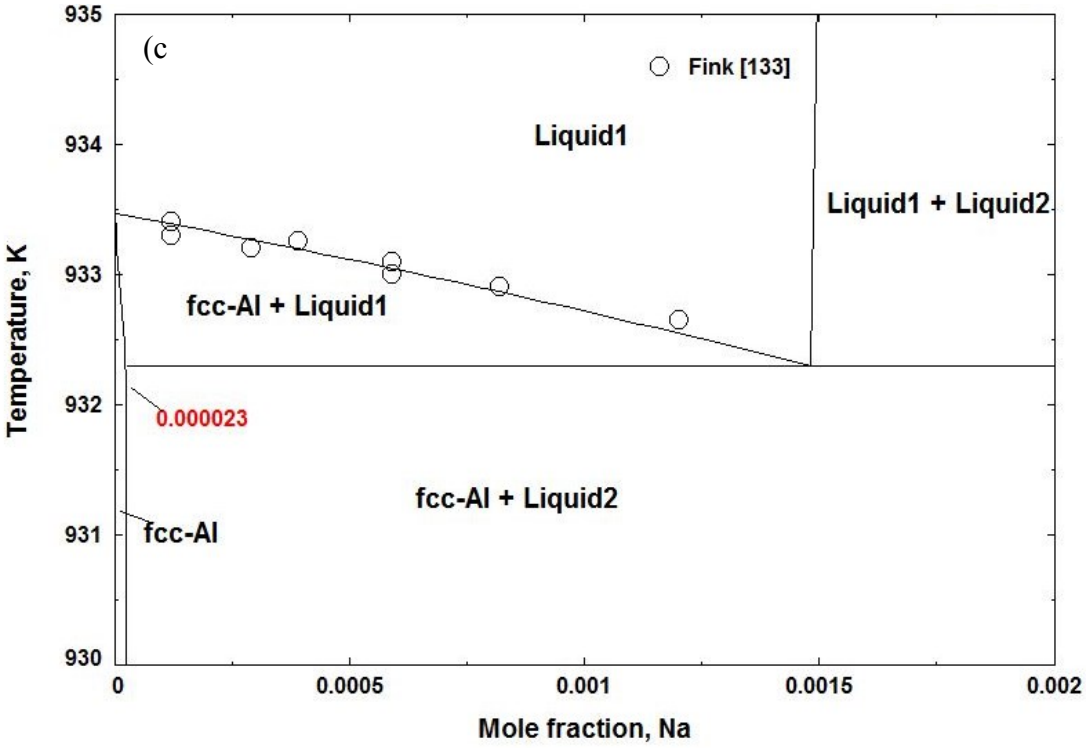

Figure 3.3 (a) Calculated Al-Na phase diagram, (b) Al-rich side of Al-Na phase diagram in comparison with experimental data, (c) enlarged view of b

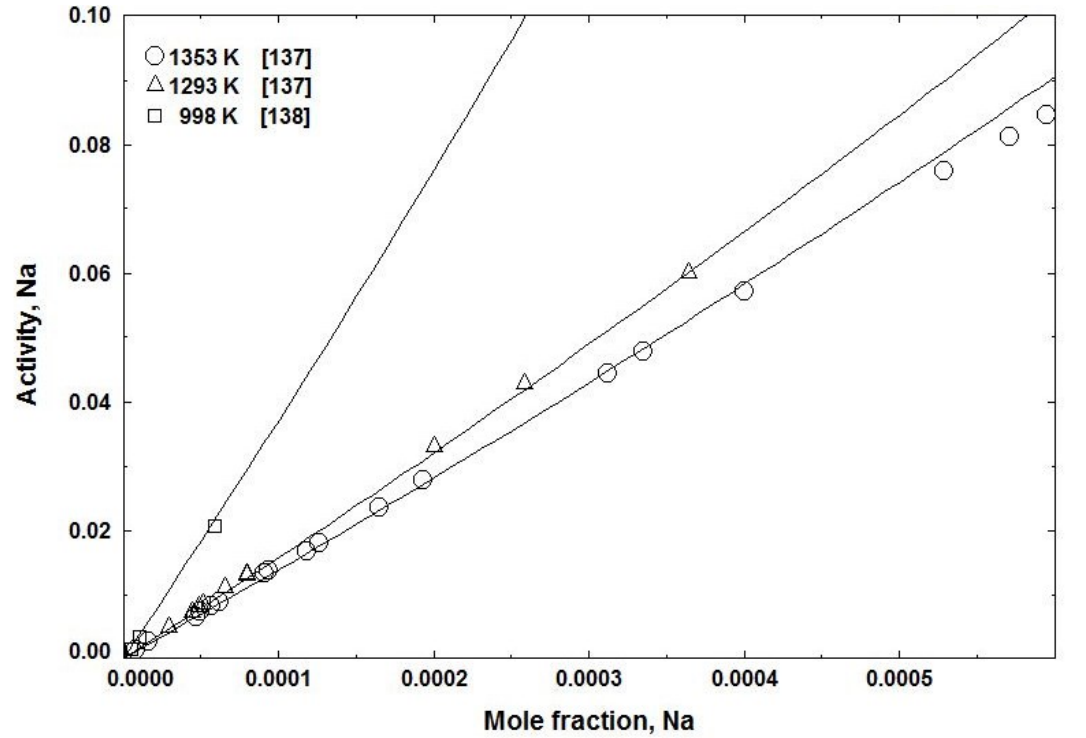

Figure 3.4 Calculated activity of Na in liquid Al-Na in comparison with experimental data

The calculated activities of Na in Al-Na liquid at 1353, 1293, and 998 K in comparison with experimental data from the literature, are presented in Figure 3.4. There is a very good agreement between the calculated activity and the experimental data for Na concentrations below 0.04 at%. For Na concentrations above 0.04 at.%, the calculated activities at 1353 K are higher than the experimental data determined by Dewing [137]. As pointed out by Dewing [160], the experimental procedure (quenching) used in [137] may have been source of errors.

3.4.1.3 Al-Mg-H system

The calculated enthalpy of formation and decomposition of $Mg(AlH_4)_2$ are given in Table 3.3 in comparison with data from the literature.

Good agreement is shown between the calculated heat of formation and decomposition of magnesium alanate and the calculations made by Palumbo *et al.* [144] and the experimental data of Claudy *et al.* [161].

***Table 3.3**: Thermodynamic properties of formation and decomposition of $Mg(AlH_4)_2$*

Reaction	Temperature, K	ΔH (kJ/mole)	Reference
$2Al + Mg + 4H_2 \rightarrow Mg(AlH_4)_2$	298.15	-79.1	This work
	298.15	-79.0[c]	[144]
	298.15	-80.33	[161]
	298.15	-82.8[c]	[145]
$Mg(AlH_4)_2 \rightarrow MgH_2 + 2Al + 3H_2$	298.15	1.8	This work
	435	1	[144]
	423	1.7	[146]
	435	0	[161]
	398-423	~ 0	[147]
	393	~ 2	[149]

[c] calculated using CALPHAD technique

The calculated temperature-pressure (PT) diagram for $Mg(AlH_4)_2$ is given in Figure 3.5a. Figure 3.5b shows the calculated reaction path of $Mg(AlH_4)_2$ at 1 bar. Figure 3.5a shows that magnesium alanate is less stable than AlH_3 and will not form even at very high pressures. At 1bar, $Mg(AlH_4)_2$ decomposes spontaneously to form MgH_2, fcc-Al, and gas phase. By increasing the temperature, MgH_2 decomposes to fcc-Al, β, and gas phase at 234°C following reaction (3.2) as can be seen in Figure 3.5b. These results are in good agreement with the literature. In fact, Palumbo *et al.* [144] calculated a temperature of 230°C for reaction (3.2) and values in the range 217-240°C have been reported using DSC experiments [146-148].

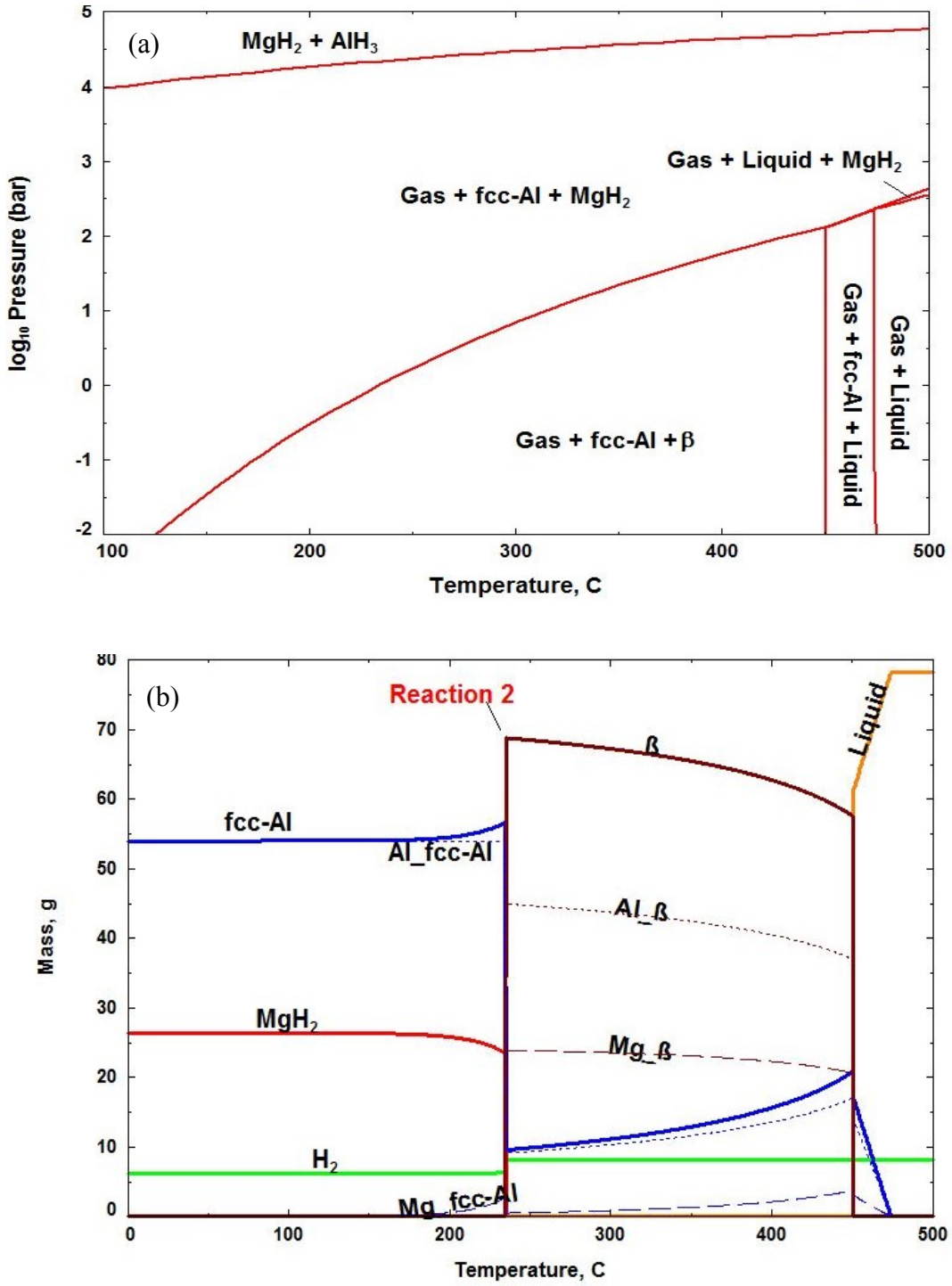

Figure 3.5 a) P-T diagram and b) decomposition reaction path, of $Mg(AlH_4)_2$ at 1 bar

As mentioned in section 3.2.1.4, Liu *et al.* [151] expressed fcc-Al as $Al_{0.9}Mg_{0.1}$ in equation (3.5) by taking into account the value of the maximum solubility of Mg in fcc-Al at 320°C as 10 at.%. However, the fact that MgH_2 decomposition kinetics was poor during the experiments and that MgH_2 started to release its hydrogen effectively at around 320°C does not indicate clearly that the composition of fcc-Al corresponds to its equilibrium composition at 320°C.

In Figure 3.5b, the different phases are presented with different colors and the Al and Mg components of each phase are presented with doted and dashed lines, respectively, with the same color as the phase. Figure 3.5b shows that the decomposition of MgH_2 is preceded by a gradual decrease in the amount of MgH_2 caused by its partial gradual decomposition with an increase in the amount of fcc-Al in which the produced Mg has dissolved.

According to these calculations, the composition of fcc-Al at 234°C is 94.89% Al, 5.10% Mg, and 2.5×10^{-7} % H, which shows that the solubility of hydrogen in fcc-Al is negligible at this temperature and the solubility of Mg in fcc-Al is equal to its solubility limit in Al-Mg system at this temperature (Figure 3.1).

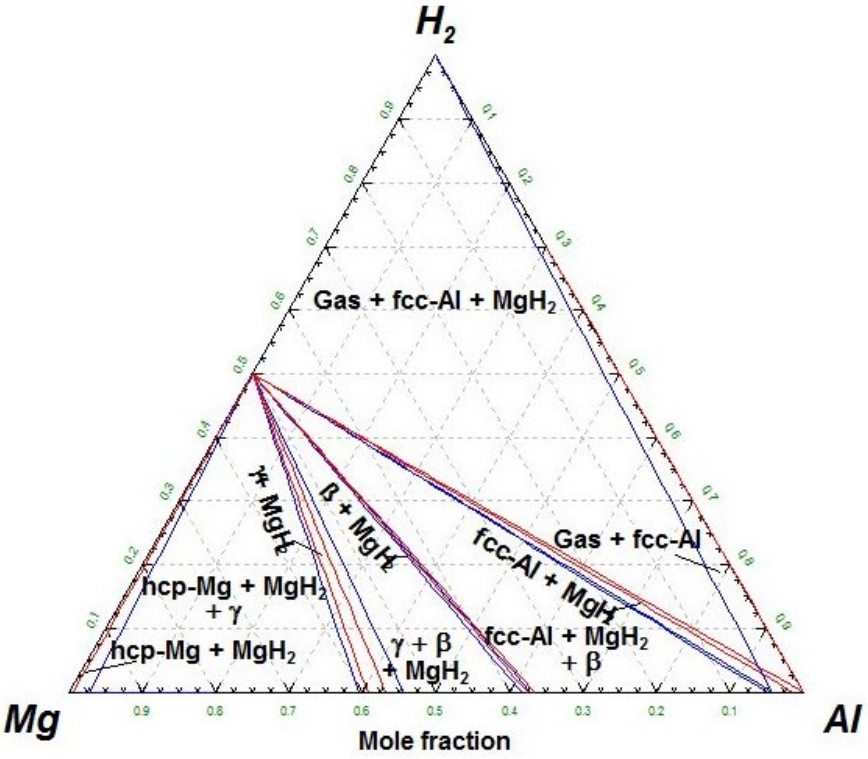

Figure 3.6 Calculated isothermal section of the Al-Mg-H_2 phase diagram at 100°C (in red) and 230°C (in blue)

The calculated vertical section of the Al-Mg-H_2 phase diagram at 100°C and 230°C is presented in Figure 3.6. It shows that the composition of the hydrided Al-Mg system depends on the hydrogen gas amount added. Above 0.5mole fraction H_2, the system is composed of gas, fcc-Al and MgH_2 phases in proportions depending on the relative amounts of Mg and Al.

3.4.1.4 Al-Mg-Na system

There are no experimental data for the Al-Mg-Na ternary system, the calculated isothermal sections at 100°C and 500°C are presented in Figure 3.7. Liquid2 corresponds to liquid Na and Liquid1 to liquid Al-Mg. Figure 3.8 shows the calculated vertical section of Al-Mg-Na system along the composition line AlNa-Mg at 1bar in comparison with Al-Mg phase diagram (dotted red line). The presented vertical sections reproduce the phase relations and the miscibility gaps in the binary phase diagrams. It can be seen that Na does not affect the phase relations in the Al-Mg phase diagram at 1 bar except the presence of bcc-Na or liquid Na, which shows the limited solubility of Na in hcp-Mg, fcc-Al, and the Al-Mg compounds. Only a small decrease in the melting point of hcp-Mg is observed when Na is added to Al-Mg mixture.

(a)

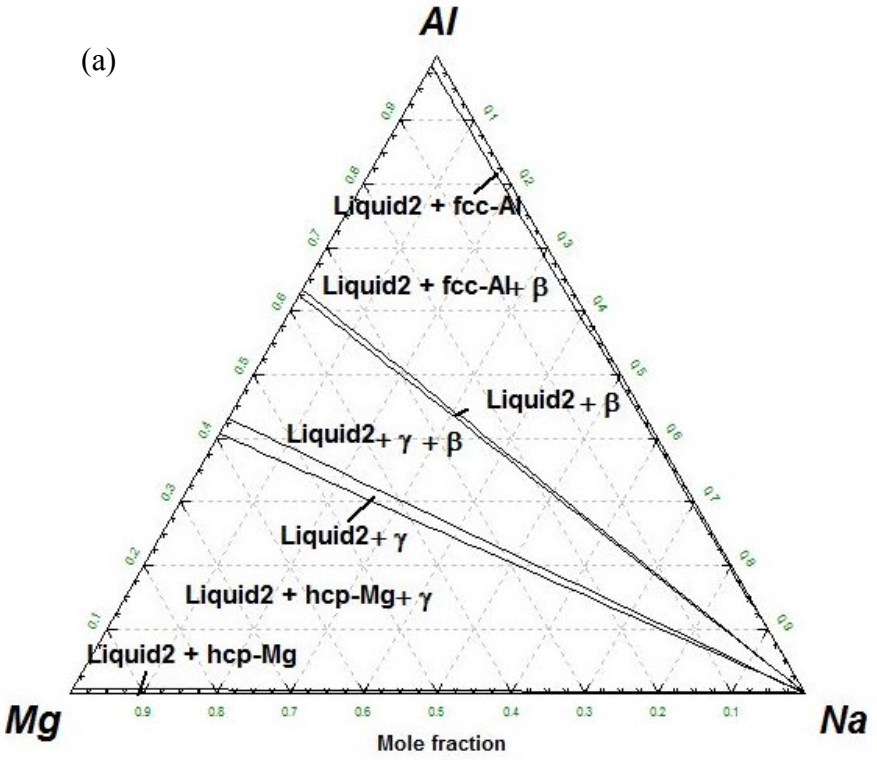

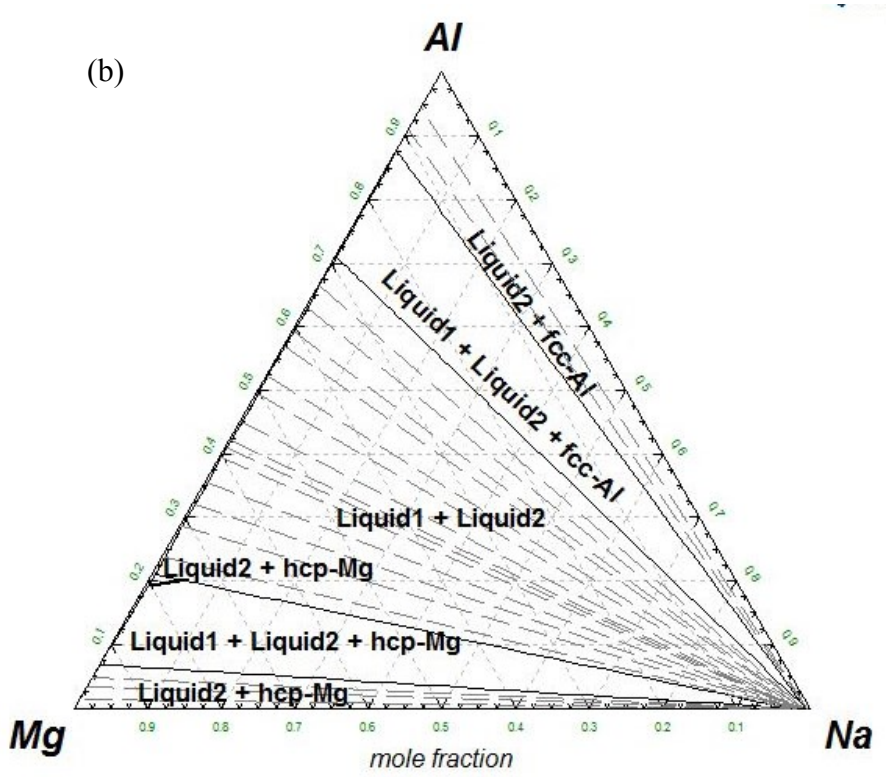

Figure 3.7 Calculated Al-Mg-Na isothermal sections at 1 bar and, a) 100°C, b) 500°C

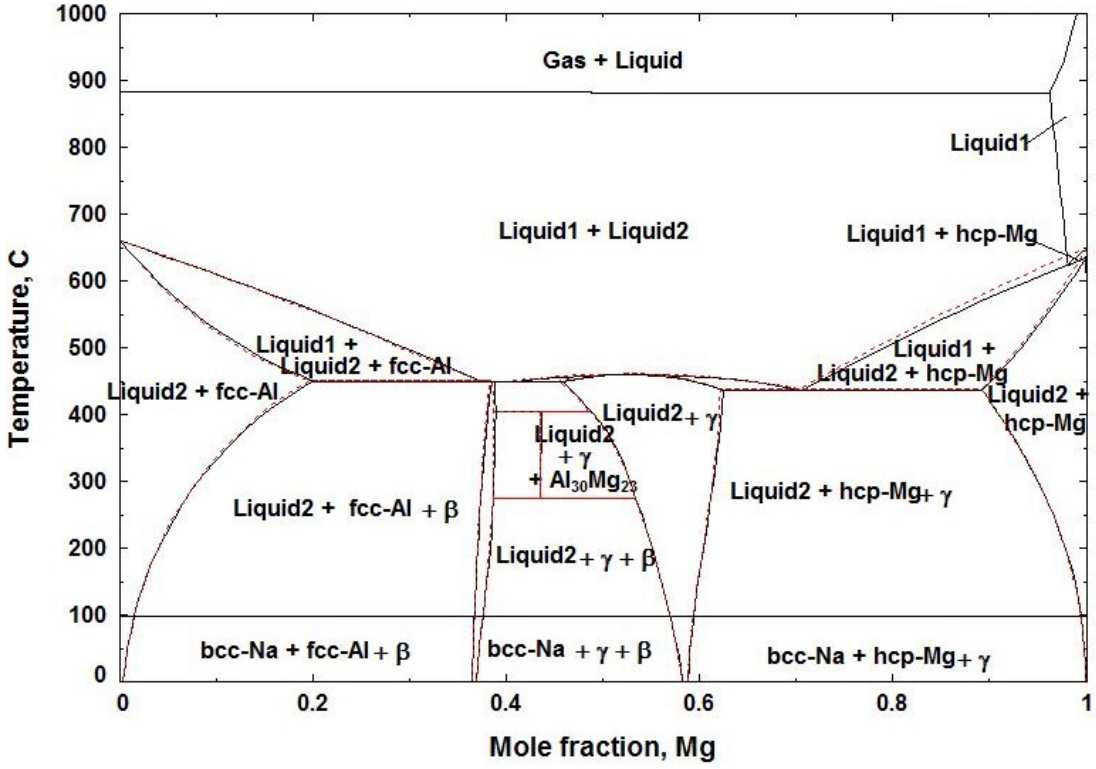

Figure 3.8 Calculated vertical section in Al-Mg-Na system along the composition line AlNa-Mg compared to the calculated Al-Mg phase diagram (dashed line) at 1 bar

3.4.1.5 Al-Na-H system

The calculated PT diagrams of $NaAlH_4$ is presented in Figure 3.9. It shows the evolution of the decomposition temperature of sodium alanates with the pressure. $NaAlH_4$ decomposes in two steps following equations (3.3) and (3.4) and the decompositions temperatures at 1 bar are 21.45°C and 106.58°C, respectively. At 10 bar, these temperatures increase to 81.68°C and 179.02°C for reactions (3.3) and (3.4), respectively.

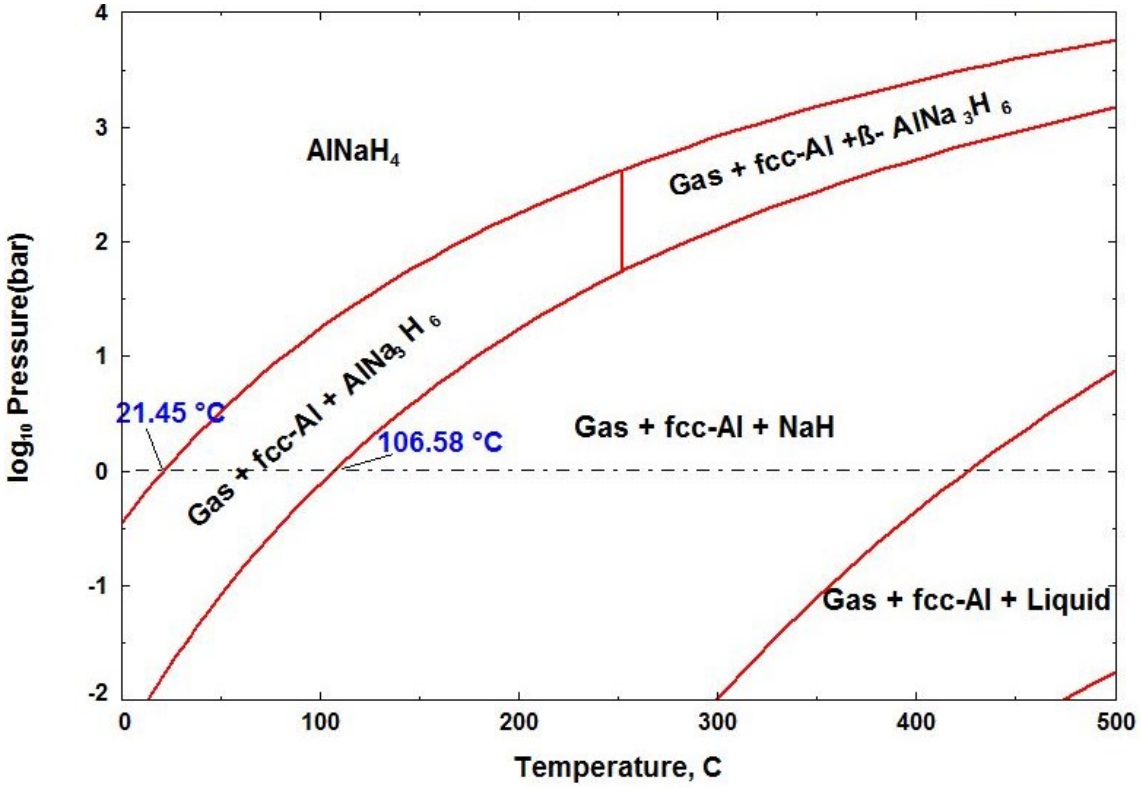

Figure 3.9 P-T diagram of $NaAlH_4$

The calculated isothermal sections of the Al-Na-H_2 system at room temperature, at 1bar and 10 bar are presented in Figure 3.10 to show the phase relations in these conditions. To show the stability of the hydrides and their decomposition temperatures in this system, vertical sections at different pressures can be calculated using the database developed in this work. As an example, the calculated vertical sections along the composition line AlH_3-NaH at 1 bar and 10 bar are shown in Figure 3.11.

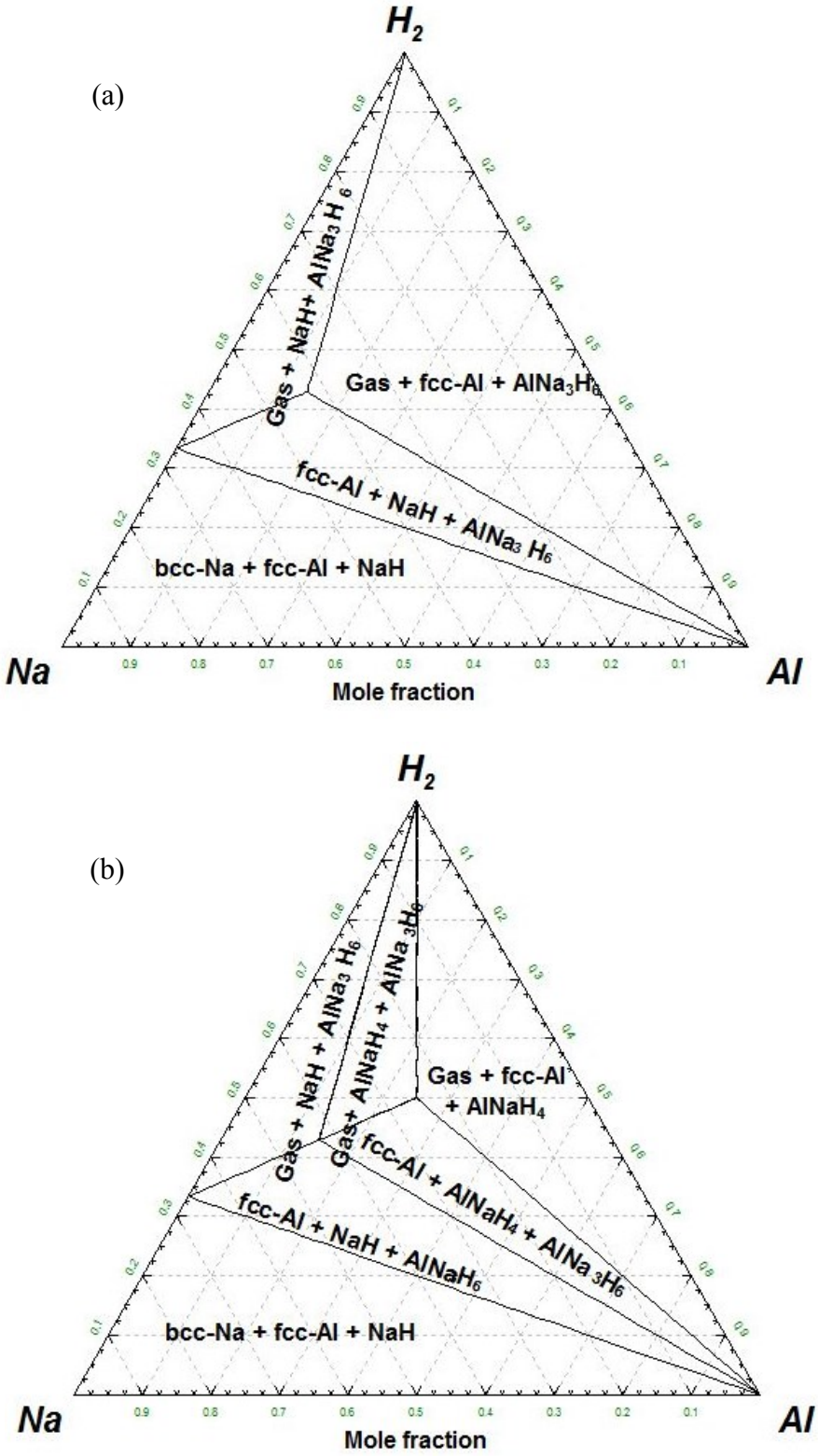

Figure 3.10 Calculated Al-Na-H_2 isothermal section at 25°C and a) 1 bar, b) 10 bar

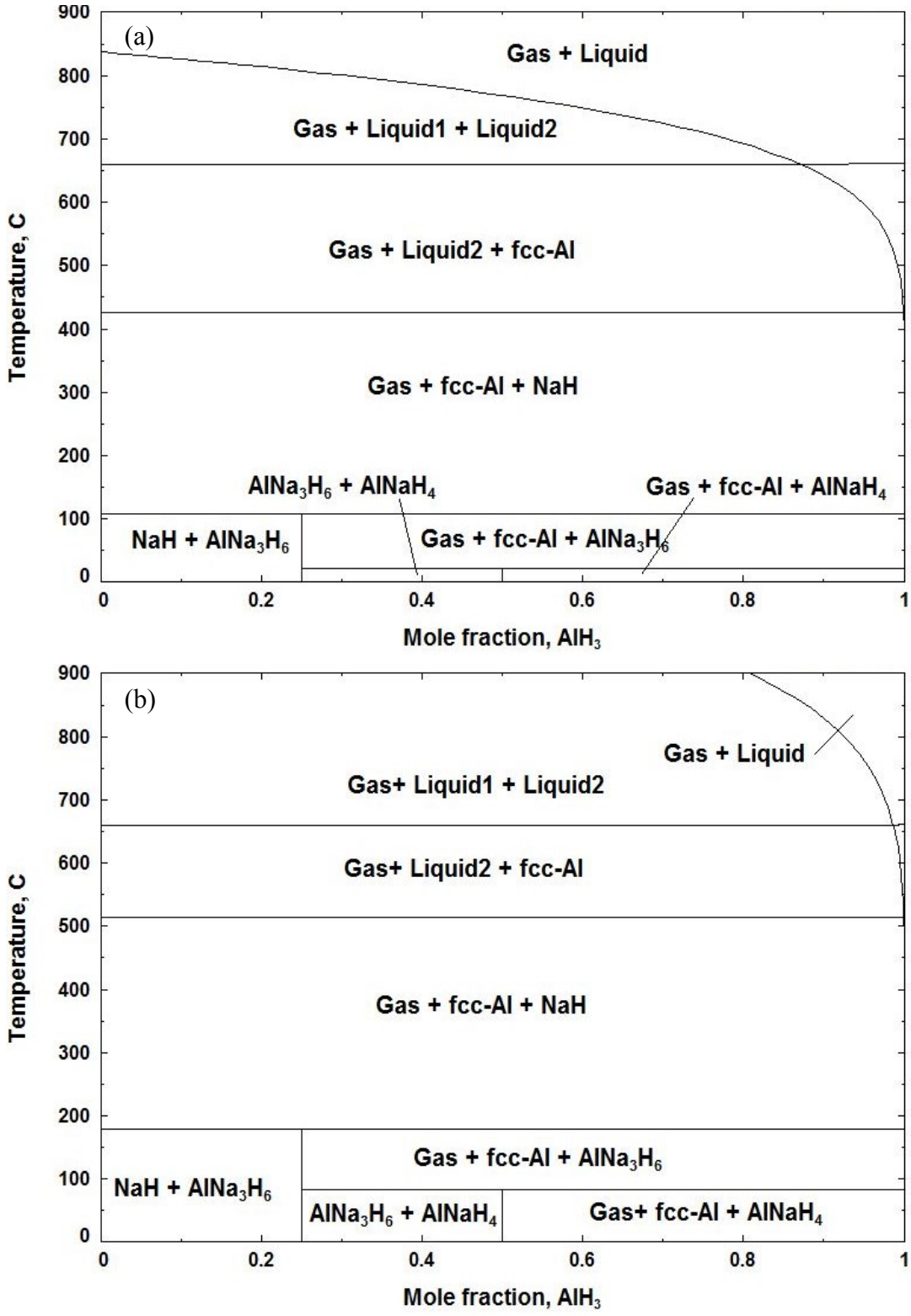

Figure 3.11 Calculated AlH_3-NaH vertical section at a) 1bar, and b) 10bar

3.4.2 Hydrogen storage analysis of Al-Mg-Na-H system using thermodynamic modeling

3.4.2.1 Al-Mg-H system

The calculated phase diagram of MgH_2+AlH_3 at 1bar is presented in Figure 3.12a. An enlarged view of MgH_2-rich part of MgH_2+AlH_3 phase diagram is presented in Figure 3.12b. It can be seen that MgH_2 decomposition process depends on Al content. Five regions are identified in Figure 3.12a separated by blue dotted lines. For AlH_3 mole fraction below 0.045, the decomposition of MgH_2 occurs in four steps according to the following reactions (the third and the fourth steps can be seen in Figure 3.12b):

$$MgH_2 + \text{fcc-Al} \xrightarrow{234°C} MgH_2 + \beta + H_2 \xrightarrow{257.8°C} MgH_2 + \gamma + H_2 \xrightarrow{283.3°C} MgH_2 + \text{hcp-Mg} + H_2$$
$$\xrightarrow{284.7< T°C< 283.3} \text{hcp-Mg} + H_2 \qquad (3.7)$$

The decomposition temperature of the last reaction in equation (3.7) varies from 284.73°C for pure MgH_2 to 283.3°C for 0.045 mole fraction of Al as can be seen in Figure 3.12b. This small difference can be explained by the solubility of Al in hcp-Mg.

For AlH_3 between 0.045 and 0.46 mole fraction, MgH_2 decomposes in three steps. For AlH_3 between 0.46 and 0.63 mole fraction, decomposition proceeds in two steps. For AlH_3 content between 0.63 and 0.95 mole fraction, MgH_2 decomposes in only one step at 234°C. It should be noted that, for AlH_3 content starting from 0.95 mole fraction, the decomposition temperature of MgH_2 decreases with increasing Al content.

The predicted reactions in the system are compared with the results of Liu *et al.* [125] on the dehydrogenation process of MgH_2+AlH_3 mixture. This composition corresponds to 0.5 mole fraction AlH_3 on Figure 3.12a where it is marked by a red doted line.

First, Liu *et al.* [125] reported that the decomposition temperature of MgH_2 in the mixture is reduced by 55°C compared to the pure MgH_2 and atributed this decrease to the interaction between MgH_2 and Al. According to our previous paper [117], the theoretical decomposition temperature of MgH_2 is 284.73°C, 50.73°C higher than the calculated first decomposition step in this mixture (234°C), which is consistent with the results of Liu *et al.* [125]. However, the temperatures they [125] reported were higher as a result of the slow kinetics and the long time required to reach equilibrium [125]. Temperatures in the ranges 217-250°C (DSC) [146, 147] and 210-220°C (in-situ XRD) [146] have also been reported.

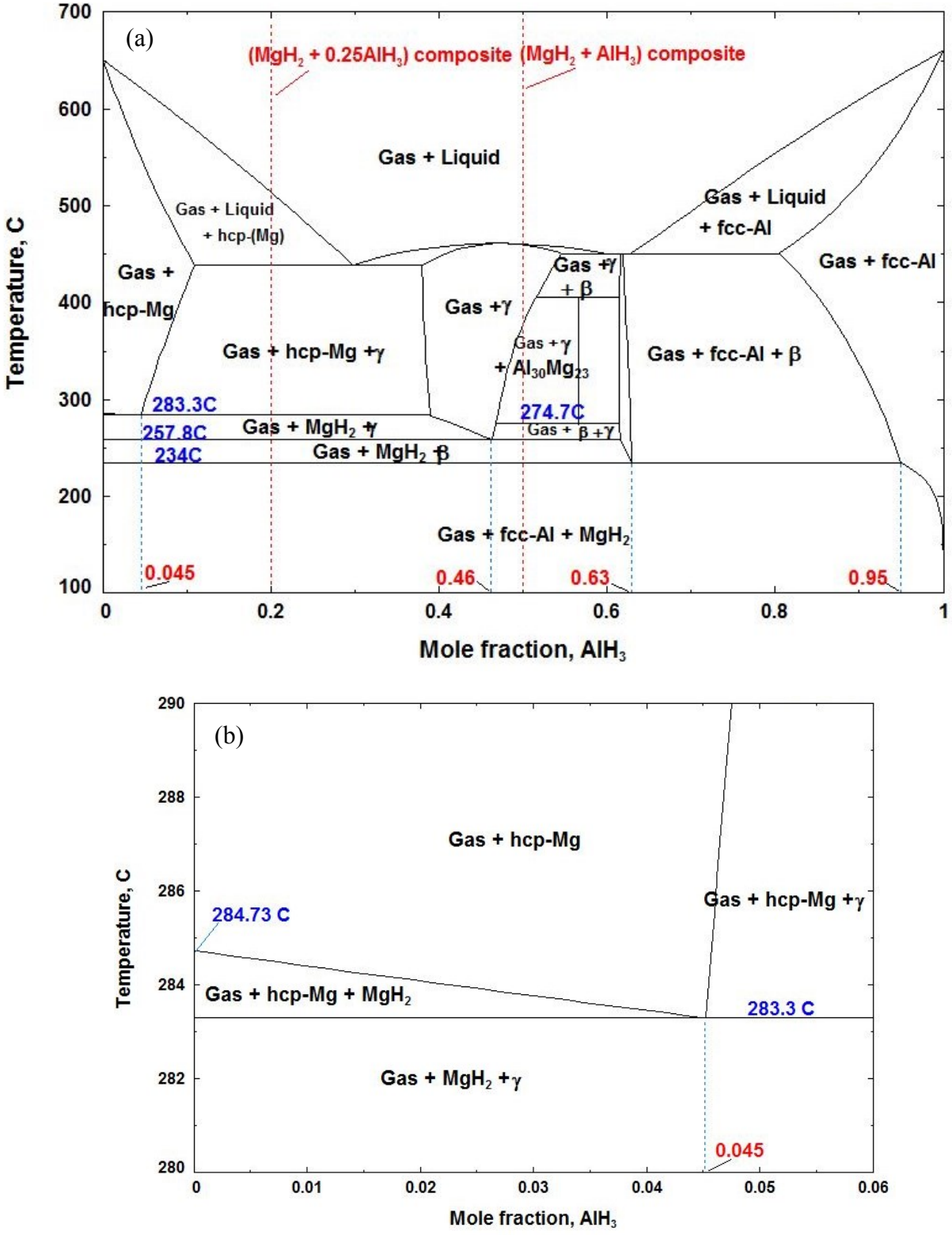

Figure 3.12 a) Calculated MgH_2-AlH_3 phase diagram at 1 bar, b) An enlarged view of a)

In their second investigation on the thermal decomposition of MgH_2/AlH_3 composites, Liu *et al.* [126], using DSC and MS-(H_2), found that the onset and peak temperatures of the first decomposition of MgH_2 in the mixtures decrease with increasing the amount of AlH_3. The onset temperatures were 252°C, 248°C, and 243°C for MgH_2/AlH_3 composites with molar ratios: 1:0.25, 1:0.5, and 1:1, respectively. The reported onset temperature for the first decomposition of MgH_2 [126] approaches gradually the calculated value of 234°C. This indicates that AlH_3, in addition to destabilizing MgH_2, improves its decomposition kinetics.

Second, Liu *et al.* [125] reported three stages during the thermal decomposition of the mixture MgH_2+AlH_3 using DSC-MS (H_2). The first stage was related to the decomposition of AlH_3. The second stage, which might be composed of two overlaping peaks [125], was attributed to the reaction of MgH_2 and Al to form γ phase. The last step was atributed to the melting of γ phase. AlH_3, as shown in Figure 3.2b, is not stable in normal conditions and will decompose spontaneously. The first stage observed by Liu *et al.* [125] can be explained by poor kinetics.

In Figure 12a, the thermal decomposition steps of MgH_2+AlH_3 composite can be followed along the doted red line marking this composition. The process is as follows:

$$MgH_2 + \text{fcc-Al} \xrightarrow{234°C} MgH_2 + \beta + H_2 \xrightarrow{257.86°C} \beta + \gamma + H_2 \xrightarrow{274.76°C} Al_{30}Mg_{23} + \gamma + H_2$$
$$\xrightarrow{379.4°C} \gamma + H_2 \xrightarrow{458.98<T°C<460.16} \text{Liquid} + H_2 \qquad (3.8)$$

Equation (3.8) shows an overall agreement with the results of Liu *et al.* [125] and gives a more detailed description of the process. This can be explained by the fact that the process suffers from poor kinetics and that the reaction temperatures are too close to observe distinct steps using DSC-MS (H_2) experiements. However, XRD analysis [125] showed that the mixture is composed of MgH_2 and Al at 200°C, and of γ phase at 400°C, which is consistent with the calculations shown in equation (8) and Figure 3.12a.

Liu *et al.* [126] investigated the structure evolution during desorption of MgH_2+$0.25AlH_3$ composites using XRD analysis of samples heated to various temperatures (from 175 to 400°C) with the same heating rate as in DSC-MS (H_2) experiements. They [126] reported a shift in the diffraction peaks of Al to small angles and the formation of β phase when the temperature was increased from 250 to 310°C. They [126] atributed Al peak shift to Mg atoms dissolution in Al lattice causing its expanssion until saturation where the new phase, β (Al_3Mg_2), formed.

However, Liu *et al.* [126] neglected the fact that this peak shift might also be caused by thermal expansion of Al lattice.

In the following step, MgH_2 reacts with β to form γ phase [126]. In the final step, the residual MgH_2 decomposes and only Mg solid solution and γ phase were detected [126].

In Figure 3.12a, the thermal decomposition steps of MgH_2+0.25 AlH_3 composite can be followed along the doted red line marking this composition. It shows a very good agreement with the results of Liu *et al.* [126] concerning the structure evolution of the composite. From Figure 3.12a, the decomposition process of MgH_2 in the composite is as follows:

$$MgH_2 + \text{fcc-Al} \xrightarrow{234°C} MgH_2 + \beta + H_2 \xrightarrow{257.86°C} MgH_2 + \gamma + H_2 \xrightarrow{283.23°C} \text{hcp-(Mg)} + \gamma + H_2 \quad (3.9)$$

Equilibrium calculations of the reaction path provide more information about the amount of phases and their composition during the thermal decomposition of the composite. In Figure 3.13, the calculated reaction path of MgH_2+0.25AlH_3 composite at 1 bar is shown. The amount of phases is expressed in gram and is presented in solid lines with different color for each phase. The amount of Al and Mg in each phase is presented with the same color as the phase, with doted and dashed lines for Al and Mg, respectively. It can be seen that, for temperatures above 200°C, the amount of fcc-Al (blue solid line) increases smoothly with temperature while the amount of MgH_2 (red solid line) decreases. Simultaneously, the Al content of fcc-Al (blue dotted line) is constant and the Mg content of fcc-Al (blue dashed line) increases smoothly, which proves that Al destabilizes MgH_2 at theses temperatures and the resulted Mg atoms dissolve in fcc-Al and increase its amount until the temperature of 234°C, where the solubility limit of Mg in fcc-Al is reached and β forms. This conclusion agrees very well with the XRD results reported in the literature[126, 148, 149, 151] observing the Al peak shift in the MgH_2/Al composites with increasing temperature until it disappears and the formation of β.

In Figure 3.13, at 234°C, it is seen that the formation of β (presented with a dark green solid line) is accompained by an abrupt decrease in the amount of MgH_2 (the solid red line). A close look at Al and Mg content in β shows that the amount of Mg in β (dashed green line) increases abruptly at 234°C too. This can be explained by the more important solubility of Mg in β. Since the first effective decomposition step of MgH_2 in MgH_2-Al mixtures is at 234°C, It can be concluded that the first effective destabilization step of MgH_2 by Al is due to the formation of β. The same conclusions can be deducted regarding the second step decomposition of MgH_2 at 257.86°C

accompained by the formation of γ. For temperatures between 257.86 and 283.23°C, the amount of MgH_2 decreases with temperature while the amount of γ increases simultaneously with the increase of the amount of Mg dissolved in it (purple dashed line). It should be noted that the amount of Al dissolved in β and γ phases (doted green and purple lines) is constant. At 283.23°C, the residual MgH_2 decomposes resulting in hcp-Mg phase.

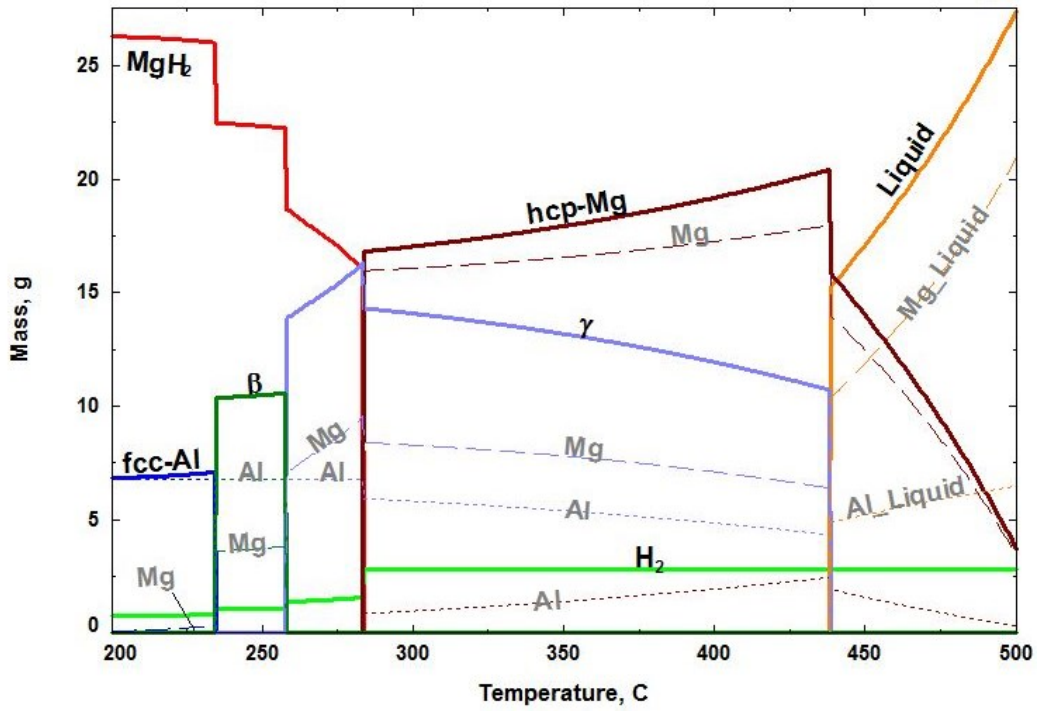

Figure 3.13 Reaction path of $MgH_2 + 0.25AlH_3$ showing the phase assemblage with temperature

The calculated PCI curve at 350°C for Mg-10 at% Al alloy is presented in Figure 3.14 and shows the presence of four plateau regions at 6.26, 12.8, 13.5, and 22 bar. The calculated hydriding reaction path of Mg-10 at% Al alloy at 350°C is presented in Figure 3.15. According to Figures 3.13 and 3.14, the initial composite is composed of hcp-Mg and γ phases. The first plateau corresponds to the formation of MgH_2 and additional γ phase from hcp-Mg. The second plateau corresponds to the hydriding of the γ phase to produce MgH_2 and $Al_{30}Mg_{23}$. The third plateau is attributed to the hydriding of $Al_{30}Mg_{23}$ to produce MgH_2 and β. The fourth plateau corresponds to the hydriding of the β phase to produce MgH_2 and fcc-Al.

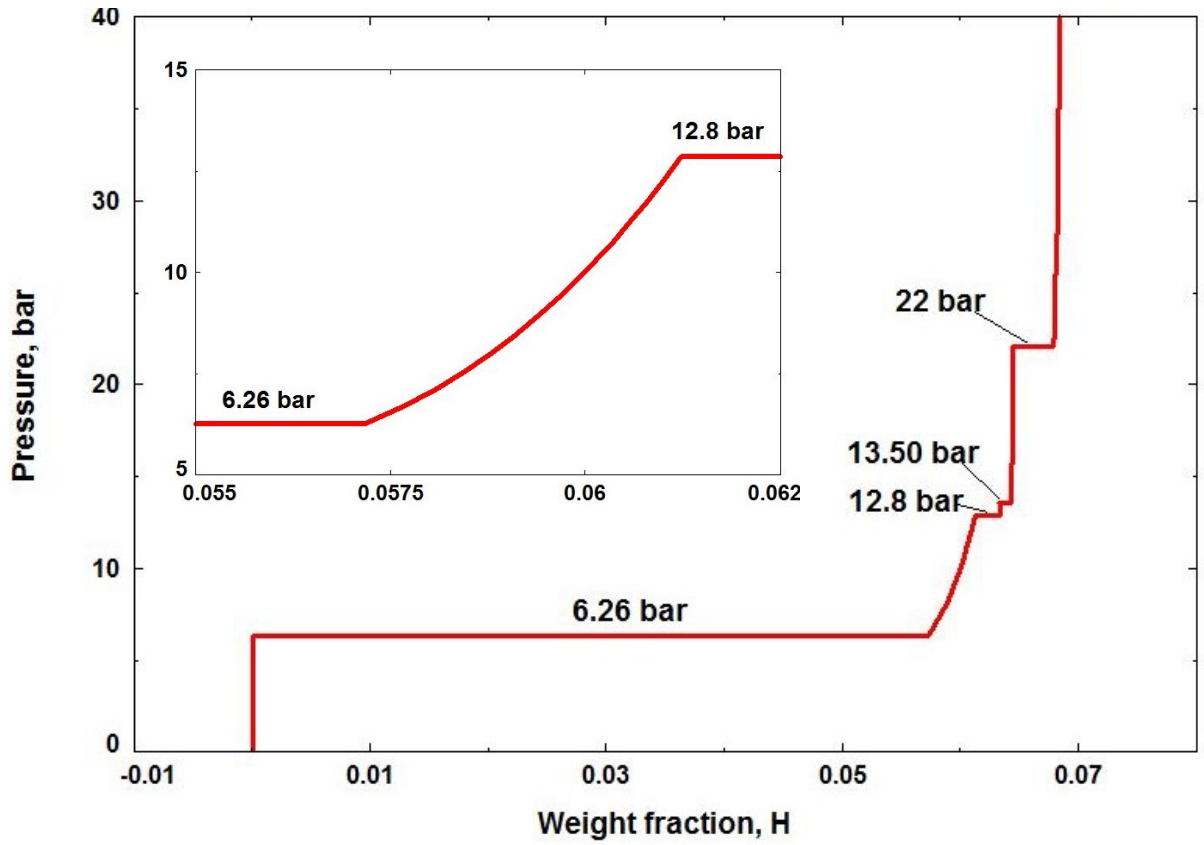

Figure 3.14 Calculated PCI curve of Mg-10at% Al at 350 °C

The results shown in Figures 3.14 and 3.15 are compared to the experimental data reported by Tanniru *et al.* [121]. These authors [121] reported the PCI curve at 350°C and the microstructural evolution of the samples (Mg-10 at% Al) during the measurements. However, they [121] could not identify the plateau pressures directly from the PCI curve because of the sloped and not well-defined plateaus resulting from the poor kinetics in addition to the small amount of hydrogen absorbed (below the theoretical capacity of the sample). For these reasons, a direct comparison between the calculated and the measured PCIs [121] is not possible. Nevertheless, the calculated plateau pressures are compared to those identified by Tanniru *et al.* [121]. Three Hydriding steps corresponding to three plateaus at 6.2, 12.7, and 22 bar have been reported [121]. These results [121] are in very good agreement with the current calculations shown in Figure 3.14 except for the calculated plateau pressure at 13.5 bar, which was not observed by these authors. This can be attributed to the small difference of pressure with the preceding step (12.8 bar) and the small

length of the plateau in addition to the poor quality of the curve. Also, microstructural analysis and phase identification at different stages of hydriding/dehydriding experiments reported by Tanniru *et al.* [121] are in good agreement with this work.

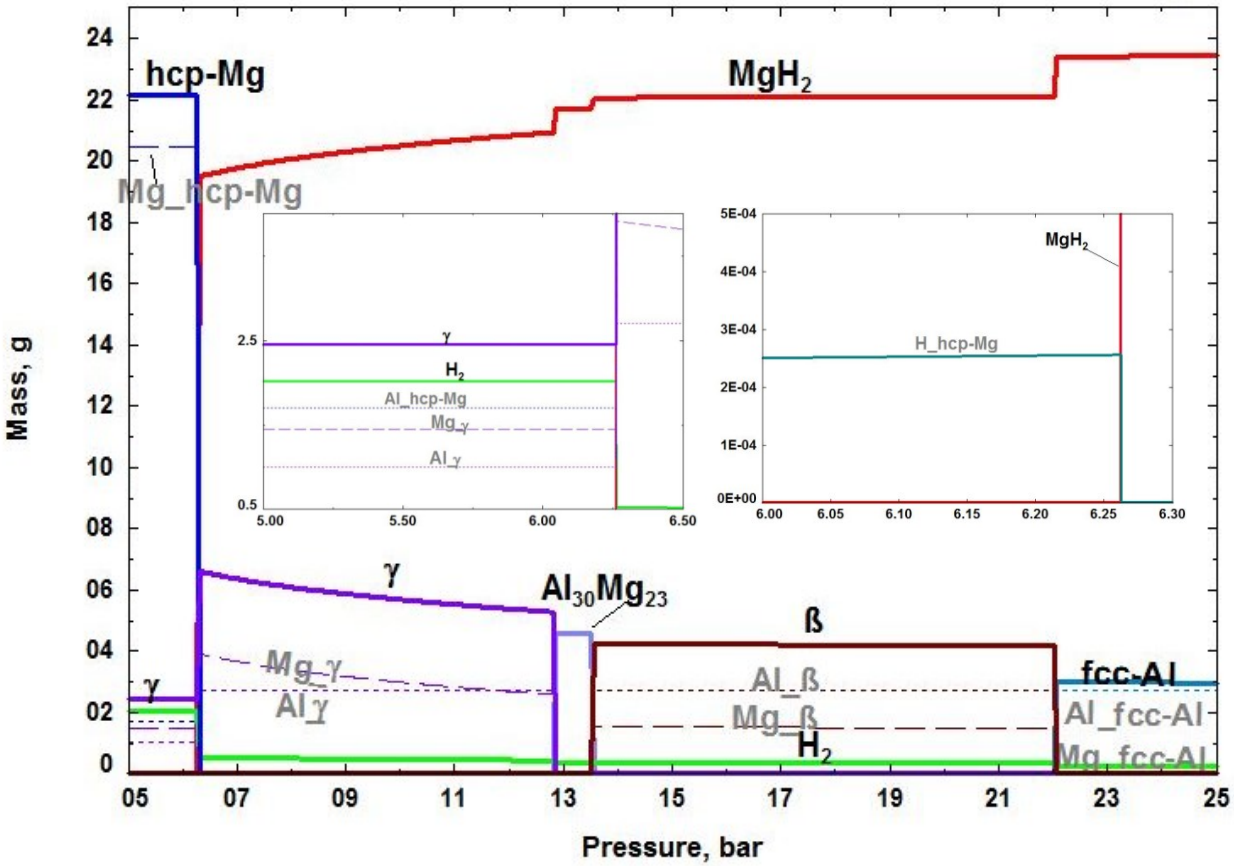

Figure 3.15 Hydriding reaction path of Mg-10at%Al at 350 °C

However, these authors [121] did not report the formation step of $Al_{30}Mg_{23}$ and therefore they combined the two-step hydriding reaction: (γ to $Al_{30}Mg_{23}$ + MgH_2 at 12.8 bar and $Al_{30}Mg_{23}$ to β + MgH_2 at 13.5 bar) in only one step: (γ to β + MgH_2 at 12.7 bar). In Figure 3.15, the amounts of Al and Mg in each phase, is presented by dotted and dashed lines, respectively, with the same color as the phase. It can be seen in Figure 3.15 that from a pressure of 6.26 and 12.8 bar, the alloy is composed of γ phase and MgH_2 and the amount of MgH_2 increases gradually in this pressure range while the amount of Mg in γ phase decreases and the amount of Al in γ phase is constant, which signifies that γ phase is being more concentrated in Al. This step takes the form

of a curved line in PCI curves (the enlarged inset in Figure 3.14) and is due to the large solubility range of γ phase. Bouaricha *et al.* [162] reported that the PCI curves of Mg-Al alloys with γ phase compositions showed slopped plateau between 8 and 15 bar, which is consistent with the trend of the PCIs calculated in this work. It can be concluded that the PCI inclined plateaus reported in the literature[156] for the Al-Mg alloys, is, in addition to kinetic factors, due to the large solubility range of γ phase, to short plateaus' length, and to the small differences between the last three plateau pressures.

Tanniru *et al.* [121] reported that the first plateau pressure increased when increasing Al content (5.4 bar, 5.7 bar, and 6.2 bar for Mg, Mg-4 at% Al, and Mg-10 at% Al, respectively) and attributed this raise in pressure to kinetic factors. To investigate the variation of the first plateau pressure with Al content, the calculated phase diagram of MgH_2-Al (Al content between 0 and 11 at% (0.11 mole fraction)) alloy at 350°C is presented in Figure 3.16.

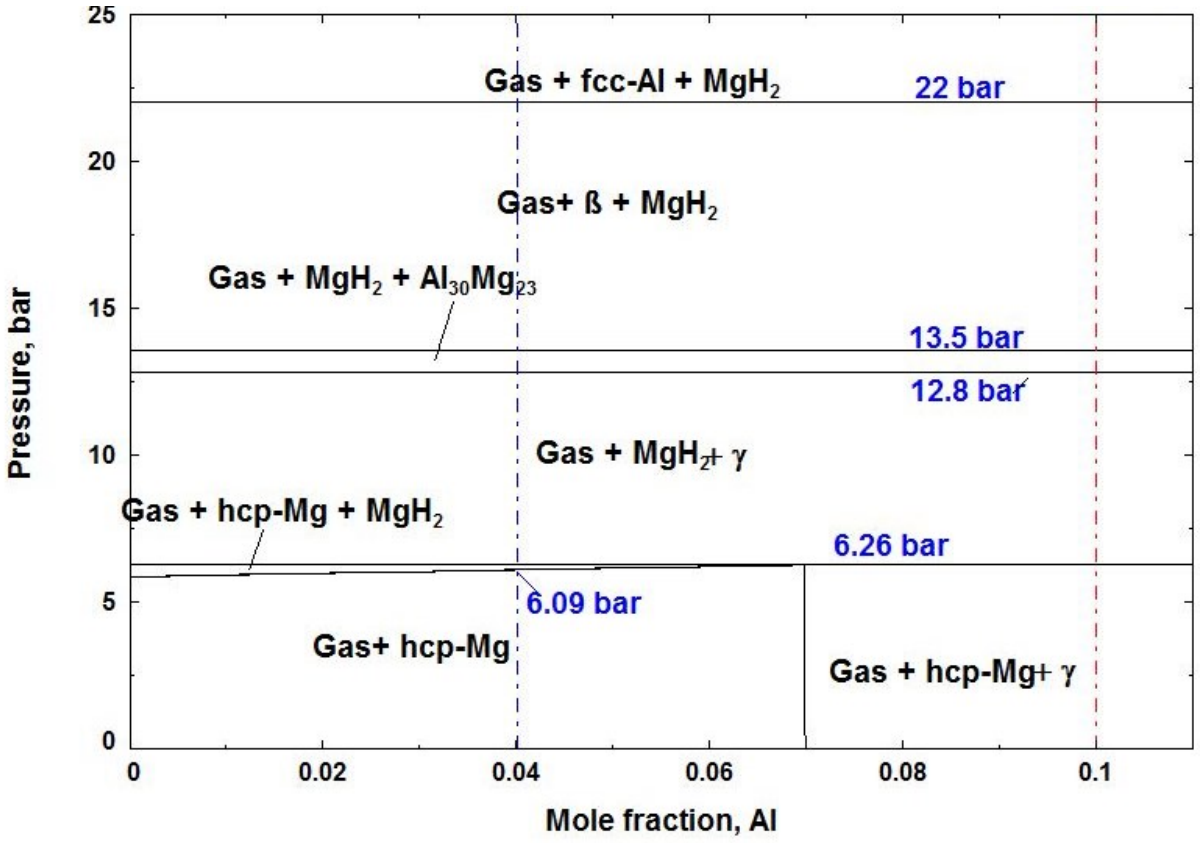

Figure 3.16 Calculated MgH_2-Al phase diagram at 350 °C

It shows that for Al content above 7 at%, the starting alloy is composed of hcp-Mg and γ phase and the hydriding of these alloys follows the same processes as for the Mg-10 at% Al alloys presented in Figures 3.13 and 14. Mg-10 at% Al composition is marked with dashed red line in Figure 3.16, which shows the four-hydriding steps with increasing the pressure. For Al content below 7 at.%, the starting alloy is composed of hcp-Mg and an additional step in the hydriding of alloys with these compositions is shown. This step occurs at a pressure which depends on the Al content and ranges between 5.84 bar for pure Mg to 6.26 bar for Al content of 7 at.%. As example, Mg-4 at% Al composition is marked with dashed blue line in Figure 3.16 and shows that the first hydriding step for alloys with this composition occurs at 6.09 bar. The calculated PCI curve at 350°C for Mg-4 at% Al alloy is presented in Figure 3.17. The enlarged portion of the first plateau shows that what can be seen as one plateau pressure is in fact composed of a curved portion starting at 6.09 bar followed by a straight one at 6.26 bar. Of course, this difference could not be observed in the experimental PCI [121] but it explains the variations in the first plateau pressure with Al content reported by Tanniru *et al.* [121].

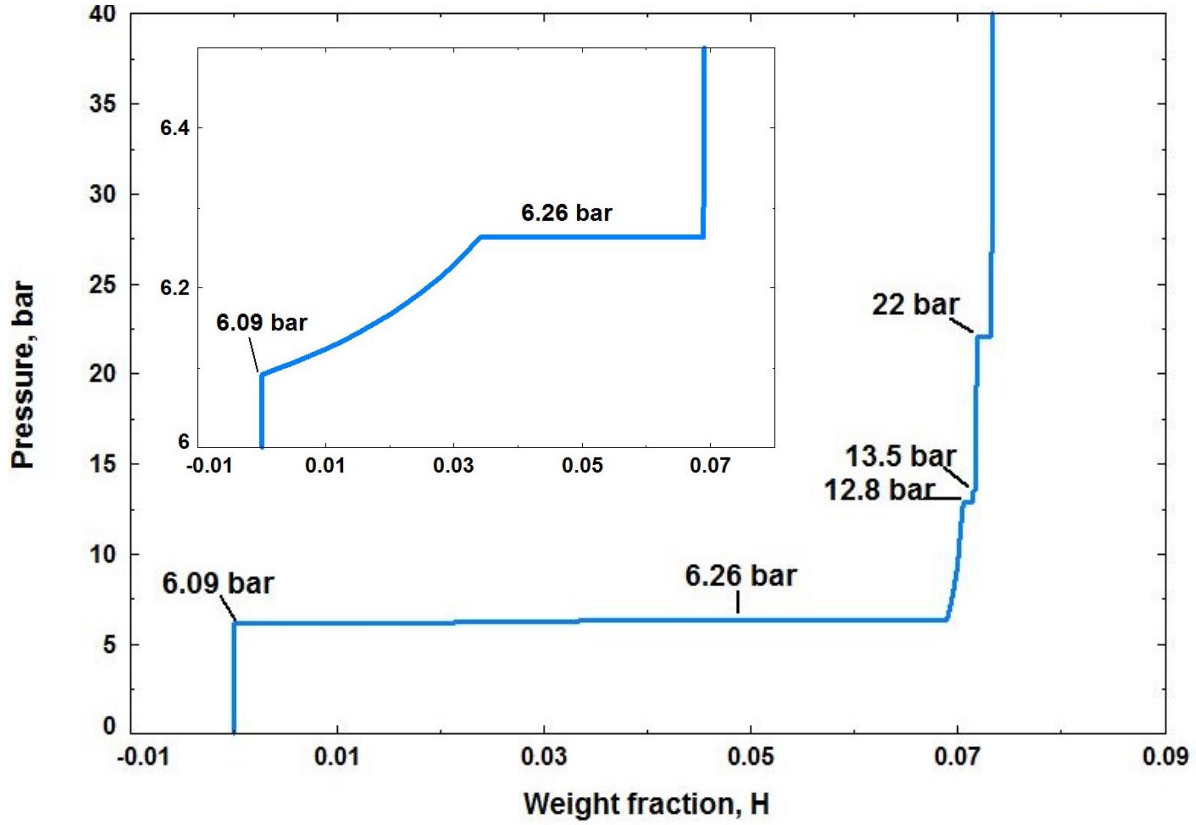

Figure 3.17 Calculated PCI curve of Mg-4at% Al at 350 °C

Figure 3.18 shows the calculated hydriding reaction pathway of Mg-4 at% Al alloy at 350°C for pressures near the first plateau pressure. It shows that MgH_2 starts forming at a pressure of 6.09 bar and its amount (red line) increases gradually with decreasing amount of hcp-Mg (blue line) as the pressure increases. The amount of Al dissolved in hcp-Mg (blue dotted line) is constant while the amount of Mg in hcp-Mg (blue dashed line) decreases which means that the hcp-Mg phase is being more concentrated in Al while MgH_2 is forming. The enlarged view shows that the amount of H in hcp-Mg decreases with the pressure too. At 6.26 bar, hcp-Mg is hydrided and γ phase forms. It can be concluded from the calculations shown in Figures 3.15, 3.16, and 3.17 that the variations in the first plateau pressure reported in the literature is due to the solubility of Al in hcp-Mg and not to kinetics factors as suggested by Tanniru *et al.* [121].

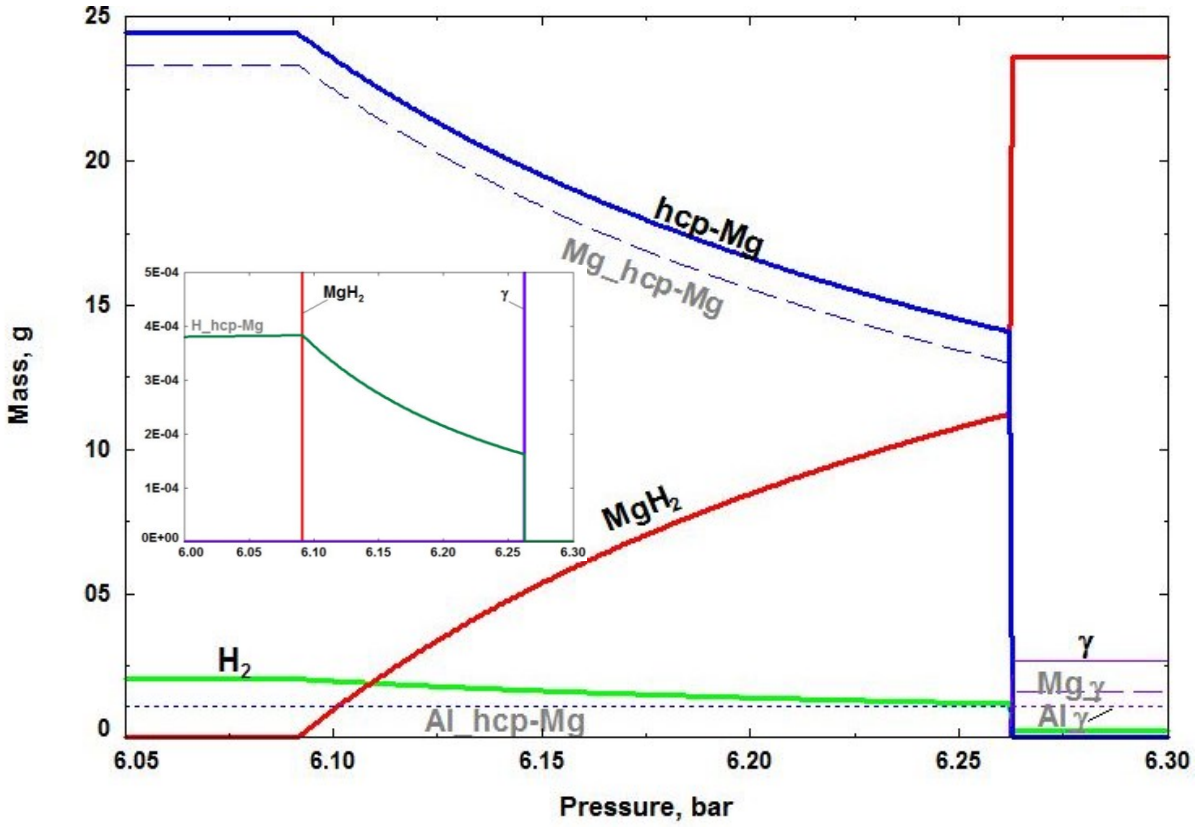

Figure 3.18 Hydriding reaction path of Mg-4at%Al at 350 °C

3.4.2.2 Al-Mg-Na-H system

As mentioned in section 3.2.2.2, Ismail *et al.* [122-124] investigated the hydrogen storage properties and the reaction pathways of MgH_2-$NaAlH_4$ (4:1)/Na_3AlH_6 (4:1) composites. In this section, their results are compared with our thermodynamic calculations.

The calculated MgH_2-$NaAlH_4$ phase diagram is presented in Figure 3.19 and shows the different reaction stages in the thermal decomposition of MgH_2/$NaAlH_4$ composites at 1 bar.

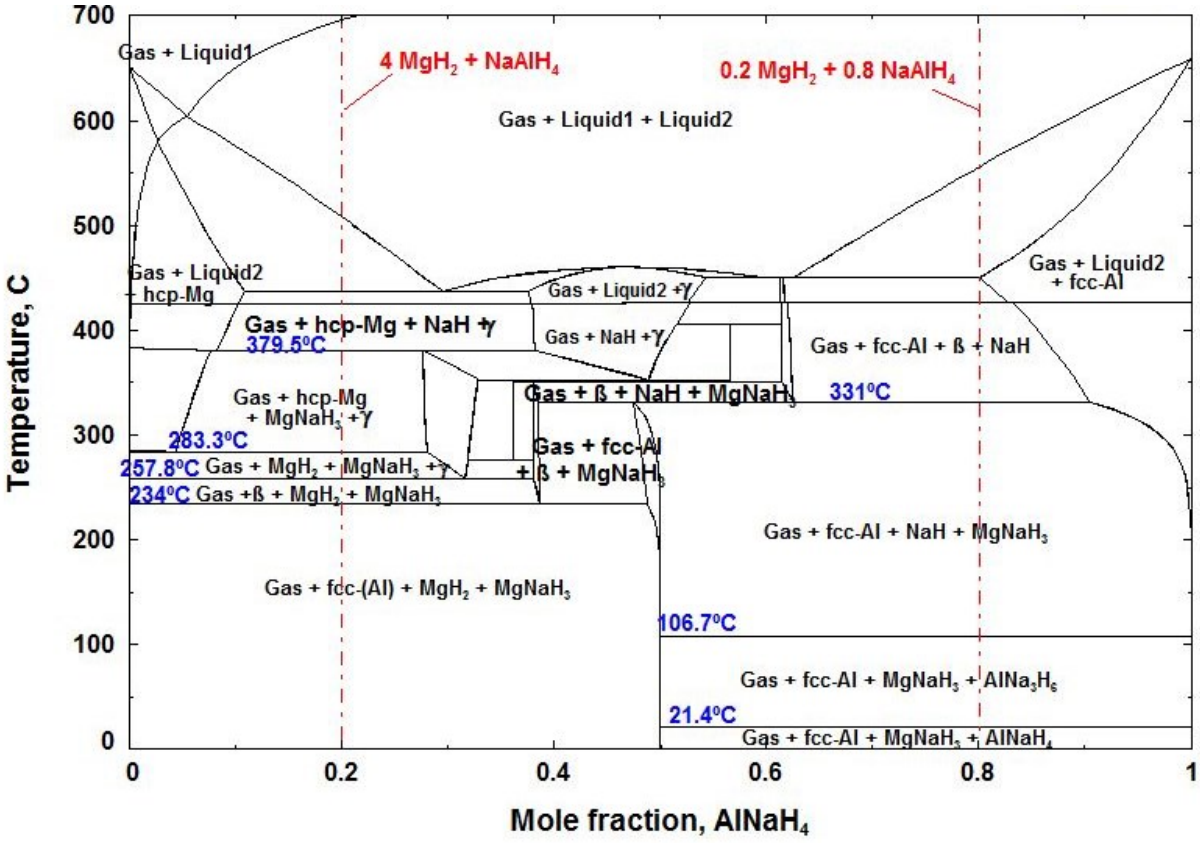

Figure 3.19 Calculated MgH_2-$AlNaH_4$ phase diagram at 1bar

It can be seen that the reaction pathway in the MgH_2/$NaAlH_4$ composites depends on the relative amounts of the components. For MgH_2-$NaAlH_4$ (4:1) composition (marked by red dashed line in Figure 19), $NaAlH_4$ reacts spontaneously with MgH_2 to form $NaMgH_3$, MgH_2, and fcc-Al. Then, as already discussed in section 3.4.2.1, MgH_2 interacts with fcc-Al and decomposes in three steps: at 234°C (where β is formed), at 257.86°C (where γ is formed), and at 283.29°C (where γ

and hcp-Mg are formed). Finally, $NaMgH_3$ and NaH decompose at 379.48°C and 424.8°C, respectively. The (TPD) results [123] showed that, four stages of $4MgH_2$-$NaAlH_4$-TiF_3 desorption have been observed in the temperatures ranges (60-200°C), (200-315°C), (315-370°C), and (after 375°C), respectively.

The results of Ismail *et al.* [122, 123] are in agreemnt with the calculations performed in this work. However, the first stage desorption reported by Ismail *et al.* [122, 123] was attributed to the reaction between a part of MgH_2 and $NaAlH_4$ to form $NaMgH_3$ and Al. This reaction happens spontaneously according to our calculation and might be kinetically hindered. Ismail *et al.* [122, 123] reported the decomposition of MgH_2 as a one step process and this might be due, in addition to kinetics factor, to the small differences in the three steps reaction temperatures (234, 257.8, and 283.29°C, respectively) calculated in this work. In addition to that, the desorption temperatures reported[123] are in a good agreement with the calculated ones at 1 bar considering the fact that the TPD experiments were performed in vacuum [122, 123].

It should be noted that according to the calculation reported in Figure 3.19 (the red dashed line for $4MgH_2 + NaAlH_3$ composition) and the results reported in section 4.2.1 Figure 3.12a (the red dashed line for MgH_2+0.25AlH_3 composition), $NaMgH_3$ does not affect the decomposition temperatures of MgH_2+Al mixtures. However, the decomposition temperature of $NaMgH_3$ is decreased from 382.63°C for pure $NaMgH_3$ [117] to 379.48°C in the MgH_2-$NaAlH_4$ (4:1) composite.

Figure 3.19 shows the reaction processes in MgH_2-$NaAlH_4$ composites for the whole composition range. According to our calculations, it is predicted that for $NaAlH_4$ content above 0.5mole fraction (in Figure 3.19), MgH_2 decomposes spontaneously and the system is initially composed of fcc-Al, $MgNaH_3$, and $AlNaH_4$. The first and the second reaction steps concern the decomposition of $AlNaH_4$ and $AlNa_3H_6$ at the hydrides' decomposition temperatures, 21.4°C and 106.7°C, respectively, which shows that these hydrides are not altered by Al or $MgNaH_3$. Between 0.62 and 0.9 mole fractions $NaAlH_4$, $NaMgH_3$ decomposes in one step at 331°C. This temperature is 51.63°C lower than the decomposition temperature of pure $NaMgH_3$. This fact proves that Al alters the decomposition process of $NaMgH_3$. The reaction pathway of 0.2Al + 0.8$NaMgH_3$ composite is presented in Figure 3.20. Al and Mg content of each phase are presented in the enlarged inset with doted and dashed lines, respectively, with the same color as

the phase. It is shown that $MgNaH_3$ decomposes in four steps with the formation of β, $Al_{30}Mg_{23}$, γ, and hcp-Mg at 331, 350.27, 352.19, and 379.48°C, respectively. In each step NaH and H_2 are formed too. It should be noted that with increasing temperature, Figure 3.20 shows that the amount of $MgNaH_3$ starts decreasing at temperatures below 331°C and that the amount of fcc-Al is increasing while its Al content is constant. The amount of NaH in the composite is increasing too. We can conclude that, when Al is added to $MgNaH_3$, some Mg starts dissolving in fcc-Al forming NaH and liberating some H_2 until fcc-Al saturation where β forms at 331°C. The same conclusion can be drawn regarding Mg solubility in β and γ.

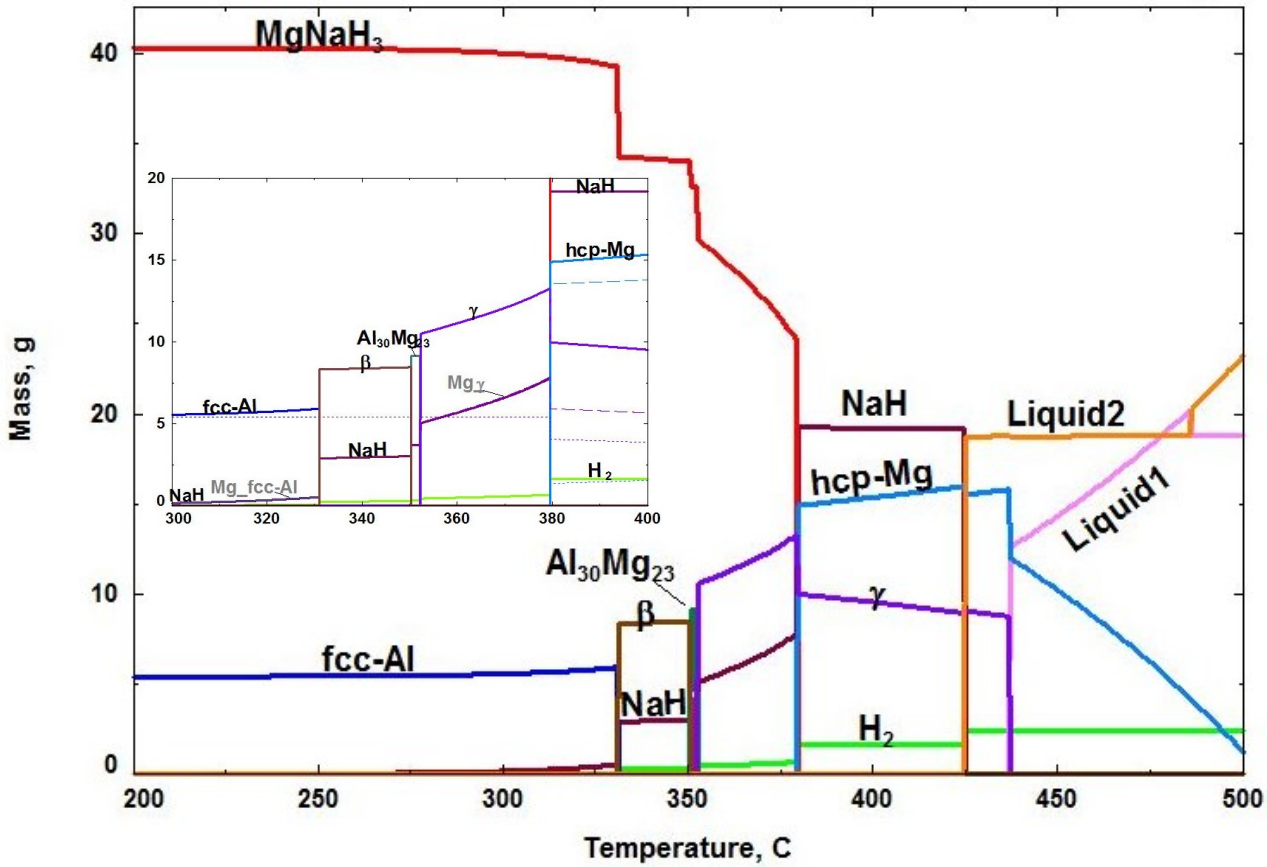

Figure 3.20 Reaction path of the reaction 0.2 Al + 0.8 $NaMgH_3$ at 1bar

Ismail *et al.* [122] demonstrated that the reactions in MgH_2-$NaAlH_4$ (4:1) composite are reversible at 30 bar H_2 pressure and 300°C, except the first one (reaction between MgH_2 and $NaAlH_4$ to form $NaMgH_3$ and Al), and that the phases present in the composite after rehydrogenation are MgH_2, $NaMgH_3$, and Al. The calculated PT diagram of MgH_2-$NaAlH_4$ (4:1) composites is shown in Figure 3.21. It shows also that at 300°C and 30 bar (marked in the Figure 3.21 by blue point), the composite is composed of MgH_2, $NaMgH_3$, and fcc-Al phases, which agree with the results of Ismail *et al.* [122, 123]. In addition to these phases, Ismail *et al.* [122, 123] reported that XRD measurements showed a small peak of β phase in addition to Al_3Ti phase when TiF_3 was added to the mixture. Al_3Ti and TiF_3 act as catalysts to improve the desorption kinetics of the mixture [122, 123].

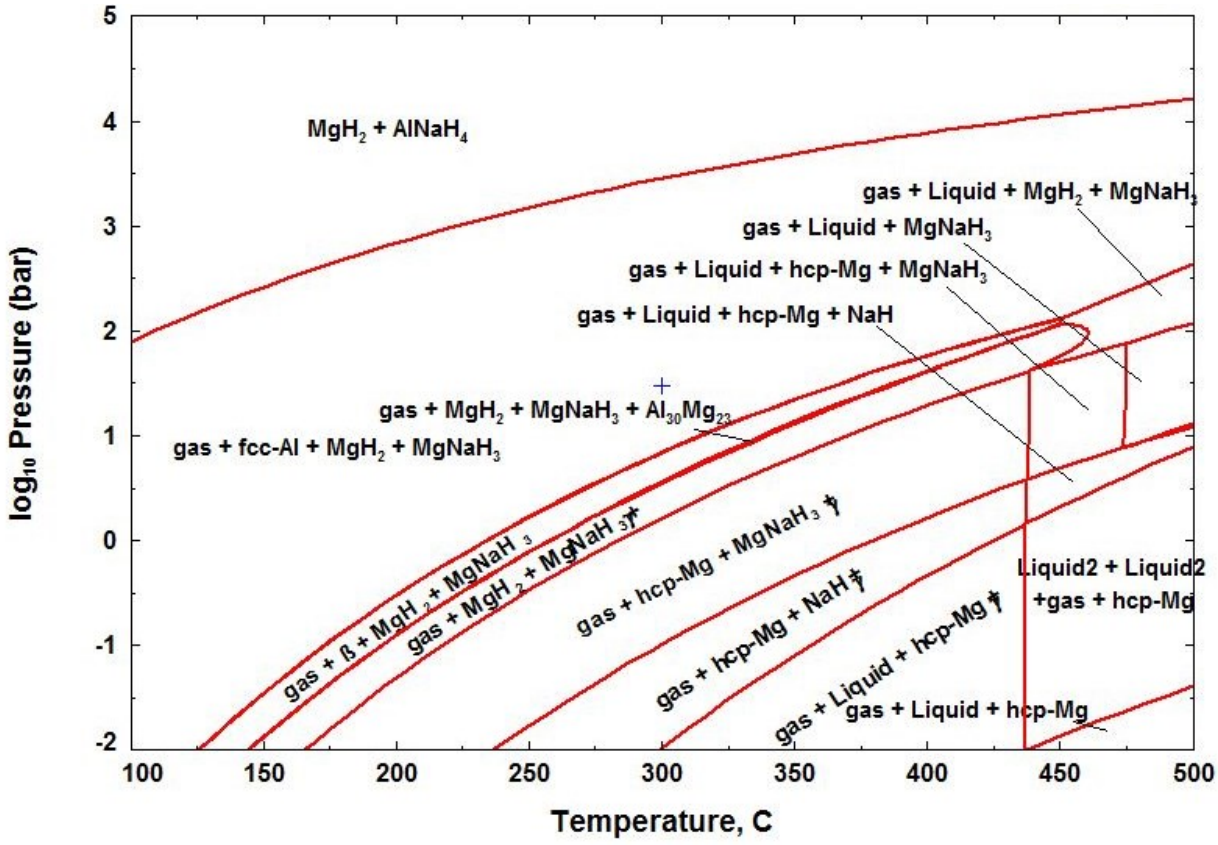

Figure 3.21 P-T diagram of $4MgH_2 + NaAlH_4$ composite

Ismail *et al.* [122, 123] showed that the absorption kinetics after the first desorption of the composite was slow compared to MgH_2 and that addition of TiF_3 did not improve it. This slow absorption kinetics has been related to the presence of β whose hydrogenation is kinetically hindered [122, 123]. It can be concluded from these calculations and the work of Ismail *et al.* [122, 123] that $NaAlH_4$ is destabilized by MgH_2 and decomposes spontaneously in the mixture MgH_2-$NaAlH_4$ (4:1). Then, the produced Al destabilizes MgH_2. But the re-hydrogenation reactions kinetics is very slow.

Ismail *et al.* [124] investigated the hydrogen storage properties of the MgH_2-Na_3AlH_6 (4:1) composite and concluded that the reaction mechanisms were similar to that of MgH_2-$NaAlH_4$ (4:1) composite. The calculated MgH_2-Na_3AlH_6 phase diagram is presented in Figure 3.22 and is very similar to the calculated MgH_2-$NaAlH_4$ phase diagram. A red dashed line in Figure 3.22 shows the MgH_2-Na_3AlH_6 (4:1) composition. It shows that MgH_2 decomposes in two steps with the formation of β phase in the first step and γ with β phases after the second step. The present calculations show the formation of $Al_{30}Mg_{23}$, which has not been reported in the literature.

Figure 3.22 shows that a small variation in the mixture composition will result in identical reaction mechanism as with MgH_2-$NaAlH_4$ (4:1) composite. It might be the case in the results published by Ismail *et al.* [124] .

The calculated PT diagram of MgH_2-Na_3AlH_6 (4:1) composites is shown in Figure 3.23. It shows that Na_3AlH_6 is not stable in this mixture even under very high pressures. XRD results [124] showed that the rehydrogenated composite at 30 bar and 300°C, was composed of MgH_2, $NaMgH_3$, Al, and a small amount of β which agrees with the calculations performed in this work (Figure 3.23) except for the existence of β which shows that its hydrogenation process is very slow.

According to the thermodynamic calculations conducted in this work, at 1 bar, $AlNaH_4$ decomposes to form $AlNa_3H_6$ and fcc-Al at 21.4°C, and $AlNa_3H_6$ decomposes to form NaH and fcc-Al at 106.7°C. When mixed with MgH_2, $MgNaH_3$ forms spontaneously from MgH_2 and $AlNaH_4$/$AlNa_3H_6$ and the resulting mixture composition depends on the relative amounts of the components.

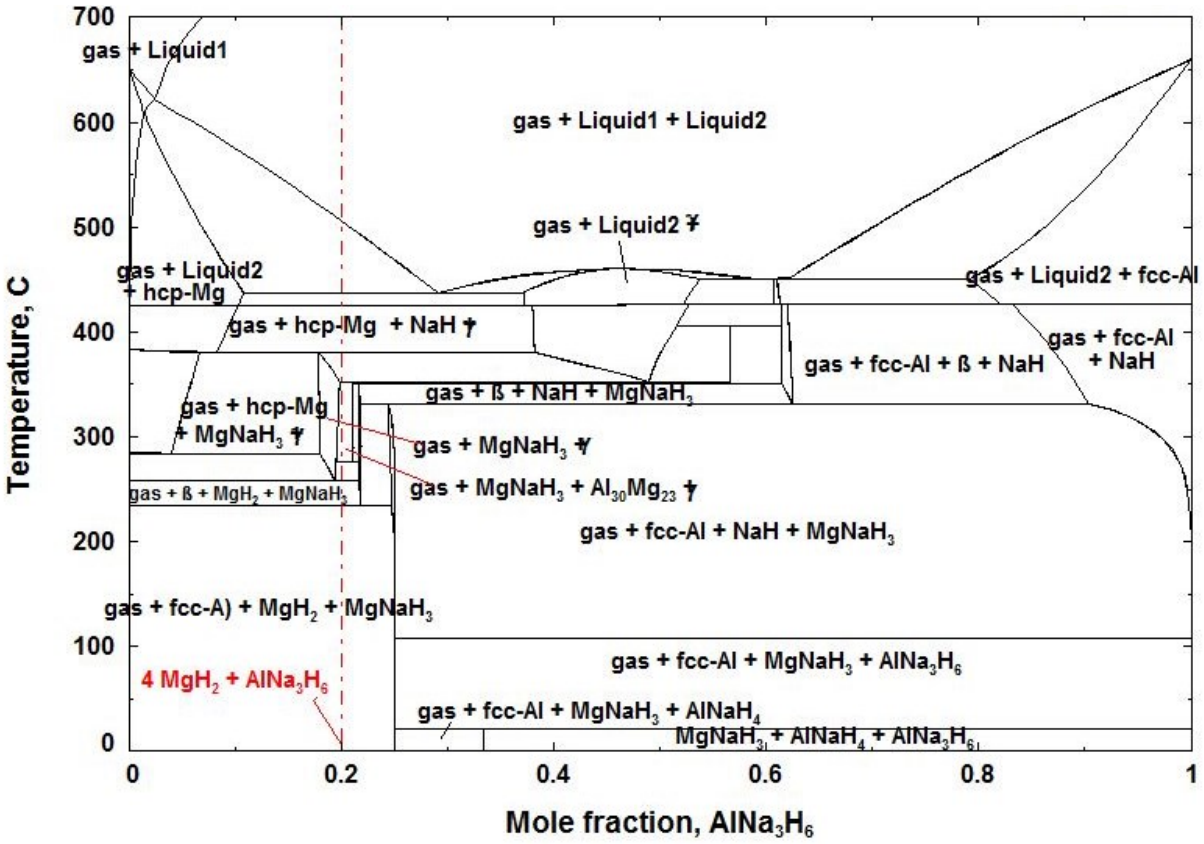

Figure 3.22 Calculated MgH_2-$AlNa_3H_6$ phase diagram at 1bar

When the number of Mg atoms in MgH_2 + $AlNaH_4$/$AlNa_3H_6$ mixture exceeds the number of Na atoms, all the $AlNaH_4$/$AlNa_3H_6$ decomposes spontaneously and the remaining decomposition steps concern the decomposition of (MgH_2 + Al) mixture and $MgNaH_3$ has only a catalytic role. When the number of Na atoms in MgH_2 + $AlNaH_4$/$AlNa_3H_6$ mixture exceeds the number of Mg atoms, MgH_2 decomposes spontaneously and the remaining steps concern the decomposition of $AlNaH_4$ and $AlNa_3H_6$ which is not affected by $MgNaH_3$.

Ismail *et al.* [124] compared hydrogen storage properties of $4MgH_2$ + $AlNaH_4$ and those of $4MgH_2$ + $AlNa_3H_6$ mixtures. TPD curves[124] show that both composites start to decompose at around 170°C, which is 10°C and 55°C lower than the decomposition temperature of the as milled $AlNaH_4$ and $AlNa_3H_6$, respectively. For this reason, Ismail *et al.* [124] concluded that MgH_2 + $AlNa_3H_6$ composite is better than MgH_2 + $AlNaH_4$ composite. However, according to our calculations, there is no difference in the decomposition process of the two composites and the mutual destabilization of MgH_2 and $AlNaH_4$/$AlNa_3H_6$ hydrides in this composition range

($4MgH_2 + AlNa_3H_6$, when number of Mg atoms exceeds number of Na atoms) does not depend on the hydrides' decomposition temperatures.

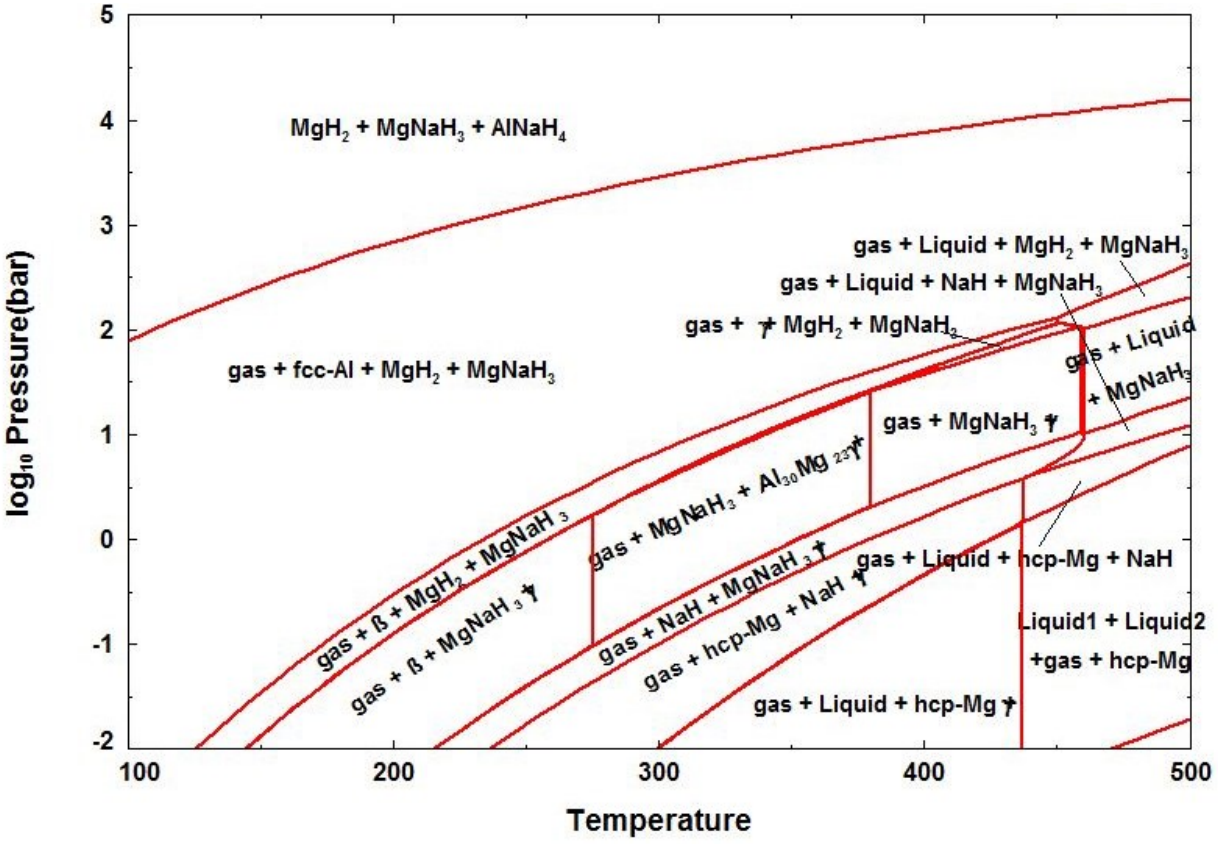

Figure 3.23 P-T diagram of $4MgH_2 + Na_3AlH_6$ composite

3.5 Conclusion

In this work, thermodynamic modeling is used to investigate the reaction mechanisms and hydrogen storage properties in the Al-Mg-Na-H system. A self-consistent database has been constructed by extrapolating the different binaries assessed in this work or taken from the literature, using the CALPHAD method.

Reaction pathways for the reaction MgH_2/AlH_3, $MgH_2/NaAlH_4$, and MgH_2/Na_3AlH_6 are calculated and show good agreement with experimental data from the literature and provide insight regarding the reaction temperatures, the amount of the products, and their composition. It

is shown that Al destabilizes MgH_2 by the formation of Al-Mg solid solutions and compounds. This process depends on Al content. The first step decomposition temperature of MgH_2 in the mixture at 1 bar is 234°C; i.e., 50.73°C lower than the decomposition temperature of MgH_2 alone and is due to the formation of β phase. The calculated pressure composition isotherms for Mg-10 at.% Al and Mg-4 at.% Al alloys at 350°C show good agreement with the experimental data and give a more detailed description of the hydriding process products and equilibrium pressures. These calculations explain the uncertainties found in the literature, especially the sloping curves and difficult plateau pressures distinction. It is shown that the first hydrogenation of Al-Mg alloys starts at higher pressure than pure Mg and depends on Al content. In fact, for Al content higher than 7 at%, the hydrogenation of hcp-Mg occurs in one step with the formation of γ phase at 6.26 bar. However, for Al content lower than 7 at%, the hcp-Mg is hydrogenated first at pressures increasing with Al content (5.84 bar for pure Mg to 6.26 bar for 7 at.% Al in Mg alloy) and is related to the solubility of Al in hcp-Mg, followed by the formation of γ phase at 6.26 bar. It is shown that the PCIs sloping reported in the literature for the Al-Mg alloys is, in addition to kinetic factors, due to the large solubility of γ phase, to short plateaus' length, and to the small differences between plateau pressures.

For $MgH_2/NaAlH_4$ and MgH_2/Na_3AlH_6, It is shown that reaction mechanisms in the composites depend on the relative amount of the components. It is demonstarted that each component of the composite destabilizes the other component in a specific composition range by the formation of $NaMgH_3$. When the number of Mg atoms in MgH_2 + $AlNaH_4/AlNa_3H_6$ mixture exceeds the number of Na atoms, all the $AlNaH_4/AlNa_3H_6$ decomposes spontaneously and the remaining decomposition steps concern the decomposition of (MgH_2 + Al) mixture and $MgNaH_3$ acts only as a catalyst.

When the number of Na atoms in MgH_2 + $AlNaH_4/AlNa_3H_6$ mixture exceeds the number of Mg atoms, MgH_2 decomposes spontaneously and the remaining steps concern the decomposition of $AlNaH_4$ and $AlNa_3H_6$ which is not affected by $MgNaH_3$ which might have a catalytic effect on the process. $MgNaH_3$ in this mixture decomposes to form β phase at 331°C, i.e., 51.6°C lower than the decomposition temperature of pure $MgNaH_3$.

Chapter 4. Thermodynamic analysis of dehydrogenation path of Mg-Al-Li-Na alloys

Abstract

A thermodynamic study on the Mg-Al-Li-Na-H system is conducted in this work in order to investigate its hydrogen storage properties. For that purpose, a thermodynamic database is constructed using the CALPHAD technique. In this work, Li is added to the previously studied Mg-Al-Na-H system and the related binaries (Li-Mg, Li-Na) and ternaries (Al-Li-Mg, Al-Li-H, Li-Mg-H) are reassessed using the Compound Energy Formalism (CEF) for the terminal solid solutions and the Modified Quasichemical Model (MQM) for the liquid phase. The quaternary hydride Na_2LiAlH_6 is assessed for the first time. The constructed database is used to calculate de/re-hydrogenation reaction pathways of MgH_2-$LiAlH_4$/Li_3AlH_6 composites in a wide temperature and pressure ranges. The results are analyzed and compared with the experimental data to better understand and predict the reaction mechanisms. It is shown that Al resulted from the decomposition of $LiAlH_4$/Li_3AlH_6 hydrides destabilizes MgH_2 by the formation of Mg-Al phases: β and γ, and that LiH does not contribute to these reactions. Only negligible amounts of hydrogen are released from LiH because of the limited solubility of Li (from LiH) in Mg at high temperatures. It is concluded that MgH_2-Li_3AlH_6 system has better reversibility than MgH_2-$LiAlH_4$ system and promising compositions (e.g. 37.09 mole% and 53.65 mole% MgH_2 contents) are predicted. Also, a new destabilization reaction is predicted in the system. The MgH_2 and Na_2LiAlH_6 hydrides destabilize mutually at 308.4 K (35.25°C) and 1 bar because of the formation of $MgNaH_3$. However, the hydrogen capacity is reduced. It is concluded that Na considerably reduces the hydrogen storage potential of the system.

Key words: Hydrogen storage, magnesium hydrides, lithium alanates, thermodynamic modeling.

4.1 Introduction

The present work is a contribution to the search and development of new materials suitable for hydrogen storage applications. In fact, the storage of hydrogen is the most critical issue for the development of hydrogen energy, especially for mobile applications [26]. Significant attention has been devoted to magnesium and its alloys as potential materials for hydrogen storage because of their high hydrogen capacity [15]. Magnesium hydride, MgH_2, can store as much as 7.6 wt. % H_2, but its thermodynamic stability is always the major problem in spite of the huge work focused on alloying and developing destabilization systems. Among these systems, Mg-Al-Li-Na-H has been reported to be very promising and many researchers focus their efforts on trying to understand reaction mechanisms and finding the best additives/catalysts to improve their hydrogen storage properties [34, 46, 123-125, 144, 163-165]. A comprehensive thermodynamic study is needed to find the best compositions in this system and to show their potential and limitations for hydrogen storage applications.

Recently Abdessameud *et al*. [117, 166] used thermodynamic modeling to construct a database that describes the Mg-Al-Na-H system for hydrogen storage application. In this work, this database is extended to include Li in the system. This work is composed of two main parts; the first one consists of the assessment of the different binaries and ternaries in this system using CALPHAD method and FactSage software [25]. The second part focuses on the analysis of hydrogen storage properties of this system in comparison with the available experimental data and on the prediction of the most promising compositions in this system.

4.2 Literature review

4.2.1 Thermodynamic properties of Mg-Al-Li-Na-H system

The Mg-Al-Na-H system was reviewed and modeled in our previous papers [117, 166] . In this section, a review of the remaining subsystems of the Mg-Al-Li-Na-H is presented.

No ternary compounds have been reported in the literature for the Al-Li-Na, Li-Mg-Na, and Li-Na-H systems. Since this work is oriented toward hydrogen storage properties, these ternaries are extrapolated from the constituent binaries using the CALPHAD method and are not included in this review.

4.2.1.1 Al-Li

A critical literature review and thermodynamic modeling of Al-Li system have been conducted by Saunders [167]. The phase diagram consists of liquid phase, terminal solid solutions fcc-Al and bcc-Li, a nonstoichiometric compound AlLi(η) and two stoichiometric compounds; Al_2Li_3 and Al_4Li_9. The liquid phase has been assessed using the substitutional solution model [167] . Harvey and Chartrand [75] used the Al-Li thermodynamic parameters published by Saunders [167] to predict the hydrogen solubility in liquid Al-Li alloys. They [75] found that the hydrogen solubility was overestimated and reassessed the Al-Li binary liquid using the modified quasichemical model and showed that Al-Li liquid alloys exhibit short range ordering. Their [75] model parameters for the liquid phase are used in this work.

Harvey [128] completed the assessment of the entire Al-Li system using the substitutional model for the terminal solid solutions fcc-Al and bcc-Li. Since the present work is dedicated to hydrogen storage applications, the fcc-Al and bcc-Li are remodeled in this work using the compound energy formalism (CEF), thus the model parameters published by Harvey [128] are changed accordingly. The thermodynamic model parameters for the compounds AlLi, Al_2Li_3 and Al_4Li_9 [128] are used in this work with minor changes in order to accommodate the newly modeled solid solutions; fcc-Al and bcc-Li. The calculated Al-Li phase diagram is presented in Figure 4.1 and the parameters used are reported in Table 4.1.

4.2.1.2 Li-H

Harvey and Chartrand [75] assessed the Li-H system using the MQM for the liquid phase. The phase diagram consists of a gas phase, bcc-Li solid solution phase, a liquid phase with miscibility gap and a hydride phase, LiH. The model parameters used to describe the Li-H system by Harvey and Chartrand [75] are used in the present work except for the bcc-Li phase, which was remodeled using the CEF. The parameters used to describe the Li-H system are reported in Table 4.1 and the calculated Li-LiH phase diagram is presented in Figure 4.2.

4.2.1.3 Li-Mg

Nayeb-Hashemi *et al.* [168] reviewed the literature on the Li-Mg system and only the literature experimental data found by these authors [168] are used in the present optimization. The phase diagram consists of three phases: Liquid, hcp-Mg and bcc-Li terminal solid solutions.

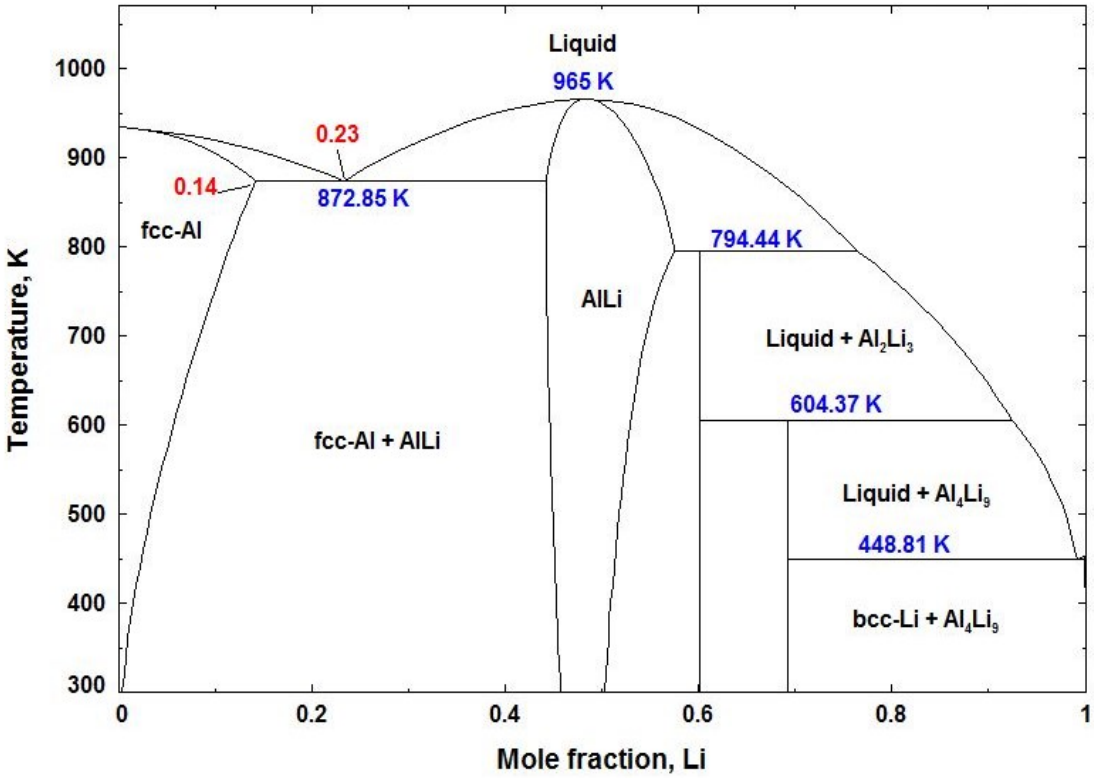

Figure 4.1 Calculated Al-Li phase diagram at 1 bar

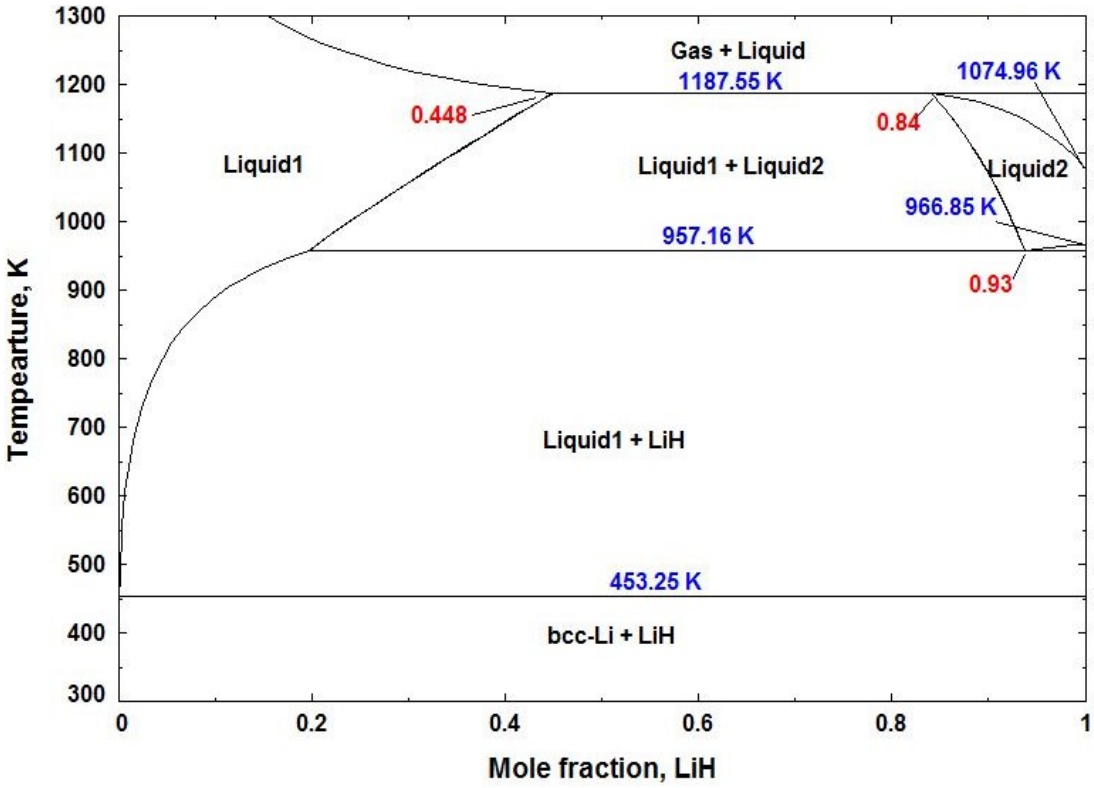

Figure 4.2 Calculated Li-LiH phase diagram at 1 bar

In the assessed phase diagram by Nayeb-Hashemi *et al.* [168], the maximum solid solubility of Li in Mg was 17 at.% Li, the maximum solid solubility of Mg in Li was 75.5 at.% Mg; and a eutectic reaction (L ↔ hcp-(Mg) + bcc-(Li)) occurred at 23 at.% Li and 861 K. The equilibrium diagram of the Li-Mg system has been widely investigated using different techniques [169-174]. Thermodynamic properties of the Li-Mg system have been investigated by Sommer [175], who measured the heat of mixing in the liquid phase at 940 K and by Saboungi and Blander [176], who measured Li activity in the Li-Mg liquid phase at 670, 735, 830 and 887 K. Gasior *et al*. [177] determined Li activities in solid and liquid Li-Mg alloys between 638 and 889 K.

Phase diagram calculations have been performed by Saboungi and Hsu [178], Nayeb-Hashemi *et al*. [168], Saunders [179], Gasior *et al*. [177], and most recently by Wang *et al*. [180]. In this work, the Li-Mg system is remodeled using the modified quasichemical model MQM for the liquid phase and CEF for the solid solutions for consistency with other systems in the same database. The results are discussed in more details in section 4.4.1.1.

4.2.1.4 Li-Na

A critical review of the Li-Na system was reported by Bale [181]. This system exhibits extensive immiscibility in the liquid and the solid phases. A monotectic reaction takes place at 443.8 K and Na compositions 3.4 and 90.2 at. % and a eutectic reaction at 365.3 K and 96.5 at. % Na [181]. The consolute point has been calculated to be at 576.35 K (303.2°C) and 35.7 at. % Na. No thermodynamic data have been reported in the literature for the Li-Na system but the phase equilibria has been widely investigated using different techniques [181]. In the present study, the experimental data [182-189] selected by Bale [181] are used. Since no experimental evidence of solid solutions has been found in the literature, Li and Na mutual solubilities are considered negligible in the present work.

Pelton [190] and Zhang *et al.* [191] assessed the Li-Na system using substitutional solution model for the liquid and solid solution phases and using the critical review of Bale [181]. However, the system are re-modeled in this work using the MQM for the liquid phase and CEF for the solid solution for consistency with other binaries showing short range ordering. The modeling results of this system are discussed in section 4.4.1.2.

4.2.1.5 Al-Li-Mg

Literature review of the Al-Li-Mg system was reported initially by Goel *et al*. [192] and Ghosh [193] and was then updated by Wang *et al*. [180]. Phase equilibria in this system were investigated by Schürmann and Voss [194] who designed a special apparatus to prepare Mg-Li-Al alloys. Phase analysis was performed by X-ray diffraction, optical metallography and electron probe microanalysis. However, Schürmann and Voss [194] did not include the Al_4Li_9 phase in their analysis of the Mg-Al-Li system and reported a ζ-phase ($Al_{11}Mg_{10}$), which is not considered as stable phase according to the widely accepted Al-Mg phase diagram [166].

Enthalpy of mixing of the Al-Li-Mg liquid was determined by Moser *et al*. [195] in the 869-1031 K temperature range using an isothermal high temperature mixing calorimeter. Schürmann and Geissler [196] constructed Al-Li-Mg isothermal sections at 473, 573, and 673 K (200, 300 and 400°C) below 60 at.% Li. Only one ternary stable compound τ ($Al_{53}Li_{33}Mg_{14}$) has been accepted in the literature [180, 196]. Considerable solubility of Li in Al-Mg solid phases and of Mg in Al-Li solid phases has been reported in the literature [196, 197]. In fact, Al-Mg compounds $Mg_{17}Al_{12}$(γ), Mg_2Al_3(β), and $Mg_{23}Al_{30}$(ε) dissolve up to about 20 at.% Li, 7 at.% Li, and 0.8 at.% Li, respectively [166]. LiAl(η) phase dissolves up to about 17 at.% Mg [196, 197].

Harvey [128] and Wang *et al*. [180] assessed the Al-Li-Mg system using the above-mentioned experimental data. Harvey [128] extrapolated the ternary liquid phase from the constituent binaries using mixed models (MQM for Al-Li and Al-Mg and substitutional solution model for Li-Mg) while Wang *et al*. [180] used substitutional solution model to extrapolate the liquid phase. In this work, the liquid phase is re-assessed using the MQM for all the binary liquids. No ternary interactions have been used in this work. The model parameters of Harvey [128] for the ternary compounds are used in this work with some modifications to attain consistency with the binary systems. The terminal solid solutions are remodeled using the CEF.

4.2.1.6 Al-Li-H

Recently, Bodak and Perrot [198] conducted a literature review on the Al-Li-H system. Two ternary hydrides have been reported in the literature. $LiAlH_4$ (P121/c1 space group [199]) is not stable at room temperature but has a theoretical hydrogen capacity of 10.6 wt. % H_2. Li_3AlH_6

($R\bar{3}$(148) space group [200]) is, in turn, stable and has a theoretical hydrogen capacity of 11.2 wt. % H_2. $LiAlH_4$ decomposes in three steps [201] through reactions (4.1) to (4.3):

$LiAlH_4 \rightarrow 1/3\ Li_3AlH_6 + 2/3\ Al + H_2$ 5.3 wt. % H_2 (4.1)

$Li_3AlH_6 \rightarrow 3LiH + Al + 3/2\ H_2$ +2.6 wt. % H_2 (4.2)

$3LiH + 3Al \rightarrow 3AlLi + 3/2\ H_2$ +2.6 wt. % H_2 (4.3)

Jang *et al* [202] assessed the thermodynamic properties of the Al-Li-H hydrides using available experimental data [203-208]. These authors [202] presented two sets of thermodynamic parameters for Li_3AlH_6 because of the contradicting pressure composition isotherm (PCI) data of Chen *et al*. [207] and Brinks *et al*. [208]. Later, Grove *et al*. [145] reassessed the thermodynamic properties of Li_3AlH_6 hydride using thermal analysis data of Claudy *et al*. [204] and first principle predictions [200, 209, 210]. The results published by Grove *et al*. [145] showed very good agreement with the PCI results of Chen *et al*. [207]. The parameters adopted by Grove *et al*. [145] are used in this work. The ternary liquid is extrapolated from the constituent binaries.

4.2.1.7 Li-Mg-H

Experimentally verified ternary phases in the H-Li-Mg system could not be found in the literature. Li *et al*. [211] predicted by means of density functional theory (DFT) the thermodynamic stability of two lithium magnesium hydrides; $LiMgH_3$ and Li_2MgH_4; at 300 K. Recently, Meggiolaro *et al*. [212] predicted, using the same method, that these hydrides are metastable and spontaneously decompose to MgH_2 and LiH.

Ikeda *et al*. [213] studied the formation of perovskite-type structure in the $Li_xNa_{1-x}MgH_3$ (x= 0, 0.17, 0.33, 0.50 and 1) hydride synthesized by ball milling NaH, MgH_2 and LiH. They did not observe the formation of $LiMgH_3$. For x = 0, X-ray diffraction showed the diffraction peaks for the perovskite structure $NaMgH_3$, the position of these peaks shifted to higher angles indicating partial substitution of Na by Li in the intermediate compositions (x= 0.17, 0.33, and 0.50) but this shift disappeared after heat treatment of the samples [107]. These results [107, 213] show that at equilibrium, Li cannot substitute Na in $NaMgH_3$ and thus, no stable ternary hydride exists in the Li-Mg-H system. Therefore, in this study, the model parameters describing the Li-Mg-H

system have been extrapolated from the constituent binaries and no ternary hydride has been included.

4.2.1.8 Quaternary phases

Three quaternary compounds, $LiMg(AlH_4)_3$, $LiMgAlH_6$, and Na_2LiAlH_6, have been reported in the literature for the Al-Li-Mg-Na-H system [46, 118, 145, 146, 214, 215].

Lithium-magnesium alanate, $LiMg(AlH_4)_3$, ($P2_1/c(14)$ [215]) contains 9.7 wt. % H_2 and has been found to decompose in two steps between 373 and 453 K (100 and 180°C) [146]. Mamatha *et al*. [146] assumed that $LiMg(AlH_4)_3$ decomposes following equations (4.4) and (4.5), where $LiMgAlH_6$ (space group P321 [215]) is an intermediate product of the decomposition of $LiMg(AlH_4)_3$. This assumption was based on the amount of hydrogen released in each step.

$$LiMg(AlH_4)_3 \rightarrow LiMgAlH_6 + 2\,Al + 3\,H_2 \quad (4.8\text{ wt. \% } H_2) \qquad (4.4)$$

$$LiMgAlH_6 \rightarrow LiH + MgH_2 + Al + 3/2\,H_2 \quad (2.4\text{ wt. \% } H_2) \qquad (4.5)$$

Mamatha *et al*. [146] showed, using DSC, that reaction (4.4) is exothermic, then not reversible, with an enthalpy value of -5 kJ/molH_2 and reaction (4.5) is endothermic with an enthalpy of 8.7 kJ/molH_2. Tang *et al*. [46] reported an enthalpy of -5.5 kJ/molH_2 and of 13.1 kJ/molH_2 for reactions (4.4) and (4.5), respectively. Tang *et al*. [46] reported that the results for reaction (4.5) agree with the results of Mamatha *et al*. [146]. Since Mamatha *et al*. [146] reported this enthalpy to be 8.7 kJ/molH_2, this suggests that the value reported by Tang *et al*. [46] for reaction (4.5) (13.1 kJ/mol H_2) might be in (kJ/mol $LiMgAlH_6$). After dehydrogenation of $LiMg(AlH_4)_3$ to form MgH_2, LiH and Al (reactions 4.4 and 4.5), Tang *et al*. [46] attempted the rehydrogenation of the products at 353 and 373 K (80 and 100°C) under 190 bar of hydrogen for 24 hours. These authors [46] found that neither $LiMgAlH_6$ nor $LiMg(AlH_4)_3$ form under these conditions.

Following the assessment of Grove *et al*. [145] for $LiMg(AlH_4)_3$ and $LiMgAlH_6$ hydrides, the above experimental data are adopted in this work to assess these two hydrides.

Na_2LiAlH_6 takes an ordered perovskite structure ($Fm\bar{3}m$ space group with a lattice constant of 7.4064(1) Å [214]) and decomposes reversibly to the binary hydrides following reaction (4.6) [118].

$$Na_2LiAlH_6 \rightarrow 2\,NaH + LiH + Al + 3/2\,H_2 \quad (3.5\text{ wt. \% } H_2) \qquad (4.6)$$

The enthalpy and/or entropy changes of reaction (4.6) were investigated using DSC [216, 217] and PCI [118, 214, 218, 219] measurements during dehydrogenation reactions. No assessment of the Na_2LiAlH_6 hydride has been reported in the literature. All these experimental data are used in the current work to establish a self-consistent database for the Mg-Al-Li-Na-H system.

4.2.2 Hydrogen storage properties

Recently, the hydrogen storage properties of the Mg-Al-Li-H system have been widely investigated [122, 220-228]. Zhang *et al*. [220] and Chen *et al*. [222] investigated the hydrogen storage properties and reaction mechanisms of ball milled MgH_2-$LiAlH_4$ composites (with different molar ratios) using thermogravimetry (TG), differential scanning calorimetry (DSC), and XRD. Zhang *et al*. [220] also investigated the non-isothermal dehydrogenation of the composites: MgH_2-LiH, MgH_2-Al, and MgH_2-LiH-Al in comparison with MgH_2-$LiAlH_4$. The effect of additives on the hydrogen storage properties and reaction mechanisms of MgH_2-$LiAlH_4$ have been also investigated [122, 223, 226].

Liu *et al*. [221, 224] investigated the MgH_2-Li_3AlH_6 composites using ball milling method, XRD analysis, thermogravimetry TGA, DSC, SEM and TEM. For comparison purposes, Liu *et al* [221] investigated the dehydrogenation of $4MgH_2$-$LiAlH_4$ composite under the same conditions and showed that Li_3AlH_6 and $LiAlH_4$ have the same destabilization effect on MgH_2 (for 4:1 mole ratio of Mg to Al).

Recently, Yap *et al*. [227] and Juahir *et al*. [228] investigated the effect of dopants on the hydrogen storage properties and reaction mechanisms of $4MgH_2$-Li_3AlH_6 composites by the addition of 10wt. % of K_2TiF_6 and Co_2NiO. In all the reported results, the dehydrogenation temperatures in the mixtures, MgH_2-$LiAlH_4$ or MgH_2-Li_3AlH_6, were lower than those of the components and the kinetics was significantly improved. Two stages of dehydrogenation of MgH_2-$LiAlH_4$ or MgH_2-Li_3AlH_6 composites have been identified during the heating process:

For MgH_2-$AlLiH_4$ composites, the first stage has been attributed to the two-step decomposition of as-milled $LiAlH_4$ (reactions (4.1) and (4.2)) [220]. In MgH_2-Li_3AlH_6 composites the first stage has been attributed to the decomposition of Li_3AlH_6 (reaction (4.2)) [221]. The second stage has been attributed to the decomposition of MgH_2 and two different dehydrogenation routes have been reported:

$4.08\ MgH_2 + 0.92\ LiH \rightarrow Li_{0.92}Mg_{4.08} + 4.54\ H_2$ (4.7)

$17\ MgH_2 + 12\ Al \rightarrow Mg_{17}Al_{12} + 17\ H_2$ (4.8)

$MgH_2 \rightarrow Mg + H_2$ (4.9)

The first route was proposed by Zhang *et al*. [220] who reported a mutual destabilization between MgH_2 and LiH to form $Li_{0.92}Mg_{4.08}$ intermediate phase in addition to the effect of Al on the dehydrogenation process of MgH_2 due to the formation of γ-phase ($Mg_{17}Al_{12}$). According to Zhang *et al*. [220] and many others [222, 225-229], the second stage of dehydrogenation of MgH_2-$LiAlH_4$ or MgH_2-Li_3AlH_6 composites occurs following reactions (4.7) and (4.8). Mao *et al*. [223] identified the Li-Mg intermediate phase that resulted from the interaction of MgH_2 and LiH as Li_3Mg_7. In turn, Liu *et al*. [221, 224] supported that LiH do not take part in the dehydrogenation reactions and the decomposition of MgH_2 proceeds following reactions (4.8) and (9). These authors argued that LiH could not be detected in XRD results because of its small amount and amorphous structure.

4.3 Thermodynamic modeling

The Mg-Al-Li-Na-H system is modeled in the current work using FactSage software [25]. The Gibbs energy functions of the pure elements (Al, Li, Mg, Na) are taken from the compilation of Dinsdale [110]. The Gibbs energy function of liquid monoatomic hydrogen estimated by Ransley and Talbot [158] is used in this work.

The liquid phase of the different binary systems is modeled using the modified quasichemical model MQM. Binary liquid parameters have been interpolated using the asymmetric Kohler-Toop technique where H is singled out as the asymmetric component [117, 166]. No ternary parameters have been added to the liquid model.

Since hydrogen atoms occupy the interstitial positions in the terminal solid solutions fcc-Al, hcp-Mg, and bcc-Li/Na, these phases are modeled using the compound energy formalism. As discussed in our previous papers [117, 166], two sublattices: $(Al,Li,Mg,Na)_1(H,Va)_1$, $(Mg,Al,Li,Na)_2(H,Va)_1$, and $(Na,Li,Al,Mg)_1(H,Va)_3$ are used to describe these solid solutions, respectively; where Mg, Al, Li, and Na atoms mix randomly in the first sublattice to allow their mutual solubility and H atom and vacancy mix in the second sublattice.

The model parameters of the compounds: $Al_{30}Mg_{23}$, AlH_3, MgH_2, $Mg(AlH_4)_2$, NaH, $NaMgH_3$, $NaAlH_4$, Na_3AlH_6 have been cited in our previous papers [117, 166] and those of the compounds: LiH [128], Al_2Li_3 [128], Al_4Li_9 [128], $Al_{53}Li_{33}Mg_{14}$ [128], $LiAlH_4$ [145], Li_3AlH_6 [145] have been taken from the literature. $LiMg(AlH_4)_3$, $LiMgAlH_6$, and Na_2LiAlH_6 are modeled in this work as stoichiometric compounds based on literature data that are found reliable [46, 118, 130, 145, 146, 215].

The nonstoichiometric compounds: β (Al_3Mg_2), γ ($Al_{12}Mg_{17}$), and AlLi are taken from Harvey [128] where they have been described by the sublattices: $(Mg,Li)_{10}(Al,Mg)_{24}(Al,Mg)_{24}$, $(Al)_{19}(Al,Mg,Li)_2(Mg,Li)_{12}$, and $(Al,Li,Mg)_1(Li,Mg,Va)_1$, respectively.

The gases: Al, Al_2, AlH, H, H_2, Li, Li_2, LiH, Mg, Mg_2, MgH, Na, Na_2, and NaH are included in this work and are considered ideal gases [117, 166] because the non-ideal contribution of the pressure to the Gibbs energy, in the pressure range of interest, is very small. Gibbs energy functions of all the gases are taken from FactPS database [25]. When present in the assessed phase diagram, the gas phase refers to all the gases that form in the considered system and cited above. The pressure reported in all the figures is the total pressure of the system.

Thermodynamic equations used to model the different phases along with the model parameters of the Mg-Al-Na-H system have been reported in our previous papers [117]. The additional model parameters assessed in the current work are listed in Table 4.1.

Table 4.1**:** *Optimized model parameters for the different phases in the Mg-Al-Li-Na-H system (G, Δg, and L in J/mole)*

Liquid Phase (MQM)	
$Z^{Al}_{AlLi} = Z^{Li}_{AlLi} = 2, \Delta g^0_{AlLi} = -25,597.8 + 15.012T - 0.1217TLnT$ $\Delta g^{10}_{AlLi} = -1.255T; \Delta g^{01}_{AlLi} = -14,126.8 + 10.3702T$	[128]
$Z^{Li}_{LiMg} = Z^{Mg}_{LiMg} = 6, \Delta g^0_{LiMg} = -3974.8 + 2.13T; \Delta g^{01}_{LiMg} = 0.698T$	This work
$Z^{Li}_{LiNa} = Z^{Na}_{LiNa} = 6, \Delta g^0_{LiNa} = 3640.08; \Delta g^{10}_{LiNa} = 2698.68 - 3.033T; \Delta g^{01}_{LiNa} = 209.2$	This work
$Z^{Li}_{LiH} = Z^{H}_{LiH} = 3; \Delta g^0_{LiH} = -106,697.2 + 33.85T - 1.58TLnT$ $\Delta g^{10}_{LiH} = 33,680.8 - 6.08T; \Delta g^{20}_{LiH} = -25,516.1$ $\Delta g^{30}_{LiH} = 7,040.9 + 5.97T; \Delta g^{01}_{LiH} = -55,745$	[128]

Terminal Solid solutions (Compound Energy Formalism) • hcp-(Mg) $(Mg,Na,Al,Li)_2(H,Va)_1$ ${}^0G_{Li:H}^{Li_2H} = 2G(Li_{hcp}) + 1/2G(H_2, gas)$; ${}^0G_{Li:Va}^{Li_2} = 2G(Li_{hcp})$ ${}^0L_{Mg,Li:Va}^{hcp} = -13,879.36$; ${}^1L_{Mg,Li:Va}^{hcp} = 7,832.64$; ${}^2L_{Mg,Li:Va}^{hcp} = 7,832.64$ ${}^0L_{Al,Li:Va}^{hcp} = -62,368$ ${}^0L_{Na,Li:Va}^{hcp} = 40000$	This work
• bcc-(Na) $(Na,Mg,Al,Li)_1(H,Va)_3$ ${}^0G_{Li:H}^{LiH_3} = G(Li_{bcc}) + 3/2G(H_2, gas) + 500,000$; ${}^0G_{Li:Va}^{Li} = G(Li_{bcc})$ ${}^0L_{Mg,Li:Va}^{bcc} = -18,209.48 + 8.25T$; ${}^1L_{Mg,Li:Va}^{bcc} = 3481$; ${}^2L_{Mg,Li:Va}^{bcc} = 265$ ${}^0L_{Li:H,Va}^{bcc} = 418,400$ ${}^0L_{Na,Li:Va}^{bcc} = 20,920$	This work
${}^0L_{Al,Li:Va}^{bcc} = -27,000 + 8T$; ${}^2L_{Al,Li:Va}^{bcc} = 3,000$	[167]
• fcc-Al $(Al,Mg,Na,Li)_1(H,Va)_1$ ${}^0G_{Li:Va}^{Li} = G(Li_{fcc})$; ${}^0G_{Li:H}^{LiH} = G(Al_{fcc}) + 1/2G(H_2, gas) + 500,000$ ${}^0L_{Al,Li:Va}^{fcc} = -26,163.199 + 9.67T$	This work
Nonstoichiometric compounds $\gamma(Al_{12}Mg_{17}) : (Mg,Li)_{10}(Al,Mg)_{24}(Al,Mg)_{24}$ $G_{Li:Al:Mg}^{\gamma} = 10G(Li_{bcc}) + 24G(Mg_{hcp}) + 24G(Al_{fcc}) - 64,310.4$ $G_{Li:Mg:Al}^{\gamma} = 10G(Li_{bcc}) + 24G(Mg_{hcp}) + 24G(Al_{fcc}) - 574,884.4 + 145.6032T$ $G_{Li:Mg:Mg}^{\gamma} = 10G(Li_{bcc}) + 48G(Mg_{hcp}) + 388,275.2$	[128]
$\beta(Al_3Mg_2) : (Al)_{19}(Al,Mg,Li)_2(Mg,Li)_{12}$ $G_{Al:Mg:Li}^{\beta} = 2G(Mg_{hcp}) + 19G(Al_{fcc}) + 12G(Li_{bcc})$-236,586.24-69.036T $G_{Al:Al:Li}^{\beta} = 21G(Al_{fcc}) + 12G(Li_{bcc})$-236,586.24-69.036T $G_{Al:Li:Li}^{\beta} = 19G(Al_{fcc}) + 14G(Li_{bcc}) + 13,807.2$ $G_{Al:Li:Mg}^{\beta} = 12G(Mg_{hcp}) + 19G(Al_{fcc}) + 2G(Li_{bcc}) + 13,807.2$	[128]

η(AlLi): (Al,Li,Mg)$_1$(Li,Mg,Va)$_1$ $G^{AlLi}_{Al:Li} = -41,338 + 18.357T + G(Al_{fcc}) + G(Li_{bcc})$ $G^{AlLi}_{Al:Va} = 19,816 + G(Al_{fcc}); G^{AlLi}_{Li:Va} = 63,000* + G(Li_{bcc}); G^{AlLi}_{Li:Li} = 2G(Li_{bcc})$ $G^{AlLi}_{Mg:Li} = -8,405 + 10.25T + G(Mg_{hcp}) + G(Li_{bcc})$ $G^{AlLi}_{Mg:Mg} = 8,368 + 2G(Mg_{hcp}); G^{AlLi}_{Mg:Va} = 4,184 + G(Mg_{hcp})$ $G^{AlLi}_{Al:Mg} = 8,293.3 - 8.368T + G(Al_{fcc}) + G(Mg_{hcp})$ $G^{AlLi}_{Li:Mg} = G(Li_{bcc}) + G(Mg_{hcp})$ $^0L^{AlLi}_{Al,Li:Va} = 2,000; {}^0L^{AlLi}_{Al:Li,Va} = -24,418.4 + 9.58T*$ $^0L^{AlLi}_{Al,Li:Li} = 11,632; {}^1L^{AlLi}_{Al,Li:Li} = 20,000*$	[128]
Stoichiometric compounds: $298.15K < T < 1000K$ (When not specified) $G_{Al_2Li_3} = 2G(Al_{fcc}) + 3\mathrm{G}(Li_{bcc})\text{-}89,690 + 33.96T$ $G_{Al_4Li_9} = 4G(Al_{fcc}) + 9\mathrm{G}(Li_{bcc})\text{-}438,967.89 + 69.28T$	[128]
$G_{LiH} = -88,297.32 + 153.52T - 22.86T\ln T - 22.315\square 10^{-3}T^2 - 5.89\square 10^{-7}T^3 - 2,370LnT$ $G_{Al_{53}Li_{33}Mg_{14}} = 53G(Al_{fcc}) + 33\mathrm{G}(Li_{bcc}) + 14\mathrm{G}(\mathrm{Mg}_{hcp})\text{-}1,324,573.135 + 2,729T$	[128]
$G_{LiAlH_4} = -330,533.6 + 4,817.71T - 811.34T\ln T + 1.23T^2 + 39.6\square 10^{-5}T^3 + 8,948,260T^{-1}$ $298K < T < 500K$ $G_{LiAlH_4} = -132,001.66 + 206.9T - 38.11T\ln T - 0.081T^2 + 1.42\square 10^{-5}T^3 - 461,924.05T^{-1}$ $500K < T < 800K$ $G_{Li_3AlH_6} = -331,337.95 + 674.27T - 110.34T\ln T - 0.081T^2 - 1.77\square 10^{-6}T^3 + 446,400T^{-1}$ $-7,110\ln T$	[145]
$G_{LiMg(AlH_4)_3} = G(LiH) + G(MgH_2) + 3G(AlH_3) + 37,221$ $G_{LiMgAlH_6} = G(LiH) + G(MgH_2) + G(AlH_3) - 1,350$ $G_{Na_2LiAlH_6} = G(LiH) + G(NaH) + G(NaAlH_4) - 36,124.41 + 47.91T$	This work

4.4 Results and discussion

4.4.1 Thermodynamic properties of Mg-Al-Li-Na-H system

4.4.1.1 Li-Mg

Figure 4.3 shows the calculated Li-Mg phase diagram in comparison with experimental data. Good agreement can be seen between the calculated phase diagram and the selected experimental data except for the calculated solubilities of magnesium in bcc-Li which were

lower than those measured by Freeth and Raynor [171]. This result was also found in the previous Li-Mg phase diagram calculations [168, 177-180] and it was not possible, in this work, to find a set of parameters that reproduce the results of [171]. Freeth and Raynor [171] reported that quenching of a sample with bcc-Li phase at higher temperature causes the precipitation of the hcp-Mg phase and this might be the source of error in the determination of the boundary (hcp-Mg + bcc-Li)/(bcc-Li). General agreement exists between the calculated phase diagram in this work and in the assessment of Saunders [179]. In the Li-rich region of the liquidus in Figure 4.3, the results by Henry and Cordiano [169], Grube *et al*. [170], and Feitsma *et al*. [172] have been chosen in this work for their close agreement and especially the resistivity measurements of Feitsma *et al*. [172], who determined the liquidus temperatures at 1 K intervals using high purity alloys.

The calculated Li solidus region of the phase diagram is in very good agreement with the results of Grube *et al.* [170]. As stated by Nayeb-Hashemi *et al*. [168], the lower solidus of Henry and Cordiano [169] has been caused by the segregation present in the alloys containing relatively high Li content.

The calculated heat of mixing for the liquid phase at 940 K is presented in comparison with the experimental data in Figure 4.4. Better agreement exists between the calculated and the measured heat of mixing [175] than the results of Saunders [179], presented in dotted line in Figure 4.4, with lower number of parameters. The calculated Li activities in the liquid phase at 670, 735, 830, and 887 K (not shown here) are very similar to the assessment of Saunders [179]. Both calculations show very good agreement with the experimental data [176]. .

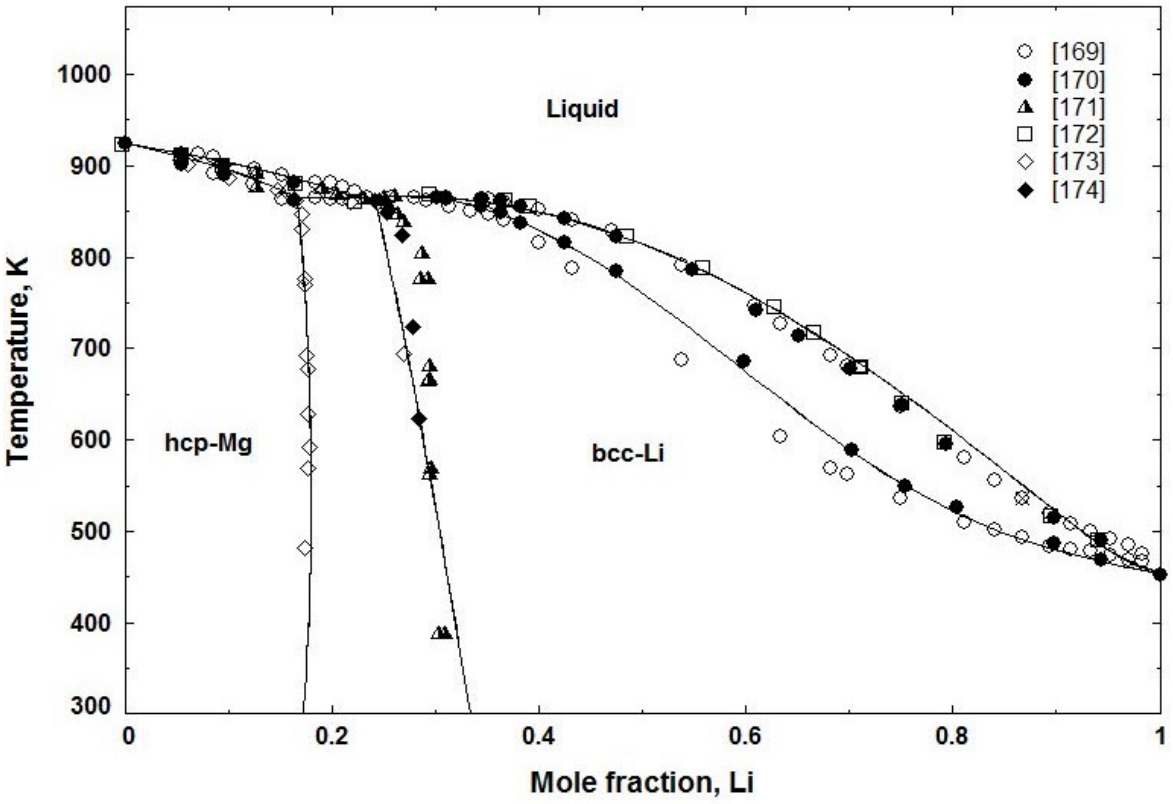

Figure 4.3 Calculated Li-Mg phase diagram in comparison with experimental data from

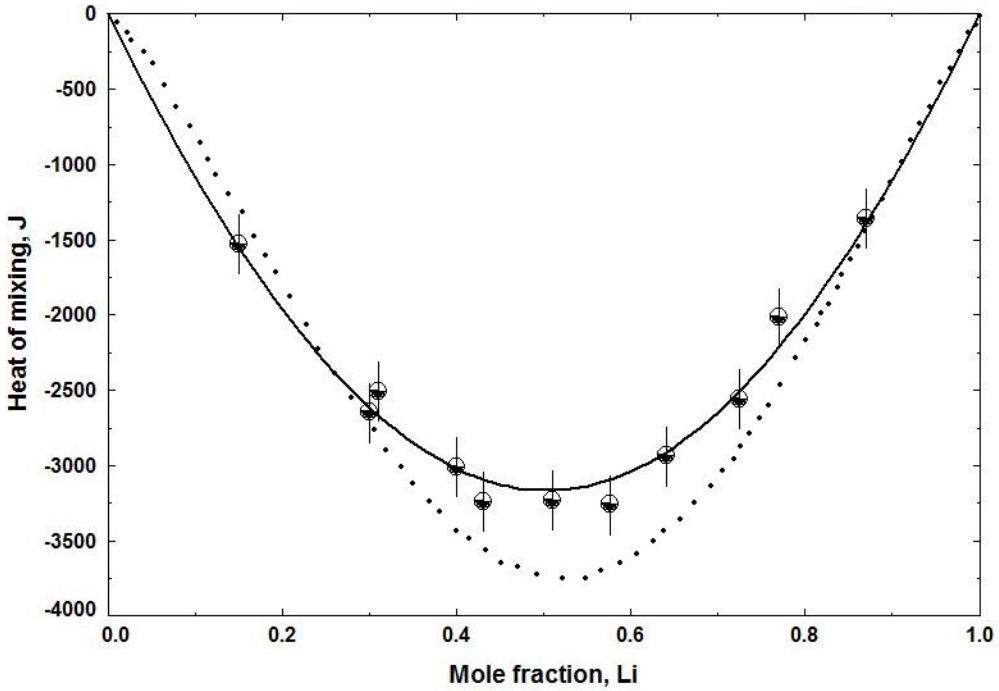

Figure 4.4 Calculated heat of mixing for liquid Li-Mg system at 940 K in comparison with experimental data [175] in this work (full line) and by saunders [179] (dotted line)

4.4.1.2 Li-Na

The calculated Li-Na phase diagram is presented in Figure 4.5 where good agreement with the experimental data from the literature is shown. Since, no thermodynamic data have been found in the literature for this system, the model parameters have been selected to reproduce the liquid miscibility gap and the bcc (Li and Na) miscibility gap. The results obtained in this work are comparable to those obtained by Zhang *et al*. [191] and deviate slightly from those of Pelton [36]. In fact, the calculations of Zhang *et al*. [191] showed better agreement with the experimental data especially near the consolute point compared to the work of Pelton [190].

4.4.1.3 Al-Li-Mg

The parameters used to model the Al-Li-Mg system are given in table 4.1. As discussed in section 4.2.1.5, Harvey [128] extrapolated the ternary liquid phase from the constituent binaries using the MQM for Al-Li and Al-Mg and substitutional solution model for Li-Mg. In this work, only the MQM is used; the model parameters of Harvey [128] for Al-Li and Al-Mg binary systems have been adopted and Li-Mg has been remodeled using the MQM in this work. As discussed in section 4.2.1.5, the parameters used by Harvey [128] for the ternary compound τ ($Al_{53}Li_{33}Mg_{14}$) and the binary compounds (where solid solubility of the third element was considered) have been adopted in this work. The terminal solid solutions fcc-Al, hcp-Mg, and bcc-Li/Na have been remodeled using the CEF. The results (not shown here) are in reasonable agreement with experimental data and comparable to those obtained by Harvey [128] for the heat of mixing of liquid and Al-Li-Mg phase diagram. As discussed in section 4.4.1.1, the calculated heat of mixing of Li-Mg liquid (using the MQM) show better agreement with the experimental data than the calculations done by Saunders [179] (which was used by Harvey [128] to extrapolate the ternary liquid in the assessment of Al-Li-Mg system). In this work, no improvement is shown with respect to the heat of mixing for the ternary liquid calculated by Harvey [128] because the available experimental data [41] covered only a small composition range.

The calculated isothermal sections at 473, 573, and 673 K (200, 300, and 400°C) are in good agreement with the experimental data [196] and comparable with the results of Harvey [128]. The calculated isothermal section at 673 K (400°C) is shown in Figure 4.6.

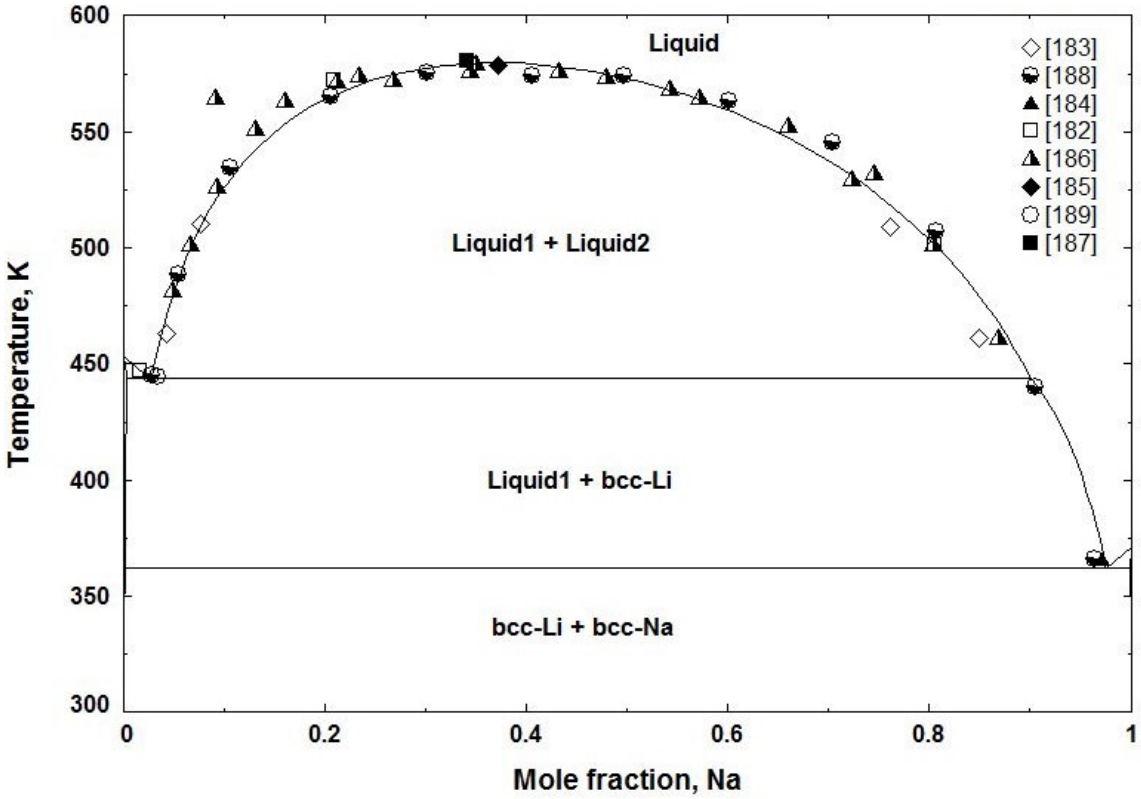

Figure 4.5 Calculated Li-Na phase diagram at 1 bar compared with experimental data

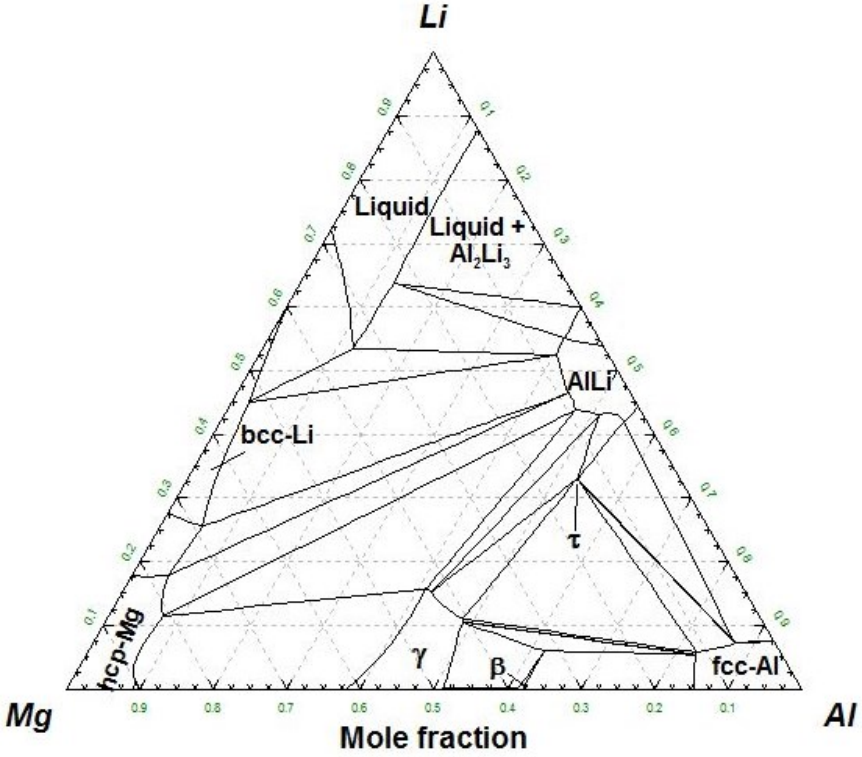

Figure 4.6 Calculated Al-Li-Mg isothermal section at 673 K and 1 bar

4.4.1.4 Al-Li-H

$LiAlH_4$ and Li_3AlH_6 hydrides are considered as stoichiometric compounds. The calculated pressure-temperature diagram and reaction path of $LiAlH_4$ composition are presented in Figure 4.7. It should be noted that "Gas" phase in Figure 4.7a refers to all the gases cited in section 4.3 including H_2 whereas Figure 4.7b shows the amount of released hydrogen. Figure 4.7a shows that $LiAlH_4$ is not stable and do not form even at very high pressures. Jang *et al*. [202] reported that, according to their calculations, Li_3AlH_6 could absorb hydrogen to form $LiAlH_4$ at pressures above 10^3 bar. However they [202] did not include AlH_3 hydride in their calculations. According to Figure 4.7b, reaction (4.1) is spontaneous and Li_3AlH_6 decomposes reversibly according to reaction (4.2) to form LiH, fcc-Al, and H_2 at 69.9°C and 1 bar. Some of the LiH decomposes at 573.6°C accompanied with the formation of AlLi and H_2 according to equation (3). Based on the current work, the remaining LiH and AlLi both melt at around 674°C forming two immiscible liquids. Liquid LiH (Liquid 2 in Figure 4.7) decomposes gradually to form liquid phase at about 701°C. Al and Li contents in fcc-Al, AlLi and Liquid phases are presented in Figure 4.7b in dashed and dotted lines, respectively, in the same color as the corresponding phase. It shows that the gradual decrease in the amount of LiH is accompanied by an increase of the Li content in fcc-Al and of the released hydrogen when the temperature is increased. This proves that there is a destabilization effect between Al and LiH because of the solubility of Li in fcc-Al which reaches its maximum at 573.6°C where AlLi forms. It can be seen in Figure 4.7b that the amount of the formed AlLi and Li dissolved in it increase with temperature while the amount of Al dissolved in AlLi is constant and the amount of the remaining LiH decreases. This shows that AlLi destabilises LiH because of the solubility of Li in AlLi.

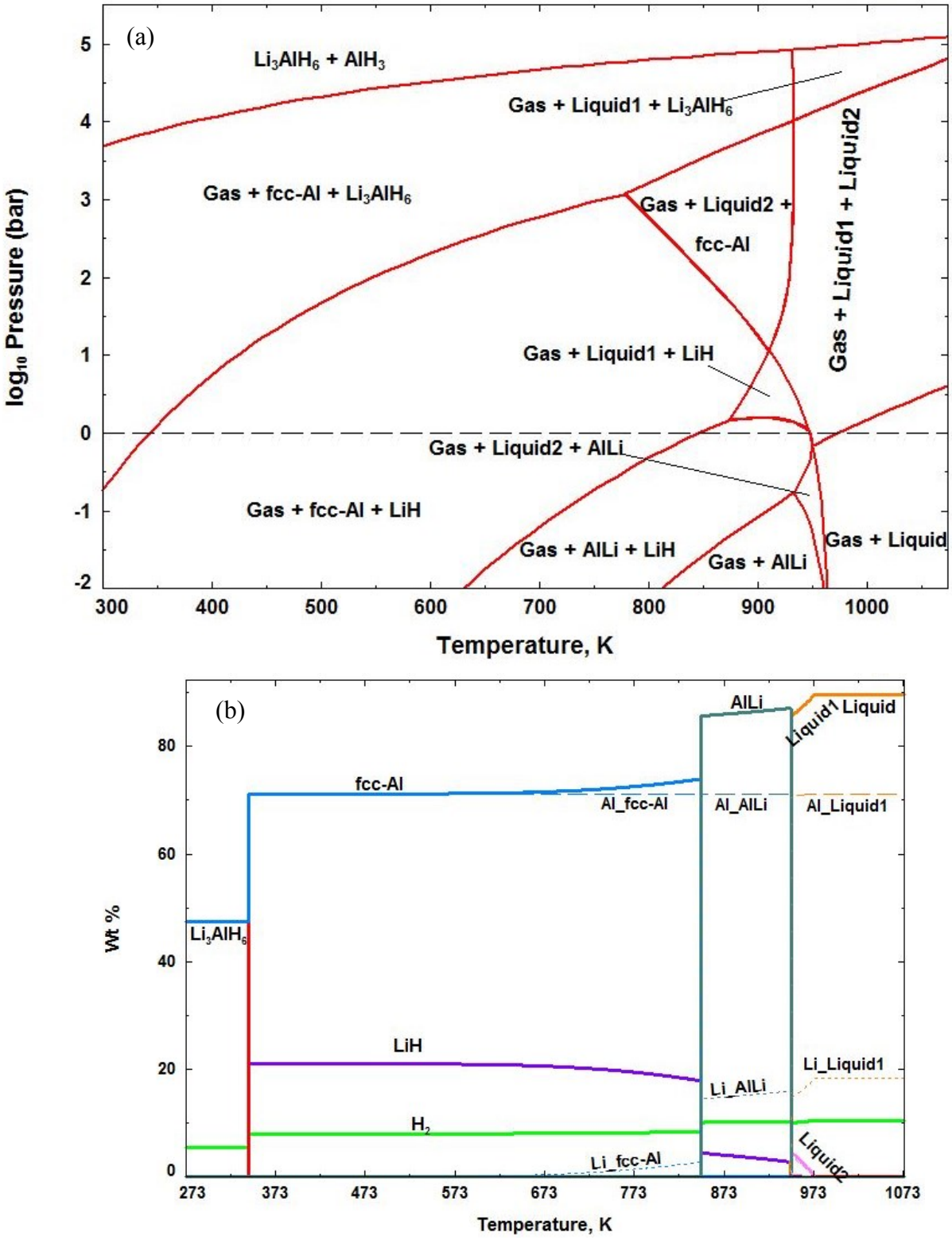

Figure 4.7 Calculated (a) Pressure-Temperature diagram and (b) Reaction path at 1 bar, for $LiAlH_4$

4.4.1.5 Li-Mg-H

As discussed in section 4.2.1.7, no experimentally confirmed ternary hydrides have been found in the Li-Mg-H system. However, some researchers reported a destabilization effect between Mg and LiH with the formation of Mg-Li compound $Li_{0.92}Mg_{4.08}$ as mentioned in section 4.2.2.

The calculated Li-Mg phase diagram presented in Figure 4.3 shows that the system is composed of only bcc-Li and hcp-Mg solid solutions, and that the solubility of Li in hcp-Mg is about 20 at. % Li. The Mg-Li compound $Li_{0.92}Mg_{4.08}$ cited in the literature [220] has the same crystal structure as hcp-Mg solid solution and its composition approaches the solid solubility limit of Li in hcp-Mg, which suggests that, when mixed with Mg, Li from LiH hydride starts dissolving in Mg until its solubility limit of about 20 at. %.

In order to investigate the effect of Mg on LiH, the calculated LiH-Mg phase diagram at 1bar is shown in Figure 4.8. It shows that LiH in the LiH-Mg mixture starts releasing hydrogen at 580.55 K (307.4°C) and the produced Li is dissolved in hcp-Mg. As the temperature increases, the solubility limit of Li, stemming from LiH, in hcp-Mg increases (following the phase boundary hcp-Mg/hcp-Mg + LiH) until it reaches a maximum of 8.3 at. % LiH at 891.65 K (618.5°C). Figure 4.8 shows that LiH hydride is too stable; only a very small amount decomposes because of the solubility of the produced Li in hcp-Mg.

4.4.1.6 Quaternary hydrides

The quaternary compounds, $LiMg(AlH_4)_3$, $LiMgAlH_6$, and Na_2LiAlH_6 are considered in this work as stoichiometric compounds and their thermodynamic parameters are reported in Table 4.1. The assessment of $LiMg(AlH_4)_3$ and $LiMgAlH_6$ hydrides is performed based on the work of Grove *et al*. [145] and using the experimental data reported by Mamatha *et al*. [146] and Tang *et al*. [46]. Figure 4.9 presents the calculated pressure-temperature diagram for $LiMg(AlH_4)_3$ composition. It shows that the two compounds, $LiMg(AlH_4)_3$ and $LiMgAlH_6$, are not stable and then, reactions (4.4) and (4.5) are not reversible which is in very good agreement with the results of Tang *et al*. [46]. Figure 4.9 shows that, at 1 bar, $LiMg(AlH_4)_3$ decomposes spontaneously to form Li_3AlH_6, MgH_2, and fcc-Al.

Na_2LiAlH_6 is thermodynamically assessed for the first time in this work. Table 4.2 summarizes the calculated enthalpy and entropy of dehydrogenation of Na_2LiAlH_6, reaction (4.6), in comparison with experimental data from the literature.

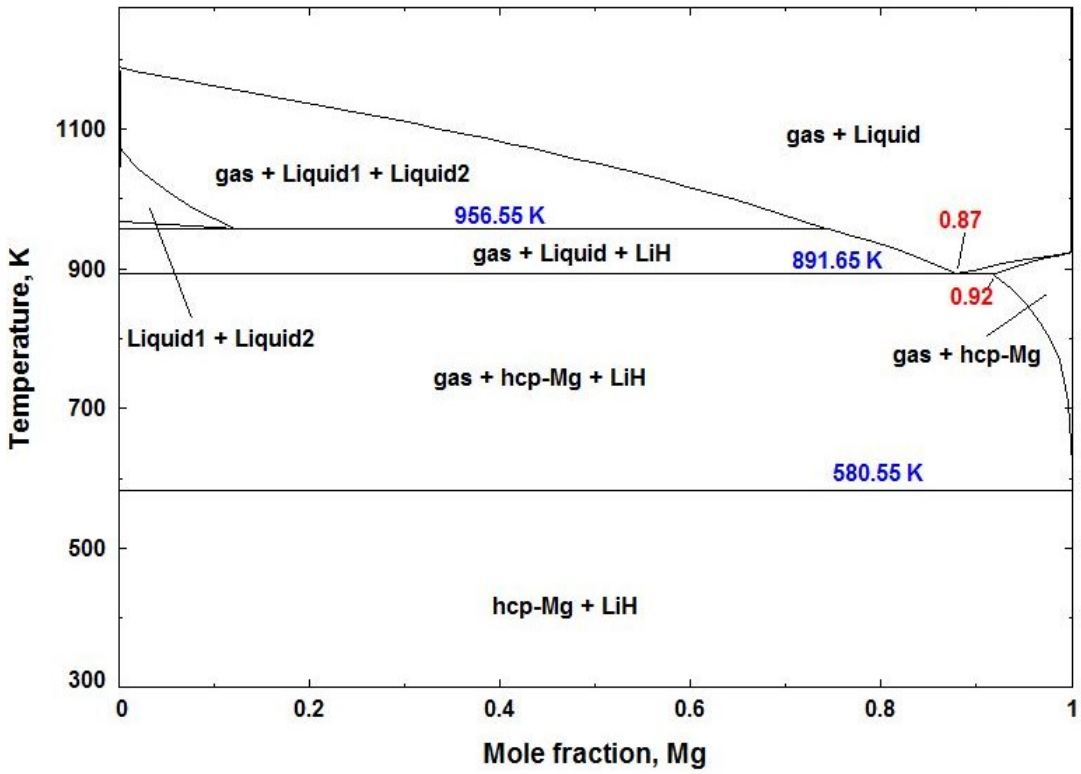

Figure 4.8 Calculated Mg-LiH phase diagram at 1 bar

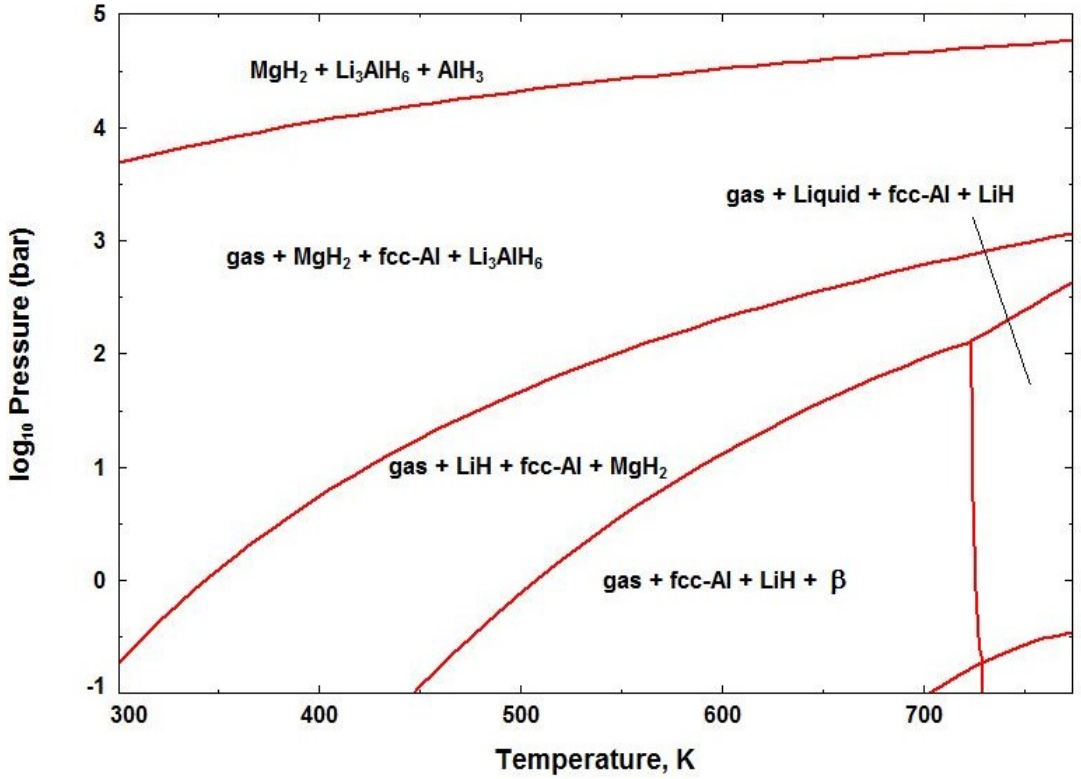

Figure 4.9 Calculated Pressure-Temperature diagram of $LiMg(AlH_4)_3$

Table 4.2: **Enthalpy and entropy for reaction (4.6): Na_2LiAlH_6 → 2 NaH + LiH + Al + 3/2 H_2**

ΔH (kJ/mol.H_2)	ΔS (J/K.mol.H_2)	Experiment	Reference
60.75	**145.1**	**-**	**This work**
62.8	-	DSC	[216]
52.3	-	PDSC (2bar H_2)	[217]
63.8	152.1	PCI	[219]
60.7±0.9	146.5 ± 1.9	PCI	[218]
56.4 ± 0.4	137.9 ± 0.7	PCI*	[218]
53.5±1.2	132.1 ± 2.4	PCI	[214]

* These values were found excluding the data point measured at 443 K (170°C)

It can be seen in Table 4.2 that Claudy *et al*. [216] and Huot *et al*. [217] reported different values for the enthalpy of reaction (4.6) using DSC experiments. It should be noted that the experimental conditions were also different. Huot *et al*. [217] realized his measurements under a hydrogen pressure of 2 bar and a heating rate of 10 K/min. Claudy *et al*. [216] experiments were under argon and with a heating rate of 1K/min. The enthalpy and entropy values for reaction (4.6) obtained from Pressure-Composition isotherms (PCI) reported in Table 4.2 are also scattered. This can be explained by the poor kinetics of reaction (4.6), the long time needed to reach equilibrium and the slopped plateaus. Wang *et al*. [219] did not show PCI curves and reported a slightly higher enthalpy change than Claudy *et al*. [216]. Fossdal *et al*. [218], in turn, showed 5 PCI curves for catalyzed Na_2LiAlH_6 for temperatures between 443 and 523 K (170 and 250°C). The plateaus were almost flat for high temperatures. Fossdal *et al*. [218] calculated two sets of values for enthalpy and entropy of reaction (4.6) reported in Table 4.2 using Van't Hoff plot. The results of Fossdal *et al*. [218] are in good agreement with Bogdanović *et al*. [118], who reported one PCI curve at 484 K (211°C) showing an equilibrium pressure of about 13 bar. The PCIs reported by Graetz *et al*. [214] or catalyzed and un-catalyzed Na_2LiAlH_6 were slopped at low temperature with only two or three data points in the plateau region. Figure 4.10 shows the calculated Van't Hoff plot for reaction (4.6) in comparison with PCI experimental data from the literature.

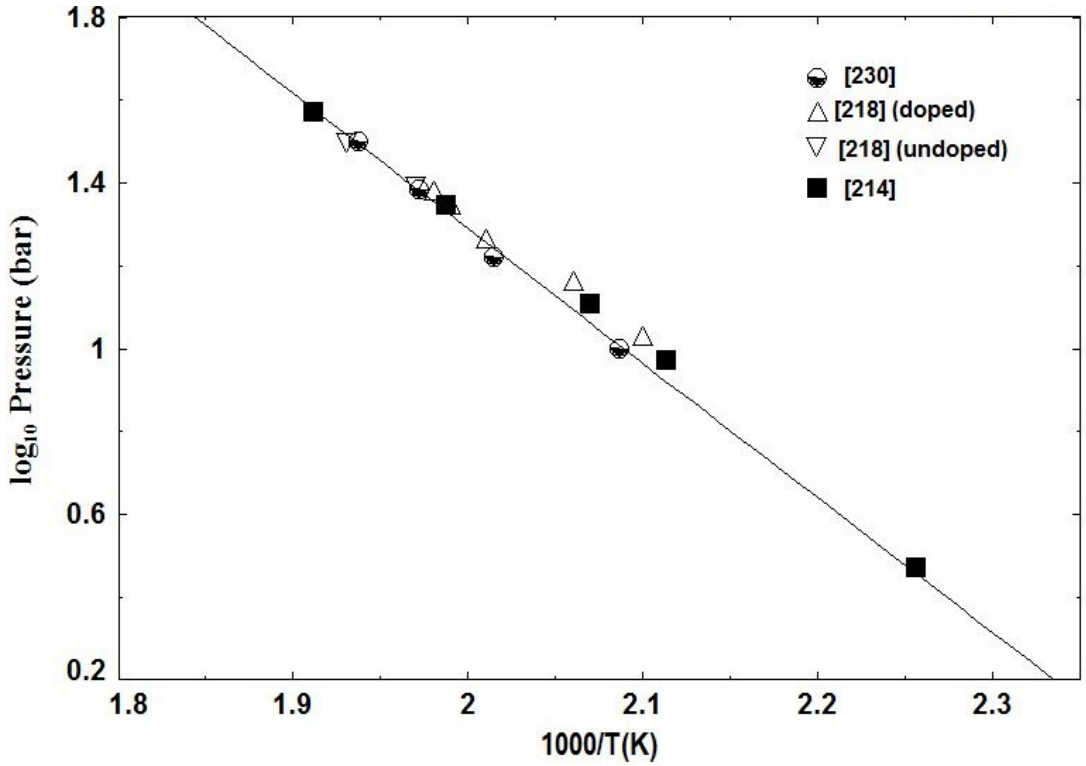

Figure 4.10 Calculated Van't Hoff plot (solid line) for the dissociation of Na_2LiAlH_6 (reaction (4.6))

Good agreement can be seen between the calculated equilibrium pressures and the experimental data [214, 218, 230]. The calculated enthalpy of reaction (4.5) in the current work is lower but approaches more the enthalpy reported by Claudy *et al*. [216] using DSC measurements. The decomposition temperature of Na_2LiAlH_6 at 1bar is calculated to be 417.23 K (144.1°C).

4.4.2 Hydrogen storage properties

The calculated MgH_2-$LiAlH_4$ phase diagram at 1 bar is presented in Figure 4.11a. It shows that $LiAlH_4$ decomposes spontaneously and the mixture is initially composed of fcc-Al solid solution, MgH_2, and Li_3AlH_6. At 343.03 K (69.9°C), Li_3AlH_6 decomposes to form LiH and fcc-Al. The remaining phase transitions concern the decomposition of MgH_2-Al mixture, which depends on the atomic ratio of Mg and Al as discussed in our previous paper [166] . The phase diagram MgH_2-Li_3AlH_6 (not presented here) is similar to the phase diagram of MgH_2-$LiAlH_4$ with respect to phase relations which proves that dehydrogenation of Al-Li hydrides in the mixture is not affected by MgH_2 and that only the Al produced following their decomposition destabilizes MgH_2. Figure 4.11a also shows that LiH does not take part in the dehydrogenation process of

MgH_2. As discussed in section 4.2.2, many authors have reported a destabilization effect between MgH_2 and LiH and claimed that this was due to the formation of Li-Mg compounds $Li_{0.92}Mg_{4.08}$ and Li_3Mg_7. However, $Li_{0.92}Mg_{4.08}$ and Li_3Mg_7 are not compounds in the widely accepted Li-Mg equilibrium phase diagram. In fact, Zhang *et al*. [220] identified, using XRD, two dehydrogenation stages in the $4MgH_2$-$LiAlH_4$ composites. The first stage was attributed to the two steps decomposition of $LiAlH_4$ (reactions (4.1) and (4.2)) and the second one to the decomposition of MgH_2 (reactions (4.6) and (4.7)) which means that the composite was composed of $Li_{0.92}Mg_{4.08}$ and γ phases. However, Zhang *et al*. [220] could detect LiH peaks in the XRD results of dehydrogenated state at 773 K (500°C) for all the MgH_2-$LiAlH_4$ composites that they investigated. Ismail *et al*. [229] reported Mg as rehydrogenation product at 673 K (400°C) besides $Li_{0.92}Mg_{4.08}$ and γ-phase for the same composite; $4MgH_2$-$LiAlH_4$, with the peaks of $Li_{0.92}Mg_{4.08}$ and Mg overlapping in the XRD patterns. Similar results have been reported by Chen *et al*. [222] for the MgH_2-$LiAlH_4$ composites with molar ratios 2.5:1 and 4:1 after dehydrogenation at 623 K (350°C). For the composites with molar ratio 1:1, Chen *et al*. [222] reported that the peaks of $Li_{0.92}Mg_{4.08}$ or Mg could not be observed in the XRD results. In TiF_3-MgH_2-$LiAlH_4$ (0.05:1:1) composites, Mao *et al*. [223] identified γ as a dehydrogenation product at 673 K (400°C), and since no LiH was detected, they [223] identified Mg_7Li_3 as a possible product; they claimed that its peaks overlap with those of γ-phase in the XRD patterns.

The calculations shown in Figure 4.11 are compared to the above-cited experimental data [220, 222, 223, 229] . MgH_2-$LiAlH_4$ (4:1) and (2.5:1) composites correspond to 80 and 71.4 mole% MgH_2, respectively, in Figure 4.11a, which shows that the dehydrogenation products of these composites at 673 K (400°C) are γ, hcp-Mg, and LiH. For MgH_2-$LiAlH_4$ (1:1) composite, Figure 4.11a shows that the dehydrogenation products are γ and LiH only.

The fact that the reported $Li_{0.92}Mg_{4.08}$ compound has the same crystal structure as hcp-Mg and its XRD peaks coincide with those of magnesium [222, 229], suggests that the phase indexed as $Li_{0.92}Mg_{4.08}$ compound might be actually hcp-Mg solid solution and that, except the small solid solubility of Li (from LiH) in hcp-Mg (as discussed in section 4.4.1.5), there is no destabilization effect between MgH_2 and LiH (reaction (4.6)). This suggestion is supported by the results of Chen *et al*. [222], who reported that, neither $Li_{0.92}Mg_{4.08}$ nor hcp-Mg were detected after dehydrogenation of MgH_2-$LiAlH_4$ (1:1) composite which is in very good agreement with the

calculations shown in Figure 4.11a. Also, the assumption of Mao *et al*. [223] concerning Mg_7Li_3 compound as a possible product (with XRD peaks overlapping with those of γ-phase) after dehydrogenation of MgH_2-$LiAlH_4$ (1:1) composite cannot be supported only by the fact that LiH peaks could not be detected in XRD results. In addition, Liu *et al*. [221, 224] did not report any Mg-Li phase in the dehydrogenation process of MgH_2-$LiAlH_4$/Li_3AlH_6 composites. These authors [221, 224] argued that peaks of LiH are not detected in XRD results due to its small amount in comparison to Mg-related phases, its lower atomic number and amorphous structure. In fact, almost all the experimental data for MgH_2-$LiAlH_4$ composites reported that LiH is produced after rehydrogenation of the composites but its XRD peaks are hardly detected or overlapped by those of Al. Also, Zhang *et al*. [220] conducted isothermal dehydrogenation of MgH_2-LiH composite at 773 K (500°C) and reported Li_3Mg_7 and $Li_{0.92}Mg_{4.08}$ as the decomposition products. However the hydrogen released from the sample did not exceeded 6 wt. % H_2 [220] that is well below the hydrogen capacity of the composite (8.82 wt. % H_2) and no other amorphous or unknown phases have been reported as other reaction products [220]. A reason for this inconsistency may be that only MgH_2 has decomposed (hcp-Mg could be indexed as $Li_{0.92}Mg_{4.08}$) and LiH could not be detected which explains the difference between the H_2 capacity of the composite and the amount of H_2 released and supports the results of this work. However, there is no other possible phase that could be indexed as Li_3Mg_7 in the decomposition products as reported by Zhang *et al*. [220].

The calculated reaction path of $4MgH_2$-$LiAlH_4$ composite is presented in Figure 4.11b. In this figure, the released hydrogen H_2, which is part of the gas phase shown in Figure 4.11a, is presented in green line and the gas phase is presented with a dotted line. Figure 4.11b shows that $LiAlH_4$ decomposes spontaneously to form Li_3AlH_6 and fcc-Al and releases 1.4 wt. % H_2. At 343.02 K (69.9°C), Li_3AlH_6 decomposes to form LiH, fcc-Al and 0.7 wt. % H_2.

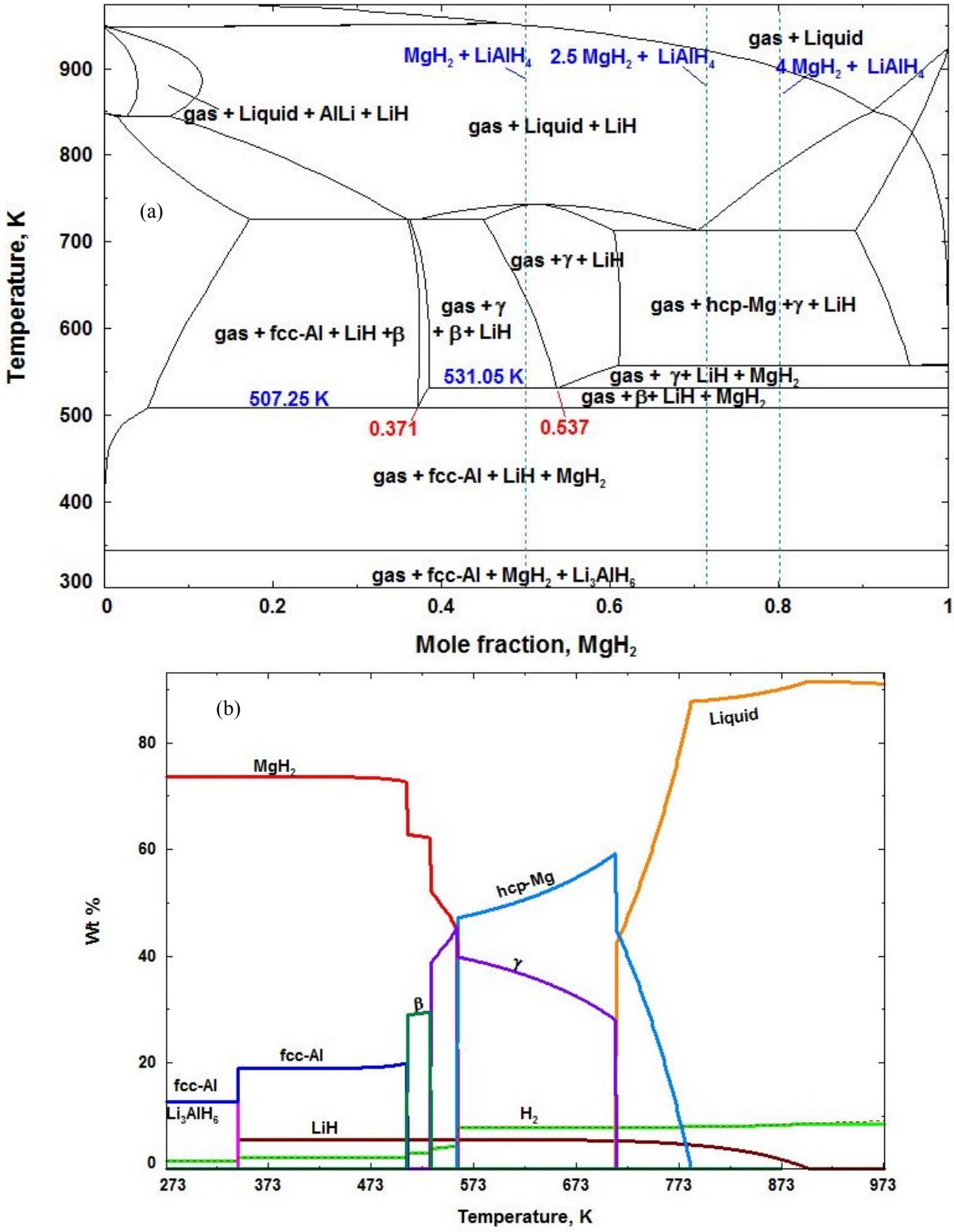

Figure 4.11 a) Calculated MgH_2-$LiAlH_4$ phase diagram at 1 bar, b) Calculated reaction path of 4 MgH_2-$LiAlH_4$ composite at 1 bar

It can be seen that during the two steps decomposition of $LiAlH_4$, MgH_2 does not play any role. From 343.03 K to 556.45 K (69.9°C to 283.3°C), MgH_2 is destabilized by the produced Al and decomposes in three steps: at 507.25 K (234.1°C) to form β-phase, at 530.65 K (257.5°C) to form γ-phase, and at 556.45 K (283.3°C) to form hcp-Mg. Additional amounts of hydrogen of 0.07 wt. % H_2, 1.56 wt. % H_2, and 4 wt. % H_2 are released in these steps, respectively. LiH does not contribute to these reactions. Figure 11b shows a small gradual decrease in the amount of LiH between 556.45 K and 711.85 K (283.3°C and 438.7°C), which can be attributed to the destabilization effect of Mg as discussed in section 4.4.1.5. With increasing temperature from 556.45 K to 784.25 K (283.3°C to 511.1°C), 0.14 wt. % H_2 is released gradually from the mixture. Finally at 899.55 K (626.4°C), all the LiH has decomposed and a total amount of 8.57 wt. % H_2 is released from the composite.

After rehydrogenation at 673 K (400°C) and 4MPa (40 bar), Zhang *et al*. [220] showed that the $4MgH_2$-$LiAlH_4$ composite contains MgH_2, LiH, and Al_3Mg_2 (β-phase). These authors [220] concluded that only MgH_2 is reversible in this composite with a loss in the hydrogen capacity because of the formation of β-phase. In turn, Chen *et al*. [222] reported that only MgH_2 and LiH can be reformed after rehydrogenation at 623 K (350°C) and 10 MPa (100 bar) in the $4MgH_2$-$LiAlH_4$ composite. Liu *et al*. [221] showed that the mixture $4MgH_2$-Li_3AlH_6 is composed of MgH_2, Al, and LiH after rehydrogenation under 623 K (250°C) and 2 MPa (20 bar) H_2. To analyze these different experimental results, the Pressure-Temperature (P-T) diagrams of the $4MgH_2$-$LiAlH_4$ composites are calculated in this work and presented in Figure 4.12. The P-T diagrams of $4MgH_2$-$LiAlH_4$ and $4MgH_2$-Li_3AlH_6 are similar. Figure 4.12 predicts the conditions (pressure and temperature) for the reversibility of the hydrogenation process of the composites $4MgH_2$- $LiAlH_4$/Li_3AlH_6. It can be seen that the calculations agree very well with all the cited experimental results [220-222] and give the conditions for the reversibility of the $4MgH_2$-Li_3AlH_6 composite. All the reported data for the undoped MgH_2-$LiAlH_4$ [220, 222] and MgH_2-Li_3AlH_6 [221] show that the dehydrogenation kinetics and temperatures of these composites were improved in comparison with the composing hydrides and related these improvements to mutual catalytic effects between the hydrides. According to this work, MgH_2 does not affect the thermodynamics of $LiAlH_4$ and Li_3AlH_6 hydrides' decomposition and then, we can conclude that the improved reactions might be due to a catalytic effect of MgH_2. However, the improvement in

MgH_2 decomposition is related to its destabilization by the resulting Al to form Mg-Al compounds, which with LiH might play a catalytic role on the decomposition of MgH_2.

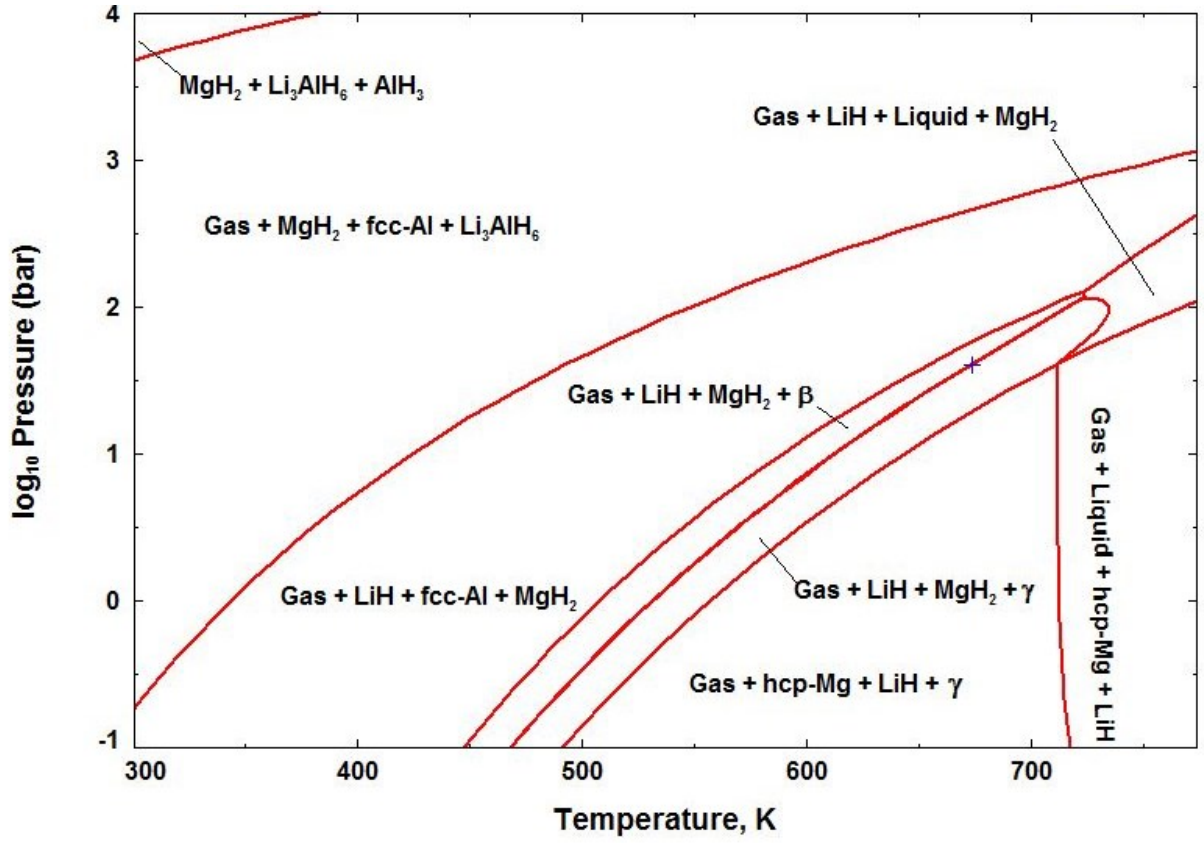

Figure 4.12 Calculated Pressure-Temperature diagram of $4MgH_2$-$LiAlH_4$ composite

The constructed database for the Mg-Al-Li-Na-H system allows predicting the dehydrogenation reaction mechanisms for all the possible composites in the system. According to our previous paper [166] . MgH_2 dehydrogenation occurs following reaction (4.10). It has been already proved [166] that destabilization of MgH_2 is due to the effect of Al. In the MgH_2-$LiAlH_4$/Li_3AlH_6 composites, Al is produced from the decomposition of $LiAlH_4$/Li_3AlH_6 and MgH_2 decomposition route depends on the ratio of Mg to Al atoms [2]. Since $LiAlH_4$ is metastable, Li_3AlH_6 is preferable as Al source for its reversibility, its hydrogen content and low decomposition temperature. The dehydrogenation of Li_3AlH_6 proceeds according to reaction (4.11). Figure 4.11a shows that for Mg composition of 37.1 mole%, MgH_2 reacts with Al to form β-phase and

releases all its hydrogen (6.07 wt. % H_2) at 507.25 K (234.1°C). For Mg composition of 53.7 mole%, MgH_2 reacts with β-phase to form γ-phase and releases all its hydrogen (6.36 wt. % H_2) at 531.05 K (257.9°C). It can be concluded that at these compositions, the maximum amount of hydrogen is released from the destabilized MgH_2. Reaction path of MgH_2-Li_3AlH_6 composites with MgH_2 content of 37.1 mole% and 53.7 mole% is calculated in this work at 1 bar and presented in Figure 4.13.

$MgH_2 \xrightarrow{557.8\ K} Mg + H_2$ (7.65 wt. %H_2), $\Delta H = 78.59$ kJ/molH_2 .....(4.10)

$Li_3AlH_6 \xrightarrow{443.1\ K} 3\ LiH + Al + 1.5\ H_2$ (5.6 wt. %H_2), $\Delta H = 33.90$ kJ/molH_2 .....(4.11)

We have already shown for the Mg-Al-Na-H system [166] that in MgH_2-$AlNaH_4$/Na_3AlH_6 composites, the component hydrides destabilize mutually and spontaneously to form a more stable hydride, $MgNaH_3$, which reduces significantly the hydrogen storage potential of the system.

As discussed in section 4.4.1.6, there is only one stable quaternary hydride in the Mg-Al-Li-Na-H system, Na_2LiAlH_6, whose decomposition path and properties are given by reaction (4.12).

$Na_2LiAlH_6 \xrightarrow{417.2\ K} Al + 2\ NaH + LiH + 1.5\ H_2$ (3.52 wt. %H_2), $\Delta H = 61.83$ kJ/molH_2 .....(4.12)

Reaction (4.12) shows that this hydride might contribute to the destabilization of MgH_2 because of its decomposition products. According to the current thermodynamic modeling, MgH_2 and Na_2LiAlH_6 destabilize mutually at 308.4 K (35.25°C) to form $MgNaH_3$. The maximum amount of hydrogen released at 308.4 K from MgH_2/Na_2LiAlH_6 composites is for MgH_2 content of 2/3 mole fraction. The reaction path of this composite at 1 bar is presented in Figure 4.14. It shows that 1.45 wt. % H_2 is released from the composite at 308.4 K (35.25°C) where $MgNaH_3$, Li_3AlH_6, and fcc-Al form. A total of 2.19 wt. % H_2 is released from the composite at 443.02 K (69.9°C) following the decomposition of Li_3AlH_6. It can be concluded that even though MgH_2 and Na_2LiAlH_6 destabilize mutually and the decomposition temperature is reduced, the formation of $MgNaH_3$ reduces the hydrogen storage potential of the system.

As a result of this work and our previous results [117, 166], it can be concluded that the addition of Na to Mg-Al-Li-H system leads to the formation of $MgNaH_3$ and thus reduces the potential of the system for mobile applications according to the recommendation of DOE [5], and that more work is needed to improve the hydrogen storage properties of Mg-Al-Li-H system.

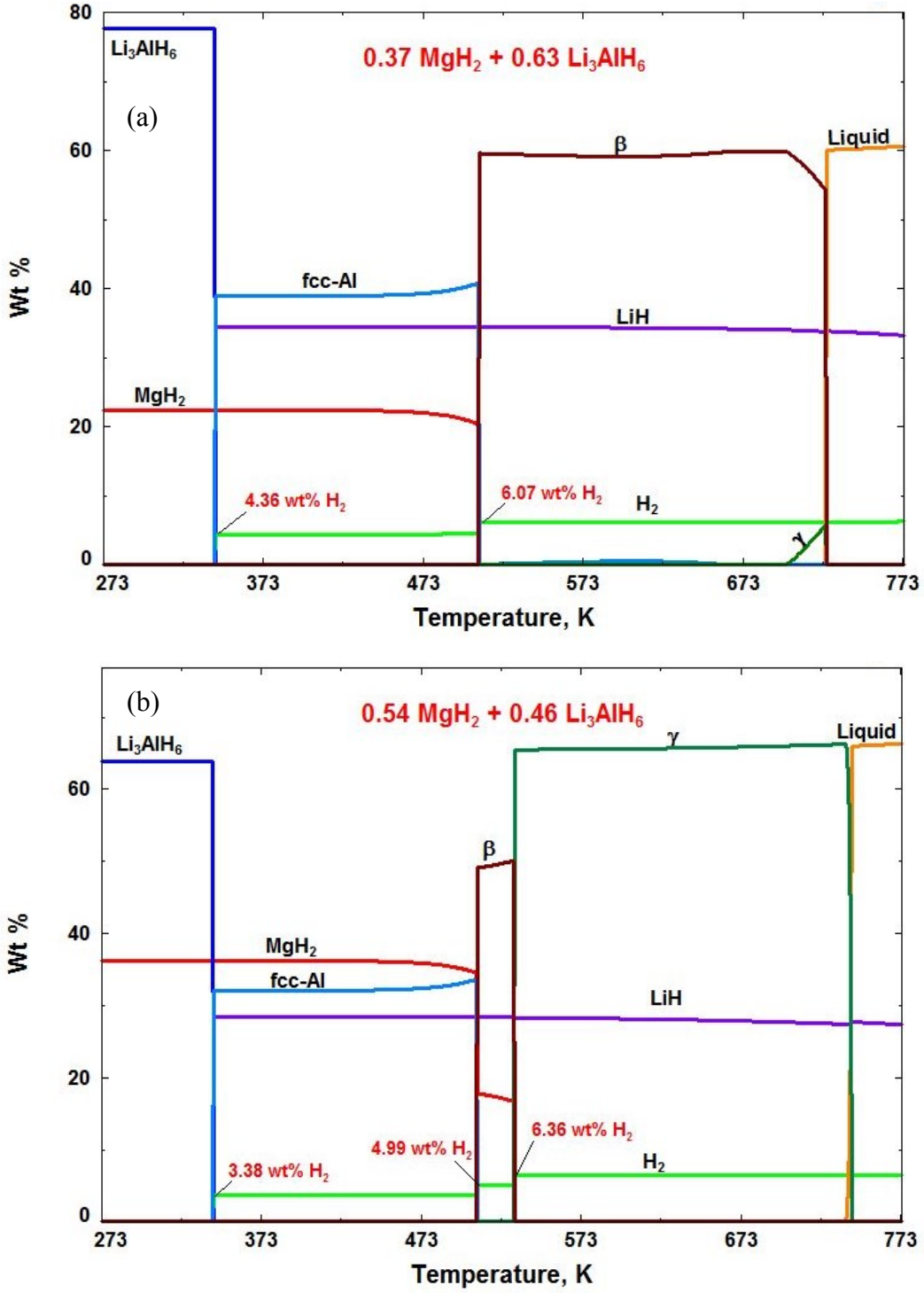

Figure 4.13 Calculated reaction path of the most promising MgH_2-$AlLi_3AlH_6$ composites at 1 bar a) 0.37 MgH_2 + 0.63 Li_3AlH_6, b) 0.54 MgH_2 + 0.46 Li_3AlH_6

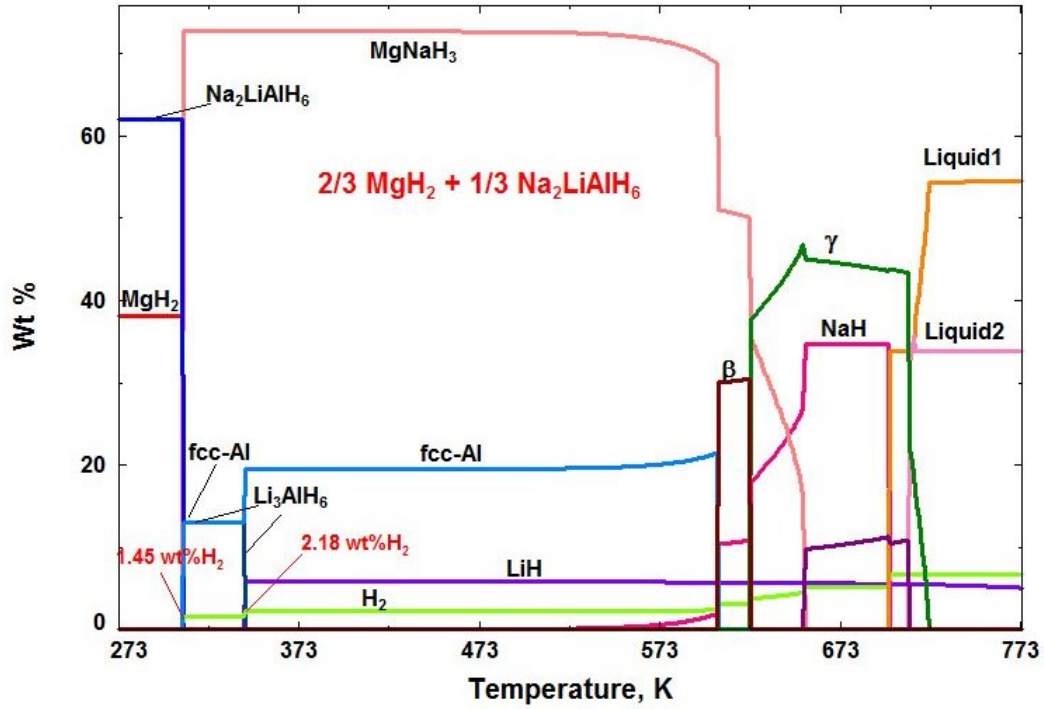

Figure 4.14 Calculated reaction path of 2/3 MgH_2 + 1/3 Na_2LiAlH_6 composite at 1 bar

4.5 Conclusions

Thermodynamic modeling is used in this work to construct a database that describes the Mg-Al-Li-Na-H system in order to study its hydrogen storage properties. Since Mg-Al-Na-H system was studied before, only Li related binaries and ternaries are re-assessed in this paper. MQM and CEF are used to describe the liquid and the solid solution phases, respectively. Reaction pathways for MgH_2-$LiAlH_4$/Li_3AlH_6 composites are calculated and compared to the experimental data from the literature. A very good agreement has been found except for Li-Mg compounds reported in the literature. It is concluded that the reported $Li_{0.92}Mg_{4.08}$ is actually hcp-Mg, because the reported XRD peaks of this compound are identical to those of hcp-Mg and no compounds exist in the accepted Li-Mg phase diagram. Also, it is found that LiH is very stable and does not contribute to the decomposition reactions of MgH_2. Nevertheless, at high temperatures, a very small amount of Li from LiH dissolves in hcp-Mg and produces a negligible amount of H_2. In the composites MgH_2-$LiAlH_4$/Li_3AlH_6, Al produced from the decomposition of $LiAlH_4$/Li_3AlH_6 destabilized MgH_2 by the formation of β- and γ-phases. It is found that the

re/dehydrogenation of the composites MgH_2- Li_3AlH_6 is reversible and that for MgH_2 content of 37.1 mole% and 53.7 mole%, 6.07 wt. % H_2 (at 507.25 K (234.1°C)) and 6.37 wt. % H_2 (at 531.05 K (257.9°C)) is released from the composite, respectively. A new destabilization reaction is predicted in this work between MgH_2 and Na_2LiAlH_6. These hydrides destabilize mutually at 308.4 K (35.25°C) and 1 bar because of the formation of $MgNaH_3$. It is concluded that Na reduces considerably the hydrogen storage potential of the system.

Chapter 5: Conclusions, Contributions and Recommendations

5.1 Conclusions

A self-consistent thermodynamic database that describes the Mg-Al-Li-Na-H system was constructed in this work using the CALPHAD method. This database is used to assess the hydrogen storage properties of the system. Thermodynamic modeling of the different constituent binaries is carried out in this work. The binary thermodynamic parameters of the liquid phases were extrapolated using the asymmetric Kohler-Toop technique.

The systems Na-H, Al-Na, Li-Mg, Li-Na, and Mg-Na were reassessed in this work using the modified quasichemical model (MQM) to describe the liquid phase, and the model parameters for Al-Mg, Al-H, Al-Li, Li-H, and Mg-H liquids were taken from the literature.

Since thermodynamic modeling is carried out in this work for hydrogen storage purposes and hydrogen atoms occupy the interstitial position in the host lattices, the terminal solid solutions hcp-Mg, fcc-Al, and bcc-Li/Na are reassessed in this work using the compound energy formalism (CEF). The gas phase is considered as ideal.

The binary MgH_2 and NaH hydrides are considered as stoichiometric and were reassessed in this work whereas the thermodynamic model parameters describing the binary compounds AlH_3, $\beta(Al_3Mg_2)$, $\gamma(Al_{12}Mg_{17})$, $Al_{30}Mg_{23}$, AlLi, Al_2Li_3 and Al_4Li_9 are taken from the literature with minor adjustments in order to be consistent with the newly modeled phases when necessary. A new thermodynamic description of $MgNaH_3$ and Na_2LiAlH_6 stable hydrides is performed in this work. Thermodynamic parameters of the ternary compounds τ ($Al_{53}Li_{33}Mg_{14}$), Na_3AlH_6 and $NaAlH_4$ are taken from the literature and the hydrides $LiMg(AlH_4)_3$, $LiMgAlH_6$ were reassessed in this work. Thermodynamic calculations of various phase diagrams and thermodynamic properties are compared with the literature experimental data when available and found to be in good agreement.

The constructed database was used to investigate the hydrogen storage properties of the Mg-Al-Li-Na system such as Pressure-Composition Isotherms (PCIs), reaction paths, and to compare the results with the experimental data from the literature. It is found that the calculations presented in this work provide more insight about the reactions when compared to experimental data from the literature. The main conclusions are:

- The hydrides AlH_3, $AlLiH_4$, $Mg(AlH_4)_2$, $LiMg(AlH_4)_3$ and $LiMgAlH_6$ are not stable at the pressure and temperature of interest and their decomposition reactions are then not reversible.
- At 1 bar, $NaMgH_3$ decomposes at 383°C to form NaH and hcp-Mg liberating 6 wt. % of hydrogen gas. It has been shown in the literature that $NaMgH_3$ improves the (de)/hydrogenation kinetic reactions when mixed with MgH_2 and that liquid Na produced from the decomposition of NaH causes capacity degradation and slow kinetics after some cycles. To avoid the formation of liquid Na phase, the best working temperatures and pressures of $NaMgH_3$ were predicted to benefit from its full catalytic role when mixed with MgH_2.
- PCIs, PT diagram, and reaction path at 1 and 0.1 bar of the MgH_2 +10 wt.% NaH mixture are predicted and show agreement with the experimental data.
- Reaction path for the reaction MgH_2/AlH_3 is calculated and shows good agreement with the experimental data from the literature and provide insight regarding the reaction temperatures, the relative amount of the reaction products, and their composition. It is shown that:
    - Al destabilizes MgH_2 by the formation of Al-Mg solid solutions and compounds. The first step decomposition temperature of MgH_2 in the mixture at 1 bar is 234°C; i.e., around 50°C lower than the decomposition temperature of MgH_2 alone and is due to the formation of β-phase.
    - The calculated pressure-composition isotherms for Mg-10 at.% Al and Mg-4 at.% Al alloys at 350°C show good agreement with the experimental data and give a more detailed description of the hydriding process products and equilibrium pressures.
    - Hydrogenation of Al-Mg alloys depends on Al content. For Al contents higher than 7 at. %, hcp-Mg is hydrogenated in one step with the formation of γ-phase at 6.26 bar. For Al contents lower than 7 at. %, the hcp-Mg is hydrogenated first at pressures increasing with Al content (5.84 bar for pure Mg to 6.26 bar for 7 at. % Al in Mg alloy) and is related to the solubility of Al in hcp-Mg, followed by the formation of γ-phase at 6.26 bar.
    - The PCIs sloping reported in the literature for the Al-Mg alloys is, in addition to kinetic factors, due to the large solubility range of γ-phase, to short plateaus' length, and to the small differences between plateau pressures.

- Reaction pathways for the reactions of $MgH_2/NaAlH_4$ and MgH_2/Na_3AlH_6 composites are calculated and show good agreement with the experimental data from the literature. The components destabilize mutually by the formation of $NaMgH_3$.
  - When Mg atomic fraction is greater than that of Na atoms, $AlNaH_4/AlNa_3H_6$ decomposes spontaneously and the remaining decomposition steps concern the decomposition of MgH_2 /Al mixture where $MgNaH_3$ acts only as a catalyst.
  - When the number of Na atoms is larger than number of Mg atoms, MgH_2 decomposes spontaneously and the remaining steps concern the decomposition of $AlNaH_4$ and/or $AlNa_3H_6$.
  - $MgNaH_3$ does take part in the decomposition of MgH_2/Al or $AlNaH_4$ and/or $AlNa_3H_6$. It has only a catalytic effect in the process as shown in the literature.
  - Al destabilizes $NaMgH_3$ by forming β-phase at 331°C, i.e., 51.6°C lower than the decomposition temperature of pure $MgNaH_3$.
- Reaction pathways for MgH_2-$AlLiH_4/AlLi_3H_6$ composites are calculated and show a very good agreement with the experimental data except for Li-Mg compounds reported in the literature. It is concluded that:
  - LiH hydride is very stable and does not contribute to the decomposition reactions of MgH_2.
  - The reported Al-Mg alloy $Li_{0.92}Mg_{4.08}$ is actually hcp-Mg, because the reported XRD peaks of this compound are identical to those of hcp-Mg and no compounds exist in the accepted Li-Mg phase diagram. Also, LiH is hardly detected in the XRD patterns.
  - Al produced from the decomposition of $AlLiH_4/AlLi_3H_6$ destabilized MgH_2 by the formation of β- and γ-phases.
  - Two compositions have been identified in the MgH_2-$AlLi_3H_6$ mixtures that show improvement with respect to MgH_2. For MgH_2 content of 37.1 mole%, 6.07 wt. % H_2 is released at 234.1°C and for MgH_2 content of 53.7 mole%, 6.37 wt. % H_2 is released at 257.9°C.
  - MgH_2 and Na_2AlLiH_6 are predicted to destabilize mutually at 35.3°C and 1 bar because of the formation of $MgNaH_3$.
- Na reduces considerably the hydrogen storage potential of the Mg-Al-Li system.

5.2 Contributions

The purpose of this thesis is to build a self-consistent database for hydrogen storage in Mg-Al-Li-Na-H system using the CALPHAD method. It is shown that this technique is able to describe simple M-H systems and to predict phase equilibrium and thermodynamic properties of complex hydrogen containing multi-component systems.

Although most of the binary M-H systems have been already described by the CALPHAD method in the literature, constructing this multicomponent self-consistent thermodynamic database has been accomplished in this thesis. For this purpose, many binary systems had to be re-optimized to become compatible with one another in terms of the use of reference states (SER) and thermodynamic models.

- In the current study, the binaries Na-H, Al-Na, Li-Mg, Li-Na, and Mg-Na have been reassessed using the modified quasichemical model (MQM) for the liquid phase and the solid solutions have been remodeled using the compound energy formalism (CEF) for all the binary systems. The MgH_2, NaH hydrides have been reassessed.
- The ternary system Mg-Na-H is optimized for the first time in this work.
- A full thermodynamic description of the ternaries Al-Mg-H, Al-Mg-Na, Al-Na-H, Al-Li-H and Li-Mg-H is provided in this work. For most of these ternaries, only solid phases (hydrides) or liquid phases have been studied in the literature.
- The $LiMg(AlH_4)_3$ and $LiMgAlH_6$ hydrides are considered as stoichiometric and have been reassessed. A new thermodynamic description for $MgNaH_3$ and Na_2LiAlH_6 stable hydrides is proposed.

The constructed database has been used to investigate the hydrogen storage properties of the Mg-Al-Li-Na system through computational thermodynamics for the first time. The present work shows the power of using computational thermodynamics to predict the properties of multi-component systems and to help for the design of new hydrogen storage materials and systems. This thesis provides a platform for such methodology.

- The stability of all the hydrides in the system has been investigated over a wide range of temperature and pressure through pressure-temperature (PT) diagrams.

- Phase diagrams and PT diagrams for hydride composites have been calculated providing details about hydrides reactions and destabilization.
- Reaction paths of (de)/hydrogenation of alloys and composites in the Mg-Al-Li-Na system have been calculated. A new understanding of reaction mechanisms is provided.
- The effect of solid solubilities on the decomposition temperatures and on pressure-temperature isotherms (equilibrium pressures and plateaus slopping) has been revealed for the first time in this work.
- The most promising compositions for hydrogen storage in the system and new destabilization reactions have been predicted.

5.3 Recommandations

The present work proves that thermodynamic modeling using the CALPHAD method is a valuable tool to investigate the hydrogen storage properties. It should be noted that thermodynamic modeling does not provide any information about the kinetics of the reactions. However, it reduces considerably the amount of experiments required to find the alloy with the best hydrogen storage properties.

- It has been found that the calculated decomposition temperatures are less than the measured ones. More theoretical and experimental work is needed to understand the kinetics limitations of some systems having favourable thermodynamic properties and the effect of catalysts on hydrogen storage properties.
- Promising compositions for hydrogen storage application have been predicted in this work. These compositions need to be studied experimentally through temperature programed desorption (TPD) measurements and de/rehydrogenation kinetics measurements in a Sievert-type pressure composition temperature (PCT) apparatus.
- The constructed database can be used for thermodynamic assessments of higher order systems. Boron stands as the best component to add to the system in order to investigate the potential of borohydrides for hydrogen storage applications from a thermodynamic viewpoint. Therefore, further work is recommended to include B in this database.

References

[1] J. Keller, L. Klebanoff, S. Schoenung and M. Gillie, "The need for hydrogen-based energy technologies in the 21st century," in *Hydrogen Storage Technology: Materials and Applications*, Lennie Klebanoff, Ed. Boca Raton: CRC Press, Taylor &Francis Group, LLC, 2012, pp. 3-30.

[2] L. Klebanoff, J. Keller, M. Fronk and P. Scott, "Hydrogen conversion technologies and automotive applications," in *Hydrogen Storage Technology: Materials and Applications*, L. Klebanoff, Ed. Boca Raton: CRC Press, Taylor & Francis Group, 2012, pp. 31-62.

[3] L. Klebanoff, Ed., "*Hydrogen Storage Technology: Materials and Applications"*. Boca Raton: CRC Press, Taylor & Francis Group, 2012.

[4] M. Hirscher, "*Handbook of Hydrogen Storage"*. Weinheim: Wiley-VCH, 2010.

[5] L. Klebanoff and J. Keller, "5 years of hydrogen storage research in the US DOE metal hydride center of excellence (MHCoE)", *Int. J. Hydrog. Energ. 38(11),* pp. 4533-4576. 2013.

[6] J. Huot, "Metal hydrides," in "*Handbook of Hyddrogen Storage, New Materials for Future Energy Storage"*, M. Hirscher, Ed. Weinhein: Wiley-VCH Verlag GmbH & Co. KGaA, 2010, pp. 81-110.

[7] D. Chandra, "Intermetallics for hydrogen storage," in *Solid-State Hydrogen Storage: Materials and Chemistry"*, G. Walker, Ed. Cambridge and Boca Raton: Woodhead Publishing Limited and CRC Press LLC, 2008, pp. 315-348.

[8] B. Chao and L. Klebannoff, "Hydrogen storage in interstitial metal hydrides," in "*Hydrogen Storage Technology: Materials and Applications"*, L. Klebanoff, Ed. Beca Raton: CRC Press, Taylor &Francis Group, 2013, pp. 109-131.

[9] A. Züttel, "Materials for hydrogen storage", *Mater. Today 6(9),* pp. 24-33. 2003.

[10] Y. Fukai, "Site occupancy and phase stability of some metal hydrides", *Z. Phys. Chem. 163(1),* pp. 165-174, 1989.

[11] I. P. Jain, P. Jain and A. Jain, "Novel hydrogen storage materials: A review of lightweight complex hydrides," *J. Alloy. Compd., 503,* pp. 303-339, 2010.

[12] V. Stavila, L. Klebanoff, J. Vajo and P. Chen, "Development of on-board reversible complex metal hydrides for hydrogen storage," in *"Hydrogen Storage Technology: Materials and Applications"*, L. Klebanoff, Ed. Boca Raton: CRC Press, Taylor & Francis Group, 2012, pp. 133-201.

[13] B. Sakintuna, F. Lamari-Darkrim and M. Hirscher, "Metal hydride materials for solid hydrogen storage: A review," *Int. J. Hydrog. Energ. 32(6)*, pp. 1121-1140, 2007.

[14] I. Jain, C. Lal and A. Jain, "Hydrogen storage in mg: A most promising material", *Int. J. Hydrog. Energ. 35(10),* pp. 5133-5144, 2010.

[15] P. Chen and M. Zhu, "Recent progress in hydrogen storage," *Mater. Today, 11(12)*, pp. 36-43, 2008.

[16] J. J. Vajo, F. Mertens, C. C. Ahn, R. C. Bowman and B. Fultz, "Altering hydrogen storage properties by hydride destabilization through alloy formation: LiH and MgH_2 destabilized with Si", *J. Phys. Chem. B 108(37),* pp. 13977-13983, 2004.

[17] P. Spencer, "A brief history of CALPHAD", *CALPHAD 32(1),* pp. 1-8, 2008.

[18] M. Hillert, "Empirical methods of predicting and representing thermodynamic properties of ternary solution phases", *CALPHAD 4(1),* pp. 1-12, 1980.

[19] F. Kohler, "Estimation of thermodynamic data for a ternary system from the corresponding binary systems", *Monatshefte Flier Chem. 91(4),* pp. 738-740, 1960.

[20] Y. M. Muggianu, M. Gambino and J. Bros, "Enthalpies of formation of liquid alloys bismuth-gallium-tin at 723K-choice of an analytical representation of integral and partial thermodynamic functions of mixing for this ternary-system", *J. Chim. Phys. Phys. -Chim. Biol. 72(1),* pp. 83-88, 1975.

[21] G. Toop, "Predicting ternary activities using binary data", *Trans. Am. Inst. Min. 233(5),* pp. 850-855, 1965.

[22] A. D. Pelton, "A general "geometric" thermodynamic model for multicomponent solutions", *CALPHAD 25(2),* pp. 319-328, 2001.

[23] B. Sundman and J. Ågren, "A regular solution model for phases with several components and sublattices, suitable for computer applications", *J. Phys. Chem. Solids 42(4),* pp. 297-301, 1981.

[24] A. D. Pelton and P. Chartrand, "The modified quasi-chemical model: Part II. Multicomponent solutions," *Metall. Mater. Trans. A 32*, pp. 1355-1360, 2001.

[25] C. Bale, A. Pelton, and W. Thompson, "*FactSage 6.4, FactSage thermochemical software and databases"*, 2013, http://www.crct.polymtl.ca/

[26] R. J. Press, K. S. V. Santhanam, M. J. Miri, A. V. Bailey and G. A. Takacs, "*Introduction to Hydrogen Technology",* John Wiley and Sons*,* New York, 2009.

[27] S. Orimo, Y. Nakamori, J. R. Eliseo, A. Zâttel and C. M. Jensen, "Complex Hydrides for Hydrogen Storage," *Chem. Rev., 107(10),* pp. 4111-4132, 2007.

[28] L. George and S. K. Saxena, "Structural stability of metal hydrides, alanates and borohydrides of alkali and alkali- earth elements: A review," *Int. J. Hydrog. Energ., 35(6),* pp. 5454-5470, 2010.

[29] G. Barkhordarian, T. Klassen, M. Dornheim and R. Bormann, "Unexpected kinetic effect of MgB_2 in reactive hydride composites containing complex borohydrides," *J. Alloy. Compd., 440(1),* pp. L18-L21, 2007.

[30] M. Dornheim, S. Doppiu, G. Barkhordarian, U. Boesenberg, T. Klassen, O. Gutfleisch and R. Bormann, "Hydrogen storage in magnesium-based hydrides and hydride composites," *Scr. Mater., 56(5),* pp. 841-846, 2007.

[31] A. Zaluska, L. Zaluski and J. O. Ström–Olsen, "Nanocrystalline magnesium for hydrogen storage," *J. Alloy. Compd. 288,* pp. 217-225, 1999.

[32] J. J. Vajo, S. L. Skeith and F. Mertens, "Reversible storage of hydrogen in destabilized $LiBH_4$", *J. Phys. Chem. B, 109(9),* pp. 3719-3722, 2005.

[33] Y. Bouhadda, N. Fenineche and Y. Boudouma, "Hydrogen storage: Lattice dynamics of orthorhombic $NaMgH_3$," *Phys. B: Condens. Matter, 406,* pp. 1000-1003, 2011.

[34] D. Pottmaier, E. R. Pinatel, J. G. Vitillo, S. Garroni, M. Orlova, M. D. Baró, G. B. M. Vaughan, M. Fichtner, W. Lohstroh and M. Baricco, "Structure and Thermodynamic Properties of the $NaMgH_3$ Perovskite: A Comprehensive Study," *Chem. Mater., 23,* pp. 2317-2326, 2011.

[35] A. Bouamrane, C. de Brauer, J. P. Soulié, J. M. Létoffé and J. P. Bastide, "Standard enthalpies of formation of sodium–magnesium hydride and hydridofluorides $NaMgH_3$, $NaMgH_2F$ and $NaMgF_2H$," *Thermochim. Acta, 326,* pp. 37-41, 1999.

[36] E. Rönnebro, D. Noréus, K. Kadir, A. Reiser and B. Bogdanovic, "Investigation of the perovskite related structures of $NaMgH_3$, $NaMgF_3$ and Na_3AlH_6," *J. Alloy. Compd., 299,* pp. 101-106, 2000.

[37] K. Ikeda, S. Kato, Y. Shinzato, N. Okuda, Y. Nakamori, A. Kitano, H. Yukawa, M. Morinaga and S. Orimo, "Thermodynamical stability and electronic structure of a perovskite-type hydride, $NaMgH_3$," *J. Alloy. Compd., 446–447,* pp. 162-165, 2007.

[38] H. Wu, W. Zhou, T. J. Udovic, J. J. Rush and T. Yildirim, "Crystal Chemistry of Perovskite-Type Hydride $NaMgH_3$: Implications for Hydrogen Storage," *Chem. Mater. 6,* pp. 2335-2342, 2008.

[39] K. Komiya, N. Morisaku, R. Rong, Y. Takahashi, Y. Shinzato, H. Yukawa and M. Morinaga, "Synthesis and decomposition of perovskite-type hydrides, MMgH3 (M = Na, K, Rb)," *J. Alloy. Compd., 453,* pp. 157-160, 2008.

[40] K. Ikeda, Y. Kogure, Y. Nakamori and S. Orimo, "Reversible hydriding and dehydriding reactions of perovskite-type hydride $NaMgH_3$," *Scripta Materialia, 53,* pp. 319-322, 2005.

[41] H. Wang, J. Zhang, J. W. Liu, L. Z. Ouyang and M. Zhu, "Catalysis and hydrolysis properties of perovskite hydride $NaMgH_3$," *J. Alloy. Compd., 580,* pp. S197-S201, 2013.

[42] D. T. Shane, R. L. Corey, J. Bowman Robert C, R. Zidan, A. C. Stowe, S. Hwang, C. Kim and M. S. Conradi, "NMR studies of the hydrogen storage compound NaMgH3," *J. Phys. Chem. C, 113*, pp. 18414-18419, 2009.

[43] O. Dolotko, N. Paulson and V. K. Pecharsky, "Thermochemical transformations in $2MNH_2$–$3MgH_2$ systems (M = Li or Na)," *Int. J. Hydrog. Energ., 35(5),* pp. 4562-4568, 2010.

[44] D. A. Sheppard, M. Paskevicius and C. E. Buckley, "Hydrogen Desorption from the $NaNH_2$−MgH_2 System," *J. Phys. Chem. C, 115,* pp. 8407-8413, 2011.

[45] S. Sartori, X. Qi, N. Eigen, J. Muller, T. Klassen, M. Dornheim and B. C. Hauback, "A search for new Mg- and K-containing alanates for hydrogen storage," *Int. J. Hydrog. Energ., 34(5),* pp. 4582-4586, 2009.

[46] X. Tang, S. M. Opalka, B. L. Laube, F. Wu, J. R. Strickler and D. L. Anton, "Hydrogen storage properties of Na–Li–Mg–Al–H complex hydrides," *J. Alloy. Compd., 446,* pp. 228-231, 2007.

[47] R. Zidan, K. L. Shanahan, D. L. Anton, A. R. Jurgensen and J. Pittman, "Development and Characterization of Novel Complex Hydrides Synthesized via Molten State Processing," *MRS Proceedings, Cambridge University Press 2005, 885,* pp. 0885-A07-02 (7 pages), 2005.

[48] S. Garroni, C. Milanese, A. Girella, A. Marini, G. Mulas, E. Menéndez, C. Pistidda, M. Dornheim, S. Suriñach and M. D. Baró, "Sorption properties of NaBH4/MH2 (M = Mg, Ti) powder systems," *Int. J. Hydrog. Energ., 35(6),* pp. 5434-5441, 2010.

[49] D. Pottmaier, C. Pistidda, E. Groppo, S. Bordiga, G. Spoto, M. Dornheim and M. Baricco, "Dehydrogenation reactions of $2NaBH_4 + MgH_2$ system," *Int. J. Hydrog. Energ., 36(7),* pp. 7891-7896, 2011.

[50] A. San-Martin and F. D. Manchester, "The H−Mg (Hydrogen-Magnesium) system," *J. Phase Equilibria, 8,* pp. 431-437, 1987.

[51] K. Zeng, T. Klassen, W. Oelerich and R. Bormann, "Critical assessment and thermodynamic modeling of the Mg–H system," *Int. J. Hydrog. Energ., 24(10),* pp. 989-1004, 1999.

[52] U. Wolf, K. Bohmhammel and G. Wolf, "A simple adiabatic low-temperature calorimeter based on a helium refrigerator system," *Thermochim. Acta, 310,* pp. 37-42, 1998.

[53] B. Bogdanović, K. Bohmhammel, B. Christ, A. Reiser, K. Schlichte, R. Vehlen and U. Wolf, "Thermodynamic investigation of the magnesium–hydrogen system," *J. Alloy. Compd., 282,* pp. 84-92, 1999.

[54] L. Belkbir, E. Joly and N. Gerard, "Comparative study of the formation-decomposition mechanisms and kinetics in LaNi5 and magnesium reversible hydrides," *Int. J. Hydrog. Energ., 6,* pp. 285-294, 1981.

[55] V. Shapovalov, N. Serdyuk and A. Semik, "Magnesium-Hydrogen and Aluminum-Hydrogen Phase Diagrams," *Dopov. Akad. Nauk Ukr. RSR, Ser. A: Fiz. -Mat. Tekh .Nauki,* pp. 99-101, 1981.

[56] J. Stampfer Jr, C. E. Holley and J. F. Scttle, "The Magnesium-Hydrogen System," *J. Am. Chem. Soc., 82,* pp. 3504-3508, 1960.

[57] V. I. Shapovalov, A. P. Semik and A. G. Timchenko, "On the solubility of hydrogen in liquid magnesium," *Metally, 3,* pp. 25-28, 1993.

[58] J. Schefer, P. Fischer, W. Hälg, F. Stucki, L. Schlapbach, J. J. Didisheim, K. Yvon and A. F. Andresen, "New structure results for hydrides and deuterides of the hydrogen storage material Mg_2Ni," *J. Less Common Metal. 74,* pp. 65-73, 1980.

[59] P. Selvam, B. Viswanathan, C. S. Swamy and V. Srinivasan, "Studies on the thermal characteristics of hydrides of Mg, Mg_2Ni, Mg_2Cu and $Mg_2Ni_{1-X}M_X$ (M=Fe, Co, Cu or Zn; $0<x<1$) alloys," *Int. J. Hydrog. Energ., 13,* pp. 87-94, 1988.

[60] D. Noréus and P. Werner, "The structure of the low temperature phase Mg_2NiH_4(LT)," *Mater. Res. Bull., 16(2),* pp. 199-206, 1981.

[61] T. Hirata, "Pressure DSC study of the hydrogenation and dehydrogenation of some intermetallic compounds Mg2Ni," *Int. J. Hydrog. Energ., 9,* pp. 855-859, 1984.

[62] A. Krozer and B. Kasemo, "Hydrogen uptake by Pd-coated Mg: absorption-decomposition isotherms and uptake kinetics," *J. Less Common Metal, 160(5),* pp. 323-342, 1990.

[63] J. Koeneman and A. Metcalfe, "The solubility of hydrogen in magnesium," *Trans. ASM, 51,* pp. 1072-1082, 1959.

[64] F. H. Ellinger, C. E. Holley Jr., B. B. McInteer, D. Pavone, R. M. Potter, E. Staritzky and W. H. Zachariasen, "The Preparation and Some Properties of Magnesium Hydride1," *J. Am. Chem. Soc., 77*, pp. 2647-2648, 1955.

[65] J. J. Reilly and R. H. Wiswall, "The Reaction of hydrogen with alloys of magnesium and nickel and the formation of Mg_2NiH_4," *Inorg. Chem., 7,* pp. 2254-2256, 1968.

[66] H. Buchner, O. Bernauer and W. Straub, "Development of high temperature hydrides for vrhicular applications," *Proc. World Hydrog. Energ. Conf.,* Zürich, 1978, pp. 1677–1687.

[67] K. J. Gross, P. Spatz, A. Züttel and L. Schlapbach, "Mechanically milled Mg composites for hydrogen storage the transition to a steady state composition," *J. Alloy. Compd., 240,* pp. 206-213, 1996.

[68] E. Akiba, K. Nomura, S. Ono and Y. Mizuno, "Pressure-composition isotherms of $MgNiH_2$ alloys," *J. Less Common Metal, 83,* pp. L43-L46, 1982.

[69] A. S. Pedersen, J. Kjøller, B. Larsen and B. Vigeholm, "Magnesium for hydrogen storage," *Int. J. Hydrog. Energ., 8,* pp. 205-211, 1983.

[70] D. F. Chernega and Y. Y. Gotvyanskii, "Permeability, Diffusion and Solubility of H in Mg-Al Alloys," *Liteinoe Proizvod*. 12, pp. 9-10, 1977.

[71] Y. C. Huang, T. Watanabe and R. Komatsu, " Hydrogen in magnesium and its alloys," *Proc. 4th Internat. Conf. Vacuum Metallurgy,* 1973, pp. 176-179.

[72] E. Øvrelid, T. A. Engh and D. Øymo, *Light Metals, TMS, Warrendale, PA*, pp. 771-78, 1994.

[73] E. Øvrelid, G. B. Fløistad, T. Rosenqvist, P. Bakke and T. A. Engh, "The effect of Sr addition on the hydrogen solubility and hydride formation in pure Mg and the alloy AZ91," *Scand. J. Metall., 27,* pp. 133-140, 1998.

[74] Z. D. Popovic and G. R. Piercy, "Measurement of the solubility of hydrogen in solid magnesium," *Metall. Mater. Trans. B Process Metall. Mater. Process. Science, 6,* pp. 1915-1917, 1975.

[75] J. P. Harvey and P. Chartrand, "Modeling the Hydrogen Solubility in Liquid Aluminum Alloys," *Metall. Mater. Trans. B, 41B,* pp. 908-924, 2010.

[76] A. San-Martin and F. D. Manchester, "The H-Na (Hydrogen-Sodium) system," *Bull. Alloy. Phase Diagr., 11,* pp. 287-294, 1990.

[77] P. Roy and D. N. Rodgers, "characterization of diffusion tube hydrogen detector in a dynamic sodium system," *Nucl. Technol., 12,* pp. 388-392, 1971.

[78] A. Herold, "Contribution to the Study of the Alkaline Hydride," *Ann.Chim., Ser., 12,* pp. 537-575, 1951.

[79] E. F. Sollers and J. L. Crenshaw, "The Dissociation Pressures of Sodium Deuteride and Sodium Hydride," *J. Am. Chem. Soc., 59,* pp. 2724-2726, 1937.

[80] D. D. Williams, J. A. Grand and R. R. Miller, "The Solubility of Sodium Hydride in Sodium," *The J. Phys. Chem., 61,* pp. 379-381, 1957.

[81] C. C. Addison, R. J. Pulham and R. J. Roy, "19. Liquid metals. Part X. Solutions of hydrogen in liquid sodium," *J. Chem. Soc.*, pp. 116-121, 1965.

[82] D. W. McClure and G. D. Halsey, "The Solubility of Hydrogen in Liquid Sodium1," *J. Phys. Chem., 69,* pp. 3542-3547, 1965.

[83] R. J. Newcombe and J. Thompson, "An electrochemical method for the determination of the solubility of hydrogen in liquid sodium," *J. Polarogr. Soc.,14,* pp. 104-108, 1968.

[84] S. A. Meacham, E. F. Hill and A. A. Gardus, "The solubility or hydrogen in sodium," Technical Report, Nb. APDA-241, *Atomic Power Development Associates*, Inc., Detroit, Mich. 1970.

[85] D. R. Vissers, J. T. Holmes, L. G. Bartholme and P. A. Nelson, "A Hydrogen Activity Meter For Liquid Sodium and Its Application to Hydrogen Solubility Measurements," *Nuc. Teehnol., 21,* pp. 235-244, 1974.

[86] O.A.Skuratov, O. N. Pavlov, V. l. Danilkin and I. V. Volkov, "Dissociation Pressure of Molten Stoichiometric Alkali Metal Hydrides," *J. Inorg. Chem., 21,* pp. 1605-1608, 1976.

[87] W. Klostermeier and E. U. Franck, "Liquid mixture of sodium and sodium hydride at high pressures and temperatures," *Phys. Chem. Chem. Phys., 86,* pp. 606-612, 1982.

[88] V. Prochazka and M. Nedved, "Chemistry of metal hydrides. VI. Mechanism of the formation of sodium hydride catalyzed by carbon monoxide," *Coll. Czech. Chem. Commun.*, *38(10)*, 2850-2854, 1973.

[89] J. R. Gwyther and C. Whittingham, "The kinetics of hydrogen removal from liquid sodium," *Mater. Behav. Phys. Chem. Liq. Met. Syst.* New York, pp. 335-343, 1982,

[90] G. F. Huttig and F. Brodkorb, "Chemistry of hydrogen. VI. Compounds of hydrogen with sodium," *Zeitschrift Fuer Anorganische Und Allgemeine Chemie, 161,* pp. 353-362, 1927.

[91] H. Hagen and A. Sieverts, "Sodium hydride. I. Preparation and density," *Z. Anorganische Und Allgemeine Chem., 185,* pp. 239-253, 1930.

[92] E. Zintl and A. Harder, "Alkali hydrides," *Z. Phys. Chem, B14,* pp. 265-284, 1931.

[93] V. G. Kuznetsov and M. M. Shkrabkina, "X-ray diffraction study of NaH and KH at temperatures from 20 to 400°C," *J. Struct. Chem, 3,* pp. 532-537, 1962.

[94] C. Qiu, S. M. Opalka, G. B. Olson and D. L. Anton, "The Na-H system: From first-principles calculations to thermodynamic modeling," *Int. J. Mater. Res., 97,* pp. 845-853, 2006.

[95] S. R. Gunn and L. G. Green, "The Heats of Formation at 25° of the Crystalline Hydrides and Deuterides and Aqueous Hydroxides of Lithium, Sodium and Potassium1," *J. Am. Chem. Soc., 80,* pp. 4782-4786, 1958.

[96] S. R. Gunn, "Heats of formation at 25° of the crystalline hydrides and aqueous hydroxides of rubidium and cesium," *The J. Physical Chemistry,* vol. 71, pp. 1386-1390, 1967.

[97] C. E. Messer, L. G. Fasolino and C. E. Thalmayer, "The Heats of Formation of Lithium, Sodium and Potassium Hydrides," *J. Am. Chem. Soc., 77,* pp. 4524-4526, 1955.

[98] H. Hagen and A. Sieverts, "Sodium hydride. II. Heat of formation," *Z. Anorg. Chem., 185*, pp. 254-266, 1930.

[99] A. Herold, "Dissociation pressure of alkali hydrides," *Compt. Rend., 228*, pp. 686-688, 1949.

[100] E. V. Sayre and J. J. Beaver, "Isotope Effect in the Vibrational Frequency Spectra and Specific Heats of Sodium Hydride and Deuteride," *J. Chem. Phys.,* vol. 18, pp. 584-594, 1950.

[101] B. Predel, "H-Na (hydrogen-sodium)," in *Ga-Gd-Hf-Zr*, O. Madelung, Ed. Springer Berlin Heidelberg, 1996, pp. 1-3.

[102] C. H. Mathewson, "Sodium-aluminum, sodium-magnesium, and sodium-zinc alloys," *Z. Anorg. Chem., 48,* pp. 191-200, 1906.

[103] M. F. Lantratov, "Thermodynamic properties of sodium-magnesium and potassium-magnesium molten alloys," *Zh. Prikl. Khim. (Leningrad), 46 (9)*, pp. 1982-1986, 1973.

[104] Klemm, W., Kunze,D., "Systems of alkali and alkaline earth metals," in *Int. Symp. Alkali Metals,* London, 1967, pp. 3-22.

[105] A. D. Pelton, "The Mg–Na (Magnesium-Sodium) system," *Bull. Alloy Phase Diagr., 5,* pp. 454-45, 1984.

[106] S. Zhang, Q. Han and Z. Liu, "Thermodynamic modeling of the Al–Mg–Na system," *J. Alloy. Compd., 419,* pp. 91-97, 2006.

[107] K. Ikeda, Y. Nakamori and S. Orimo, "Formation ability of the perovskite-type structure in $Li_xNa_{1-x}MgH_3$ (x = 0, 0.5 and 1.0)," *Acta Mater., 53,* pp. 3453-3457, 2005.

[108] D. M. Banus, J. J. McSharry and E. A. Sullivan, "The Sodium-Sodium Hydride-Hydrogen System at 500-600°," *J. Am. Chem. Soc., 77(7),* pp. 2007-2010, 1955.

[109] D. A. Sheppard, M. Paskevicius and C. E. Buckley, "Thermodynamics of Hydrogen Desorption from NaMgH3 and Its Application As a Solar Heat Storage Medium," *Chem. Mater., 23,* pp. 4298-4300, 2011.

[110] A. T. Dinsdale, "SGTE data for pure elements," *CALPHAD, 15,* pp. 317-425, 1991.

[111] J. M. W. Chase, Ed., *NIST-JANAF Thermochemical Tables, (NIST,Washington, DC),* 1998.

[112] A. Pelton, S. Degterov, G. Eriksson, Student, C Robelin Ph D and Y. Dessureault, "The modified quasichemical model I—Binary solutions," *Metall. Mater. Trans. B, 31,* pp. 651-659, 2000.

[113] Z. Qiao, X. Xing, M. Peng and A. Mikula, "Thermodynamic criterion for judging the symmetry of ternary systems and criterion applications," *J. Phase Equilib., 17,* pp. 502-507, 1996.

[114] K. Frisk, "A thermodynamic evaluation of the Cr-N, Fe-N, Mo-N and Cr-Mo-N systems," *CALPHAD, 15,* pp. 79-106, 1991.

[115] M. L. Post and J. J. Murray, "Mg_2Ni hydride: In situ heat conduction calorimetry of the phase transition near 510 K," *J. Less Common Metal., 134(8),* pp. 15-26, 1987.

[116] K. J. Gross, P. Spatz, A. Züttel and L. Schlapbach, "Mechanically milled Mg composites for hydrogen storage the transition to a steady state composition," *J. Alloy. Compd., 240,* pp. 206-213, 1996.

[117] S. Abdessameud, M. Mezbahul-Islam and M. Medraj. Thermodynamic modeling of hydrogen storage capacity in mg-na alloys. *The Scientific World J. 2014(Article ID 190320, 16 pages),* 2014.

[118] B. Bogdanović and M. Schwickardi, "Ti-doped alkali metal aluminium hydrides as potential novel reversible hydrogen storage materials," *J. Alloy. Compd*. *253,* pp. 1-9, 1997.

[119] C. Qiu, S. M. Opalka, G. B. Olson and D. L. Anton, "Thermodynamic modeling of the sodium alanates and the Na–Al–H system," *Z. Metall., 97,* pp. 1484-1494, 2006.

[120] M. Tanniru, D. K. Slattery and F. Ebrahimi, "A study of stability of MgH_2 in Mg–8at% Al alloy powder," *Int. J. Hydrog. Energ., 35,* pp. 3555-3564, 2010.

[121] M. Tanniru, D. K. Slattery and F. Ebrahimi, "A study of phase transformations during the development of pressure-composition-isotherms for electrodeposited Mg–Al alloys", *Int. J. Hydrog. Energ. 36(1),* pp. 639-647, 2011.

[122] M. Ismail, Y. Zhao, X. Yu, J. Mao and S. Dou, "The hydrogen storage properties and reaction mechanism of the MgH_2–$NaAlH_4$ composite system," *Int. J. Hydrog. Energ., 36,* pp. 9045-9050, 2011.

[123] M. Ismail, Y. Zhao, X. Yu and S. Dou, "Improved hydrogen storage performance of MgH_2–$NaAlH_4$ composite by addition of TiF_3," *Int. J. Hydrog. Energ., 37,* pp. 8395-8401, 2012.

[124] M. Ismail, Y. Zhao and S. Dou, "An investigation on the hydrogen storage properties and reaction mechanism of the destabilized MgH_2-Na_3AlH_6 (4: 1) system," *Int. J. Hydrog. Energ., 38*, pp. 1478-1483, 2013.

[125] H. Liu, X. Wang, Y. Liu, Z. Dong, G. Cao, S. Li and M. Yan, "Improved hydrogen storage properties of MgH_2 by ball milling with AlH_3: preparations, de/rehydriding properties, and reaction mechanisms," *J. Mater. Chem. A, 1,* pp. 12527-12535, 2013.

[126] H. Liu, X. Wang, Y. Liu, Z. Dong, H. Ge, S. Li and M. Yan, "Hydrogen Desorption Properties of the MgH_2–AlH_3 Composites," *J. Phys. Chem. C, 118,* pp. 37-45, 2014.

[127] C. Qiu, G. B. Olson, S. M. Opalka and D. L. Anton, "Thermodynamic evaluation of the Al-H system," *J. Phase Equilib. Diffus., 25,* pp. 520-527, 2004.

[128] J. Harvey, "Developpement d'une base de donnees thermodynamique pour la modelisation de la solubilite d'hydrogène dans les alliages d'aluminium," *ProQuest Dissertations and Theses,* vol. Ecole Polytechnique, Montreal (Canada), Canada, M.Sc.A., 2007.

[129] A. San-Martin and F. Manchester, "The Al-H (aluminum-hydrogen) system," *J. Phase Equilib., 13,* pp. 17-21, 1992.

[130] J. Graetz, J. Reilly, V. Yartys, J. Maehlen, B. Bulychev, V. Antonov, B. Tarasov and I. Gabis, "Aluminum hydride as a hydrogen and energy storage material: past, present and future," *J. Alloy. Compd., 509,* pp. S517-S528, 2011.

[131] J. L. Murray, "The Al−Na (Aluminum-Sodium) system," *J. Phase Equilib., 4,* pp. 407-410, 1983.

[132] E. Scheuber, "Study of the Solubility of Sodium in Aluminum," *Z. Metall., 27,* pp. 83-85, 1935.

[133] W. Fink, L. Willey and H. Stumpf, "Equilibrium Relations in Aluminum-Sodium Alloys of High Purity," *Trans.AIME 175,* pp. 364-371, 1948.

[134] C. E. Ransley and H. Neufeld, "The solubility relationships in the Aluminum-Sodium and Aluminum-Silicon-Sodium systems," *J. Inst. Met. 78,* pp. 25-46, 1950.

[135] S. Hansen, J. Tuset and G. Haarberg. "Thermodynamics of liquid Al-Na alloys determined by using CaF_2 solid electrolyte", *Metall. Mater. Trans. B 33(4),* pp. 577-587, 2002.

[136] P. Fellner, M. Korenko, V. Danielik and J. Thonstad, "The content of sodium in aluminium during electrolysis of the molten systems Na_3AlF_6–NaCl–Al_2O_3 and NaF–NaCl," *Electrochim. Acta, 49,* pp. 1505-1511, 2004.

[137] E. Dewing, "Thermodynamics of system NaF-AlF_3. 3. Activities in liquid mixtures," *Metall. Trans., 3,* pp. 495-501, 1972.

[138] R. Brisley and D. Fray, "Determination of the sodium activity in aluminum and aluminum silicon alloys using sodium beta alumina," *Metall. Trans. B14,* pp. 435-440, 1983.

[139] L. Rokhlin and V. Ivanchenko, "Al-H-Mg," in *Light Metal Ternary Systems: Phase Diagrams, Crystallographic and Thermodynamic Data, vol. 11A3*, G. Effenberg, S. Ilyenko ed., S. I. G. Effenberg, Ed. Germany: Springer-Verlag Berlin Heidelberg, 2005, pp. 64-70.

[140] W. Baukloh and F. Oesterlen, "The solubility of hydrogen in aluminum and some aluminum alloys", *Z. Metall., 30,* pp. 386-389, 1938.

[141] T. Watanabe, Y. Tachihara, Y. Huang and R. Komatsu, "Effects of various alloying elements on the solubility of H in Mg", *J. Jpn Inst. Light Metal., 26(4),* pp. 167-174, 1976.

[142] E. Øvrelid, T. Engh and D. Øymo, "Light metals", TMS, Warrendale, vol. PA, pp. 771-778, 1994.

[143] K. N. Semenenko, V. N. Verbettskii, A. V. Kotchukov and A. N. Sytnikov, "Reaction of magnesium containing intermetallic compounds and alloys with hydrogen," *Vestn. Mosk. Uni. Ser. 2: Khim, 24,* pp. 16-27, 1983.

[144] M. Palumbo, F. Torres, J. Ares, C. Pisani, J. Fernandez and M. Baricco, "Thermodynamic and ab initio investigation of the Al–H–Mg system," *CALPHAD, 31,* pp. 457-467, 2007.

[145] H. Grove, O. M. Løvvik, W. Huang, S. M. Opalka, R. H. Heyn and B. C. Hauback, "Decomposition of lithium magnesium aluminum hydride," *Int. J. Hydrog. Energ., 36,* pp. 7602-7611, 2011.

[146] M. Mamatha, B. Bogdanović, M. Felderhoff, A. Pommerin, W. Schmidt, F. Schüth and C. Weidenthaler, "Mechanochemical preparation and investigation of properties of magnesium, calcium and lithium–magnesium alanates", *J. Alloy. Compd. 407(1),* pp. 78-86, 2006.

[147] R. Varin, C. Chiu, T. Czujko and Z. Wronski, "Mechano-chemical activation synthesis (MCAS) of nanocrystalline magnesium alanate hydride [$Mg(AlH_4)_2$] and its hydrogen desorption properties", *J. Alloy. Compounds 439(1),* pp. 302-311, 2007.

[148] Y. Kim, E. Lee, J. Shim, Y. W. Cho and K. B. Yoon, "Mechanochemical synthesis and thermal decomposition of mg $(AlH_4)_2$", *J. Alloy. Compounds 422(1),* pp. 283-287, 2006.

[149] V. Iosub, T. Matsunaga, K. Tange and M. Ishikiriyama, "Direct synthesis of $Mg(AlH_4)_2$ and $CaAlH_5$ crystalline compounds by ball milling and their potential as hydrogen storage materials", *Int. J. Hydrog. Energ. 34(2),* pp. 906-912, 2009.

[150] M. Sterlin Leo Hudson, D. Pukazhselvan, G. Irene Sheeja and O. Srivastava, "Studies on synthesis and dehydrogenation behavior of magnesium alanate and magnesium–sodium alanate mixture", *Int. J. Hydrog. Energ. 32(18),* pp. 4933-4938, 2007.

[151] Y. Liu, Y. Pang, X. Zhang, Y. Zhou, M. Gao and H. Pan, "Synthesis and hydrogen storage thermodynamics and kinetics of mg $(AlH_4)_2$ submicron rods", *Int. J. Hydrog. Energ. 37(23),* pp. 18148-18154, 2012.

[152] M. Mintz, Z. Gavra, G. Kimmel and Z. Hadari, "The reaction of hydrogen with magnesium alloys and magnesium intermetallic compounds", *J. Less Common Metal. 74(2),* pp. 263-270, 1980.

[153] Z. Gavra, Z. Hadari and M. H. Mintz, "Effects of nickel and indium ternary additions on the hydrogenation of Mg-Al intermetallic compounds," *J. of Inorganic and Nuclear Chemistry, 43,* pp. 1763-1768, 1981.

[154] A. Zaluska, L. Zaluski and J. Ström-Olsen, "Structure, catalysis and atomic reactions on the nano-scale: a systematic approach to metal hydrides for hydrogen storage," *Applied Physics A, 72,* pp. 157-165, 2001.

[155] C. Shang, M. Bououdina, Y. Song and Z. Guo, "Mechanical alloying and electronic simulations of (MgH_2- M) systems (M= Al, Ti, Fe, Ni, Cu and Nb) for hydrogen storage," *Int. J. Hydrog. Energ., 29,* pp. 73-80, 2004.

[156] A. Andreasen, "Hydrogenation properties of Mg–Al alloys," *Int. J. Hydrog. Energ., 33,* pp. 7489-7497, 2008.

[157] Y. Nakamori, A. Ninomiya, G. Kitahara, M. Aoki, T. Noritake, K. Miwa, Y. Kojima and S. Orimo, "Dehydriding reactions of mixed complex hydrides", *J. Power Sources 155(2),* pp. 447-455. 2006.

[158] C. Ransley and D. Talbot, "Hydrogen porosity in metals with special reference to aluminum and its alloys", *Z. Metall. 46(5),* pp. 328-337, 1955.

[159] H Hemmes and A Driessen and,R.Griessen, "Thermodynamic properties of hydrogen at pressures up to 1 Mbar and temperatures between 100 and 1000K," *J. of Physics C: Solid State Physics, 19*, pp. 3571, 1986.

[160] E. W. Dewing. Thermodynamics of the system NaF-AIF3: Part VI. revision. *Metall. Trans. B 21(2),* pp. 285-294, 1990.

[161] P. Claudy, B. Bonnetot and J. Letoffe, "Preparation and physicochemical properties of magnesium alanate," *J. Therm. Anal., 15,* pp. 119-128, 1979.

[162] S. Bouaricha, J. Dodelet, D. Guay, J. Huot, S. Boily and R. Schulz, "Hydriding behavior of Mg–Al and leached Mg–Al compounds prepared by high-energy ball-milling", *J. Alloy. Compd. 297(1),* pp. 282-293, 2000.

[163] Y. W. Cho, J. Shim and B. Lee, "Thermal destabilization of binary and complex metal hydrides by chemical reaction: A thermodynamic analysis", *CALPHAD 30(1),* pp. 65-69, 2006.

[164] J. Urgnani, M. Di Chio, M. Palumbo, M. Feuerbacher, J. Fernandez, F. Leardini and M. Baricco. Hydrogen absorption and desorption in rapidly solidified Mg-Al alloys. *J. Phys. Conf. Ser. 144(1),* pp. 12-16. 2009.

[165] W. Hsu, C. Yang, C. Tan and W. Tsai. In situ synchrotron X-ray diffraction study on the dehydrogenation behavior of LiAlH 4–MgH 2 composites. *J. Alloy. Compd., 599,* pp. 164-169, 2014.

[166] S. Abdessameud and M. Medraj. Understanding the hydrogen storage behavior of promising Al–Mg–Na compositions using thermodynamic modeling, *Mater. Renew. Sustain. Energ. 5(2),* pp. 1-29. 2016.

[167] N. Saunders, "Calculated stable and metastable phase equilibria in Al-Li-Zr alloys," *Z. Metall., 80,* pp. 894-903, 1989.

[168] A. Nayeb-Hashemi, J. Clark and A. Pelton, "The Li-Mg (lithium-magnesium) system," *J. of Phase Equilibria, 5,* pp. 365-374, 1984.

[169] O. H. Henry and H. V. Cordiano, "The Lithium-Magnesium Equilibrium Diagram," *Trans.AIME, 101,* pp. 319-332, 1934.

[170] G. Grube, H. Zeppelin and H. Bumm, "Elektrische Leitfähigkeit und Zustandsdiagramm bei binären Legierungen. 11. Mitteilung. Das System Lithium- Magnesium," *Z. Elektrochem. Angewandte Phys. Chem., 40,* pp. 160-164, 1934.

[171] W. Freeth and G. Raynor, "The systems magnesium-lithium and magnesium-lithium-silver," *J. Inst. Metal., 82,* pp. 575-580, 1954.

[172] P. Feitsma, T. Lee and W. Van der Lugt, "Electrical transport properties and phase diagram of the liquid binary lithium-magnesium system," *Physica B C, 93,* pp. 52-58, 1978.

[173] W. Hume-Rothery, G. Raynor and E. Butchers, "Equilibrium relations and some properties of magnesium-lithium and magnesium-silver-lithium alloys," *J. Inst. Metal., 71,* pp. 589-601, 1945.

[174] J. Catterall, "Solubility of Magnesium in Lithium," *Nature, 169,* pp. 336, 1952.

[175] F. Sommer, "Thermodynamic Investigation of Liquid Li-Mg Alloys," *Z. Metall., 70,* pp. 359-361, 1979.

[176] M. Saboungi and M. Blander, "Electromotive force measurements in molten lithium-magnesium alloys," *J. Electrochem. Soc.;(United States), 122(12),* pp. 1631-1634, 1975.

[177] W. Gasior, Z. Moser, W. Zakulski and G. Schwitzgebel, "Thermodynamic studies and the phase diagram of the Li-Mg system," *Metall. Mater. Trans. A, 27,* pp. 2419-2428, 1996.

[178] M. Saboungi and C. C. Hsu, "Computation of isothermal sections of the Al-Li-Mg system," *CALPHAD, 1,* pp. 237-251, 1977.

[179] N. Saunders, "A review and thermodynamic assessment of the Al-Mg and Mg-Li systems," *CALPHAD, 14,* pp. 61-70, 1990.

[180] P. Wang, Y. Du and S. Liu, "Thermodynamic optimization of the Li–Mg and Al–Li–Mg systems," *CALPHAD, 35,* pp. 523-532, 2011.

[181] C. Bale, "The Li-Na (Lithium-Sodium) system," *J. of Phase Equilib., 10,* pp. 265-268, 1989.

[182] H. Schürmann and R. Parks, "Paraconductivity in binary metallic liquids above the critical point," *Phys. Rev. Lett., 27,* pp. 1790-1793, 1971.

[183] P. Feitsma, J. Hallers, F. Werff and W. Van der Lugt, "Electrical resistivities and phase separation of liquid lithium-sodium alloys," *Physica B C, 79,* pp. 35-52, 1975.

[184] M. G. Down, P. Hubberstey and R. J. Pulham, "Sodium–lithium phase diagram: redetermination of the liquid immiscibility system by resistance measurement," *J.Chem.Soc., Dalton Trans.,14,* pp. 1490-1492, 1975.

[185] H. Endo, H. Hoshino, K. Tamura and M. Mushiage, "Phase separation of liquid binary mixtures containing metals under pressure," *Solid State Commun, 32*, pp. 1243-1246, 1979.

[186] F. A. Kanda, R. C. Faxon and D. V. Keller, "The Determination of the Liquid Immiscibility Boundaries of the Lithium-Sodium and Thallium-Selenium Systems by the Liquid Density Method," *Phys Chem Liq, 1,* pp. 61-72, 1968.

[187] E. Wu and H. Brumberger, "Critical small-angle X-ray scattering of the liquid sodium-lithium system," *Phys. Lett. A, 53,* pp. 475-477, 1975.

[188] O. Salmon and D. Ahmann, "The Lithiuim–Sodium Liquid Metal System," *J. Phys. Chem., 60,* pp. 13-14, 1956.

[189] W. Howland and L. Epstein, "The Binary System Sodium-Lithium," *Advan. Chem. Ser, 19,* pp. 34-41, 1957.

[190] A. D. Pelton, "Calculation of phase equilibria and thermodynamic properties of the Li-Na-H system," *Z. Metall./Mater. Res. Adv. Tech., 84,* pp. 767-772, 1993.

[191] S. Zhang, D. Shin and Z. Liu, "Thermodynamic modeling of the Ca–Li–Na system," *CALPHAD, 27,* pp. 235-241, 2003.

[192] N. Goel and J. Cahoon, "The Al-Li-Mg System (Aluminum-Lithium-Magnesium)," *Bull. Alloy Phase Diagr., 11,* pp. 528-546, 1990.

[193] G. Ghosh, "Aluminium-lithium-magnesium ," in *MSIT Ternary Evaluation Program, in MSIT Workplace, Effenberg, G. (Ed.), MSI, Materials Science International Services GmbH, Stuttgart, (Crys. Structure, Equi. Diagram, Assessment, 48),* 1993.

[194] E. Schürmann and H. Voss, "Investigation of the Melting Equilibria of Mg-Li-Al Alloys," *Giessereiforschung, 33,* pp. 33-53, 1981.

[195] Z. Moser, R. Agarwal, F. Sommer and B. Predel, "Calorimetric studies of liquid Al-Li-Mg alloys," *Z. Metall., 82,* pp. 317-321, 1991.

[196] E. Schürmann and I. Geissler, "Solid Phase Equilibrium inMg-Rich Alloys of the Al-Ii-Mg System," *Giessereiforschung,. 32,* pp. 163-174, 1980.

[197] H. Voss, "Development of an Apparatus for Melting Lithium-Containing Magnesium--Aluminium Alloys and their Use in Thermal Analysis," *Thesis, Tech.Univ.Clausthal*, 1979.

[198] O. Bodak and P. Perrot, "Al-H-Li," in *Light Metal Ternary Systems: Phase Diagrams, Crystall. Thermodyn. Data, 11A3*, G. Effenberg, S. Ilyenko ed., S. I. G. Effenberg, Ed. Germany: Springer-Verlag Berlin Heidelberg, 2005, pp. 58-63.

[199] N. Sklar and B. Post, "Crystal structure of lithium aluminum hydride", *Inorg. Chem. 6(4),* pp. 669-671, 1967.

[200] S. Chung and H. Morioka, "Thermochemistry and crystal structures of lithium, sodium and potassium alanates as determined by ab initio simulations," *J. Alloy. Compd., 372,* pp. 92-96, 2004.

[201] W. E. Garner and E. W. Haycock. The thermal decomposition of lithium aluminium hydride. *Proceedings of the Royal Society of London A: Math., Phys. Eng. Sci. the Royal Society. 211(1106),* pp. 335-351, 1952.

[202] J. Jang, J. Shim, Y. W. Cho and B. Lee, "Thermodynamic calculation of LiH↔ Li_3AlH_6↔ $LiAlH_4$ reactions," *J. Alloy. Compd., 420,* pp. 286-290, 2006.

[203] M. B. Smith and G. E. Bass Jr, "Heats and Free Energies of Formation of the Alkali Aluminum Hydrides and of Cesium Hydride." *J. Chem. Eng. Data, 8,* pp. 342-346, 1963.

[204] P. Claudy, B. Bonnetot, J. Letoffe and G. Turck. Determination of thermodynamic constants of simple and complex hydrides of aluminum. 4. enthalpy of formation of $LiAlH_4$ and Li_3AlH_6. *Thermochim. Acta 27(1-3),* pp. 213-221, 1978.

[205] A. J. Bard, R. Parsons and J. Jordan, *Standard Potentials in Aqueous Solution, 6,* CRC press, 1985.

[206] T. N. Dymova, D. P. Aleksandrov and V. N. Konoplev, "Spontaneous and thermal decomposition of lithium tetrahydroaluminate $LiAlH_4$: the promoting effect of mechanochemical action on the process," *Russ. J. Coord. Chem., 20,* pp. 297-285, 1994.

[207] J. Chen, N. Kuriyama, Q. Xu, H. T. Takeshita and T. Sakai, "Reversible hydrogen storage via titanium-catalyzed LiAlH4 and Li3AlH6", *J. Phys. Chem. B 105(45),* pp. 11214-11220, 2001.

[208] H. Brinks, A. Fossdal, J. Fonneløp and B. Hauback, "Crystal structure and stability of $LiAlD_4$ with TiF_3 additive," *J. Alloy. Compd., 397,* pp. 291-295, 2005.

[209] O. Løvvik, S. M. Opalka, H. W. Brinks and B. C. Hauback, "Crystal structure and thermodynamic stability of the lithium alanates $LiAlH_4$ and Li_3AlH_6", *Phys. Rev. B, 69(13),* pp. 134117: (1-9), 2004.

[210] J. K. Kang, J. Y. Lee, R. P. Muller and W. A. Goddard III, "Hydrogen storage in $LiAlH_4$: Predictions of the crystal structures and reaction mechanisms of intermediate phases from quantum mechanics," *J. Chem. Phys., 121,* pp. 10623-10633, 2004.

[211] D. Li, T. Zhang, S. Yang, Z. Tao and J. Chen, "Ab initio investigation of structures, electronic and thermodynamic properties for Li–Mg–H ternary system," *J. Alloy. Compd., 509,* pp. 8228-8234, 2011.

[212] D. Meggiolaro, G. Gigli, A. Paolone, F. Vitucci and S. Brutti, "Incorporation of lithium by MgH_2: an ab initio study," *J. Phys. Chem. C, 117,* pp. 22467-22477, 2013.

[213] K. Ikeda, Y. Kogure, Y. Nakamori and S. Orimo, "Formation region and hydrogen storage abilities of perovskite-type hydrides," *Prog. Solid State Chem., 35,* pp. 329-337, 2007.

[214] J. Graetz, Y. Lee, J. Reilly, S. Park and T. Vogt, "Structures and thermodynamics of the mixed alkali alanates", *Phys. Rev. B 71(18),* pp. 184115-: (1-7), 2005.

[215] H. Grove, H. Brinks, R. Heyn, F. Wu, S. Opalka, X. Tang, B. Laube and B. Hauback, "The structure of $LiMg(AlD_4)_3$," *J. Alloy. Compd. 455(1),* pp. 249-254. 2008.

[216] P. Claudy, B. Bonnetot, J. Bastide and L. Jean-Marie, "Reactions of lithium and sodium aluminium hydride with sodium or lithium hydride. Preparation of a new alumino-hydride of lithium and sodium $LiNa_2AlH_6$," *Mater. Res. Bull., 17*, pp. 1499-1504, 1982.

[217] J. Huot, S. Boily, V. Güther and R. Schulz. Synthesis of Na_3AlH_6 and Na_2LiAlH_6 by mechanical alloying. *J. Alloy. Compd. 283(1),* pp. 304-306, 1999.

[218] A. Fossdal, H. Brinks, J. Fonneløp and B. Hauback, "Pressure–composition isotherms and thermodynamic properties of TiF_3-enhanced Na_2LiAlH_6", *J. Alloy. Compd., 397(1),* pp. 135-139, 2005.

[219] P. Wang, L. Ma, Z. Fang, X. Kang and P. Wang, "Improved hydrogen storage property of Li-Mg-B-H system by milling with titanium trifluoride," *Energ. Environ. Sci., 2,* pp. 120-123, 2009.

[220] Y. Zhang, Q. F. Tian, S. S. Liu and L. X. Sun, " The destabilization mechanism and de/re-hydrogenation kinetics of MgH_2–$LiAlH_4$ hydrogen storage system," *J. Power Sources, 185,* pp. 1514-1518, 2008.

[221] S. Liu, L. Sun, J. Zhang, Y. Zhang, F. Xu, Y. Xing, F. Li, J. Zhao, Y. Du and W. Hu, "Hydrogen storage properties of destabilized MgH_2-Li_3AlH_6 system", *Int. J. Hydrog. Energ., 35(15),* pp. 8122-8129, 2010.

[222] R. Chen, X. Wang, L. Xu, L. Chen, S. Li and C. Chen, "An investigation on the reaction mechanism of $LiAlH_4$–MgH_2 hydrogen storage system", *Mater. Chem. Phys. 124(1),* pp. 83-87, 2010.

[223] J. Mao, Z. Guo, X. Yu, M. Ismail and H. Liu "Enhanced hydrogen storage performance of $LiAlH_4$–MgH_2–TiF_3 composite", *Int. J. Hydrog. Energ. 36(9),* pp. 5369-5374, 2011.

[224] S. Liu, L. Sun, F. Xu, J. Zhang, Z. Cao and Y. Liu, "Improved dehydrogenation of MgH_2–Li_3AlH_6 mixture with TiF_3 addition" *Int. J. Hydrog. Energ. 36(18),* pp. 11785-11793, 2011.

[225] Q. Wan, P. Li, Z. Li, F. Zhai, X. Qu and A. A. Volinsky, "Improved hydrogen storage performance of MgH_2–$LiAlH_4$ composite by addition of $MnFe_2O_4$," *J. Phys. Chem.C, 117(51),* pp. 26940-26947, 2013.

[226] N. S. Mustafa and M. Ismail, "Enhanced hydrogen storage properties of $4MgH_2 + LiAlH_4$ composite system by doping with Fe_2O_3 nanopowder," *Int. J. Hydrog. Energ., 39(15),* pp. 7834-7841, 2014.

[227] F. H. Yap, M. Ishak and M. Ismail, "Enhanced hydrogen storage performance of destabilized $4MgH_2$–Li_3AlH_6 system doped with Co_2NiO nanopowder", *Int. J. Hydrog. Energ., 40(32),* pp. 10131-10138, 2015.

[228] N. Juahir, F. H. Yap, N. Mustafa and M. Ismail, "Hydrogen storage properties of $4MgH_2$–Li_3AlH_6 composite improved by the addition of K_2TiF_6". *Int. J. Hydrog. Energ. 40(37),* pp. 12713-12720, 2015.

[229] M. Ismail, Y. Zhao, X. Yu and S. Dou, "Effect of different additives on the hydrogen storage properties of the MgH_2-$LiAlH_4$ destabilized system" *Rsc. Adv., 1(3),* pp. 408-414, 2011.

[230] F. Wang, Y. Liu, M. Gao, K. Luo, H. Pan and Q. Wang, "Formation reactions and the thermodynamics and kinetics of dehydrogenation reaction of mixed alanate Na_2LiAlH_6," *J. Phys. Chem. C, 113,* pp. 7978-7984, 2009.